

**COMPARATIVE STUDY OF WIND LOADS
ESTIMATED FROM NUMERICALLY SIMULATED
WIND TUNNEL TEST RESULTS AS PER THE
PROVISIONS OF BANGLADESH NATIONAL
BUILDING CODE**

MD. IMAM HOSSAIN

M.Sc. ENGINEERING THESIS



**DEPARTMENT OF CIVIL ENGINEERING
MILITARY INSTITUTE OF SCIENCE AND TECHNOLOGY
DHAKA, BANGLADESH**

MARCH 2022

**COMPARATIVE STUDY OF WIND LOADS ESTIMATED FROM
NUMERICALLY SIMULATED WIND TUNNEL TEST RESULTS AS
PER THE PROVISIONS OF BANGLADESH NATIONAL
BUILDING CODE**

MD. IMAM HOSSAIN (SN. 1015110005)

**A Thesis Submitted in Partial Fulfillment of the Requirements for the Degree of
Master of Science in Civil Engineering**



**DEPARTMENT OF CIVIL ENGINEERING
MILITARY INSTITUTE OF SCIENCE AND TECHNOLOGY
DHAKA, BANGLADESH**

MARCH 2022

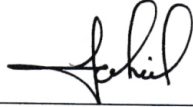
**COMPARATIVE STUDY OF WIND LOADS ESTIMATED FROM
NUMERICALLY SIMULATED WIND TUNNEL TEST RESULTS AS
PER THE PROVISIONS OF BANGLADESH NATIONAL
BUILDING CODE**

M.Sc. Engineering Thesis

By

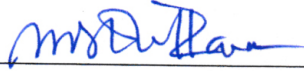
MD. IMAM HOSSAIN (SN. 1015110005)

Approval as to style and content by the Board of Examination on 31 March 2022



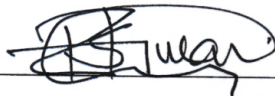
Lt Col Md Jahidul Islam, PhD, Engrs
Associate Professor of Civil Engineering
MIST, Dhaka

Chairman (Supervisor)
Board of Examination



Dr. Shohel Rana
Associate Professor of Civil Engineering
BUET, Dhaka

Member (External)
Board of Examination



Maj Md. Soebur Rahman, PhD, PEng, Engrs
Associate Professor of Civil Engineering
MIST, Dhaka

Member
Examination



Col Nasir Uddin Ahmed
Dean of Civil Engineering Faculty
MIST, Dhaka

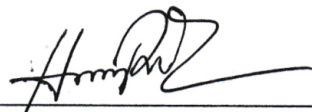
Dean of the Department
Member (Ex-Officio)

Department of Civil Engineering, MIST, Dhaka

**COMPARATIVE STUDY OF WIND LOADS ESTIMATED FROM
NUMERICALLY SIMULATED WIND TUNNEL TEST RESULTS AS
PER THE PROVISIONS OF BANGLADESH NATIONAL
BUILDING CODE**

DECLARATION

I hereby declare that the study reported in this thesis entitled as above is my own original work and has not been submitted before anywhere for any degree or other purposes. Further I certify that the intellectual content of this thesis is the product of my own work and that all the assistance received in preparing this thesis and source have been acknowledged and cited in the reference Section.



Md. Imam Hossain

**COMPARATIVE STUDY OF WIND LOADS ESTIMATED FROM
NUMERICALLY SIMULATED WIND TUNNEL TEST RESULTS AS
PER THE PROVISIONS OF BANGLADESH NATIONAL
BUILDING CODE**

M.Sc. Engineering Thesis

By

Md. Imam Hossain

DEDICATION

Dedicated to my parents for supporting and encouraging me to believe in
myself.

ACKNOWLEDGEMENT

First of all, I would like to express my sincere gratitude to the Almighty Allah for his mercy and blessing and for giving me this opportunity to complete this research peacefully.

I would like to express my sincere gratitude to my thesis supervisor Lt Col Md Jahidul Islam, PhD, Engrs, Associate Professor, Department of Civil Engineering, MIST, for providing me excellent guidance and continuous assistance throughout the study. His constant advice, assertions, and appreciation were very vital and irrevocable. Without his motivation, it wouldn't have been possible for me to finish my paper. I am very much thankful to him for his encouragement throughout the study.

I wish to express my gratitude and thanks to Dr. Iftekhar Anam, Professor, Department of Civil Engineering, University of Asia Pacific, for his valuable time, dynamic direction and recommendations.

I would like to express my sincere gratitude to Maj Md. Soebur Rahman, PhD, PEng, Engrs (Associate Professor), and Dr. G M Jahid Hasan (Professor), Department of Civil Engineering, MIST, for providing me excellent guidance and continuous assistance throughout the study. I express my gratitude and thanks to Dr. Shohel Rana (Associate Professor), Department of Civil Engineering, BUET for his valuable recommendations. Their constant advice, assertions, and appreciation were very vital and irrevocable. I am very much thankful to them for their encouragement throughout the study.

I also express my heartiest thanks to the Head of the Department and other faculty members of the Department of Civil Engineering, MIST, who helped me by providing their important suggestions and cooperation.

I am very much grateful to the officers and staff of the Department of Civil Engineering, MIST, for their cooperation and assistance throughout my study.

Indeed, this page of acknowledgment shall never be able to touch the horizon of the generosity of those who tendered their help to me.

ABSTRACT

COMPARATIVE STUDY OF WIND LOADS ESTIMATED FROM NUMERICALLY SIMULATED WIND TUNNEL TEST RESULTS AS PER THE PROVISIONS OF BANGLADESH NATIONAL BUILDING CODE

Bangladesh has recently landed in the era of tall buildings. Wind load generally governs over earthquakes for tall buildings. However, research on the effect of wind load on structures is limited in Bangladesh. International and local codes evaluate wind effects on regular shape buildings. But they are not recommended for complex-shaped structures. For those, a wind tunnel test is required. This research aimed to determine the performance of the local codes in calculating the wind effect on structures such as BNBC 2020 and BNBC 2006 in addition to the numerical wind tunnel. The other objective was to formulate empirical equations from the numerical wind tunnel test data to improve the evaluation process of wind effect, precisely the wind pressure coefficient (C_p). Computational Fluid Dynamic analysis in a finite element software, named RWIND, was used to perform the numerical wind tunnel test. The numerical model was first validated with physical wind tunnel test data. Four-building of the various geometric property was modeled and simulated to compare the wind pressure coefficient. Another twenty models with different length-width ratios were simulated and analyzed to develop empirical equations for calculating the wind pressure coefficient. The study concluded that the proposed empirical equations evaluate the wind loads better than the BNBC 2020. The proposed empirical equations demonstrated a mean variation of about 15 percent in the long direction to the numerical wind tunnel, while the BNBC 2020 showed about 50 percent variation. Moreover, in the short direction, the proposed equations showed a mean variation of about 28 percent compared to 53 percent of the BNBC 2020. The BNBC 2020 and BNBC 2006 showed a considerable variation in calculating the wind pressure coefficient. The story-wise average variation ranged from 47% to 53% in the long direction and 37% to 47% in the short direction. The numerical wind tunnel following the BNBC 2020 showed relatively less variation in the calculation of the shear force than the BNBC-2020 manual, and the average variation was 20% to 30% in the long direction and 16% to 33% in the short direction.

সারসংক্ষেপ

COMPARATIVE STUDY OF WIND LOADS ESTIMATED FROM NUMERICALLY SIMULATED WIND TUNNEL TEST RESULTS AS PER THE PROVISIONS OF BANGLADESH NATIONAL BUILDING CODE

বাংলাদেশ সম্প্রতি উঁচু ভবনের যুগে অবতরণ করেছে। বায়ু লোড (wind load) সাধারণত উঁচু ভবনের জন্য ভূমিকম্পের (earthquake) চেয়ে বেশি প্রাধান্য পায়। তারপরও কাঠামোর উপর বায়ু লোডের প্রভাব নিয়ে গবেষণা বাংলাদেশে সীমিত। আন্তর্জাতিক এবং স্থানীয় কোডগুলি সাধারণত স্বাভাবিক আকৃতির বিল্ডিংগুলিতে বাতাসের প্রভাব মূল্যায়ন করে কিন্তু জটিল আকৃতির কাঠামোর জন্য বায়ু টানেল (wind tunnel) সুপারিশ করা হয়েছে। জটিল আকৃতির কাঠামোর কার্যকারিতা নির্ধারণ করার জন্য বায়ু টানেল পরীক্ষা প্রয়োজন। এই অধ্যয়নের লক্ষ্য ছিল সংখ্যাসূচক বায়ু টানেল (numerical wind tunnel) এর সাথে কাঠামোতে বায়ুর প্রভাব নির্ণয় করার ক্ষেত্রে স্থানীয় কোডগুলির (BNBC-2020, BNBC-2006) কার্যকারিতা তুলনা করা। অধ্যয়নের আরেকটি লক্ষ্য ছিল বায়ুর প্রভাব মূল্যায়ন প্রক্রিয়া উন্নত করার জন্য সংখ্যাসূচক বায়ু টানেল (numerical wind tunnel) পরীক্ষার ফলাফল থেকে বায়ু চাপ সহগ (wind pressure coefficient, C_p) এর প্রায়োগিক সমীকরণ (empirical equation) তৈরি করা। RWIND নামক একটি সফটওয়্যার গণনামূলক তরল গতিশীল বিশ্লেষণ (computational fluid dynamic, CFD) এবং একটি সংখ্যাসূচক বায়ু টানেল (numerical wind tunnel) পরীক্ষার জন্য ব্যবহৃত হয়েছে। K-Epsilon মডেলটি এই গবেষণায় ব্যবহার করা হয়েছে, যাতে ফলাফলগুলিতে ভাল সামঞ্জস্য আছে। সংখ্যাসূচক মডেলটি প্রথমে পরীক্ষালব্ধ বায়ু টানেল পরীক্ষার ফলাফল দিয়ে যাচাই করা হয়েছিল। চারটি ভিন্ন আকারের মডেল তৈরি করা হয়েছিল, এবং বাতাসের চাপ সহগ (wind pressure coefficient, C_p) পরিপ্রেক্ষিতে কোডগুলির মূল্যায়ন বৈশিষ্ট্যের তুলনা করার জন্য সিমুলেট করা হয়েছিল। এছাড়াও বিভিন্ন দৈর্ঘ্য-প্রস্থ অনুপাতের আরও বিশটি মডেল সিমুলেট করা হয়েছিল এবং বায়ুচাপ সহগ (wind pressure coefficient, C_p) গণনা করার জন্য প্রায়োগিক সমীকরণ (empirical equation) তৈরির জন্য বিশ্লেষণ করা হয়েছিল। সমীক্ষাটি উপসংহারে পৌঁছেছে যে প্রস্তাবিত পরীক্ষামূলক সমীকরণগুলি (empirical equations) BNBC-2020 এর তুলনায় বায়ু লোড ভালভাবে অনুমান করে। দীর্ঘ দিকে প্রস্তাবিত পরীক্ষামূলক সমীকরণগুলি (empirical equations) সংখ্যাসূচক বায়ু সুডঙ্গ (numerical wind tunnel) এর তুলনায় প্রায় ১৫ শতাংশের

গড় পরিবর্তন দেখায়, যেখানে BNBC 2020 প্রায় ৫০ শতাংশ পরিবর্তন দেখায়। এছাড়াও, সংক্ষিপ্ত দিকে প্রস্তাবিত সমীকরণগুলি BNBC 2020 এ ৫৩ শতাংশের তুলনায় গড়ে প্রায় ২৮ শতাংশ পরিবর্তিত হয়। BNBC-2020 এবং BNBC-2006 বায়ুচাপ সহগ (wind pressure coefficient, C_p) গণনা করার ক্ষেত্রে যথেষ্ট পার্থক্য দেখিয়েছে, যেখানে ভবনের তলা-ভিত্তিক গড় পরিবর্তন দীর্ঘ দিকে ৪৭ থেকে ৫৩ শতাংশ এবং সংক্ষিপ্ত দিকে ৩৭ থেকে ৪৭ শতাংশ পর্যন্ত ছিল। BNBC-2020 অনুসরণকারী সংখ্যাসূচক বায়ু টানেল (numerical wind tunnel) হাতে শিয়ার ফোর্সের গণনায় তুলনামূলকভাবে কম তারতম্য দেখায় এবং গড় তারতম্য ছিল দীর্ঘ দিক থেকে ২০ থেকে ৩০ শতাংশ এবং সংক্ষিপ্ত দিকে ১৬ থেকে ৩৩ শতাংশ।

LIST OF SYMBOLS

Acceleration	x	Standard Deviation	σ
Atmospheric pressure	P	Stiffness matrix	$[k]$
Boundary layer value of first grid pt	v	Surface shear stress	C_{sd}
Coef dependent on terrain roughness	α	Temperature	T
Constant Velocity	U	Terrain exposure constant	l
Coriolis parameter	f	Time	t
Density	ρ	Total internal energy	e
Density of air	ρ_a	Turbulence frequency	$\rho\theta$
Displacement	x	Turbulence intensity in i -th direction	TI_i
Distance	d	Turbulent kinetic energy	K
Dynamic viscosity	μ	Velocity	x
Elevation or height	z	Viscous damping	c
Equivalent height	\bar{z}	von Karman's constant	k
Flexibility matrix	$[a]$	Natural circular frequency	$\rho\omega_0$
Force	F	Radius	r
Frequency	f	Rate-of-strain tensor	\bar{S}_{ij}
Friction velocity	u_*	Roughness coefficient of terrain	z
integral length scale in i -th direction	L_i		
Kinematic velocity	v		

LIST OF TABLES

Table 3.1: Dimensions of study models.....	53
Table 4.1: Length-width ratios of structures considered in modelling	81
Table 4.2: Proposed linear equations to calculate pressure coefficient	97
Table 4.3: Comparison of base shear in Long Direction	107
Table 4.4: Comparison of base shear in Short Direction	109

LIST OF FIGURES

Figure 1.1: Flowchart of the study	5
Figure 2.1: Wind profile in different boundary layers	8
Figure 2.2: Variation of wind velocity with time	10
Figure 2.3: Schematic representation of mean and gust pressure	10
Figure 2.4: Wind Components	11
Figure 2.5: Simplified two-dimensional flow of wind	11
Figure 2.6: (a) Wind flow and pressure distribution (b) Pressure on surface	16
Figure 2.7: Flowchart of wind Load Calculation (BNBC 2006)	17
Figure 2.8: Flowchart of wind Load Calculation (BNBC 2020)	20
Figure 2.9: Infinitesimal fluid element model of flow	24
Figure 2.10: Model of infinitesimally small element fixed in space including mass flux diagram	24
Figure 2.11: Model used for the derivation of the x-component of momentum equation.	26
Figure 2.12: Surface mounted cube: Comparison of mean wind pressure coefficients between wind tunnel experiments and numerical simulation by using several turbulence models	33
Figure 2.13: Cubical building in ABL flow. Comparison of pressure coefficient profiles on the vertical section using several turbulence models	33
Figure 2.14: Silsoe 6m cube: Comparison of mean pressure coefficient between full-scale measurement, wind tunnel and numerical simulations- cube skewed at 45- degree	34
Figure 2.15: Low-rise building: Comparison of wind pressure coefficients experiment and numerical	35
Figure 2.16: The TTU Building: Comparison between mean pressure coefficient profiles for straight wind computational and WT and field measurement	37

Figure 2.17: The TTU Building in ABL flow condition: Comparison of pressure coefficient profiles on the vertical section between wind tunnel experiments and numerical simulations.....	37
Figure 2.18: Mean wind pressure coefficient on CAARC building model	38
Figure 2.19: Comparison between the mean pressure coefficients of CAARC in a simulated ABL flow using LES with various turbulence models and BLWT experiment	39
Figure 2.20: Relationship between RFEM/RSTAB and RWIND Simulation.....	40
Figure 2.21: Manual Model Import in RWIND Simulation	41
Figure 2.22: Automatic Model Import in RWIND	42
Figure 2.23: Flow Field Results in Volume Space	43
Figure 2.24: Different results of the aerodynamics analysis in RWIND Simulation	44
Figure 2.25: Model of a multi-storeyed building.....	46
Figure 2.26: Linear analysis of structure	47
Figure 2.27: Response spectrum analysis	48
Figure 2.28: Time History analysis.....	48
Figure 2.29: Nonlinear Direct Integration analysis.....	49
Figure 2.30: Pushover analysis	50
Figure 3.1: Numerical wind tunnel measurements	52
Figure 3.2: Simulation parameters in RWIND	53
Figure 3.3: (a) Simulation parameters model selection, turbulence consideration (b) Wind tunnel dimensions.....	54
Figure 3.4: RWIND's Graphical representation of (a) external pressure coefficient (C_p) and (b) streamlines turbulence	54
Figure 3.5: Graphical representation of pressure co-efficient at a specific elevation.....	55
Figure 3.6: One of the numerical study models in ETABS	56
Figure 3.7: Numerical wind tunnel measurements	57

Figure 3.8: Model and Computational Domain at RWIND.....	57
Figure 3.9: (a) Topological imperfections of CAD models (b) Examples of automatically simplified models	58
Figure 3.10: Mesh generation of the model	58
Figure 3.11: 1:400 scale model for Wind Tunnel test	60
Figure 3.12: Values of Mean Pressure Coefficients (C_p) over the Perimeter at 2H/3	61
Figure 3.13: Pressure Coefficients (C_p) at Windward and Leeward Surface	61
Figure 4.1 Six Storied Building	64
Figure 4.2: Contours of C_p in Windward wall and Side wall of the six storied building in Numerical Wind Tunnel Test	65
Figure 4.3: Comparison of story shear of the six storied building in the long direction ...	67
Figure 4.4: Comparison of story shear of the six storied building in the short direction ..	67
Figure 4.5: Ten Storied Building	68
Figure 4.6: Contours of C_p in Windward wall and Sidewall of the ten storied building in Numerical Wind Tunnel Test	69
Figure 4.7: Comparison of story shear of the ten storied building in the long direction ...	71
Figure 4.8: Comparison of story shear of the ten storied building in the Short direction .	71
Figure 4.9: Twenty Storied Building	72
Figure 4.10: Contours of C_p in Windward wall and Sidewall of the twenty storied building in Numerical Wind Tunnel Test	73
Figure 4.11: Comparison of story shear of the twenty storied building in the long direction	75
Figure 4.12: Comparison of story shear of the twenty storied building in the Short direction	75
Figure 4.13: Forty Storied Building.....	76
Figure 4.14: Contours of C_p in Windward wall and Sidewall of the forty storied building in Numerical Wind Tunnel Test	77

Figure 4.15: Comparison of story shear of the forty storied building in the Long direction	79
Figure 4.16: Comparison of story shear of the forty storied building in the Short direction	79
Figure 4.17: Geometry and wind direction of a typical building	80
Figure 4.18: Considered zones of a structure	81
Figure 4.19: Windward pressure coefficient for $L/B = 0.50$	83
Figure 4.20: Leeward pressure coefficient for $L/B = 0.50$	85
Figure 4.21: Windward pressure coefficient for $L/B = 0.67$	86
Figure 4.22: Leeward pressure coefficient for $L/B = 0.67$	88
Figure 4.23: Windward pressure coefficient for $L/B = 1.0$	89
Figure 4.24: Leeward pressure coefficient for $L/B = 1.0$	91
Figure 4.25: Windward pressure coefficient for $L/B = 2.0$	92
Figure 4.26: Leeward pressure coefficient for $L/B = 2.0$	94
Figure 4.27: Windward pressure coefficient for $L/B = 3.0$	95
Figure 4.28: Leeward pressure coefficient for $L/B = 3.0$	97
Figure 4.29: Proposed Windward pressure coefficient at zone A	98
Figure 4.30: Proposed Windward pressure coefficient at zone B	99
Figure 4.31: Proposed Windward pressure coefficient at zone C	99
Figure 4.32: Proposed Leeward pressure coefficient at zone A	100
Figure 4.33: Proposed Leeward pressure coefficient at zone B	100
Figure 4.34: Proposed Leeward pressure coefficient at zone C	100
Figure 4.35: Comparison of story shear of the six storied building in the long direction	101
Figure 4.36: Comparison of story shear of the six storied building in the short direction	102
Figure 4.37: Comparison of story shear of the ten storied building in the long direction	103

Figure 4.38: Comparison of story shear of the ten storied building in the short direction	103
Figure 4.39: Comparison of story shear of the twenty storied building in the long direction	104
Figure 4.40: Comparison of story shear of the twenty storied building in the short direction	105
Figure 4.41: Comparison of story shear of the forty storied building in the long direction	106
Figure 4.42: Comparison of story shear of the forty storied building in the short direction	106
Figure 4.43: Comparison of base shear in the long direction	108
Figure 4.44: Comparison of base shear in the Short direction.....	109

TABLE OF CONTENTS

ACKNOWLEDGEMENT	i
ABSTRACT.....	ii
LIST OF SYMBOLS	v
LIST OF TABLES	vi
LIST OF FIGURES	vii
TABLE OF CONTENTS.....	xii
CHAPTER 1: INTRODUCTION.....	1
1.1 General.....	1
1.2 Effect on Structure Due to Wind Force	2
1.3 Research Significances	3
1.4 Objectives of the Study.....	4
1.5 Outline of Methodology.....	5
1.6 Organisation of the Thesis	5
CHAPTER 2 : LITERATURE REVIEW	7
2.1 Introduction.....	7
2.2 Atmospheric Boundary Layer.....	7
2.2.1 Wind Speed Profile	7
2.2.1.1 The Logarithmic Law	8
2.2.1.2 The Power Law	9
2.2.2 Wind Turbulence	9
2.3 Design Wind Pressures	11
2.3.1 Wind Velocity Pressure	12
2.3.2 Wind Pressure Coefficient	12
2.3.3 Gust Effect Factor	17
2.4 Provisions for Wind Load – BNBC 2006.....	17

2.4.1	Design Wind Pressure.....	18
2.4.2	Exposure Categories	18
2.4.3	Local Topography Coefficient.....	18
2.4.4	Overall Pressure Coefficient.....	19
2.4.5	Wind Gust Coefficient	19
2.4.6	Combined Height and Exposure Coefficient	19
2.5	Provisions for Wind Load – BNBC 2020.....	19
2.5.1	Design Wind Pressure.....	20
2.5.2	Exposure Categories	20
2.5.3	Structural Importance Factor	21
2.5.4	Wind Pressure Coefficient	21
2.5.5	Velocity Pressure Exposure Coefficient.....	22
2.5.6	Wind Gust Coefficient	22
2.6	Computational Fluid Dynamics	23
2.6.1	The Continuity Equation.....	23
2.6.2	The Momentum Equation	25
2.7	Background of CFD Modelling	27
2.8	The k- ϵ Turbulence Model.....	28
2.8.1	Turbulence Energy Transport Equation.....	29
2.8.2	Turbulence Dissipation Transport Equation	30
2.8.3	Final Form of the Standard k- ϵ Turbulence Model.....	31
2.9	Computational Evaluation of Wind Load on Buildings	32
2.9.1	Illustration of Wind Loads on Low-Rise Buildings.....	34
2.9.2	Wind Load Estimation on High-Rise Buildings	38
2.10	Wind Simulation and Analysis Software.....	39
2.10.1	Dlubal RWIND and RFEM	40

2.10.2	ETABS.....	45
2.11	Summary	50
CHAPTER 3 : METHODOLOGY		51
3.1	Introduction.....	51
3.2	Numerical Modelling	52
3.2.1	Study Model in RFEM.....	52
3.2.2	Wind Simulation in RWIND	53
3.2.3	Simulation Output Pressure Co-efficient (C_p)	54
3.2.4	Numerical Model in ETABS	55
3.3	Numerical Wind Tunnel Model Validation	56
3.3.1	Geometric Dimension	57
3.3.2	Meshing of the Model.....	58
3.3.3	Turbulence Models and Analysis Methods.....	59
3.3.4	Boundary Conditions	59
3.3.5	Result Verification	60
3.4	Summary	60
CHAPTER 04 : RESULTS ANALYSIS AND DISCUSSIONS.....		63
4.1	Introduction.....	63
4.2	Comparison of Story Shear Due to Wind Force	63
4.2.1	Six Storied Regular Shape Building	64
4.2.1.1	Building Parameters According to BNBC-2006.....	65
4.2.1.2	Building parameters According to BNBC-2020.....	65
4.2.1.3	Pressure Co-efficient from Numerical Wind Tunnel Test.....	65
4.2.2	Ten Storied Regular Shape Building	68
4.2.2.1	Building Parameters According to BNBC-2006.....	68
4.2.2.2	Building parameters According to BNBC-2020.....	68

4.2.2.3	Pressure Co-efficient from Numerical Wind Tunnel Test.....	69
4.2.3	Twenty Storied Regular Shape Building	72
4.2.3.1	Building Parameters According to BNBC-2006.....	72
4.2.3.2	Building parameters According to BNBC-2020.....	72
4.2.3.3	Pressure Co-efficient from Numerical Wind Tunnel Test.....	73
4.2.4	Forty Storied Regular Shape Building.....	76
4.2.4.1	Building Parameters According to BNBC-2006.....	76
4.2.4.2	Building parameters According to BNBC-2020.....	76
4.2.4.3	Pressure Co-efficient from Numerical Wind Tunnel Test.....	77
4.3	Evaluation of Pressure Coefficient Due to Wind Force.....	80
4.3.1	Pressure Coefficient for Length to Width Ratio is 0.5.....	82
4.3.2	Pressure Coefficient for Length to Width Ratio is 0.67.....	85
4.3.3	Pressure Coefficient for Length to Width Ratio is 1.0.....	88
4.3.4	Pressure Coefficient for Length to Width Ratio is 2.0.....	91
4.3.5	Pressure Coefficient for Length to Width Ratio is 3.0.....	94
4.4	Proposed Pressure Coefficient Equations	97
4.4.1	Comparison of Story Shear	101
4.4.1.1	Six Storied Regular Shape Building	101
4.4.1.2	Ten Storied Regular Shape Building	102
4.4.1.3	Twenty Storied Regular Shape Building	104
4.4.1.4	Forty Storied Regular Shape Building.....	105
4.4.2	Total Base Shear Comparison.....	107
4.5	Summary	110
CHAPTER 05 : CONCLUSIONS AND RECOMMENDATIONS.....		111
5.1	Introduction.....	111
5.2	Conclusions.....	111

5.3 Recommendations for Future Work.....	112
REFERENCES	114
APPENDICES	A1
Appendix A: Story share calculation of six storied regular shape building.....	A1
Appendix B: Story share calculation of ten storied regular shape building.....	B1
Appendix C: Story share calculation of twenty storied regular shape building.....	C1
Appendix D: Story share calculation of forty storied regular shape building.....	D1
Appendix E: Pressure coefficient for $L/B = 0.5$	E1
Appendix F: Pressure coefficient for $L/B = 0.67$	F1
Appendix G: Pressure coefficient for $L/B = 1.0$	G1
Appendix H: Pressure coefficient for $L/B = 2.0$	H1
Appendix I: Pressure coefficient for $L/B = 3.0$	I1
Appendix J: Story shear comparison for six storied building using proposed equations	J1
Appendix K: Story shear comparison for ten storied building using proposed equations	K1
Appendix L: Story shear comparison for twenty storied building using proposed equations	L1
Appendix M: Story shear comparison for forty storied building using proposed equations	M1
Appendix N: Provisions for Wind Load – BNBC 2006.....	N1
Appendix O: Provisions for Wind Load – BNBC 2020.....	O1

CHAPTER 1

INTRODUCTION

1.1 General

Revolutionary developments in science, commerce, advances in construction technology, high-strength materials, and innovation in architectural approaches have led to the construction of super-tall structures. Contemporary high-rise buildings are significantly thinner, more flexible, and lighter than their old counterpart's previous ones. Engineers went from convention to symmetry cross-sections to more complex and heterogeneous shapes with large buildings. The shape of the structure plays an essential role in the structure's resistance to loads and reactions caused by wind. Wind loads for tall buildings cannot be generalized because of the significant variation of the heights and shape and the environment of a building. The advancements in heights and shapes result in a lack of sufficient damping and a low structure's natural frequency. These undesirable conditions cause excessive vibration, poor operating conditions, and discomfort of occupants under the influence of wind. This increase in wind loads with altitude causes problems related to the excitation vortex, and wind-induced dynamics respond within the range of gusts. This oscillating motion produces by dynamic motion that is sensed by the occupants and can create an annoyance. Therefore, wind-induced building movements are also in performance design ranges. It must meet service requirements such as the occupant's discomfort from the building's lateral motion. Strong wind may become the major force for a particular structure: tall slender and inadequate stiff result in a collapse of the structure. Wind pressure coefficient (C_p) is an aerodynamics effect to structures that highly depend on the aspect ratio, shape of the structures, façade's position, and others.

According to Taranath (1988, 2010), tall buildings cannot be defined in terms of any specific number of floors or storey height, but the dividing line should be where the design of the structure moves from the field of statics to structural dynamics. From the structural engineer's point of view, however, a tall building may be defined as one that, because of height, is affected by lateral forces due to wind or earthquake actions to an extent that they play an important role in the structural design (Smith and Coull, 1991). As indicated in the definition for a high-rise building in Section 202 of the 2015 International Building Code (IBC), a building is considered a high-rise when there is an "occupied floor" more than 75 feet above the lowest level of fire department vehicle access. The occupied floor, in this

case, was referring to the “occupied floor” of the highest story and not the level of the occupied roof.

1.2 Effect on Structure Due to Wind Force

Windstorm damage to buildings and other structures has been a fact of life for humans since they emerged from the cave until the present day. The development of construction techniques and roof shapes for small residential buildings, which have typically incurred the most damage during extreme winds, has relied heavily on trial and error. In past centuries, heavy masonry construction was once thought to be the best way to withstand wind forces. The difference in pressure between the exterior and interior of a building governs envelope net wind load and the subsequent wind-driven rain infiltration. Even though the contribution of internal pressure to the total design wind load on building envelope is significant, there are very few studies performed as compared to that of external pressure. Most internal and external pressure related studies were conducted in Boundary Layer Wind Tunnels (BLWT) (Amanuel et al., 2013). Unlike the external pressure, internal pressure is highly influenced by the size and location of dominant openings and the internal volume of the building. In retrospect, these factors are governed by Strouhal and Reynolds number which cannot be represented accurately in small scale wind tunnel studies. For wind load application, minimization of the internal pressure to reduce the net design pressure might be an effective target. This can be achieved by sealing and blocking any opening on the building envelope.

Similarly higher differential pressure (external versus internal) can lead to movement of moisture (or wind driven rain) through a building envelope. From energy efficiency point of view, however, vent openings are necessary to help control temperature of the interior building and minimize energy cost. This, generally, underscores the necessity of a parametric evaluation of internal and external pressures on low-rise buildings to address the effective design wind loads under the constraints of natural ventilation for energy efficiency (Masaru et al., 2009).

The introduction of steel and reinforced concrete as construction materials and the beginnings of stress analysis methodologies for structural design characterized the nineteenth century. The introduction of computer methods in the second half of the twentieth century was further developed. Major structural failures due to wind action have

periodically provoked engineers' interest in wind forces. Long-span bridge collapses were common. The Brighton Chain Pier in England was in service in 1823 and collapsed due to the gusty wind in 1836. In Scotland, the Tay Bridge was one of the most spectacular structures then, which collapsed in 1879.

Moreover, the Tacoma Narrows Bridge in Washington State, the United States of America, was the most prominent, collapsed in 1940 with the dynamic action of wind having a significant role (Holmes, 2007). One Indiana Square is a 36-story (504 ft) building in Indianapolis, Indiana, United States. After being damaged by' tornado-force, winds reaching speeds of more than 130 km/h (80.7 mph) on April 2, 2006, the building underwent external restoration. This storm made winds strong enough to cause significant damage to the façade and structural elements of 16 of the tower's 36 stories, resulting in millions of dollars in losses and the restriction of streets and businesses for many days. The extent of the devastation provoked dispute over whether it was caused by a tornado, a downburst, or strong straight-line winds. The measured wind speed was very close to the recommended ASCE 7-10 national standard for typical design wind speeds for buildings. The recommended speeds are based on geographic areas, with the southeast Florida region having the highest wind speed values (Duffin, 2014).

1.3 Research Significances

The advancement of science, technologies, and construction, along with the economic status of the People's Republic of Bangladesh, has stimulus for the development of skyscrapers in the country. Moreover, the growing population in urban societies and increasing pressure on the limited but expensive land area have also contributed a lot to the evolution of high-rise buildings. These structures are significantly affected by lateral forces such as wind load.

The Bangabandhu Iconic Tri-Tower is an under-construction skyscraper project and the centerpiece of the Purbachal Central Business District development project. There will be a 71-story Liberation Tower with a height of 323 m (1,060 ft) and a 52-story Language Tower with a height of 244 m (801 ft) in addition to the 111-story Legacy Tower with a height of 465 m (1526 ft) (The Business Standard , 2021). Lateral deflection of the Legacy Tower due to the lateral forces will be controlled using the tuned mass damper like the

Taipei 101 tower (The Business Standard , 2021). The Purbachal CBD will include 38 other towers ranging from 35 to 50 floors.

The construction of such skyscrapers in the country will be fostered rapidly soon. Bangladesh National Building Code (BNBC) provides the tools for engineers to calculate the wind pressures for designing the regular-shaped building. Where regular-shaped building properties are defined as (i) building height to minimum lateral dimension ratio not more than 5.0, (ii) building natural frequency in the first mode is equal or more than 1 Hz, (iii) simple diaphragm, and no unusual geometrical irregularity, etc. (BNBC, 2006). Significant modifications of wind load calculation have been suggested in the new building design code BNBC-2020 compared to the previous code BNBC-2006. However, the code does not consider the uneven effects (turbulence, torsional effect, etc.) on building due to a cross-wind, vortex shedding, and instability for galloping or flutter. Furthermore, special consideration is required for channeling impacts in the wake of upwind obstructions (BNBC, 2020).

Calculation of wind load is critical for tall, unusually shaped buildings or buildings located in hurricane-prone areas. The BNBC-2020 recommends performing a wind tunnel test. Wind tunnel testing provides more accurate design information, but it is expensive and time-consuming (Soligo, 2019). Alternatively, numerical simulation of the wind tunnel is an easy and effective tool for engineers to evaluate the design information of the concerned building (Daemei, 2019).

Therefore, this study compared the provisions of BNBC-2006 and BNBC-2020 and numerical simulation of wind tunnel test results for induced wind load for various types of structures.

1.4 Objectives of the Study

This work aims to identify the response of structures subjected to wind load. For this purpose, the following objectives have been established to organize the effort:

- i. To evaluate the response of various real structures (low-rise, high-rise, and tall building) due to wind load according to the provisions of BNBC 2006 and BNBC 2020

- ii. To compare the results of codes with the numerically simulated results from the wind tunnel test

1.5 Outline of Methodology

In this research, initially, wind effects on these structures are determined manually to make comparisons. A numerical simulation has been carried out for different structure with various length-width ratios using numerical wind tunnel to understand the local and the international code's process of evaluating the wind load and finally to formulate empirical equations for determination of the wind pressure coefficients at various section of the surface of a structure. Flow chart of the methodology is shown in Figure 1.1 below.

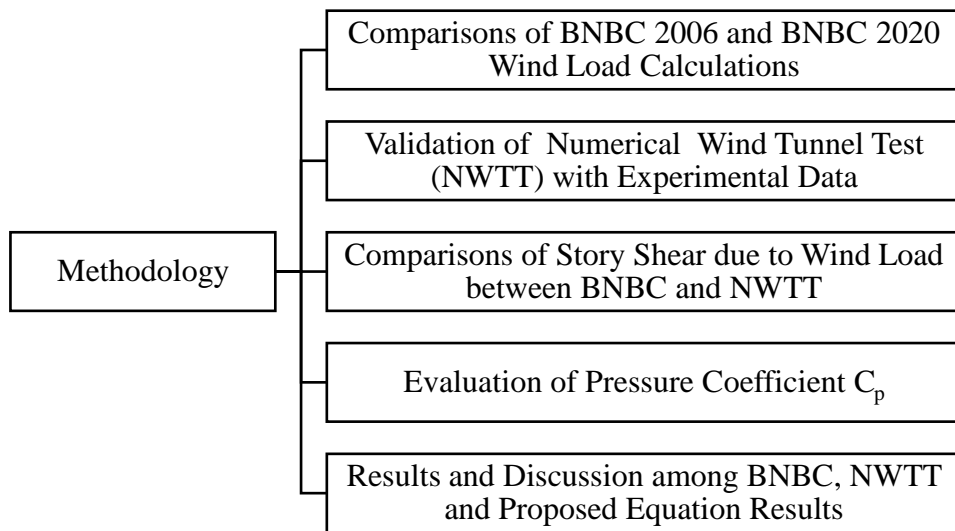


Figure 1.1: Flowchart of the study

1.6 Organisation of the Thesis

This study attempted to assess the wind pressure coefficient on the surface of structures, an aerodynamic property, and evaluate the effects of different pressure coefficients on various surfaces of structures. Local and global standards were also studied, and comparison was performed in calculating the lateral base shear or story shear and numerical wind tunnel test results. The whole thesis has been organized as follows:

Chapter 2 presents a basic summarized historical review of the numerical wind tunnel test and its output, especially the pressure coefficient. This chapter also provides the

background for calculating wind pressure and its parameters according to Bangladesh National Building Code and related international codes and standards.

Chapter 3 presents verification work between an experimental wind tunnel performed in the Tong Ji University and the numerical model performed in RWIND software for this study. This chapter also describes the parameters of numerical wind tunnel simulation and its procedure.

Chapter 4 presents the results and discussions about the findings from numerical wind tunnel tests such as pressure coefficient, story shear, etc. This chapter is divided into three sections (i) Calculation of the shear force due to the lateral wind load by the standards, (ii) Effect of variable coefficients at different points of surfaces of structures using numerical wind tunnel (CFD analysis), (iii) Performance of proposed empirical equations for calculation of the variable coefficients at specified zones of structures. Moreover, the proposed pressure coefficient equations from different length-to-width ratios were also described in this chapter.

Chapter 5 presents conclusions drawn from this study and provides recommendations for further work.

CHAPTER 2

LITERATURE REVIEW

2.1 Introduction

The wind is the air moving relative to the earth produced by several forces such as forces generated by the rotation of the earth and the pressure differences in the atmosphere, which are the results of the differential solar heating of different parts of the earth's surface. Eddies of wind power it to be turbulent or gusty. Flutter, a coupled motion, is a combination of bending and torsion and the vortex, which can lead to a crosswind response of a structure. Serviceability considerations are important criteria a designer must take care of. The wind is one of the major forces that can cause collapse to any structure, create motion on the structure while moving, and result in vibration to the structure. Humans are very sensitive to vibration even though the structure responds to a relatively low level of stress and strain. The average wind speed tends to increase with height while the gustiness decreases with height. Slender tall structures are relatively more sensitive to the wind load.

2.2 Atmospheric Boundary Layer

Frictional forces play a vital part in the balance of forces on moving air as it approaches the earth's surface. This zone stretches up to 500 to 1,000 meters in height for heavier storms like convective depressions. The area affected by friction is called the atmospheric boundary layer; in many respects, it resembles a turbulent boundary layer on a solid surface at high wind speeds. All of this turbulence redistributes pollutants and other atmospheric components as well as heat, moisture, and wind drag inside the boundary layer. By doing this, it significantly influences how the weather (temperature, humidity, wind speed, air quality, etc.) is experienced by those of us who live on the surface.

2.2.1 Wind Speed Profile

The Atmospheric Boundary Layer features change depending on the topographical conditions. The influence of neighboring structures and topography in the loading of the structure of interest is considered and included in design standards such as the ASCE 7-05. As shown in Figure 2.1, there are three main types of terrain that will impact the form and thickness of the boundary layer. Nominal height of boundary layer Z_g depends on the

exposure and V_z indicates the mean wind speed at height Z aboveground. Since the BNBC 2020 and BNBC 2006 regard urban and suburban regions to have the same exposure, the BNBC classifies terrain into three categories. The surface boundary layer is a region of turbulence that exists in urban areas and rises to a height of about a quarter of a mile above ground. The ground effect no longer affects the horizontal airflow above this layer. The majority of human activity takes place at this boundary layer, where the wind speed at this height is known as the gradient wind speed.

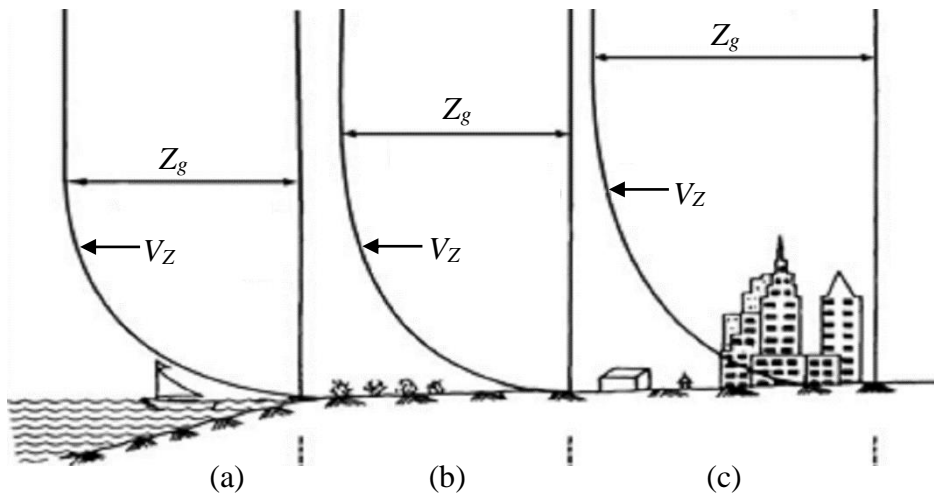


Figure 2.1: Wind profile in different boundary layers; (a) Marine/Unobstructed Areas, (b) Open Terrain (c) Urban and Suburban Terrain (Taranath, 2004)

2.2.1.1 The Logarithmic Law

The most accurate mathematical expression in strong wind conditions is the 'logarithmic law.' The logarithmic law was derived initially for the turbulent boundary layer on a flat plate by Prandtl. It can be derived in several ways. Note that near the ground, the effect of the earth's rotation (Coriolis forces) and molecular viscosity can be neglected because of the turbulent flow (Holmes, 2007). Equation 2.1 is the simplest derivation of boundary layer-

$$U_{(z)} = \frac{\mu_0}{k} \log_e \left(\frac{z}{z_0} \right) \dots \dots \dots (2.1)$$

\bar{U} is the rate of change of mean wind speed, Z is the height above the ground, Z_0 is the roughness length, k is the surface drag coefficient.

2.2.1.2 The Power Law

The power law has no theoretical foundation, but it is simple to integrate over height, which is useful for determining bending moments at the base of a tall building is given by equation 2.2. The power-law may be used to connect the mean wind speed at any height z to that at 10 m (Holmes, 2007).

$$v_z = v_{zref} \left(\frac{v}{v_z} \right)^{\frac{1}{\alpha}} \dots\dots\dots (2.2)$$

With changes in terrain roughness, height range, and average time, the α exponent will change. Design standards such as ASCE 7-05, ASCE 7-10, BNBC 2020 have their own sets of coefficients for the mentioned equations, demonstrated in section 2.4.

2.2.2 Wind Turbulence

The movement of the wind is turbulent. Since air has a very low viscosity, about 1/16th that of water, it is difficult to give a concise mathematical definition of turbulence. Air movement faster than 2-3 miles per hour (0.9-1.3 m/s) is turbulent, so air particles move randomly in all directions. This differs mainly from the laminar flow of heavy liquid particles moving parallel to the direction of flow. For structural design purposes, wind speed can be thought of as having two components: an average velocity component that increases with height and a turbulent velocity that remains constant at height (Taranath, 2004). Figure 2.2 describes the variation of wind velocity with time.

Similarly, the wind pressures, which are proportional to the square of the velocities is also fluctuate as shown in Figure 2.3. In equation 2.3, the total pressure P_t at any instant t is given by the relation-

$$P_t = P' + P \dots\dots\dots (2.3)$$

Where, P_t is the pressure at instant t , P' is the average or mean pressure, and P is the instantaneous pressure fluctuation.

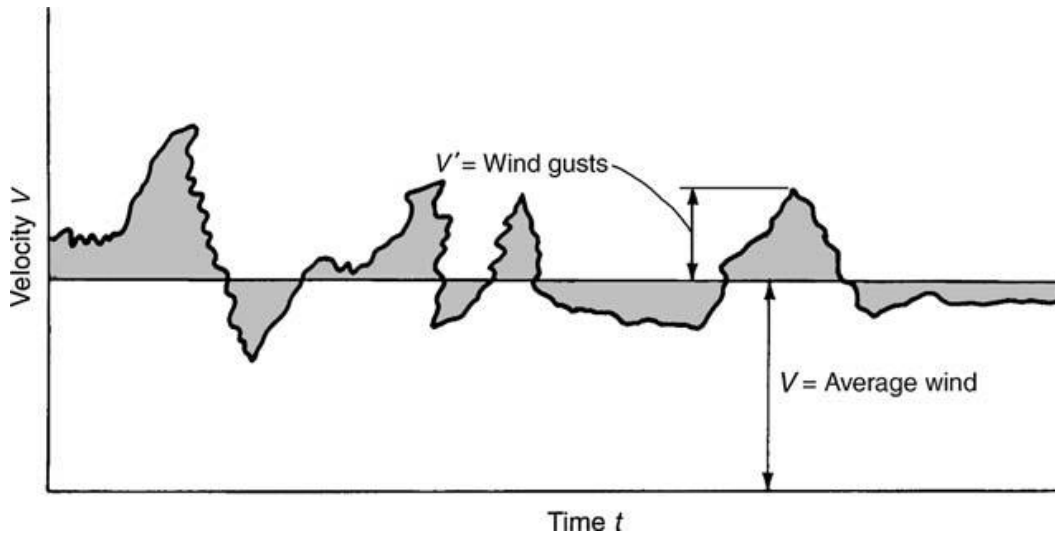


Figure 2.2: Variation of wind velocity with time; at any instant t , Velocity, $V_t = V' + V$ (Taranath, 2004)

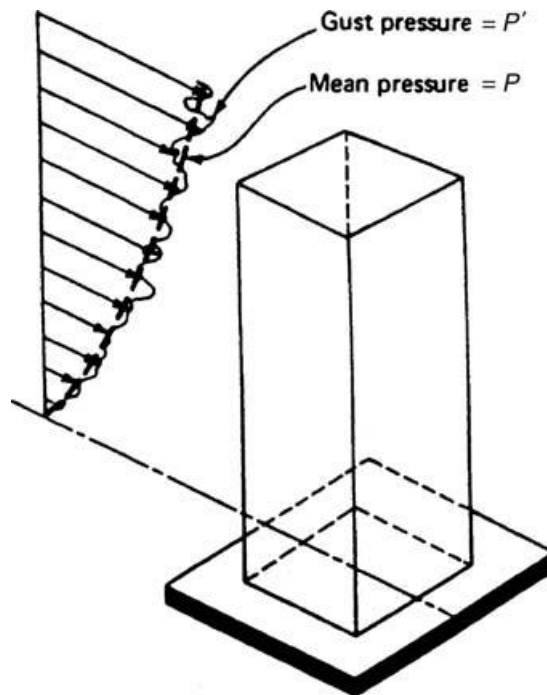


Figure 2.3: Schematic representation of mean and gust pressure (Taranath, 2004)

Wind buffeting on a bluff body is generally deflected in three mutually perpendicular directions, resulting in forces and moments in all three directions. Although all six components, as indicated in Fig.1.3, are important in aeronautical engineering, the force and moment corresponding to the vertical axis (lift and yawing moment) are of lesser significance in civil and structural work. As a result, aside from uplift effects on large roof areas, wind flow is simplified and considered two-dimensional, as shown in Fig.1.4, with along and transverse wind.

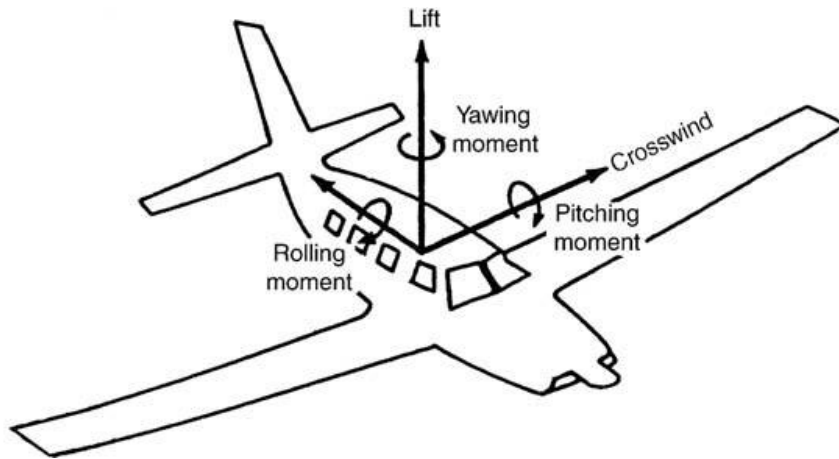


Figure 2.4: Wind Components (Taranath, 2004)

Drag forces are referred to as along wind (or simply wind), while crosswind is referred to as transverse wind. For large buildings, the crosswind reaction, which causes motion in a plane opposed to the wind's direction, often prevails over the along-wind response. Consider a prismatic building subjected to a smooth wind flow.

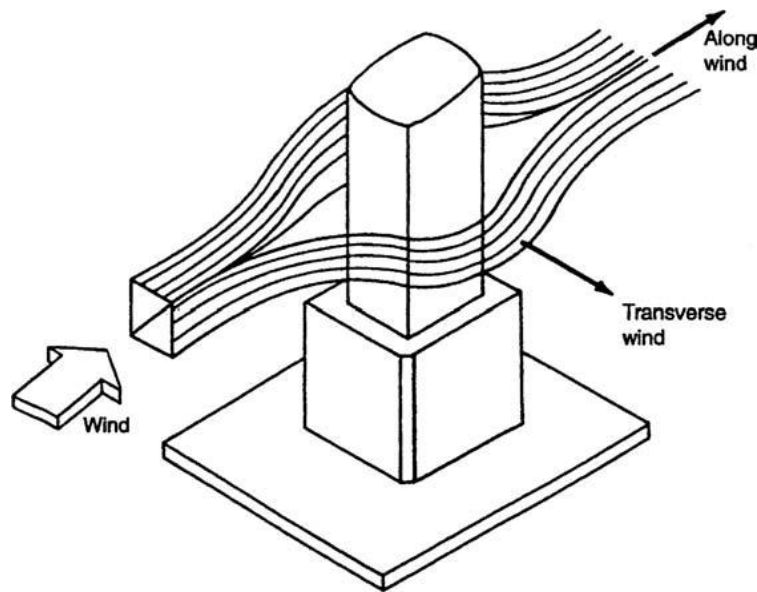


Figure 2.5: Simplified two-dimensional flow of wind (Taranath, 2004)

2.3 Design Wind Pressures

Wind Loading is the effect of the atmosphere passing by a stationary structure attached to the earth's surface. Atmospheric and Aerodynamic effects control wind loads. In equation 2.4, the design wind pressure (P) general equation is a product of three terms of wind.

$$P = q \times G \times C_p \dots\dots\dots (2.4)$$

Where, q is the Velocity Pressure (Atmospheric Effects), C_p is the External Pressure Coefficient (Aerodynamic Effects), G is the Gust Effect Factor (Combination of both).

2.3.1 Wind Velocity Pressure

When a surface stop moving air or wind, the dynamic energy in the wind is transformed to pressure. The pressure q is given by equation 2.5, established on the surface of a building due to a mass of air with density ρ , moving at a velocity v is given by Bernoulli's equation:

$$q = \frac{1}{2} \rho v^2 \dots\dots\dots (2.5)$$

The density of air ρ is 0.0765 pcf (1.25 kg/m³), for conditions of the standard atmosphere, temperature 15°C or, 59°F, and barometric pressure (29.92 in. of mercury). If velocity given in the wind map is in mph, reduces as equation 2.6-

$$q = \frac{1}{2} \left[\frac{0.0765 \text{ pcf}}{32.2 \text{ ft/s}^2} \right] \left[\frac{5280 \text{ ft}}{\text{mile}} \times \frac{1 \text{ hr}}{3600 \text{ s}} \right] v^2$$

$$q = 0.00256 v^2 \dots\dots\dots (2.6)$$

The general formula for wind load is $F = A \times P \times C_d$, where F denotes the force or wind load, A is the object's projected area, P denotes the wind pressure, and C_d denotes the drag factor. Although this equation is helpful for calculating the wind load on a single object, it does not comply with building code standards for new construction design.

2.3.2 Wind Pressure Coefficient

The wind pressure coefficients (C_p), which indicate the wind-induced pressure at a certain place over a body in relation to the freestream wind pressure, are non-dimensional coefficients. Equation 2.7 can be used to compute wind-pressure coefficients:

$$C_p = \frac{p - p_\infty}{\frac{1}{2} \rho U_\infty^2} \dots\dots\dots (2.7)$$

where p is the pressure at the point of interest, P_∞ is the pressure in the freestream, ρ is the freestream air density, and U_∞ is the freestream wind velocity at the specific height of the building.

Wind pressure coefficients (C_p) are important values for building engineering applications, such as calculating wind loads or wind-induced air infiltration, and especially for tall buildings that are more susceptible to wind forces. Wind pressure coefficients are influenced by several parameters, such as building geometry, the position of the façade, exposure, and wind directions (Charisi et al., 2019). In building science, wind effects are intimately linked to building load and natural ventilation. Numerous studies have been conducted to investigate wind flow mechanisms and establish wind properties on structures.

Significantly, air flows around buildings have been proved susceptible and complicated according to the results of more than 50 years' investigation (Blocken, 2014), generally showing large variability with wind features, building configuration, and site characteristics. To create actual wind pressure coefficients, full-scale and wind-tunnel measurements are regarded the most precise methods. It is not necessary to reproduce boundary conditions, use physical models, or do any down-scaling during full-scale measurements. Using the other hand, on wind-tunnel measurements, the user may accurately adjust the approach-flow, including wind speed, direction, and turbulence. Full-scale measurements are difficult, costly, and time-consuming to perform. Similarly, wind tunnel measurements are expensive and need a lot of knowledge. In low-rise buildings with simple geometry, full-scale experiments for determining wind-induced pressures have previously been performed (Blocken, 2014). Full-scale measurements have also been used to validate reduced-scale measures, such as wind-tunnel testing, and have shown agreement, making wind-tunnel tests a useful tool for determining wind pressure coefficients (Blocken, 2014).

After long-term meteorological monitoring and wind tunnel tests, wind profiles such as exponential law, logarithmic law, and modified logarithmic law were established using regression methods. These models are widely accepted and implemented in contemporary research, even though the values of various parameters in published international wind standards and codes differ (Kwon & Kareem, 2013). Meanwhile, these profiles are critical in turbulent models, which have an impact on the accuracy of numerical simulation in Computational Fluid Dynamics (CFD) approaches.

Various researchers (Murakami & Mochida, 1988; Murakami et al., 1987) tested the performance of turbulent models such as the standard k-turbulent model and big eddy

simulation when predicting an unstable wind field around a cubic model. Even though all calculated findings were in good agreement with experimental data, the later approach performed significantly better when computing unstable fields. Various k-models were used to calculate three-dimensional steady fields to analyze wind pressure and velocity distributions on and around buildings (Baskaran & Stathopoulos, 1994; Stathopoulos & Baskaran, 1996), making significant progress in wind characteristics exploration and promoting inclusive research on wind environment.

Many experts have recently confirmed the interference effect caused by nearby structures, which is regarded as a type of site impact. Wind flows can overlap, interact, neutralize, and offset when original wind fields are disrupted by newly constructed structures. When a building is constructed in front of a principal building, the negative zone is completely covered, resulting in higher mean and peak negative pressures on the principal building. Lam et al. (2008) evaluated wind pressure on a row of square-shaped tall buildings using both experimental and numerical methods, concluding that sheltered structures were subjected to reduced wind loads and directions when compared to isolated buildings. Kim et al. (2011) conducted systematic experiments to investigate the fluctuation of peak pressure on major structures due to interference effects. Peak pressure was discovered to be directly linked to following arranged structures in terms of wind direction, building height ratio, and design. Negative wind effects became much more intense as the interference distance decreased.

Hui et al. (2012) used particle image velocimetry to show interference effects of various rectangular buildings, where both unfavorable positive and negative peak pressures were converted to the margins and corners of principal buildings. Yu et al. (2015) conducted a thorough investigation of the interference impacts of two different buildings with varying breadth and height ratios, as well as three various configurations: tandem, oblique, and parallel scenarios. Negative pressures were also considerably increased in tandem and parallel circumstances when compared to isolated buildings.

Engineers and architects are increasingly pursuing unique suggestions; yet the wind pressure acting on these structures with unusual shapes is quite complex. Researchers (Tanaka et al., 2012) measured the wind characteristics of square-shaped tall buildings with corner cut, setbacks, and helical configurations, finding that the helical configuration endured better wind fields than other types of novelties, allowing it to be used to reduce

wind loads significantly. Moreover, they discovered that as the twist angle increased, both overturning moments and spectral densities tended to decrease, with only minor variations observed when the twist angle was greater than 180° . Kim and Kanda (2013) studied tapered and set-back tall structures in order, finding that mean pressure on the windward side was nearly identical, but the negative side was clearly different due to geometry differences. Set back models suffered a lower value in terms of minimum pressure coefficients than square prisms. Others, suppose houses were built in a hilly terrain field. Li et al. (2017) investigated the link between wind loads on various shaped buildings and their aspect ratios and side ratios and found that wind loads on rectangle shaped buildings were more vulnerable to aspect ratios and side ratios than those on circular-shaped models.

In the case of sophisticated structures, such as high-rise buildings and non-conventional architectural systems, numerical analysis using computational fluid dynamics (CFD) simulations is commonly used to determine wind loads. The CFD simulations are seen as replacing traditional full and reduced scale measurements, and they need a high level of knowledge and skill to achieve high quality and reliability (Hoxey, 2008). To calculate the air flows, fluctuating C_p values are more accurate than those calculated by the conventional method of using mean C_p values (Charisi et al., 2019).

Combined effect of environmental and geometrical conditions on the wind pressure distribution (Grosso, 1992), as shown in Figure 2.6, around buildings with sufficient accuracy. The degree of accuracy is proportional to the availability of data from wind tunnel or real-scale tests for the regression analysis upon which the developed model is based.

Wind pressure on buildings is intimately connected to surrounding structures and their geometric shapes, according to existing research. Because the shelter effect experienced by the leeward side varies with the enlargement of windward, it is logical to assume that the horizontal dimension of an isolated building will likewise influence wind pressure distribution. Only a few scholars, however, have looked at the relationship between building proportions and wind patterns. Lin et al. (2005) used a wind tunnel test to analyze wind effects, concluding that building aspect ratio and side ratio might influence the wind load of both square and rectangular-shaped tall buildings. Furthermore, it was insufficient that general wind pressure on separate buildings was not revealed and compared.

Generally, a few efforts have focused impact of building plane dimension on wind pressure distribution. Consequently, this study is devised to respond to this issue, through numerically predicting wind pressure coefficient on and around rectangular-shaped tall buildings.

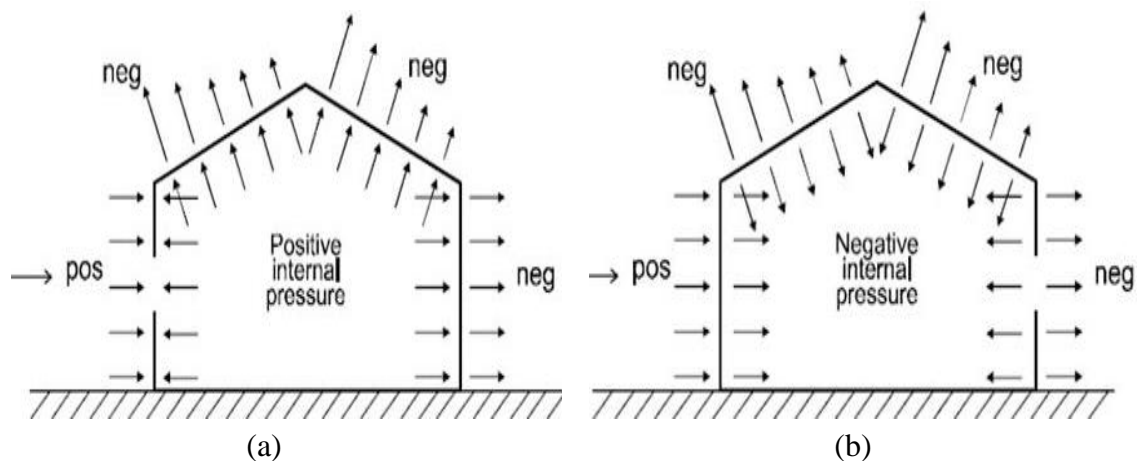


Figure 2.6: (a) Wind flow and pressure distribution (b) Pressure on surface (Taranath, 2004)

Three-dimensional stable wind fields will be estimated using the Re-Normalisation Group (RNG) k-turbulent model in CFD approach, as in earlier research (Braun & Awruch, 2009; Dagneu et al., 2016; Zhang & Gu, 2008; Huang et al., 2007). The following part will primarily cover the computational domain, grid arrangement, boundary conditions, solution methods, and solver control, all of which can have an impact on the correctness and effectiveness of numerical simulation. Meanwhile, complete scenario information, including height-width (HW) and height-thickness (HT), will be supplied.

Section 3.3.5 will compare computed results with experimental data of the Commonwealth Advisory Aeronautical Research Council (CAARC) standard models to ensure the validity and reliability of our research. Overall, the goal of this study is to provide engineers and architects with a foundational understanding of natural ventilation in both indoor and outdoor environments.

2.3.3 Gust Effect Factor

The gust effect factor provides for additional dynamic amplification of loading in the along-wind direction caused by the interaction of wind turbulence with structure. A cross-wind loading effect, vortex shedding, instability brought on by galloping or flutter, or dynamic torsional effects are not taken into account. Wind tunnel results should be used in the design of structures that are subject to these effects. G can be calculated using one of three ways. The first two are for structures that are inflexible, and the third is for structures that are flexible or dynamically sensitive.

2.4 Provisions for Wind Load – BNBC 2006

The wind pressure of a structure depends on the height, exposure (whether the place is open terrain or congested area), basic wind speed, gust effect, and importance or priority of the structure. Wind pressure or velocity increases from zero at the structure's base and increases with a height almost exponentially according to the wind speed profile. Flowchart of wind load calculation according BNBC 2006 is shown in Figure 2.7.

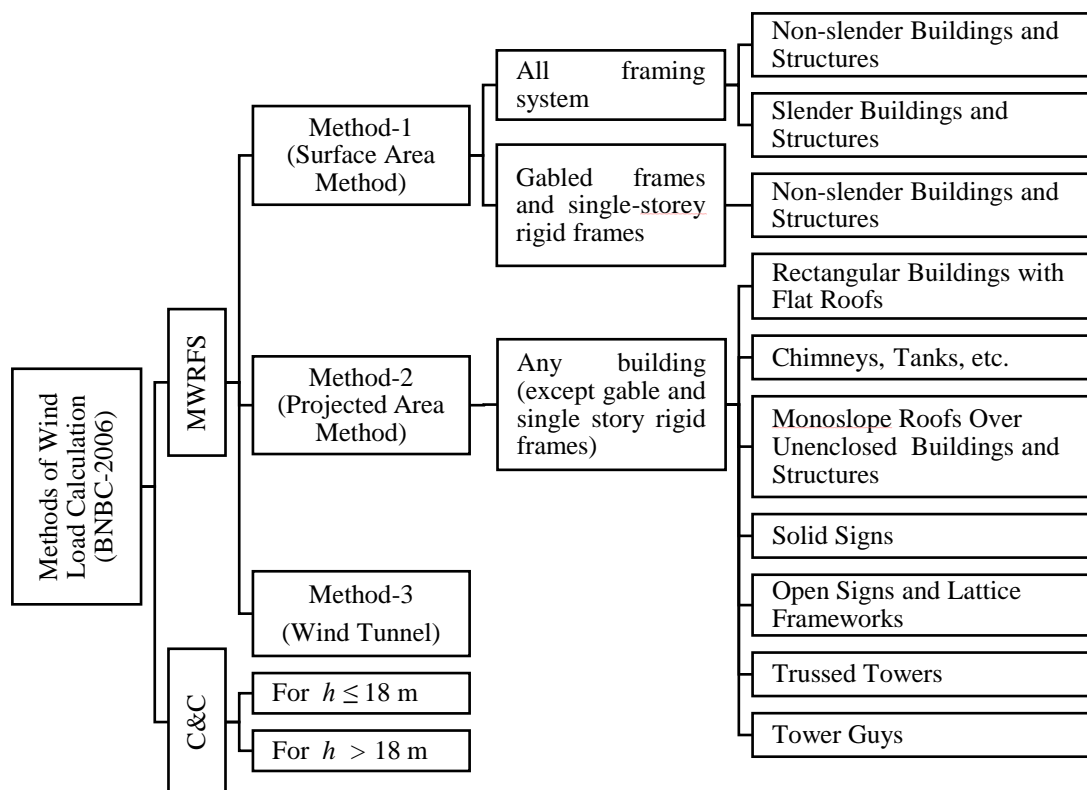


Figure 2.7: Flowchart of wind Load Calculation (BNBC 2006)

2.4.1 Design Wind Pressure

The sustained wind pressure can be used to compute the design wind pressure by multiplying it by the pressure coefficients due to wind gust and turbulence as well as local terrain. Equation 2.8 is the design wind pressure on a surface at any height z above ground.

$$P_z = 0.00256 C_G C_t C_p C_I V_b^2 \dots\dots\dots (2.8)$$

where C_G = Wind gust coefficient, C_t = Local topography coefficient, and C_p = Pressure coefficient.

2.4.2 Exposure Categories

As mentioned earlier, the ASCE 7-05 regard four exposure categories while the BNBC considers only three merging the urban and suburban together.

Exposure A: Urban and sub-urban areas, industrial areas, wooded areas, hilly or other terrain covering at least 20 percent of the area with obstructions of 6 meters or more in height and extending from the site at least 500 meters or 10 times the height of the structure, whichever is greater.

Exposure B: Open terrain with scattered obstructions having heights generally less than 10 m extending 800 m or more from the site in any full quadrant. This category includes airfields, open parklands, sparsely built-up outskirts of towns, flat open country, and grasslands.

Exposure C: Flat and unobstructed open terrain, coastal areas, and riversides facing large bodies of water, over 1.5 km or more in width. Exposure C extends inland from the shoreline 400 m or 10 times the height of the structure, whichever is greater.

2.4.3 Local Topography Coefficient

Wind speeds up over Hills, Ridges, Escarpments. Ridge is an elongated crest of a hill, characterized by strong relief in two directions and Escarpment is a cliff or steep slope generally separating two levels or gently sloping areas, while Hill is a land surface characterized by strong relief in any horizontal direction. The factor can be calculated from Table N.2 in Appendix-N using the height to multiplied length ratio.

2.4.4 Overall Pressure Coefficient

The pressure coefficient is a dimensionless factor described in section 2.3.2. The wind pressure coefficient was considered for the whole structure in the BNBC 2006 as shown in Table N.3 of Appendix-N and called the overall pressure coefficient.

2.4.5 Wind Gust Coefficient

According to the US Meteorological Department, gusts are declared when the peak wind speed reaches at least 16 knots and the difference in wind speed between the peaks and lulls is at least 9 knots. Typically, a gust of wind lasts under 20 seconds. A knot is a unit of speed equal to one nautical mile per hour, which is exactly 1.852 kilometres per hour, or 1.151 miles per hour, or 0.514 meters per second. Bangladesh National Building code 2006 addressed the wind gust factor, as shown in Table N.4 of Appendix-N.

2.4.6 Combined Height and Exposure Coefficient

The atmospheric boundary condition, as described in section 2.2, was addressed by the Bangladesh National Building Code 2006, as shown in Table N.5 of Appendix-N.

2.5 Provisions for Wind Load – BNBC 2020

The wind pressure of a structure depends on altitude, exposure (whether the location is an open area or a densely populated area), the underlying wind speed, the gust effect, the importance or priority of the structure, and the wind direction. Wind pressure or speed increases from zero at the base of the structure and increases almost exponentially with height according to the wind speed profile. Determining the wind load for this code is similar to ASCE 7-05.

New features in the BNBC 2020 are how to determine the gust and direction coefficients and how to determine the basic wind speed. If the structure is rigid, the gust factor can be used at 0.85. If not, it can be determined by an expression. Wind load calculation according BNBC 2020 is shown in Figure 2.8.

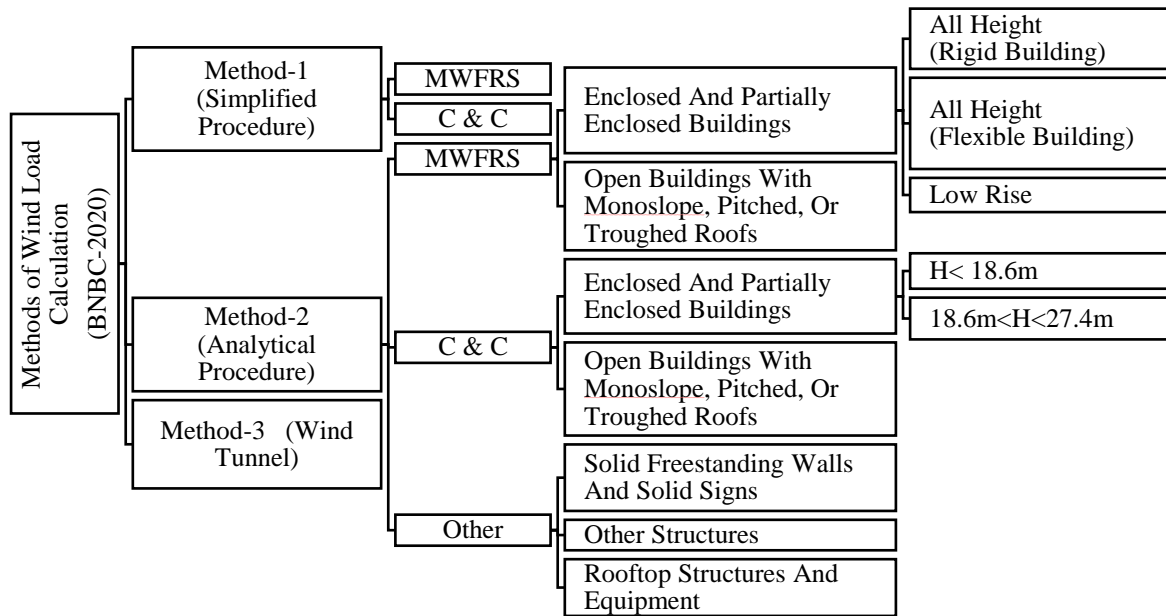


Figure 2.8: Flowchart of wind Load Calculation (BNBC 2020)

2.5.1 Design Wind Pressure

The sustained wind pressure can be used to compute the design wind pressure by multiplying it by the necessary pressure coefficients owing to wind gust and turbulence as well as local terrain. At any height z above ground, the design wind pressure on a surface is expressed by equation 2.9 and 2.10.

$$q_z = 0.00256 I K_z K_{zt} K_D V_b^2 \dots \dots \dots (2.9)$$

$$p_z = q_z G C_{p-ww} - q_h G C_{p-lw} \dots \dots \dots (2.10)$$

Where Structural importance factor (I), Velocity pressure exposure co-efficient (K_z), Topographic factor (K_{zt}), Gust-effect factor (G), Wind directionality factor (K_d), External pressure co-efficient windward (C_{p-ww}), External pressure co-efficient leeward (C_{p-lw}), Basic wind speed (V), Wind directionality factor (K_d).

2.5.2 Exposure Categories

Surface Roughness A: Urban and suburban areas, wooded areas, or other terrains with numerous closely-spaced obstructions having the size of single-family dwellings or more extensive.

Surface Roughness B: Open terrain with scattered obstructions having heights generally less than 9.1 m. This category includes flat open country, grasslands and all water surfaces in cyclone-prone regions.

Surface Roughness C: Flat, unobstructed areas and water surfaces outside cyclone-prone regions. This category includes smooth mud flats and salt flats.

Exposure A: Exposure A shall apply where the ground surface roughness condition, as defined by Surface Roughness A, prevails in the upwind direction for a distance of at least 792 m or 20 times the height of the building, whichever is greater.

Exception: For buildings whose mean roof height is less than or equal to 9.1 m, the upwind distance may be reduced to 457 m.

Exposure B: Exposure B shall apply for all cases where Exposures A or C do not apply.

Exposure C: Exposure C shall apply where the ground surface roughness, as defined by Surface Roughness C, prevails in the upwind direction for a distance greater than 1,524 m or 20 times the building height, whichever is greater. Exposure C shall extend into downwind areas of Surface Roughness A or B for a distance of 200 m or 20 times the height of the building, whichever is greater. The category resulting in the largest wind forces shall be used for a site located in the transition zone between exposure categories.

2.5.3 Structural Importance Factor

The structural importance factor was addressed in the BNBC 2020. However, it has considered the velocity, importance category, and mean reoccurrence interval, as shown in Table O.1 of Appendix-O.

2.5.4 Wind Pressure Coefficient

Wind pressure coefficient, a dimensionless factor, is described in section 2.3.2. The wind pressure coefficient was considered for structure side-wise in the BNBC 2020, as shown in Table O.2 of Appendix-O. Wind pressure coefficient for windward wall and sidewall is constant, 0.8 and -0.7, respectively. On the other hand, for the leeward wall, it depends on the length-width ratio of the structure

2.5.5 Velocity Pressure Exposure Coefficient

The atmospheric boundary condition, as described in section 2.2, was addressed by the Bangladesh National Building Code 2006, as shown in Table O.3 of Appendix-O.

2.5.6 Wind Gust Coefficient

Wind gust effect on structures was described in sections 2.3.3 and 2.4.5. The BNBC 2020 suggested a rigid structure of 0.85, similar to the BNBC 2006. For flexible structure, equations are expressed in Table O.4 of Appendix-O.

Equations given to calculate the wind gust effect on a flexible structure in the Table above include a few sub equations for influential factors such as intensity of turbulence, resonant response factor, background response factor, peak factor for background response, peak factor for resonant response, and peak factor for wind response.

Table O.5 in Appendix-O represents the parameters required for the background response factor. The background response factor is a function of several parameters as well, such as damping ratio, the horizontal dimension of the building measured normal to wind direction, building height, the natural frequency of the structure, and basic wind speed. Table O.6 represents constants values essential for the determination of the background response factor, which is a must to calculate the wind gust effect on a flexible structure.

Table O.7 in Appendix-O represents essential parameters for the approximate time period. Determination of structure, whether the structure is flexible or rigid, requires a time period. If the time period is more than 1 second or the frequency is higher than 1 Hz, the structure is a rigid structure.

The directionality factor (K_d) used in the BNBC 2020 wind load provisions for components and cladding is a load reduction factor intended to take into account the less than 100% probability that the design event wind direction aligns with the worst-case building aerodynamics.

By taking into account the dependence of wind speed, the frequency of occurrence of high winds, and the aerodynamic characteristic on wind direction, the Directionality Factor K_d is defined as a parameter that makes the design more reasonable. The frequency of

occurrence and paths of typhoons, climatological variables, significant topographical influences, and other variables all affect the wind Directionality Factor K_d .

Directionality Factor K_d , as shown in Table O.8 of Appendix-O, has been calibrated with combinations of loads specified in BNBC 2020, Sec 2.7. This factor shall only be applied when used in conjunction with

2.6 Computational Fluid Dynamics

CFD is a discipline of fluid mechanics that analyzes and solves problems involving fluid flows using numerical analysis and data structures. "Computational Fluid Dynamics is the art of replacing the integrals or the partial derivatives in the equations with discretized algebraic forms, which in turn are solved to obtain numbers for the flow field values at discrete points in space and/or time" (Anderson, 1992). CFD produces a set of numbers because of the process. Since it processes the manipulation of thousands and millions of numbers, the high-speed digital computer has enabled the practical expansion of this issue.

The physical features of any fluid flow are based on three fundamental principles that can be described mathematically using either integral or partial differential equations in a general form.

- i. The conservation of mass (Continuity Equation)
- ii. The second law of Newton (Momentum Equation, $F = ma$)
- iii. The conservation of energy (First law of thermodynamics)

2.6.1 The Continuity Equation

Figure 2.9 (a) describes an example of a flow model. The fluid is travelling through this fluid element, which is fixed in space. On the other hand, in Figure 2.9 (b), the fluid is moving along a streamline with a velocity equal to the local flow at each point.

A Cartesian coordinate system is used to explain the fluid flow, in which velocity and density are functions of both space (x , y , and z) and time (t). This stationary element has a mass flow going through it. Consider the element's perpendicular to the x -axis left and right faces, as shown in Figure 2.10.

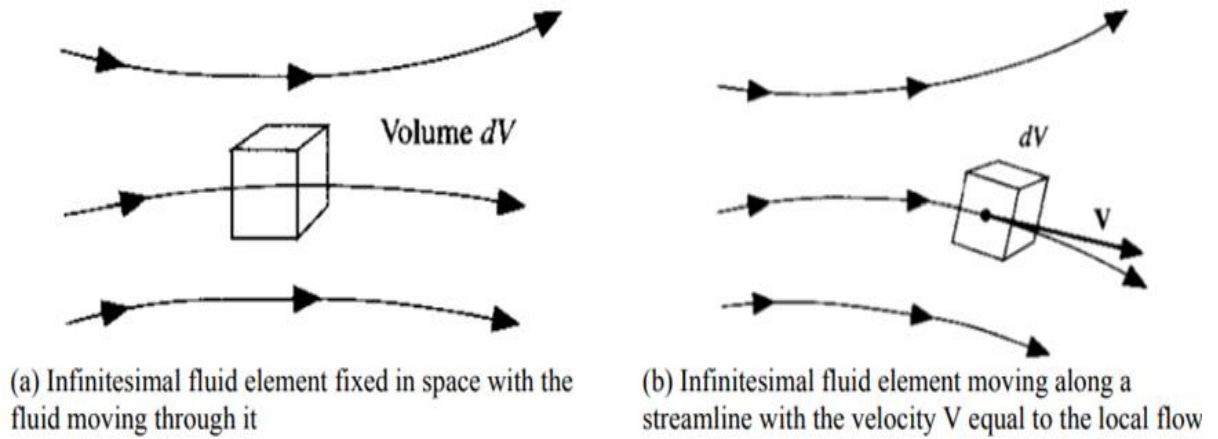


Figure 2.9: Infinitesimal fluid element model of flow (Anderson, 1992)

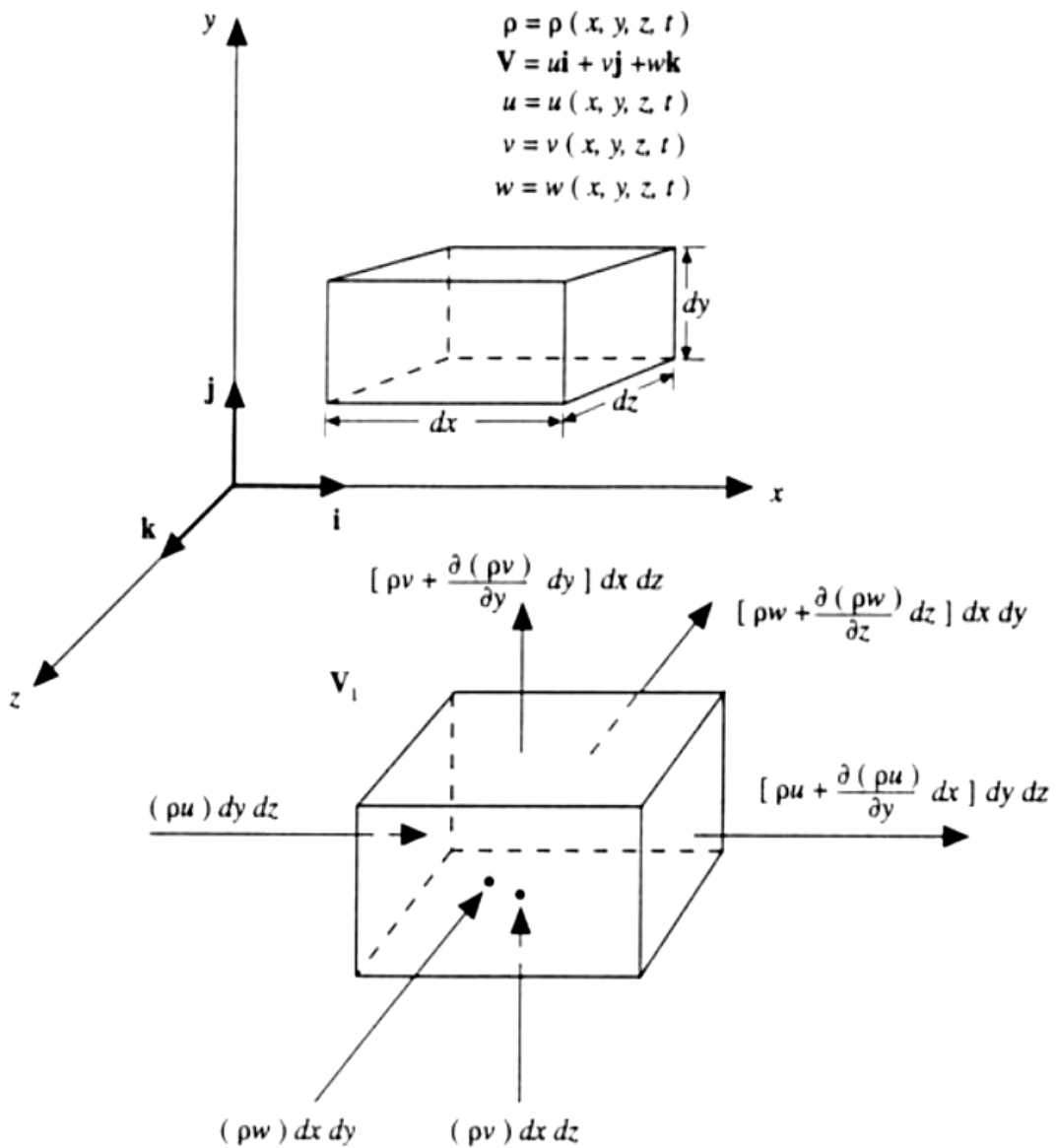


Figure 2.10: Model of infinitesimally small element fixed in space including mass flux diagram (Anderson, 1992)

Here $(\rho u) \cdot dy \cdot dz$ is the mass flow across the left face with area $(dy \cdot dz)$ is given by equation 2.11 and 2.12. Because velocity and density are spatially dependent, the values of the mass flux across the right face will differ from those on the left. Thus, the mass flow can be represented as $\left[\rho u + \frac{\partial(\rho u)}{\partial x} \cdot \partial x \right] dy \cdot dz$ over the right face. So, the changes are

$$\rho u (dy \cdot dz) - \left[\rho u + \frac{\partial(\rho u)}{\partial x} \cdot \partial x \right] dy \cdot dz \dots\dots\dots (2.11)$$

$$Change = \rho - \left[\frac{\partial(\rho w)}{\partial z} \right] dx \cdot dy \cdot dz \dots\dots\dots (2.12)$$

The expression can be rendered in a similar way for faces that are perpendicular to the y and z axes. Note that equation 2.13 is the positive x, y, and z directions, u, v, and w are all positive by convention. As a result, the element's net mass flow is given by

$$Net\ mass\ flow = - \left[\frac{\partial(\rho u)}{\partial x} + \frac{\partial(\rho v)}{\partial y} + \frac{\partial(\rho w)}{\partial z} \right] dx \cdot dy \cdot dz$$

$$The\ time\ rate\ of\ mass\ increase = \frac{\partial \rho}{\partial t} (dx \cdot dy \cdot dz) \dots\dots\dots (2.13)$$

The physical principle that masses is conserved can be expressed in words as follows: the net mass flow out of the element must equal the time rate of decrease of mass inside the element (Anderson, 1992) is given by equation 2.14.

$$- \left[\frac{\partial(\rho u)}{\partial x} + \frac{\partial(\rho v)}{\partial y} + \frac{\partial(\rho w)}{\partial z} \right] (dx \cdot dy \cdot dz) = \frac{\partial \rho}{\partial t} (dx \cdot dy \cdot dz)$$

$$\frac{\partial \rho}{\partial t} + \left[\frac{\partial(\rho u)}{\partial x} + \frac{\partial(\rho v)}{\partial y} + \frac{\partial(\rho w)}{\partial z} \right] = 0$$

$$\frac{\partial \rho}{\partial t} + \nabla \cdot (\rho V) = 0 \dots\dots\dots (2.14)$$

wherein Cartesian coordinates, the vector operator nabla ∇ , is defined as $\frac{\partial}{\partial x} i + \frac{\partial}{\partial y} j + \frac{\partial}{\partial z} k$

2.6.2 The Momentum Equation

The momentum equation is based on Newton's second law of motion, which describes how objects behave when all external forces are imbalanced. The net force operating on a body is determined by two variables: the net force acting on the body and the mass of the object, according to the physical principle of the law. According to Newton's second law, the rate

of change in momentum of a fluid particle equals the sum of the forces acting on the particle (Anderson, 1992).

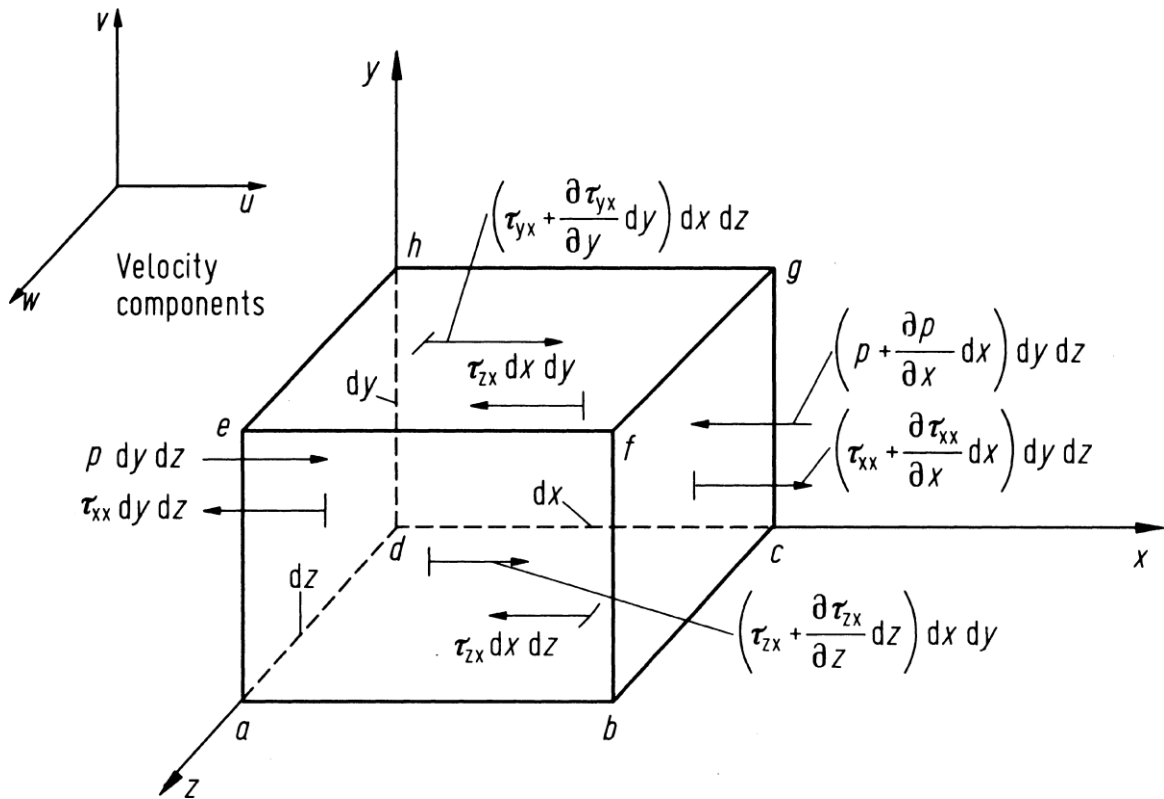


Figure 2.11: Model used for the derivation of the x-component of momentum equation (Anderson, 1992)

Based on Newton's concept, the element is subjected to two forces. The first is body forces, which act directly on the fluid element's volumetric mass. Electric, magnetic, and gravitational forces are examples of these forces that act at a distance. Surface forces, which act directly on the fluid element's surface, are the second type. They are caused by two factors: (a) the pressure distribution imposed on the surface by the outside fluid surrounding the fluid element, and (b) the shear and normal stress distributions imposed on the surface by the outside fluid pressing on the surface through friction, as shown in Figure 2.11 and equation 2.15 (Anderson, 1992).

$$\rho \frac{Du}{Dt} = -\frac{\partial p}{\partial x} + \frac{\partial \tau}{\partial x} + \frac{\partial \tau}{\partial y} + \frac{\partial \tau}{\partial z} + \rho f \dots \dots \dots (2.15)$$

2.7 Background of CFD Modelling

It is helpful to understand the basics of CFD modelling. Most CFD software products solve a series of equations known as the Navier-Stokes (NS). These equations are based on two conservation laws. Conservation of Mass and Momentum Conservation (Newton's Second Law) was developed by Navier and Stokes in the 1880s. The resulting four equations are time-varying, non-linear, and highly interconnected. Regardless of how these equations are solved, the field of velocity and pressure changes over time. Unfortunately, few analytic solutions to these equations apply to flow, which is in a quasi-steady state, effectively restricted (e.g., bounded by boundaries), and essentially in a non-turbulent region. To extend its applicability outside the analysis solution, two ways to solve these equations are direct numerical simulation (DNS) or non-linear simplification and meshing. DNS is practical only for basic research studies on simple problems.

A third solution to address the temporary nature of the liquid flow was proposed by Osborne Reynolds in the 1890s (Reynolds, 1895). It consisted of decomposing (decomposing) the time-varying velocities into averaging and fluctuating components, substituting them into the Navier-Stokes's equation, and averaging the equations. In this way, the Reynolds average Navier-Stokes (RANS) equation was born. One of the consequences of this mathematical formulation is forming a set of stress tensors as a quadratic derivative. These stress tensors need to be modelled to solve the RANS equation, resulting in turbulent closure. The closure of these stress tensors leads to the turbulence model that CFD users are most familiar with. The basis of these models is that the effects of the stress tensor can be treated as a form of viscosity. This is often referred to as vortex viscosity. This assumption is that the -turbulence is isotropic (e.g., uniform in all directions) and the model is "tuned" based on the turbulent flows they were compared to. This adjustment is important because the constants present in the turbulent shutter are not universally applicable. Most flows generate turbulence in one direction, which is transmitted, so the isotropic assumption also fails, which means that turbulence fluctuations can be stronger than in one direction.

Most CFD users use a two-equation model, a variant of the $k-\epsilon$ model. This model adds two equations to Navier-Stokes's equation to explain turbulence's kinetic energy transport (k) and dissipation (ϵ). There are other variants RNG, feasible $k-\epsilon$, etc.). Although the two models of equations such as $k-\epsilon$ and its derivative are intuitively easy to understand and

mathematically relatively stable, these turbulent closures have flow separation, vortex or recirculation zones, or geometry that is sometimes called "strong streamline curvature." One might have noticed that these features are all flow phenomena present when wind passes around buildings. There are some reasons for the failure of two-equation closures to reasonably simulate these features. These limitations prevent RANS-based simulation models from accurately predicting flow around buildings. There is no RANS closure model with a single set of parameters that can accurately model multiple types of flow regimes. On the other hand, these limitations do not exist in wind tunnel tests since the flows are physically modelled using the same fluid properties; hence the wind tunnel methodology accurately represents these flow conditions. Most of the available CFD software uses these sorts of turbulence closures, which should be of concern to users.

2.8 The k-ε Turbulence Model

The k-epsilon (k-ε) turbulence model is the most widely used model in computational fluid dynamics (CFD) to predict mean flow characteristics in turbulent flow situations. It's a two-equation model with two transport equations that provides a general explanation of turbulence (partial differential equations, PDEs). The K-epsilon model was developed to improve the mixing-length model and to discover an alternative to algebraically prescribing turbulent length scales in flows of moderate to high complexity. The Jones-Launder k-ε turbulence model is the most widely used of all k-ε turbulence models.

To begin the quick discussion, I'll refer back to the explanation in the preceding paragraphs, which states that 2-equation closure models have two additional transport equation 2.16 and 2.17, which in the case of the k-ε turbulence model are the turbulence kinetic energy k and the turbulence dissipation ε:

$$\mu_t = \rho C_\mu \frac{k^2}{\epsilon} \dots \dots \dots (2.16)$$

This eddy viscosity dimensional grounds-based relation relating the Reynolds Stresses to the mean strain rate:

$$\nu_t = \frac{u'v'}{du/dy} \dots \dots \dots (2.17)$$

2.8.1 Turbulence Energy Transport Equation

Obtaining a transport equation 2.18 for the total kinetic energy is a simple mathematical step of forming a dot product of Navier–Stokes equations (NSE) with the velocity vector:

$$\frac{\partial}{\partial t} \left(\frac{1}{2} |U|^2 \right) + U \cdot \nabla \left(\frac{1}{2} |U|^2 \right) = -\nabla \cdot (\rho U) + \nu \Delta \left(\frac{1}{2} |U|^2 \right) \dots \dots \dots (2.18)$$

Equation 2.19 found after defining the total kinetic energy:

$$\frac{1}{2} |U|^2 = \frac{1}{2} (u^2 + v^2 + w^2) \equiv K \dots \dots \dots (2.19)$$

A transport equation 2.20 for the total kinetic energy could be written as:

$$K_t + U \cdot \nabla K = -\nabla \cdot (\rho U) + \nu \Delta K \dots \dots \dots (2.20)$$

Decomposing the velocity vector according to Reynold’s decomposition and defining the turbulent kinetic energy is given by equation 2.21.

$$k \equiv \frac{1}{2} (\overline{u'^2} + \overline{v'^2} + \overline{w'^2}) = \bar{k}' \dots \dots \dots (2.21)$$

Allows the construction of an energy transport equation for the mean flow by the same procedure as the total kinetic energy transport equation 2.22 was constructed (i.e., dot product of the mean velocity with RANS equations):

$$\bar{u} \cdot \nabla \bar{k} = -\nabla \cdot (\bar{\rho} \bar{u}) + \nu \Delta \bar{k} - \bar{u} \cdot R(u', u) \dots \dots \dots (2.22)$$

The next steps consider time (or ensemble) averaging the total kinetic energy transport equation and the subtraction of the mean flow energy transport equation. Then after tedious manipulations on the result, a transport equation for the turbulence kinetic energy transport equation 2.23 is achieved (Tennekes and Lumley form):

$$\bar{u}_j \cdot \frac{\partial k}{\partial x_j} = -\frac{\partial k}{\partial_j} \left(\overline{p' u'_j} + \frac{1}{2} \overline{u'_i u'_i u'_j} - 2 \overline{\nu u'_i s'_{ij}} \right) - \overline{u'_i u'_i s'_{ij}} - 2 \overline{\nu s'_{ij} s'_{ij}} \dots \dots \dots (2.23)$$

The systematic identification and simplification of the terms in the original transport equation by physical reasoning now begins, coming after each creation of the closure transport equation's mathematical endeavor. They are identified as follows for the turbulence kinetic energy equation (because the advection of turbulent energy is on the left side of the equation above):

1. Pressure works due to only turbulence.
2. Transport of turbulent kinetic energy due to fluctuations.
3. Diffusive transport of turbulence kinetic energy.
4. Turbulence production, or to be more precise the amplification of the Reynolds stress tensor by the mean strain.
5. Dissipation rate of turbulence kinetic energy.

The acknowledgement that each of the terms has been identified shall allow to not go into the surgical simplification of each of the initial turbulence kinetic energy transport equation terms, but just to add that it is the part where the witchcraft comes into play in turbulence modeling. As the final transport equation for the kinetic turbulence kinetic energy shall soon be presented, one should ask as to why should we expect so many simplifying assumptions to so many terms in the initial equation to even satisfy a transport equation 2.24 in the first place well, here goes:

$$\frac{\partial k}{\partial t} + \bar{u}_j \frac{\partial k}{\partial x_j} = -\overline{u'_i u'_j} \frac{\partial \bar{u}_i}{\partial x_j} - \epsilon + \frac{\partial}{\partial x_j} \left[(v + vT/\sigma_k) \frac{\partial k}{\partial x_j} \right] \dots\dots\dots (2.24)$$

2.8.2 Turbulence Dissipation Transport Equation

Now, let's build an equation for the dissipation of turbulence. In order to achieve this, we first use local isotropy for the dissipation. It is a little more difficult to defend local isotropy in the Reynolds decomposition even though it seems reasonable (maybe for large eddy simulation (LES) it actually is somewhat), as the fluctuating term in RANS does not accurately represent high wave-number (small spatial scale) behavior in general. Before presenting the final turbulence dissipation and transport equation, it should be noted that its derivation is significantly more challenging. However, in order to simplify the interpretation of the surgically simplified equation, it should be noted that it has many similarities to the kinetic energy equation 2.25, albeit with some significant differences:

$$\frac{\partial \epsilon}{\partial t} + \bar{u}_j \frac{\partial \epsilon}{\partial x_j} = -C_{\epsilon 1} \frac{\epsilon}{k} \overline{u'_i u'_j} \frac{\partial \bar{u}_i}{\partial x_j} - C_{\epsilon 2} \frac{\epsilon^2}{k} + \frac{\partial}{\partial x_j} \left[(v + vT/\sigma_\epsilon) \frac{\partial \epsilon}{\partial x_j} \right] \dots\dots\dots (2.25)$$

2.8.3 Final Form of the Standard k-ε Turbulence Model

After “constructing” (lazy-wise) both equations and defining the relations between the transported variables from equation to the eddy viscosity the final form of the standard k-ε turbulence model may be presented by equation 2.26 to 2.30:

$$k_t + \bar{u} \cdot \nabla k = P - \epsilon + \nabla \cdot \left[\left(\nu + \frac{\nu_T}{\sigma_k} \right) \nabla k \right] \dots\dots\dots (2.26)$$

$$\epsilon_t + \bar{u} \cdot \nabla \epsilon = C_{\epsilon 1} \frac{\epsilon}{k} P - C_{\epsilon 2} \frac{\epsilon^2}{k} + \nabla \cdot \left[\left(\nu + \frac{\nu_T}{\sigma_\epsilon} \right) \nabla \epsilon \right] \dots\dots\dots (2.27)$$

$$P = -\overline{u'_i u'_j} \frac{\partial \bar{u}_i}{\partial x_j} \dots\dots\dots (2.28)$$

$$-\overline{u'_i u'_j} = 2\nu_T \overline{s_{ij}} - \frac{2}{3} k \delta_{ij} \dots\dots\dots (2.29)$$

$$\nu_T = C_\nu \frac{k^2}{\epsilon} \dots\dots\dots (2.30)$$

Subsequently to performing the surgical identification of the different terms in the transport equation, it should be remembered that we are still left out with some added constants to be calibrated. In turbulence modeling calibration of the model is at least as important as the derivation of the model itself. Calibration is achieved with the help of experimental and numerical results of the type of flow that should be modeled. The calibration process is also the first step in which the range of validity of the model would be revealed to close inspection and not just postulated from physical reasoning. For the standard k-ε turbulence model the calibrated closure constants are (Henk Kaarle Versteeg, 2007):

$$C_\nu = 0.09, C_{\epsilon 1} = 1.44, C_{\epsilon 2} = 1.92, \sigma_k = 1.0, \sigma_\epsilon = 1.3$$

2.9 Computational Evaluation of Wind Load on Buildings

The majority of numerical research refers to the basic cube form exposed to wind perpendicular to its face for testing and confirming the correctness of computational evaluations of wind pressures (Stathopoulos, 2002 and 2003). This is related to the cube's simple design, which includes key intricate parts of a real building flow, and the amount of full-scale and experimental results in the literature. Several researchers studied the surface-mounted cube, Silsoe 6m cube, numerically and experimentally, as shown in Figure 2.12. Wright and Easom (2003) used standard $k - \epsilon$ to compare the mean pressure coefficient on the surface of the Silsoe cube, RNG $k - \epsilon$ models (Yakhot et al., 1992) are obtained from the renormalization group of study of Navier-Stokes equations, and MMK $k - \epsilon$ models (Tsachiya et al., 1997), which aim to enhance the prediction of turbulent kinetic energy and eddy viscosity for a bluff body field, and Launder et al. (1975) developed the DSM (Differential Stress Model), a more complicated anisotropic turbulence model. The RNG $k - \epsilon$ model's forecast is more accurate than the Boundary Layer Wind Tunnel (BLWT) data, especially in the windward face, where the standard $k - \epsilon$ model overestimates the suction pressure. The separation region prediction accuracy has improved with the revised $k - \epsilon$ models. However, such changes are made on a case-by-case basis, and additional enhancements are only made for certain situations. C_p values derived using LES simulation by Lim et al. (2009) were more consistent with experimental results.

On course meshes, Köse and Dick (2010) studied the performance of RANS, hybrid RANS/LES, and implicit LES (ILES) turbulence models. The study found no significant differences between the outcomes of the RANS and hybrid (DED SST) simulations in cases with coarse meshes, as shown in Figure 2.13. The failure of the LES model in the outer region to behave as a pure LES is blamed for the poor prediction of the mean C_p at the front and side faces in the hybrid model. The coarseness of the grid utilized in the simulation is to blame for this. Both the LES and ILES were claimed to produce superior results when the meshes utilized in the simulations were coarse. Figure 2.14 demonstrates that the mean C_p is over-predicted by CFD and experimentally acquired pressure coefficients, albeit the error appears to be minimized when compared to a 45-degree wind angle of attack (Wright and Easom, 2003). Because of the reduced flow impingement, the standard $k - \epsilon$ to the prediction for the cube with the normal wind angle of attack is as expected.

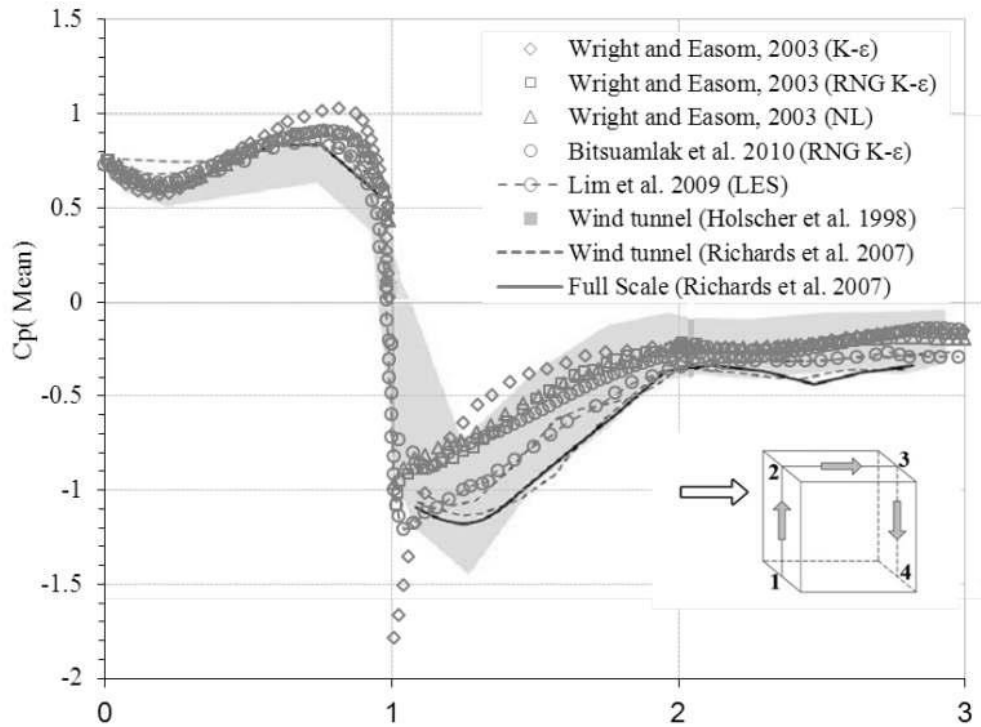


Figure 2.12: Surface mounted cube: Comparison of mean wind pressure coefficients between wind tunnel experiments and numerical simulation by using several turbulence models (Bitusamlak et al., 2010)

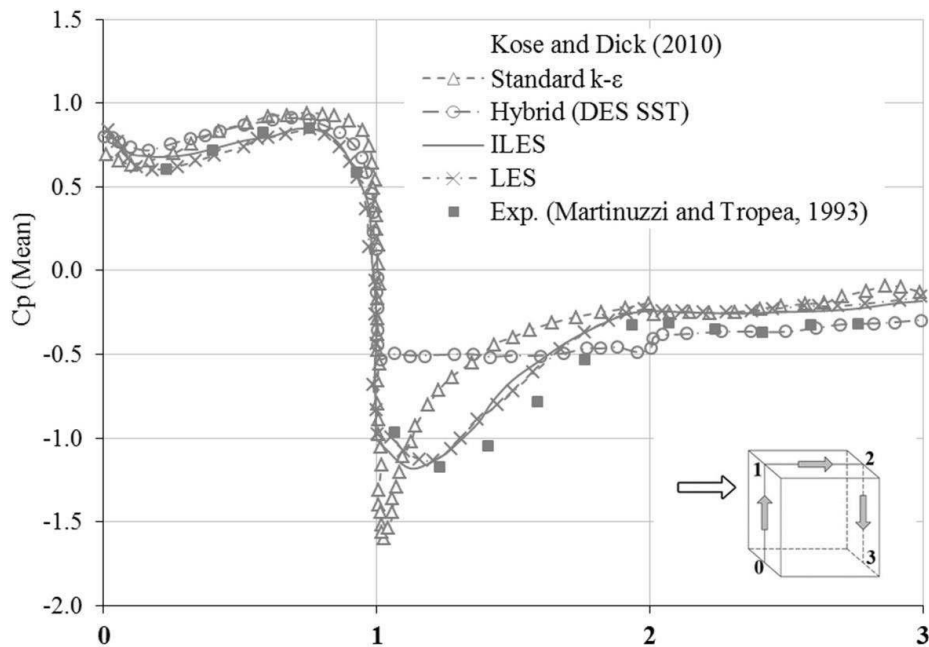


Figure 2.13: Cubical building in ABL flow. Comparison of pressure coefficient profiles on the vertical section using several turbulence models (Köse and Dick, 2010)

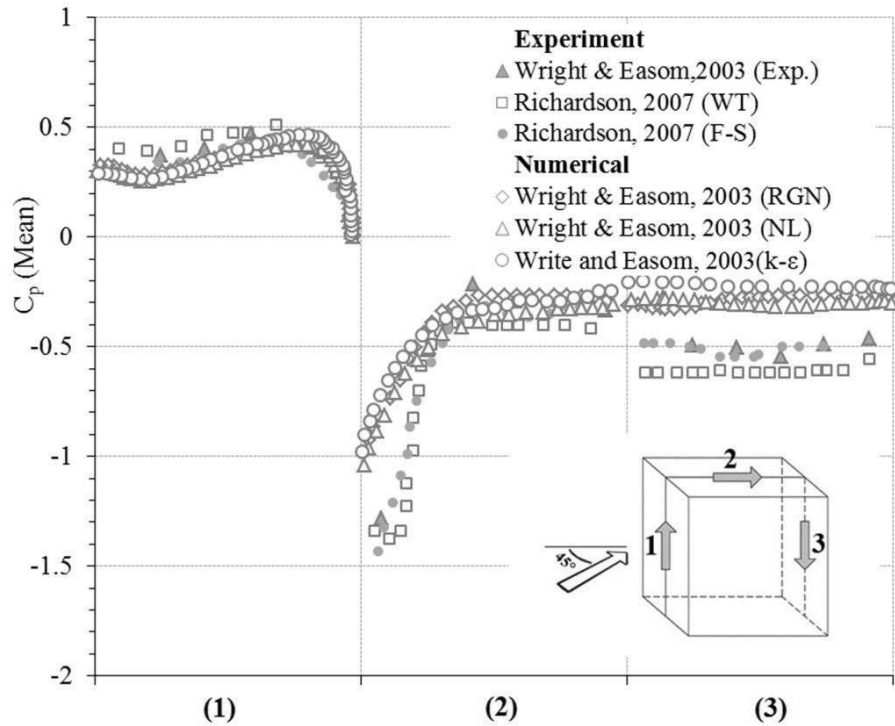


Figure 2.14: Silsoe 6m cube: Comparison of mean pressure coefficient between full-scale measurement, wind tunnel and numerical simulations- cube skewed at 45-degree (Köse and Dick, 2010)

2.9.1 Illustration of Wind Loads on Low-Rise Buildings

Regarding wind load evaluation of low-rise buildings, several numerical studies have been published. The mean pressure coefficients of short structures with a size of $H: H: 0.5H$ were predicted by Tsuchiya et al. (1997) and Nozawa and Tamura (2002). On the mid-vertical plane of a low-rise building, Figure 2.15 shows the distribution of time-averaged pressure coefficients. Because the approaching flow did not separate from the leading edge of the roof due to the impinging flow, the standard $k - \epsilon$ overestimates the C_p value on the frontal face. The approaching flows simulated with the modified $k - \epsilon$ models, $k - \epsilon - \phi$ (Kawamoto et al., 1998), and the MMK model (Tsuchiya et al., 1997) were separated from the leading edge of the roof, resulting in an improved prediction of the mean C_p at the windward face that was in closer agreement with the experiment data carried out by Kondo (1997). Figure 2.15 shows the distribution of time-averaged pressure coefficients on the mid-vertical plane of a low-rise building. Because of the impinging flow, the approaching flow did not separate from the leading edge of the roof, the standard $k - \epsilon$ overestimates the C_p value on the frontal face. On the other hand, the approaching flows simulated with the modified $k - \epsilon$ models, $k - \epsilon - \phi$ (Kawamoto et al., 1998), and the MMK model (Tsuchiya et al., 1997)

were separated from the leading edge of the roof and they resulted an improved prediction of the mean C_p at the windward face that were in closer agreement with the experiment data carried by Kondo (1997). Another interesting finding is that in all of the $k - \epsilon$ models, the lack of velocity fluctuation due to the vortex shedding effect resulted in lower kinetic energy output behind the building. While Nozawa and Tamura's (2002) LES simulation accurately anticipated the pressure coefficients on the building's surfaces. However, the same study found that the LES overestimated the rms coefficient on the roof due to the difference in the inlet velocity profile.

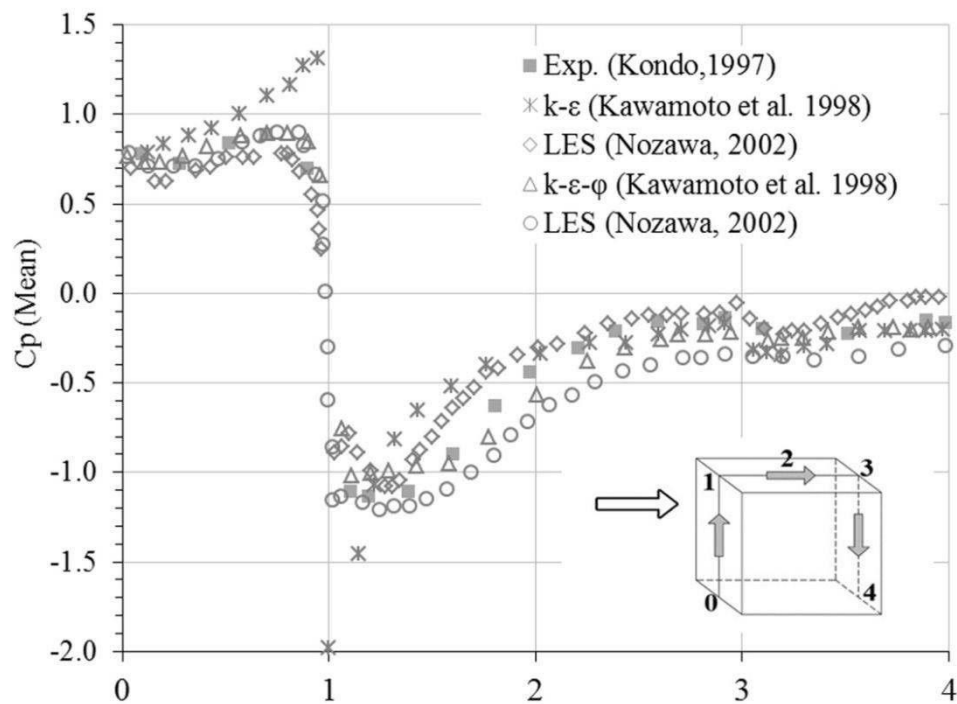


Figure 2.15: Low-rise building: Comparison of wind pressure coefficients experiment and numerical (after Nozawa & tamura,2002)

The TTU building is one of the most thoroughly researched standard short buildings for wind loading. Senthoran et al. (2004) use Kato and Launder's (1993) modified $k - \epsilon$ turbulence model to assess the wind-induced pressure fluctuation of TTU. The inflow turbulence fluctuation is generated using a stochastic approach. The improved MMK model (Launder and Kato, 1993), which reduces superfluous kinetic energy production in the impinging zone, performed better, and the results are in good agreement with experimental and field data (Figure 2.16). Recently, Köse and Dick (2011) investigated the influence of inflow circumstances on the quality of the mean pressure distribution on the same building using an implicit LES (ILES) and LES simulations. Figure 2.17 shows a comparison of the

LES and ILES predictions along the centerline of a vertical plane of the TTU. After correcting the inflow turbulence by lowering the kinetic energy, improvements in the mean C_p value were found. There was a significant difference between the numerical and BLWT predictions in both investigations (Selvam, 1997; Köse and Dick, 2011). The overproduction of the mean C_p on the windward face and roof surfaces, in particular. Strong distortion of the oncoming flow velocity profile in the incident region is the primary source of overproduction. This illustrates how incoming turbulence affects the wind pressure load distribution.

There is also a push to use Partially Averaged Navier-Stokes (PANS) turbulence modeling for wind effect evaluation as an alternative to the hybrid RANS/LES model. Using coarse computational meshes, the PANS modeling tries to capture/or resolve energy-containing structures at a realistic computational cost. For simulating the unresolved scales, the method employs the Boussinesq approximation methodology (Abdol-Hamid and Girimaji, 2005). To determine the wind-pressure load on a square cylinder, Song and Park (2009) used a two-stage PANS simulation. Figure 2.16 indicates that their PANS simulation accurately anticipated the mean C_p of the windward face for various grid resolution instances, while somewhat over-predicting the pressure distributions on the sidewalls. The case with fine grids accurately replicated the velocity in the wake and recirculation region, and the high-resolution simulation accurately predicted the mean C_p on the leeward face and the mean drag coefficient. The PANS method appears to be on the right track in terms of addressing some of the grid dependence difficulties that come up when using hybrid RANS/LES turbulence simulation. Although a comparison of the cost-effectiveness and prediction accuracy of PANS with the hybrid RANS/LES and LES would have offered more information on the cost-effectiveness and prediction accuracy of PANS.

Overall, the CFD results for time-averaged wind loads on low-rise buildings were in good agreement with the measured BLWT and field data. More work is needed, however, to estimate peak wind loads using some of the models, such as LES. In addition to the mean and rms values, numerical study should look into how well the peak loads compare to the experimental data. As a result, CWE application for design wind load evaluation will have a firm foundation.

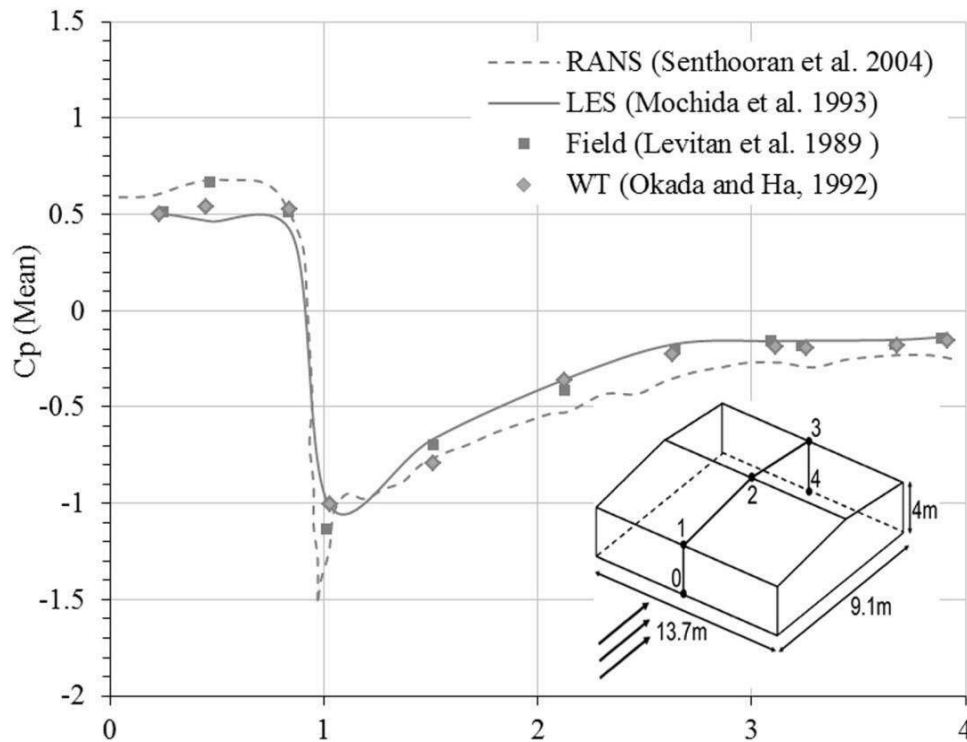


Figure 2.16: The TTU Building: Comparison between mean pressure coefficient profiles for straight wind computational and WT and field measurement (after Senthoooran et al., 2004)

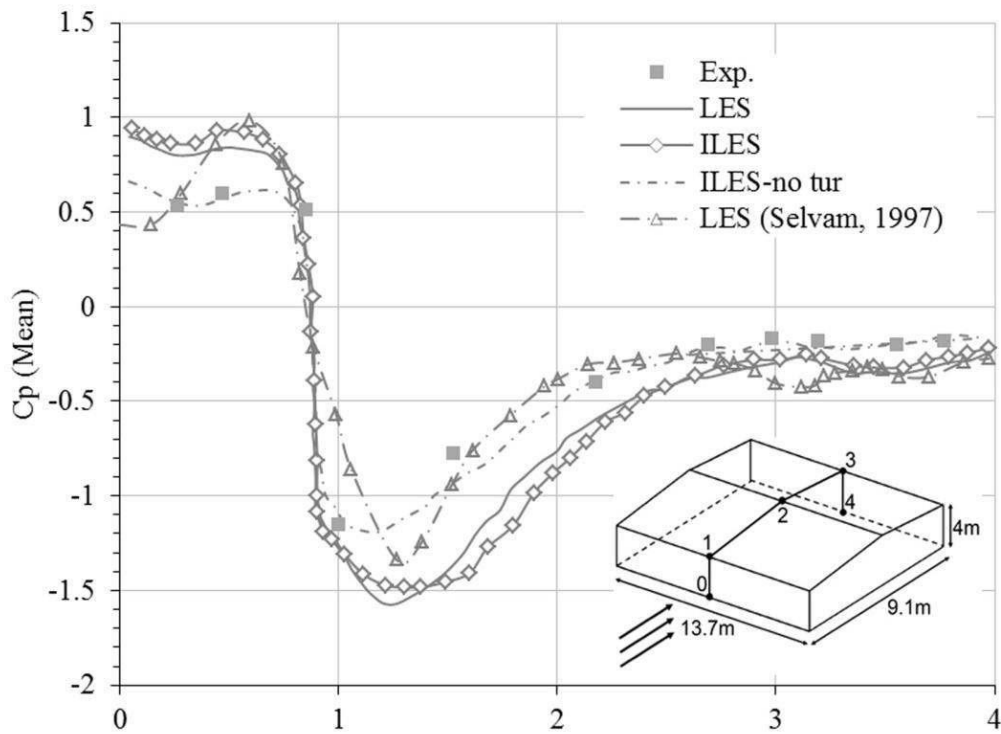


Figure 2.17: The TTU Building in ABL flow condition: Comparison of pressure coefficient profiles on the vertical section between wind tunnel experiments and numerical simulations (after Köse and Dick, 2011)

2.9.2 Wind Load Estimation on High-Rise Buildings

Several wind engineering experimental laboratories utilize the Commonwealth Advisory Aeronautical Research Council (CAARC) building model (Melbourne, 1980) for calibration and validation reasons when studying external aerodynamic loads of tall buildings. The Computational Wind Engineering (CWE) community is also evaluating the performance of numerical wind load evaluation strategies for tall buildings using the same model. The authors conducted a short analysis of several inflow turbulence production strategies for large eddy simulation (LES) as part of their review study. Figure 2.19 shows numerical and physical wind tunnel data for the mean pressure coefficient operating on the windward and leeward faces of the CAARC building model, as calculated by several numerical approaches. RWDI Inc. carried out the Boundary Layer Wind Tunnel (BLWT) test. Even in terms of the quantitative agreement, the pressure coefficient distributions are very similar. Figure 2.18 shows a comparison of the mean pressure coefficients derived at $2/3$ of H (H is the height of the CAARC building model) from multiple computational (LES and RANS $k - \epsilon$) and experimental studies of the CAARC building model. The RANS based on the $k - \epsilon$ model had a good agreement with the BLWT data. A significant disparity was seen on the side face, where the flow divided due to the acute corner. Similar experiments (Huang et al., 2007, Braun and Awruch, 2009) revealed a satisfactory C_p prediction on the windward face, but a little departure from the BLWT measurements on the side and leeward faces.

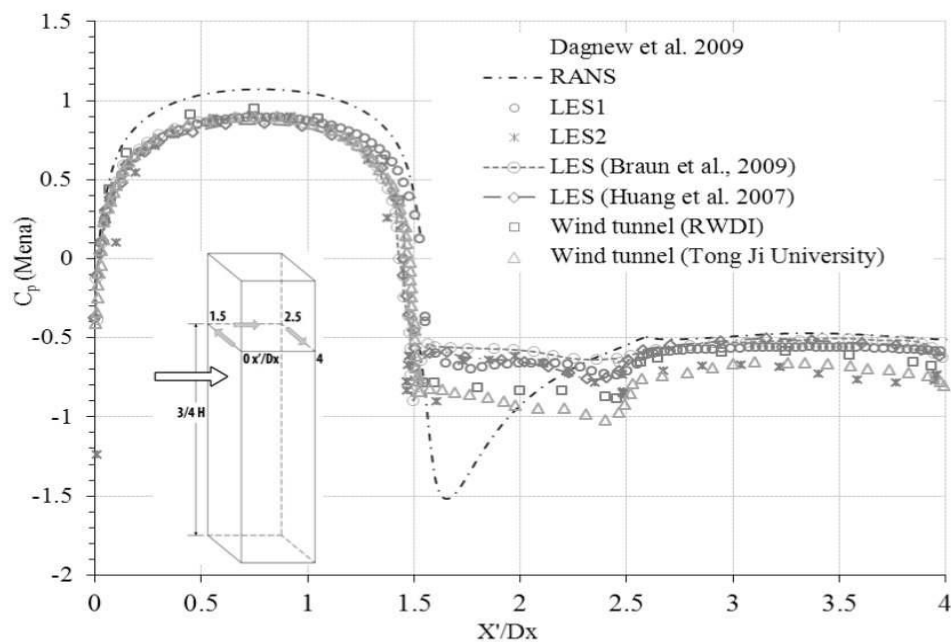


Figure 2.18: Mean wind pressure coefficient on CAARC building model

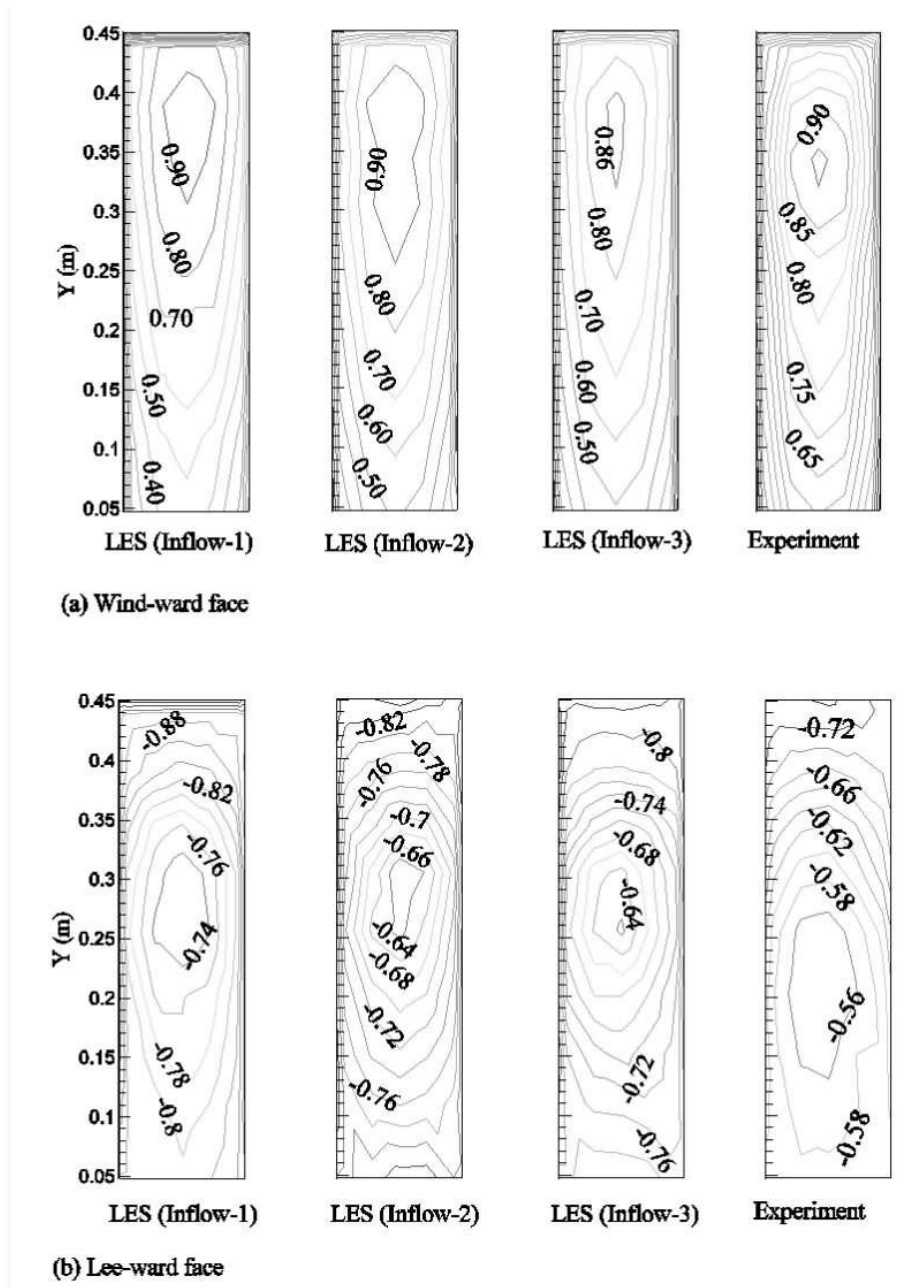


Figure 2.19: Comparison between the mean pressure coefficients of CAARC in a simulated ABL flow using LES with various turbulence models and BLWT experiment

2.10 Wind Simulation and Analysis Software

Although with complex buildings, our wind simulation technology functions as a wind tunnel and enables you to see colorful pressure maps on our model to understand the effects of the wind in RWIND simulation software. Pressure Coefficient is calculated using the formula $\text{Pressure Coefficient} = (\text{Surface pressure at a location} - \text{Free stream Pressure}) / (\text{Free stream dynamic pressure})$. This formula describes the value of local pressure at a given point in terms of free stream pressure and dynamic pressure. The symbol for pressure coefficient is C_p . The pressure function object in the simulation software can convert an

input pressure field into derived forms in a number of different methods, including static pressure, total pressure, and the pressure coefficient described in equations 2.31 to 2.33.

Pressure coefficient calculator uses pressure

$$\text{Static pressure, } p = \rho p_k \dots\dots\dots (2.31)$$

$$\text{Total pressure, } p_t = p_{ref} + p + 0.5\rho|u|^2 \dots\dots\dots (2.32)$$

$$\text{Pressure coefficient, } C_p = \frac{p}{0.5\rho_\infty|u_\infty|^2} \dots\dots\dots (2.33)$$

Where, p is the static pressure, ρ is density of air, p_k is the kinematic pressure, p_{ref} is the Reference pressure level, u is the velocity, p_∞ is the free stream pressure and u_∞ is the free stream velocity.

2.10.1 Dlubal RWIND and RFEM

RWIND Simulation is a stand-alone tool used for static and dynamic analysis alone or in conjunction with the RFEM/RSTAB programs. There is a native relationship between RFEM/RSTAB and RWIND Simulation due to the basic assumption regarding the computation of wind loads for structures with the transfer of forces to the structural model, as shown in Figure 2.20. This link allows any RFEM or RSTAB model with wind load specification to be exported to RWIND Simulation via a particular interface, and wind loads to be received on the surfaces of the elements after the computation (Anderson, 1992).

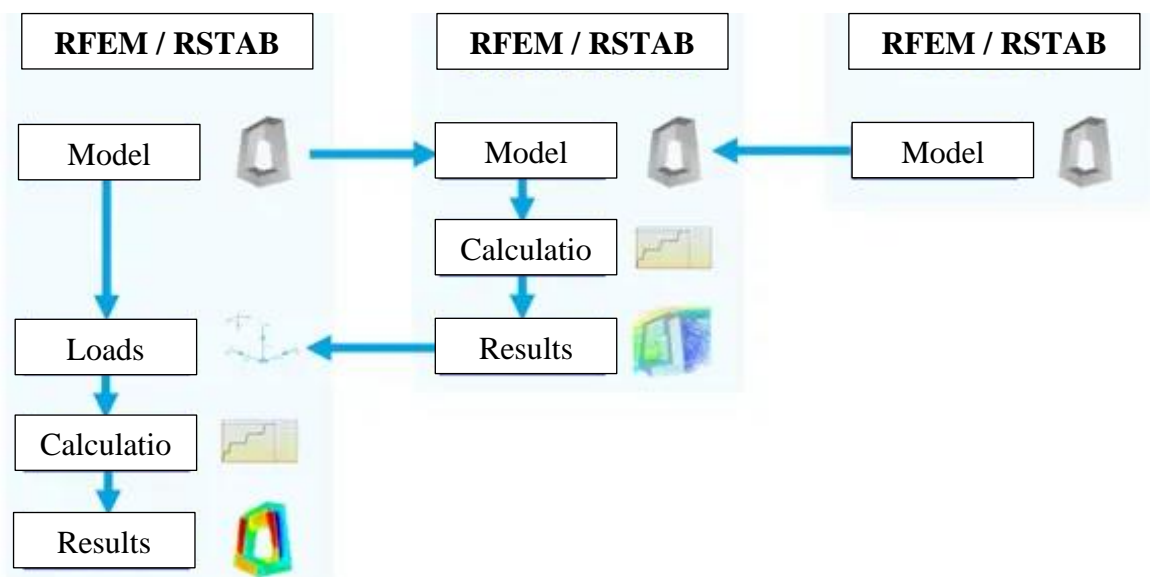


Figure 2.20: Relationship between RFEM/RSTAB and RWIND Simulation (Dlubal Software GmbH, 2022)

Projects are used to organize RWIND Simulation. Each project includes all flow field results in the wind tunnel and surface results on the objects and object geometry orientated to the wind flow in a numerical wind tunnel with a defined incoming wind force. The incoming wind load is a wind velocity profile and turbulence intensity over a height at the wind tunnel's entrance. To describe a project, you have two alternatives.

If users merely want to do a wind load study in RWIND Simulation, use a 3D data model to import the geometry surrounded by flows to the project's numerical wind tunnel, align it in the wind tunnel, and describe the incoming wind load in the dialogue box, as shown in Figure 2.21. Using this application, the model can be imported as triangularized model geometry in STL format or as ParaView model geometry in VTP format.

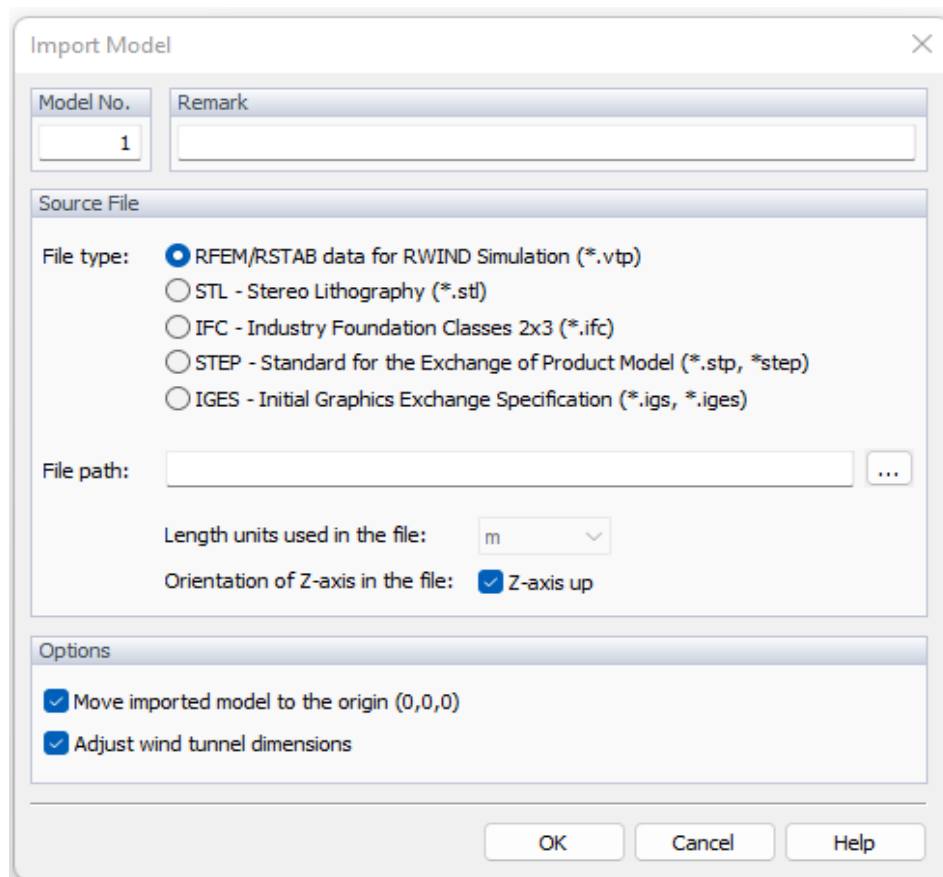


Figure 2.21: Manual Model Import in RWIND Simulation (Dlubal Software GmbH, 2022)

To keep all connections in a wind load analysis using the wind loads in the RFEM and RSTAB structural analysis tools, the primary model must be created as a structural model in RFEM or RSTAB. In this case, using an interface application in RFEM and RSTAB, you can define the wind load (manually or according to the standard) for different wind

directions, and the structural model with all members, surfaces, solids, and 3D objects for the wind directions is automatically exported to the RWIND Simulation wind tunnel projects, as shown in Figure 2.22 (Dlubal Software GmbH, 2021).

There will be no further constraints when importing the model into RWIND Simulation. The accessible interfaces import the geometry data with orientation options to the numerical wind tunnel and construct the corresponding boundary conditions for the numerical flow analysis on the surfaces, regardless of whether the flow around the object is an organic shape or a sharp-edged block.

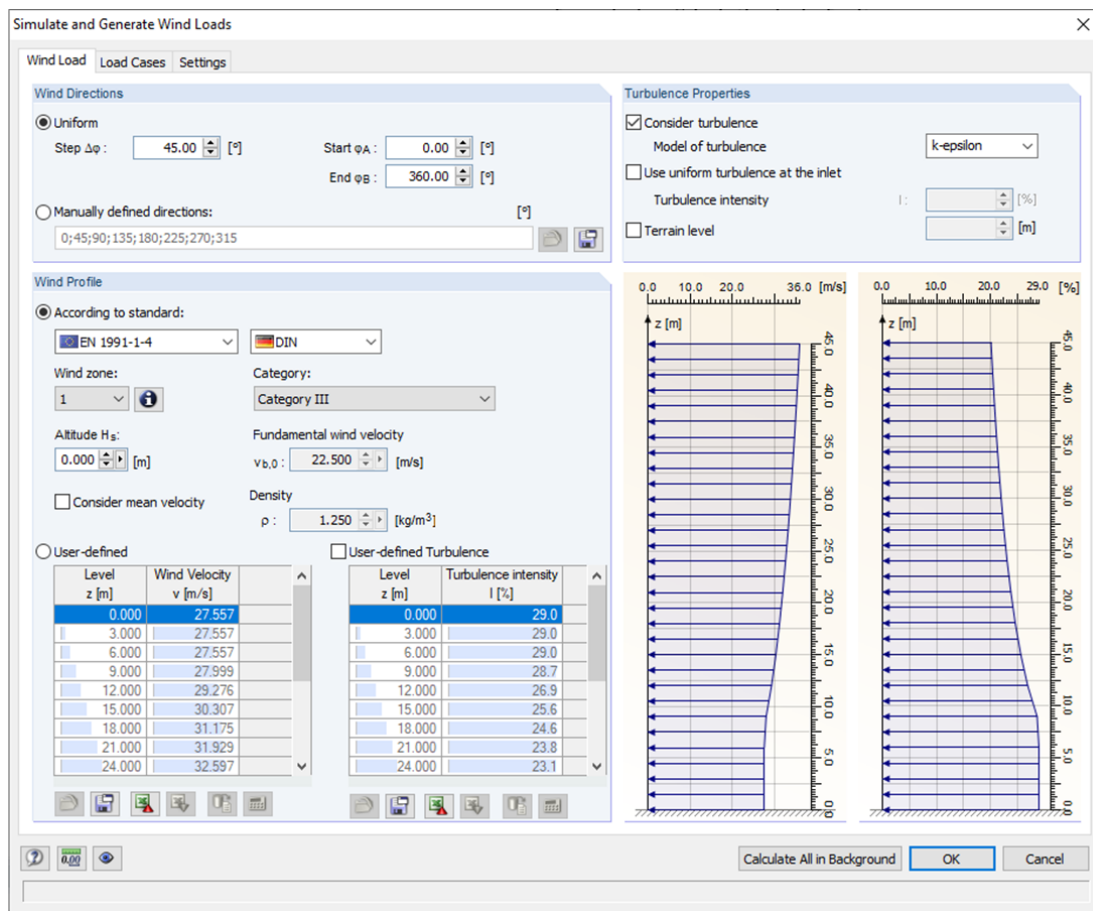


Figure 2.22: Automatic Model Import in RWIND (Dlubal Software GmbH, 2022)

The program presents two primary result types for characterizing the wind flow around the objects and its effect when the iterative simulation procedure reaches the convergence requirement.

On the one hand, by presenting three-dimensional flow fields characterized by layers by displaying Wind speeds, directions, pressures, turbulence qualities, and Streamlines.

(Dlubal Software GmbH, 2021). In addition to these resulting load cases in RFEM and RSTAB, more results of the aerodynamics analysis in RWIND Simulation are obtained, as shown in Figure 2.23, which display the flow problem as a whole (Dlubal Software GmbH, 2022):

- Pressure on the structure surface
- Pressure field about structure geometry
- Velocity field about structure geometry
- Velocity vectors about structure geometry
- Flow lines about structure geometry
- Forces on member-shaped structures that were originally generated from member elements
- Convergence diagram
- Direction and size of the flow resistance of the defined structures

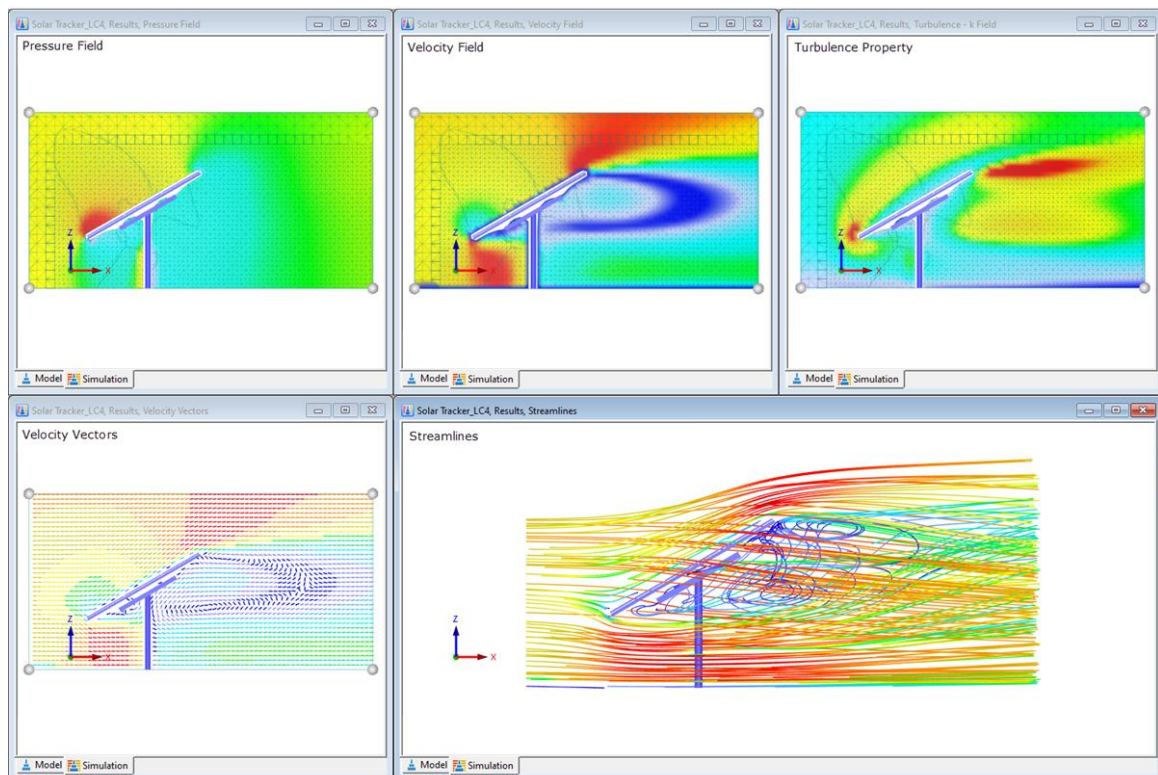


Figure 2.23: Flow Field Results in Volume Space (Dlubal Software GmbH, 2022)

These results are displayed in the RWIND Simulation environment and evaluated graphically, as shown in Figure 2.24. Since the flow results about the structure geometry are confusing in the overall display, you can see freely movable section planes for the separate display of the "solid results" in a plane. Accordingly, in the 3D branched

streamline result, an animated display in the form of moving lines or particles is shown in addition to a structural representation. This option helps to represent the wind flow as a dynamic effect. All results can be exported as a picture or, especially for the animated results, as a video.

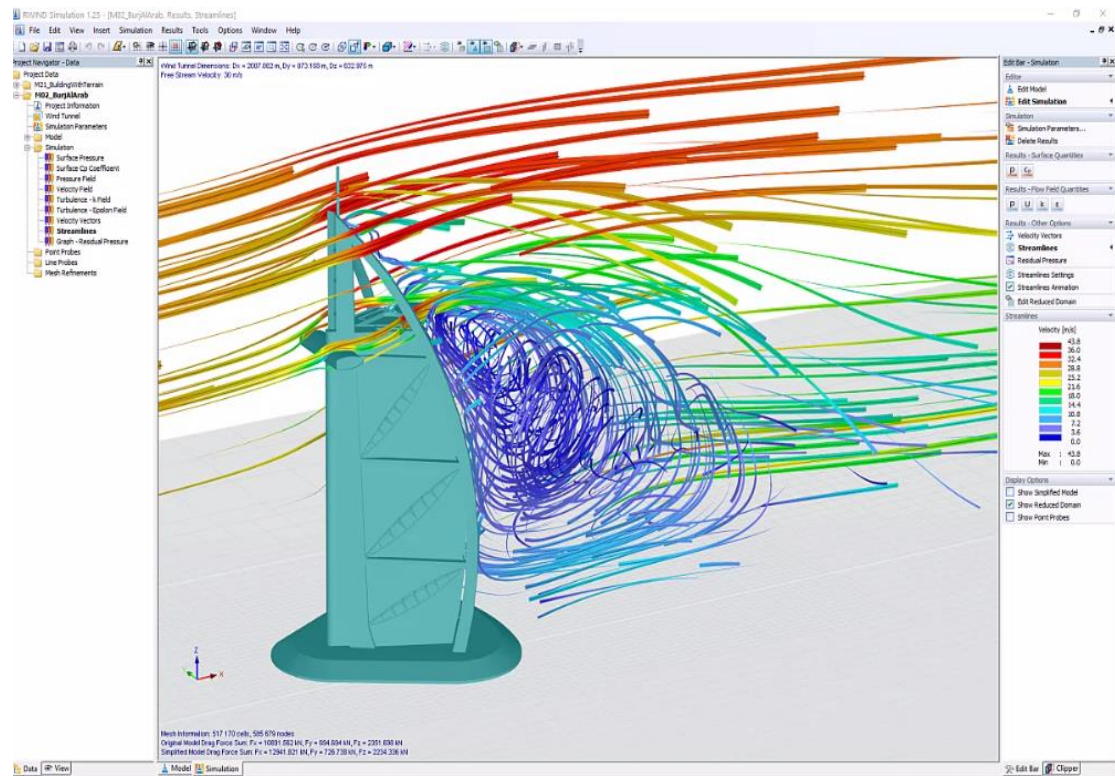


Figure 2.24: Different results of the aerodynamics analysis in RWIND Simulation (Dlubal Software GmbH, 2022)

The RWIND has some excellent features (Dlubal Software GmbH, 2022) including:

- i. 3D incompressible wind flow analysis with OpenFOAM[®] software package
- ii. Direct model import from RFEM or RSTAB including neighbouring and terrain models (3DS, IFC, STEP files)
- iii. Model design via STL or VTP files independent of RFEM or RSTAB
- iv. The simple model changes using Drag and Drop and graphical adjustment assistance
- v. Automatic corrections of the model topology with shrink wrap networks
- vi. Option to add objects from the environment (buildings, terrain)
- vii. Wind load determined over the height of the building, depending on standard-specific parameters (velocity, turbulence intensity)

- viii. K-epsilon and K-omega turbulence models
- ix. Automatic mesh generating adjusted to the selected depth of detail
- x. Parallel calculation with optimal utilization of the capacity of multicore computers
- xi. Results in just minutes for low-resolution simulations (up to 1 million cells)
- xii. Results within a few hours for simulations with medium/high resolution (1-10 million cells)
- xiii. Graphical display of results on the Clipper/Slicer planes (scalar and vector fields)
- xiv. Graphical display of streamlines
- xv. Streamline animation (optional video creation)
- xvi. Definition of point and line samples
- xvii. Display of aerodynamic pressure coefficients
- xviii. Graphical display of turbulence properties in the wind field
- xix. Optional meshing using the boundary layer option for the area near the model surface
- xx. Consideration of rough model surfaces possible
- xxi. Optional use of a second-order numerical scheme
- xxii. Documentation possible in the RFEM and RSTAB printout report

2.10.2 ETABS

ETABS is a designing programming item that obliges multi-story building investigation and plan. Demonstrating instruments and layouts, code-based burden remedies, examination strategies, and arrangement methods all coordinate with the matrix-like calculation extraordinary to this class of design. Fundamental or progressed frameworks under static or dynamic conditions might be assessed utilizing ETABS. For a refined appraisal of seismic execution, modular and direct-incorporation time-history investigations might couple with P-Delta and Large Displacement impacts. Nonlinear connections and concentrated PMM or fiber pivots might catch material nonlinearity under monotonic or hysteretic conduct. Natural and incorporated highlights make utilizations of any intricacy pragmatic to execute. Interoperability with a progression of plan and documentation stages makes ETABS an organized and useful instrument for plans which range from basic 2D edges to expound current elevated structures (Computers and Structures Inc., 2022). ETABS is one of the most user-friendly software used widely. Graphical visualization, customized animation, element-wise customization options, and

options of more than one window make the modelling work attractive, as shown in Figure 2.25.

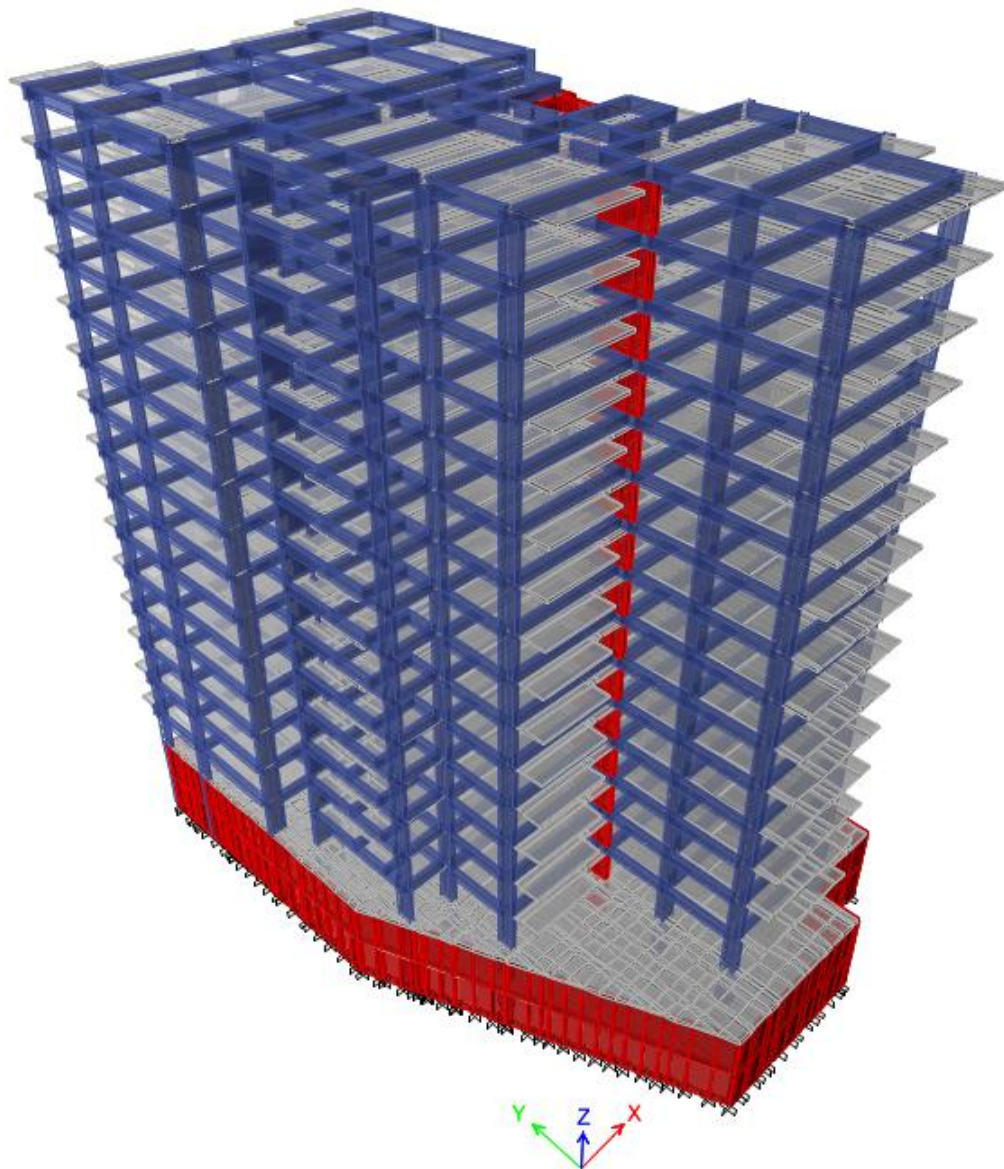


Figure 2.25: Model of a multi-storeyed building (Computers and Structures Inc., 2021)

Static Analysis: It can do static analysis for user-specified vertical and lateral floor or story loads. Vertical loads on the floor are transmitted to the beams and columns by bending the floor components when floors are represented with out-of-plane bending capacity. Otherwise, vertical loads on the floor are automatically converted to span loads on nearby beams or point loads on adjacent columns, eliminating the need to explicitly model the secondary framing and automating the laborious job of transferring floor tributary loads to the floor beams. Figure 2.26 represents a linearly analyzed structure.

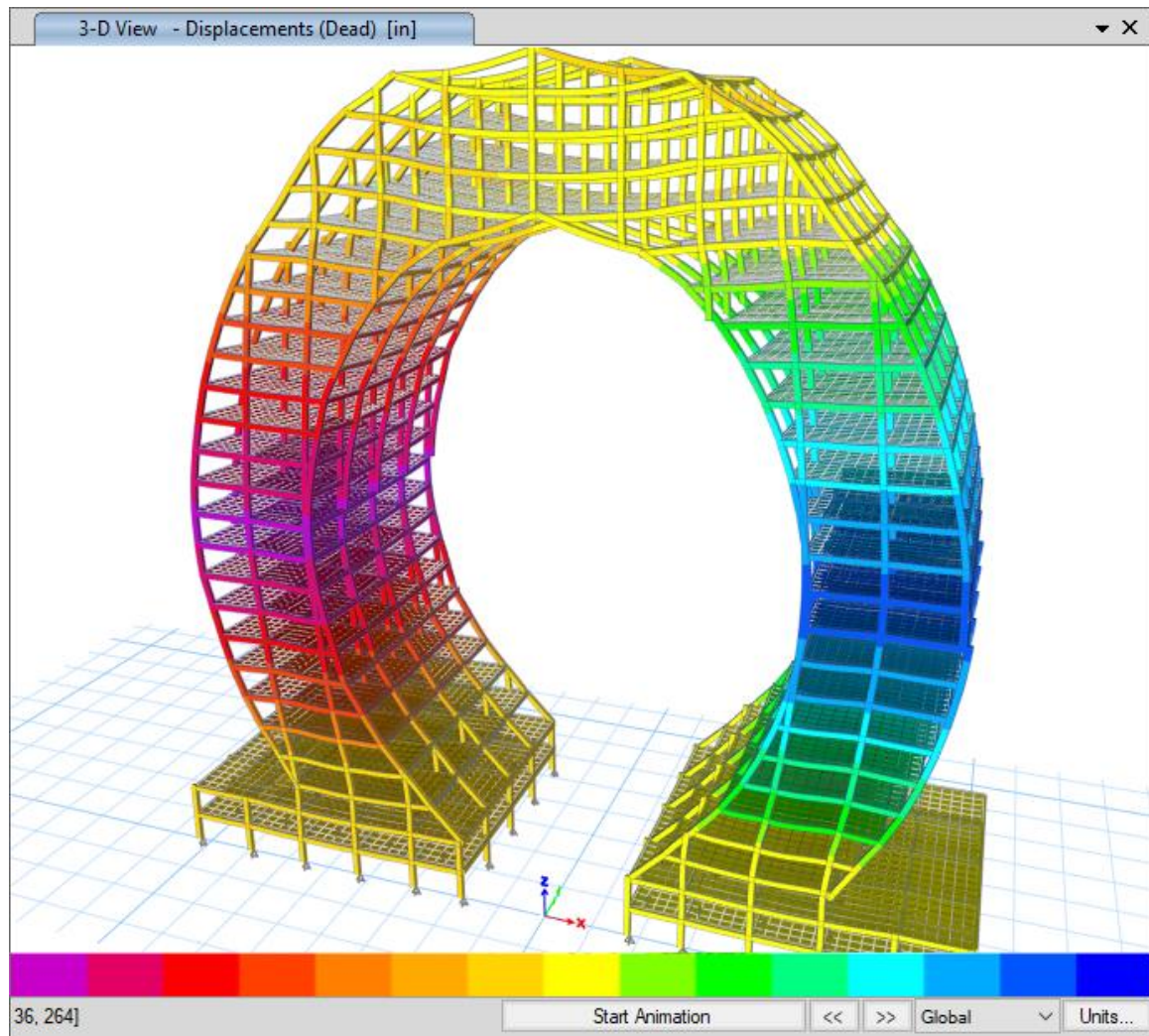


Figure 2.26: Linear analysis of structure (Computers and Structures Inc., 2021)

P-delta analysis captures the softening and stiffening effects of compression and tension. For linear load scenarios, a single P-delta analysis under gravity and sustained loads may be utilized to adjust the stiffness, which can then be superposed. Alternatively, complete nonlinear P-delta effects can be studied for each combination of loads. All aspects have P-delta effects, smoothly incorporated into analysis and design (Computers and Structures Inc., 2021).

Response spectrum analysis determines the statistically probable response of the structure to seismic loads. This linear analysis uses ground acceleration records that respond to seismic loads and site conditions rather than ground motion records over time, as shown in Figure 2.27. This method is highly efficient and considers the dynamic behavior of the structure.

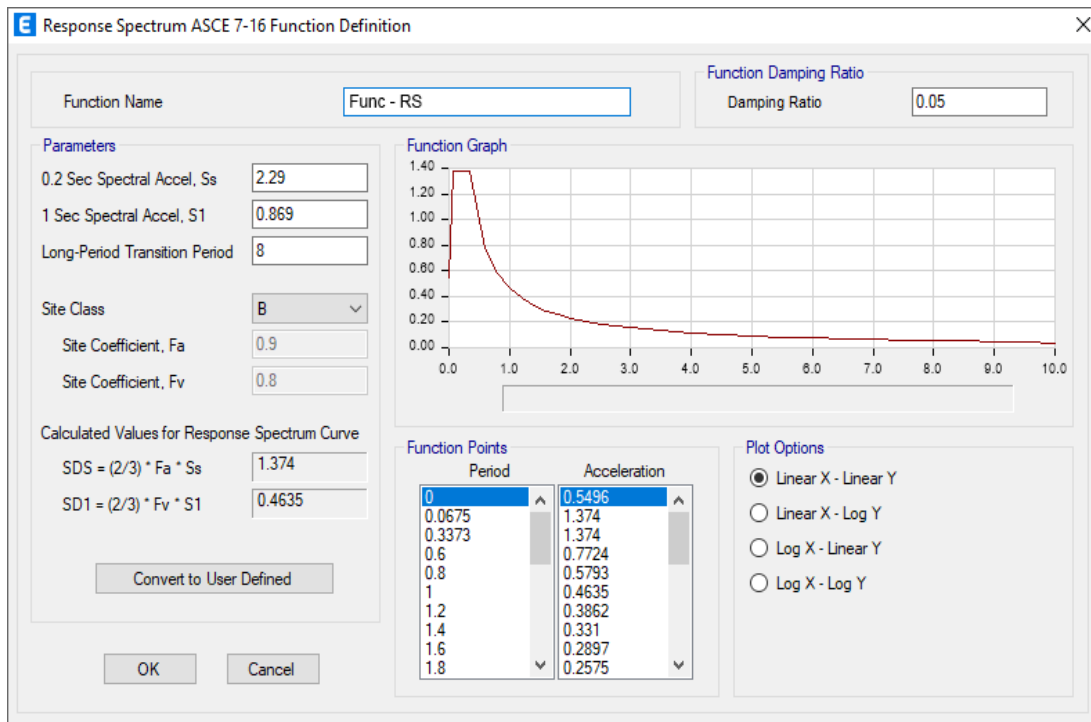


Figure 2.27: Response spectrum analysis (Computers and Structures Inc., 2021)

Time History analysis captures the step-by-step response of a structure to ground-based seismic motion and other types of loads such as explosions, machinery, wind, waves, and more. The Time History analysis uses a seismograph, unlike the response spectrum graph, as shown in Figure 2.28.

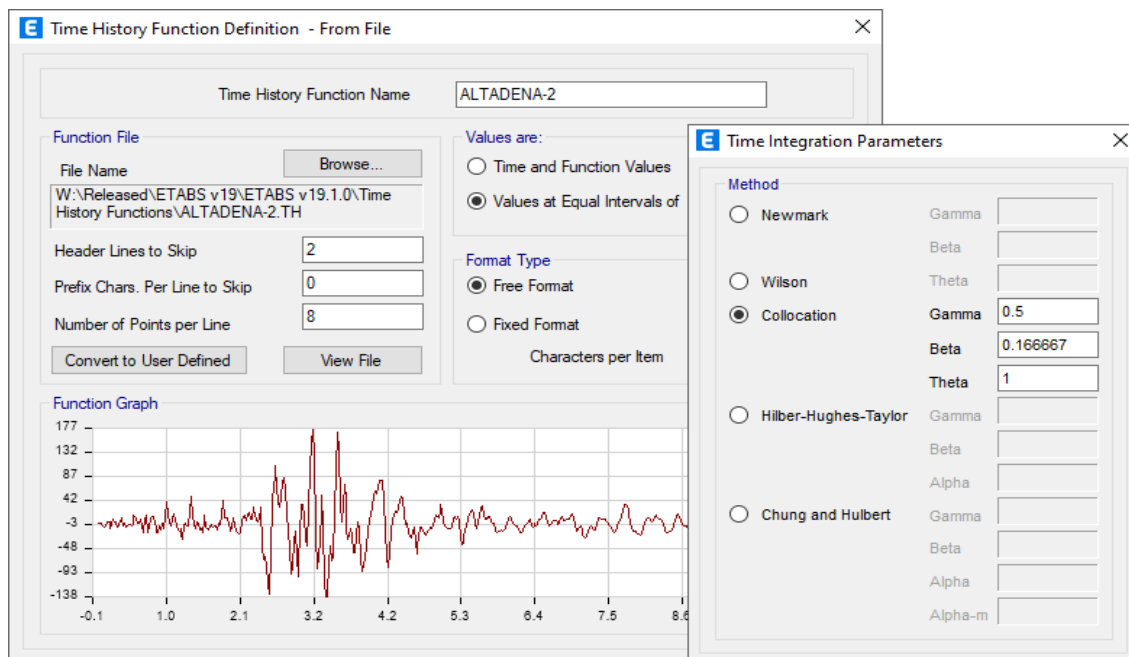


Figure 2.28: Time History analysis (Computers and Structures Inc., 2021)

This analysis can use modal superposition or direct integration, and both can be linear or nonlinear. The Modal Nonlinear Method, also known as FNA for Fast Nonlinear Analysis, is highly efficient and accurate for many problems. The direct integration method is even more general and can handle significant distortions and highly nonlinear behaviors, as shown in Figure 2.29. Nonlinear time analyzes can be chained with other nonlinear cases (including stepwise construction), addressing many applications (Computers and Structures Inc., 2021).

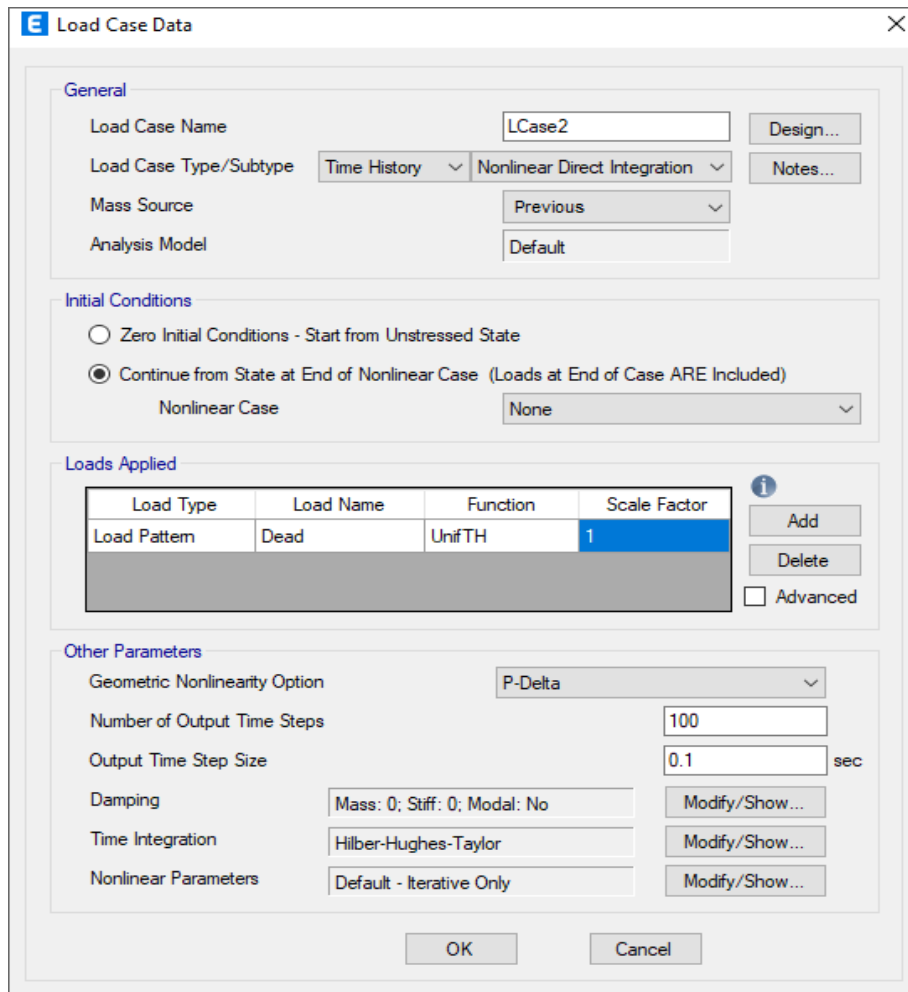


Figure 2.29: Nonlinear Direct Integration analysis (Computers and Structures Inc., 2021)

Pushover analysis features in ETABS include the implementation of FEMA 356 and the hinge and fiber hinge option based on stress-strain, as shown in Figure 2.30. The nonlinear layered shell element enables users to consider the plastic behavior of concrete shear walls, slabs, steel plates, and other finite area elements in the pushover analysis. Force deformation relations are defined for steel and concrete hinges.

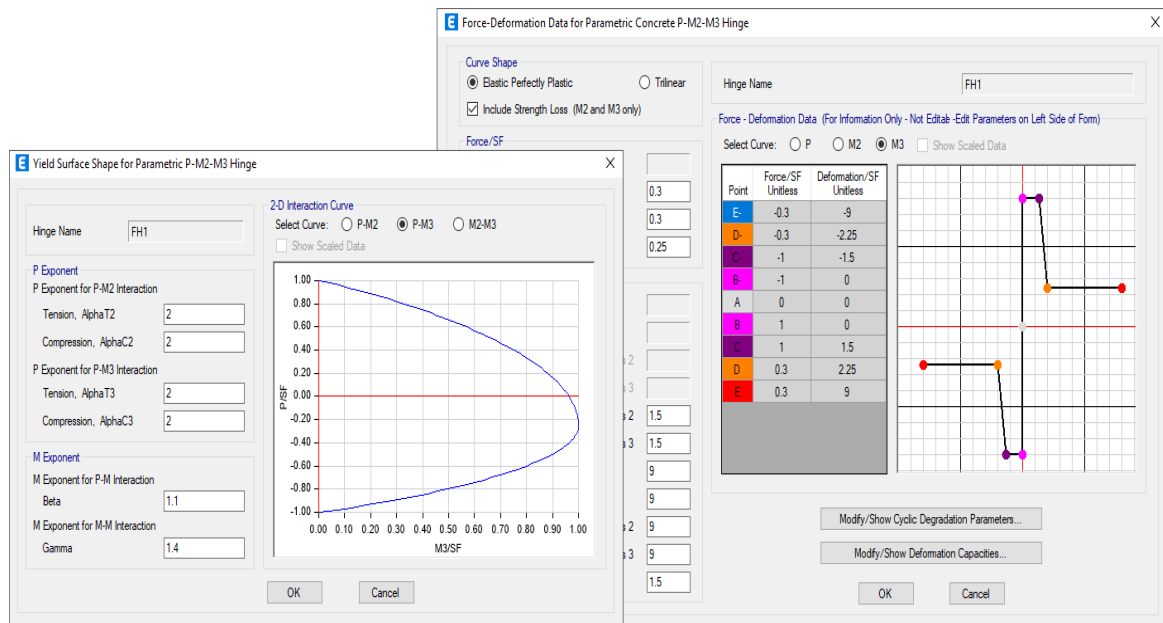


Figure 2.30: Pushover analysis (Computers and Structures Inc., 2021)

2.11 Summary

This chapter of the thesis reviewed several literature concerning the wind pressure coefficient and some of the basic wind terminologies such as the atmospheric boundary layer, wind speed profile, and wind turbulence. Bangladesh National Building Code (BNBC) wind load was also reviewed for the interest of the study. Computational fluid dynamics (CFD) is a science that, with the help of digital computers, produces quantitative predictions of fluid-flow phenomena based on the conservation laws (conservation of mass, momentum, and energy) governing fluid motion. The k-epsilon turbulence model was discussed along with the basics of the CFD. Discussion on the numerical wind tunnel RWIND and ETABS were discussed briefly. Features of both the software were expressed, such as the ability of CFD analysis of the RWIND in wind simulation and its incredible outputs, and different types of analysing capabilities of the ETABS.

CHAPTER 3

METHODOLOGY

3.1 Introduction

Physical wind tunnel test, the most accurate method of measuring the wind flow parameters, is recommended for any complex, essential structures. However, since it is not available in all parts of the world and is expensive, the wind scientist and engineers came up with an alternative solution: The numerical simulation of wind tunnel test. Mechanisms of the numerical wind tunnel had already been discussed in Chapter 2. Validation of numerical model is always essential for any new study. Therefore, a numerical wind tunnel model was validated using a Dlubal RWIND simulation, a computer program. The experimental or physical wind tunnel test data was extracted from the study of Dagnev et al. (2009).

Methodology of the study includes five steps including

- i. Comparison of Bangladesh National Building Code (BNBC) 2006 and 2020 in determination of the wind load effect on structure with manual calculation.
- ii. Numerical modelling and validation of the numerical wind tunnel test.
- iii. Comparison of wind load in terms of story share between Bangladesh National Building codes and the numerical wind tunnel test.
- iv. Evaluation of wind pressure coefficient for all the structures modelled for the study.
- v. Results analysis and proposal of the empirical equations for wind pressure coefficient and performance evaluation of the proposed equations.

Wind load on structures were calculated according to both the Bangladesh National Building Code (BNBC) and then a comparison was made. For better understanding on how local and international codes evaluate the wind effects, the Uniform Building Code (UBC 94) and ASCE 7-05 were also included to the comparison. Numerical wind simulation was performed in the simulation software namely “RWIND” and validation of the numerical wind tunnel was performed and described in sections 3.2 & 3.3. Upon successful validation of the numerical wind tunnel test, a parametric study was performed. A Comparison was then performed in terms of story share between Bangladesh National Building code and the numerical wind tunnel.

Wind pressure coefficients found from the simulation were evaluated and the idea of using different wind pressure coefficients of the surface of structures were implemented. Performance of the use of variable wind pressure were observed with care. Analysis of the test results was done and proposal of the empirical equations for wind pressure coefficient and performance evaluation of the proposed equations were performed before reaching to the conclusion of the study.

3.2 Numerical Modelling

Upon completing the numerical model validation, study structures were modelled in two well-known sophisticated software, namely Dlubal RFEM and CSI ETABS. Models created in the Dlubal RFEM were sent to the Dlubal RWIND simulation software for wind simulation. The structural response of the buildings was analyzed in the CSI ETABS.

3.2.1 Study Model in RFEM

Since the numerical wind tunnel RWIND accepts modelling in the RFEM, a total number of four structures with variable geometric properties was modelled in RFEM, commercial software for structural analysis, discussed in Chapter two. Figure 3.1 represent a twenty storied building, one of the numerical models whose length is 140 feet, width is 76 feet, and height is 200 feet. Geometric properties of four types building structures such as length, width, height, and least dimension to height ratio were described in the Table 3.1.

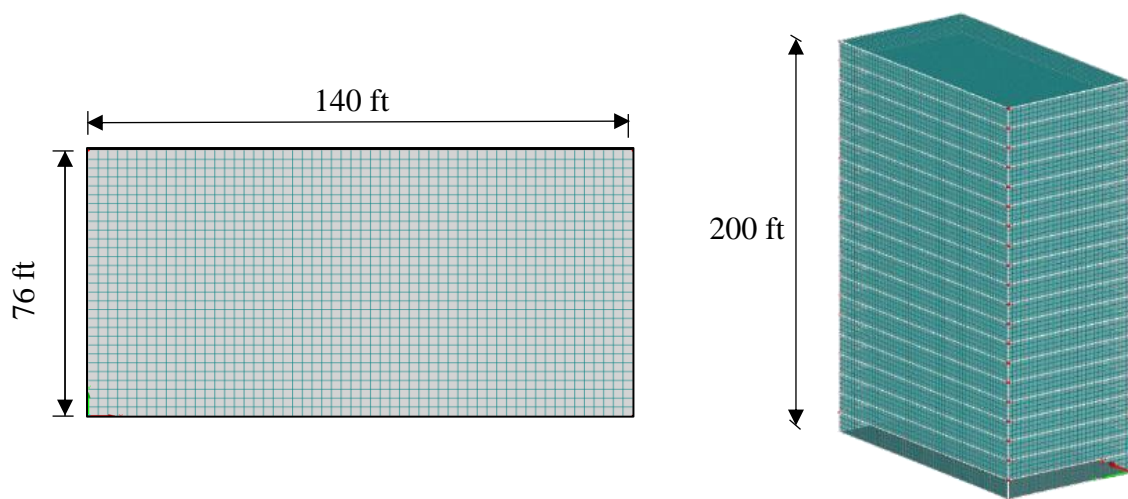


Figure 3.1: One of the numerical study models in RFEM

Table 3.1: Dimensions of study models

Structure Name	Length (ft)	Width (ft)	Height (ft)	Least dimension to height ratio
6 storied	40	50	62	1.52
10 storied	50	75	100	2.00
20 storied	78	140	202	2.59
40 storied	80	120	400	5.00

3.2.2 Wind Simulation in RWIND

Upon completing the modelling part in RFEM, wind simulation was performed in the numerical wind tunnel RWIND. Several simulation parameters were assigned during the process, such as the wind direction, velocity profile, wind mean speed, wind turbulence, mesh intensity, iteration, wind speed profile etc. shown in Figures 3.2 and 3.3. All of these parameters are essential in determining wind effect in structures. At the same time, the k-epsilon model was chosen, OpenFOAM numerical solver was selected, and wind tunnel dimensions were adjusted standing on the ground.

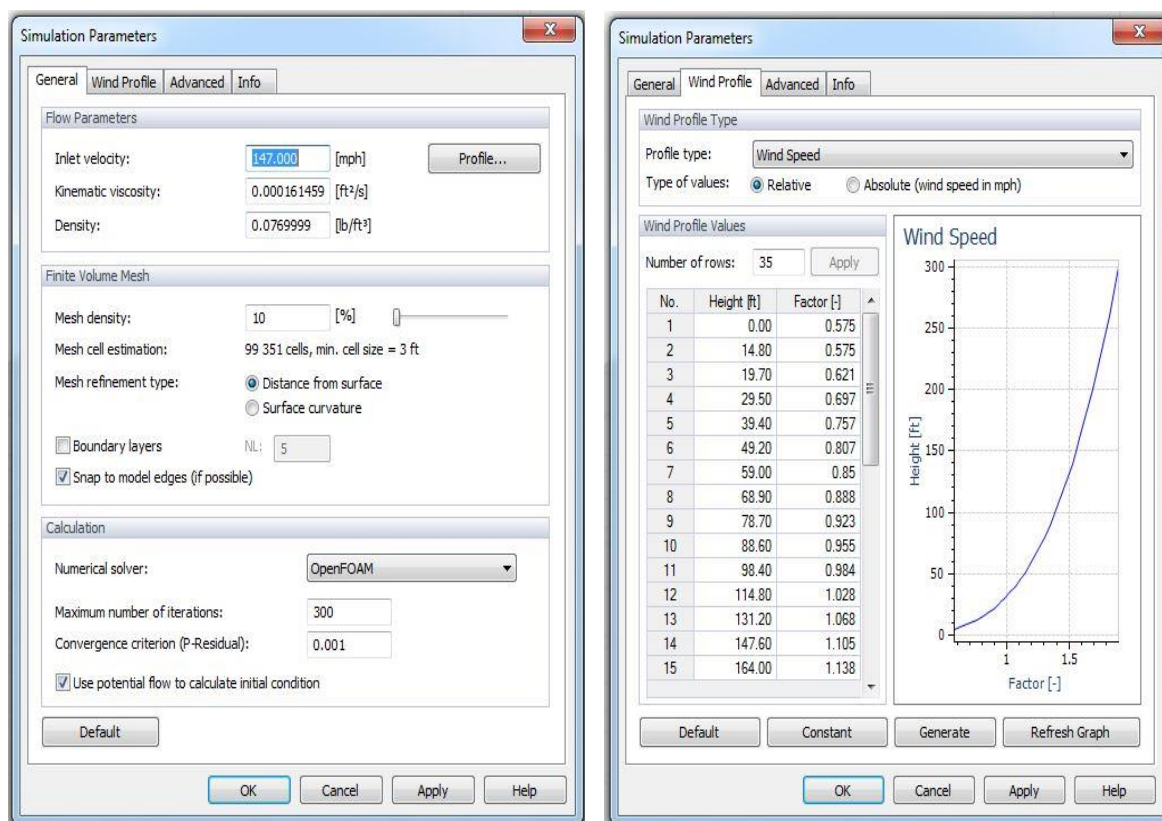


Figure 3.2: Simulation parameters in RWIND (Dlubal Software GmbH, 2021)

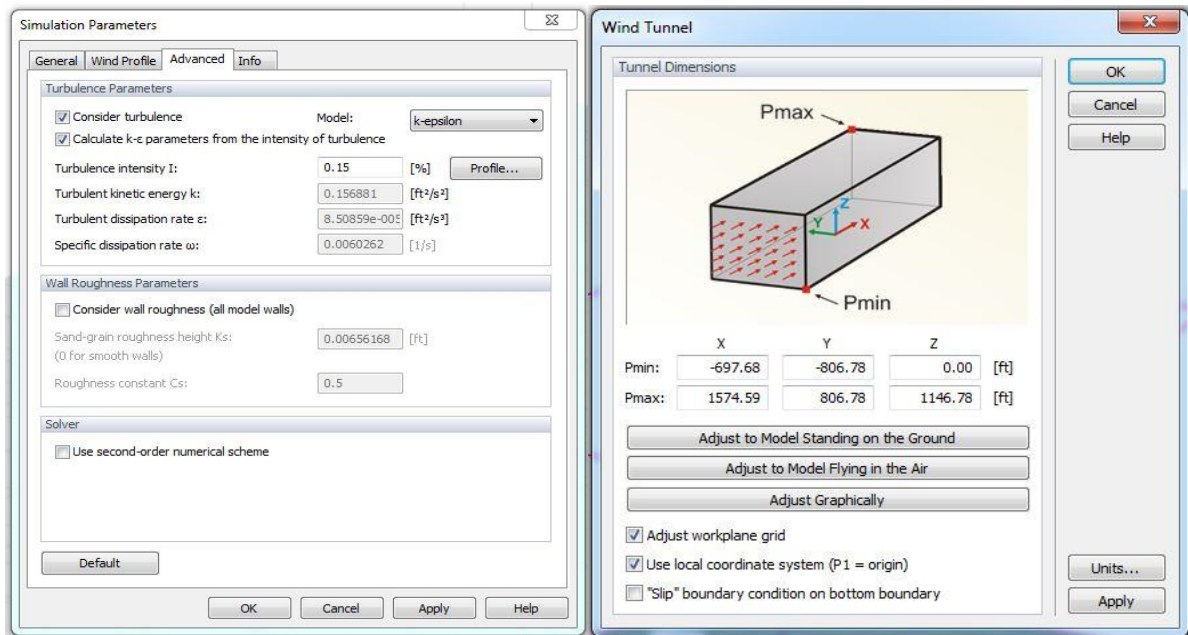


Figure 3.3: (a) Simulation parameters model selection, turbulence consideration (b) Wind tunnel dimensions (Dlupal Software GmbH, 2021)

3.2.3 Simulation Output Pressure Co-efficient (C_p)

Once the simulation parameters were assigned successfully, with the help of the simulation result, the output of the simulation was ready to be extracted. Colormap on the surface represents a range of values of specific parameters such as the wind pressure coefficients, as shown in Figure 3.4 (a). If pointed by a mouse cursor on the surface of the simulated structure, the software shows the value at the particular point. The software has several features, including isolines, color map, color points, color edges, and streamlines turbulence etc., as shown in Figure 3.4 (b).

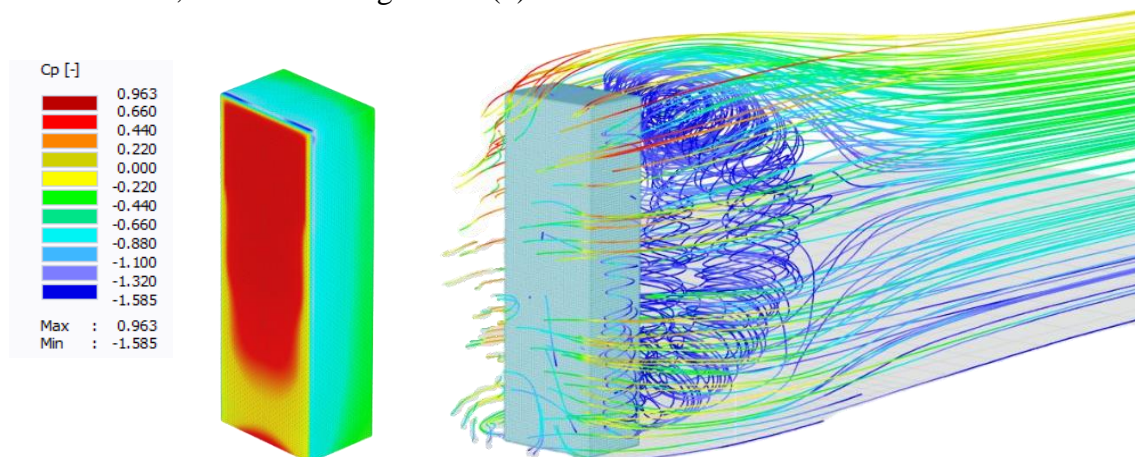


Figure 3.4: RWIND's Graphical representation of (a) external pressure coefficient (C_p) and (b) streamlines turbulence

External pressure coefficient (C_p) and surface pressure are the software’s surface quantities results as output. Moreover, the flow field quantities were the pressure field, velocity field, turbulence-kinetic energy, and turbulence-dissipation rate. The other options were velocity vectors, streamlines, residual pressure, and graph along the line. This study was concerned only with the external pressure coefficient (C_p); hence, it was the only output from the RWIND simulation software taken into consideration.

“Graph along line” was the command that assisted a lot in creating a graphical output of pressure coefficient from the software automatically at a specific elevation, as shown in Figure 3.5. The pressure coefficient along the perimeter was extracted as output. If it was not available had to make it manually, which would have been nearly impossible to ensure accuracy.

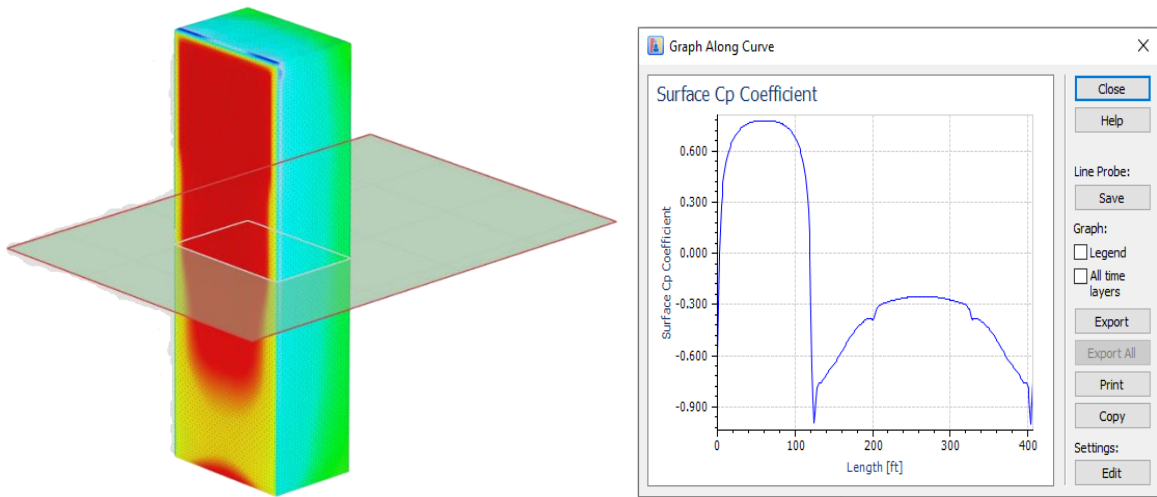


Figure 3.5: Graphical representation of pressure co-efficient at a specific elevation

The arithmetic mean of the pressure coefficients on the surface of the simulated model was considered to use various values at different zones to increase accuracy. Several line graphs were plotted at variable heights, mainly the 3rd and 7th feet of each story, and then the arithmetic mean was considered. Absolute fluctuating C_p values from the numerical wind tunnel as an input for any other structural analysis software, especially ETABS, is impractical.

3.2.4 Numerical Model in ETABS

CSI-ETABS is one of the most popular commercial software structural designer’s use for analysis, design, and evaluation features, which has already been discussed in Chapter 2.

All the study models were modelled in ETABS to analyze the story shear due to the wind effect. Geometric properties were the same as the models of the RFEM. Size and thickness of the structural components or stiffness of the structure do not play any role in the story shear due to the wind load. Material properties for all the study models were kept identical. No external lateral loading was applied, except the wind load and the self-load of the structural elements; since the self-load has nothing to do with the story shear, this loading did not raise any question.

Upon completing the frame modelling, the calculated mean story C_p found from the wind simulation in RWIND was assigned to the structure with the help of “none areas” created vertically to the wind direction shown in Figure 3.6.

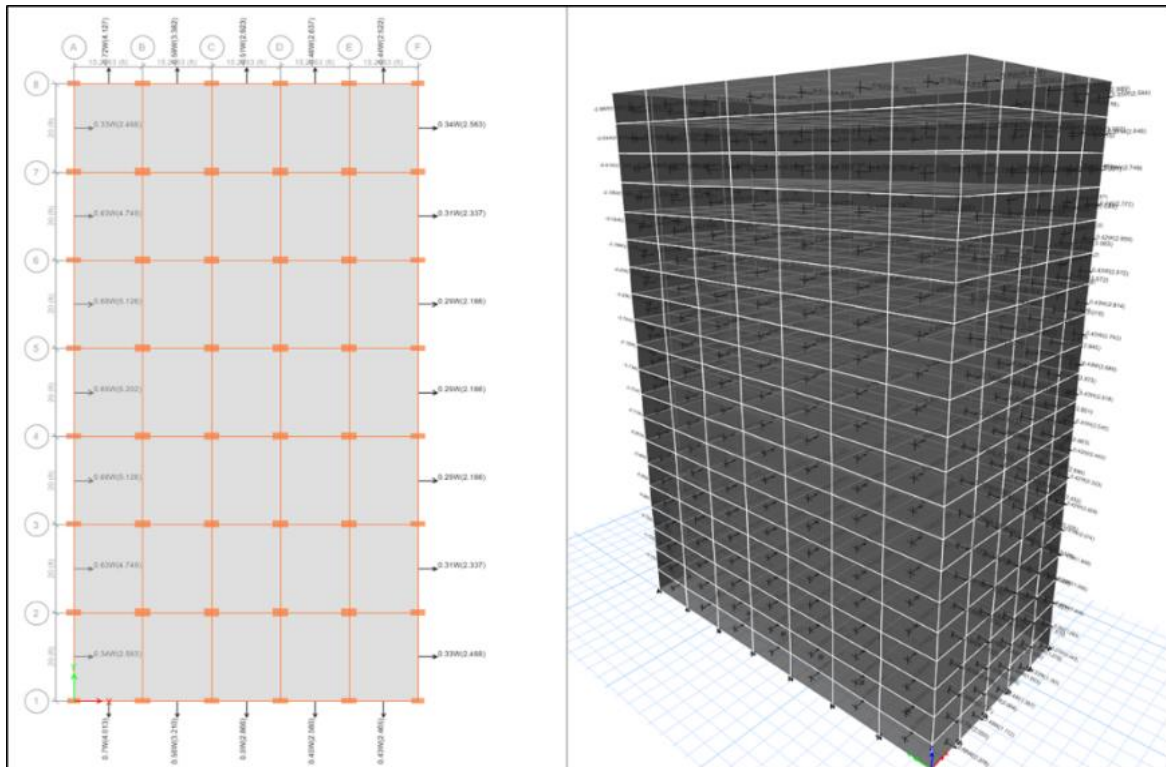


Figure 3.6: One of the numerical study models in ETABS

3.3 Numerical Wind Tunnel Model Validation

The Navier-Stokes Equations can be solved numerically for fluid flow by using a computer. Now CFD can be applied to complicated fluid flow studies due to advanced development in computer technology over the last few years. It became one of the important tools in wind-related research (Liaw, 2005).

3.3.1 Geometric Dimension

In this study, CFD simulation was done by RWIND Simulation Solver that many flow dynamics researcher uses for the general-purpose program. The geometric modelling of numerical simulation has shown in Figure 3.1. Cartesian coordinate system (x , y , and z) was used for identifying flow direction where X -axis aligned with streamwise and normal to the wall and vertical direction aligned with Y -axis and Z -axis respectively. To minimize the blockage effect, tunnel size considered $33B$ along streamwise, $20B$ is normal to the wall and $2H$ in vertical direction respectively, where B is the depth and H is the height of the building, as shown in Figure 3.7.

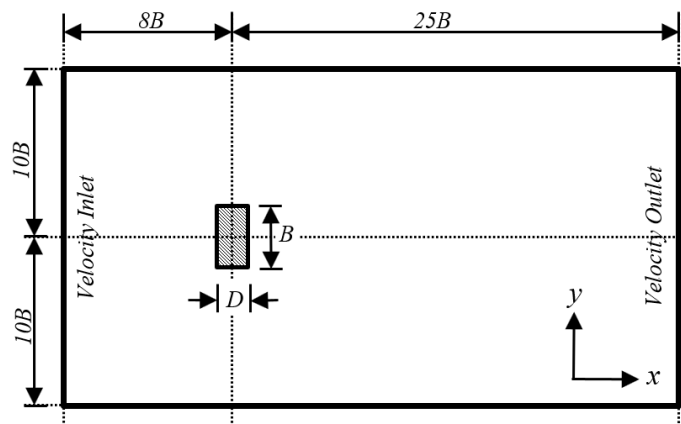


Figure 3.7: Numerical wind tunnel measurements (Dagnev et al., 2009)

The verification model shape is rectangular with a dimension parallel to the wind is 100.0 ft, perpendicular to the wind is 150.0 ft, and height is 600.0 ft. In the numerical wind tunnel test, the wind tunnel dimensions are 4950.0 ft in the windward direction and 3000.0 ft in the spanwise direction, and the total height is twitching the model size equal to 1200.0 ft, as shown in Figure 3.8.

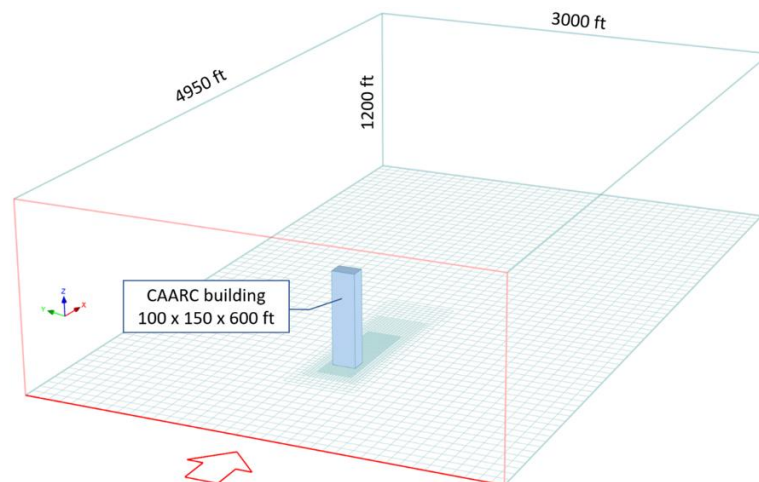


Figure 3.8: Model and Computational Domain at RWIND (Dagnev et al., 2009)

3.3.2 Meshing of the Model

The meshing of a structure is very important because the output values may vary if the unstructured mesh is used. Also, a large number of mesh is time-consuming for analysis. To generate a finite volume mesh, the model must be topologically correct. The term “topologically correct” then means that these triangles must form a closed triangular mesh, i.e., each mesh edge has exactly two adjacent triangles and that the triangles must not intersect or touch each other except common edges. The exact definition of a “topologically correct” model is more complicated, but we don’t want to go into all the details here (Dlubal Software GmbH, 2021). The problem is that CAD models are usually not topologically correct – triangles of a 3D object often intersect with triangles of another object, the model boundary is not closed, etc. In RWIND Simulation, model boundaries are defined by triangles and use simplified models to ensure a topologically correct model, as shown in Figure 3.9. Therefore, an optimum number of mesh was used in the regular shaped model of this study, as shown in Figure 3.10.

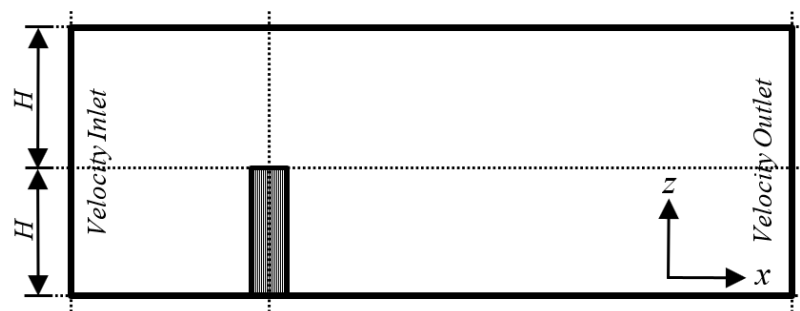


Figure 3.9: (a) Topological imperfections of CAD models (b) Examples of automatically simplified models (Dlubal Software GmbH, 2021)

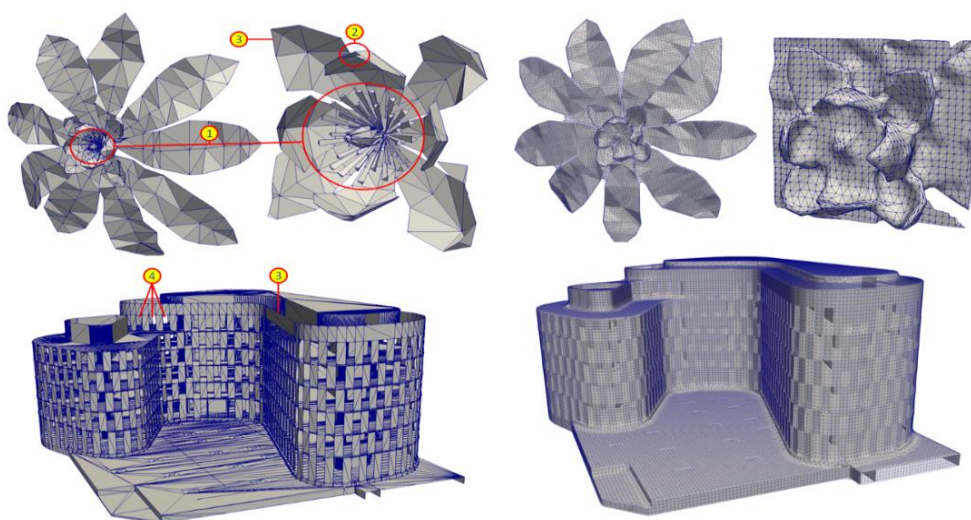


Figure 3.10: Mesh generation of the model (Dagnev et al., 2009)

3.3.3 Turbulence Models and Analysis Methods

The analysis between the fluid flow and the dynamic behavior body plays an important role. Bluff body shape is common for buildings, and accurate flow measurement is difficult for this shape. Due to the nature of flow separation, unsteadiness, wake, and reattachment, the flow characteristics around the building are very complicated. There is much turbulence analyzing models; three are suited under this study consideration. Namely, k-ε modelling, large eddy simulation (LES), and direct numerical simulation (DNS) satisfy all the CFD problem's requirements.

Instead, RWIND Simulation uses a different technique where flow variables, such as velocity or pressure, are decomposed into mean (averaged) components and fluctuating components. In other words, governing equations of fluid motion are averaged to remove the small scales, resulting in a modified set of computationally less laborious equations to solve. Those equations are referred to as “Reynolds-averaged Navier-Stokes equations” (RANS). To solve RANS in RWIND Simulation, the k-ε turbulence model is used, introducing two transport equations for the turbulence properties: the first is the transport equation of the turbulence kinetic energy k, and the second equation governs the transport of the dissipation rate ε of k. This method represents the most widely used and tested model for CFD calculations. Robustness, economy, and reasonable accuracy for a wide range of turbulent flows applications explain its popularity in industrial flow simulations.

3.3.4 Boundary Conditions

The mean wind profile represents the wind velocity concerning the height and shows homogenous terrain horizontally that has been power law. It is a simple equation because many researchers and engineers widely use this empirical equation. The velocity profile in wind tunnel test and CFD simulation takes the following power law is given by equation 3.1:

$$V_z = 2.01V_g \left(\frac{z}{z_g} \right)^{2/\alpha} \dots\dots\dots (3.1)$$

Where V_g is the wind speed at the height of the building models, α is the exponent of the velocity profile, which depends on exposure category.

3.3.5 Result Verification

For verification, wind tunnel test results of the Commonwealth Advisory Aeronautical Council (CAARC) building are compared with numerical wind simulation in the RWIND program. The geometrical modelling for the numerical simulation of the CAARC building model was built in a 1:400 scale rigid model, as shown in Figure 3.11, for wind tunnel testing. Results of wind tunnel tests are collected from different literature (Dagnew et al., 2009).



Figure 3.11: 1:400 scale model for Wind Tunnel test (Liaw, 2005)

The velocity profile for numerical wind tunnel test in CFD simulation takes the following power-law as equation 3.2 is exponent of 0.16 for verification test results:

$$V_z = V_g \left(\frac{z}{z_g} \right)^\alpha \dots\dots\dots (3.2)$$

A turbulent intensity is applied 15percent in the inlet boundary condition. Other boundaries are considered slip conditions at the top and two sides and pressure outlet conditions in the outflow of the control volume.

The RWIND simulation results and experimental results according to the wind tunnel test on the windward face are in close comparison, as shown in Figure 3.12 and Figure 3.13. Around 15% differences between the measured and the calculated data are observed on the sidewall and leeward faces, mainly depending on the boundary mesh and turbulence model.

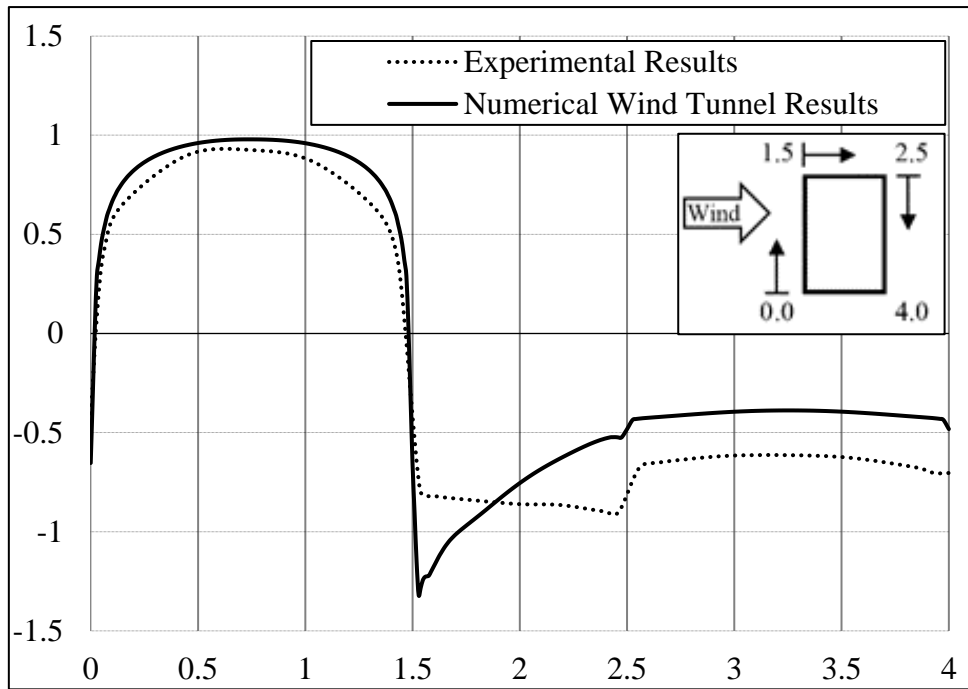


Figure 3.12: Values of Mean Pressure Coefficients (C_p) over the Perimeter at $2H/3$

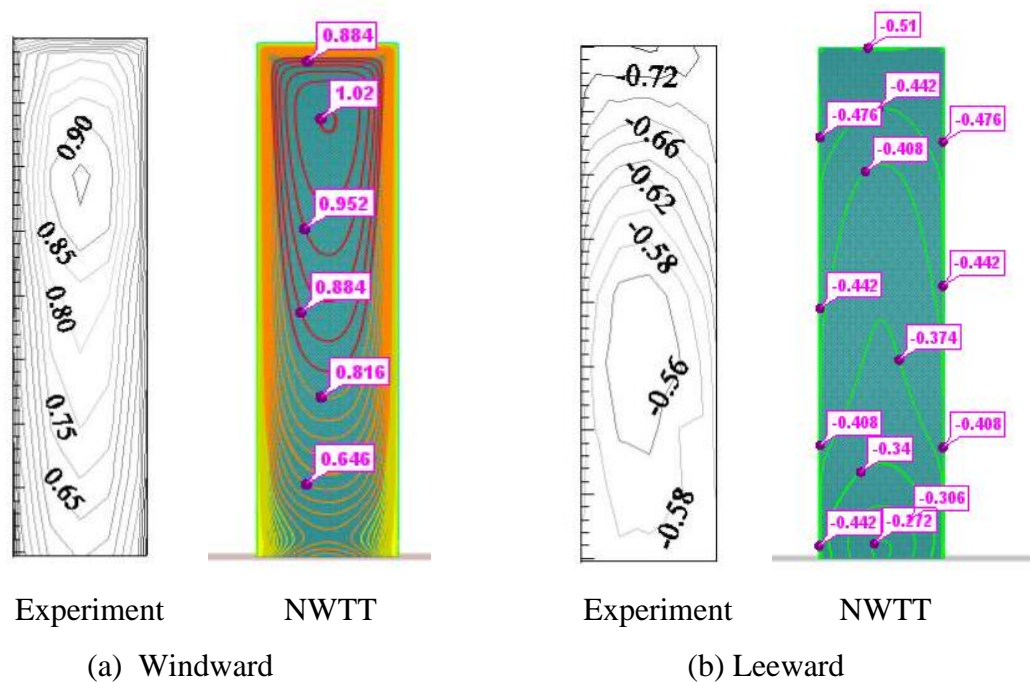


Figure 3.13: Pressure Coefficients (C_p) at Windward and Leeward Surface

The result of the analyzed model showed great similarities with the numerical values of Dagnev et al., (2009) and the experimental values in the windward side, while inconsistency could be observed in the leeward sides of the model, overall, could be termed as good results.

3.4 Summary

Numerical modelling and validation were performed in this chapter. To validate the numerical wind tunnel (RWIND), physical wind tunnel data of a particular structure was extracted from a study by Dagneu et al., (2009). The numerical model was done similarly to the study, 33 times of structure width (B) along the streamwise direction and 20 times of structure width (B) normal to the wall were the dimensions of the wind tunnel. The dimension of the full-scale model was 100 ft in length, 150 ft in width, and 600 ft in height. For validation purposes, the k-epsilon turbulence model and a similar wind profile were used. Results from the wind tunnel test indicate closer results compared to the physical windward test data in the windward face. However, fluctuations were observed on the leeward side within a threshold limit of around 10~15%.

CHAPTER 04

RESULTS ANALYSIS AND DISCUSSIONS

4.1 Introduction

Wind pressure coefficients (C_p) are influenced by various parameters, including building geometry, facade detailing, position on the facade, the degree of exposure/sheltering, wind speed, and wind direction (D.Cóstola et al., 2009). As it is practically impossible to consider the full complexity of pressure coefficient variation, relatively simplified methods are appreciable. Model of different heights was considered as the wind pressure coefficient depends on the boundary condition. Models of different lengths, widths, and heights were assessed to understand the effect of geometric properties in determining the wind pressure coefficient.

This study emphasized numerical models to conclude with empirical equations to predict the relatively accurate value of the pressure coefficient. The main approach was to use a variable pressure coefficient at a variable height of the structures and reach closer with respect to the numerical wind tunnel.

4.2 Comparison of Story Shear Due to Wind Force

A comparison was conducted as a part of this study between the wind force evaluating standards such as ASCE 7-05, UBC 94, BNBC 2006, BNBC 2020, and the equivalent numerical wind tunnel to some of these standards, especially the BNBC 2006 and the BNBC 2020. The wind speed profile was collected from these standards in the equivalent numerical wind tunnel simulation.

Main Wind Force Resisting System (MWFRS) is defined as “an assemblage of structural elements to provide support and stability for the overall structure.” Typically, members who receive loading from two surfaces are designed to resist MWFRS loading. For example, consider a moment-resisting frame building with a roof and wall panels as figure 3.6. Engineers would design the moment frames and the spread footings at the base of the frames to resist MWFRS loading from the lateral wind pressure on the wall panels and positive/negative wind pressure on the roof panels. Size, thickness, stiffness of the structural components such as beam, column, slab do not influence the wind pressure

coefficient, but the geometric properties of the whole system such as length, width, and height of the system.

Six to ten storied buildings are commonly seen in the major cities in Bangladesh. Newly constructed buildings are crossing the conventional height and are in a race of being the tallest one. The latest addition in the race is the Bangabandhu Iconic Tri-Tower, with three skyscrapers of Fifty-one, Seventy-one, and one hundred and eleven storied buildings. Moreover, the Purbachal development project will include 38 more buildings ranging from 35 to 50 stories (The Business Standard , 2021).

Four models with four different story heights were used to analyse and simulate the wind effect in this study. A six storied, a ten storied, a twenty storied, and a forty storied building were modelled. Geometric properties, wind loading considerations according to codes, results are presented below.

4.2.1 Six Storied Regular Shape Building

Figure 4.1 represents the Main Wind Force Resisting System (MWFRS) with six floors modelled in ETABS. The structure's total height is 62 feet, where the bottom story is 12 feet, and the typical story height is 10 feet. The length and width of the structure are 50 feet and 40 feet, respectively.

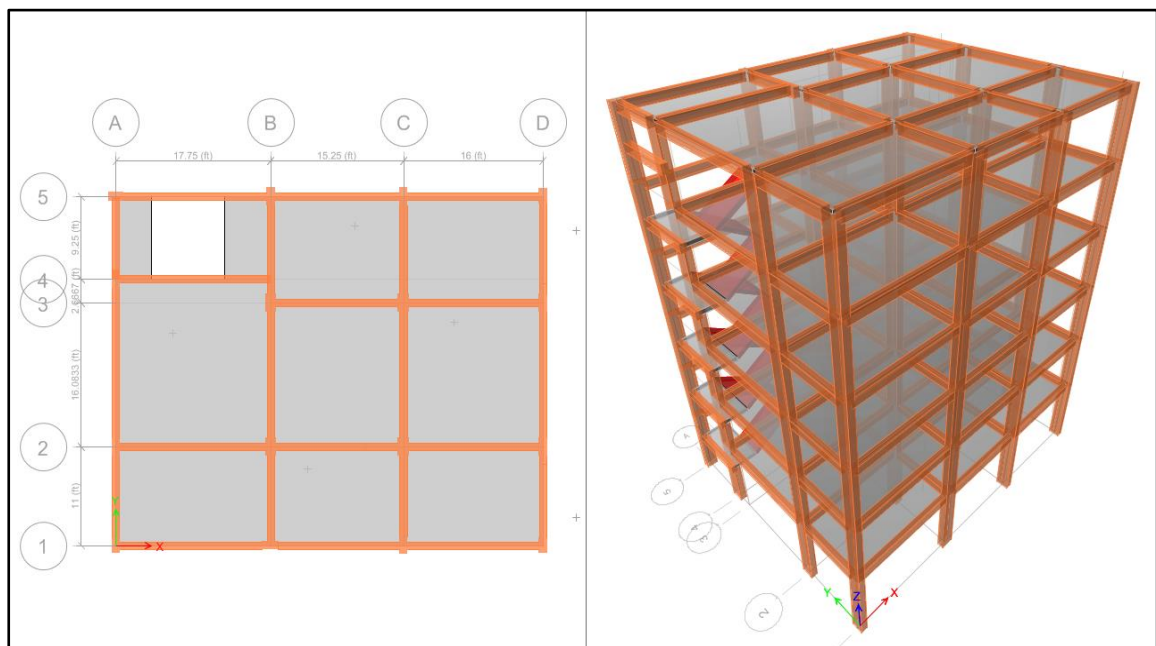


Figure 4.1: Six Storied Building

4.2.1.1 Building Parameters According to BNBC-2006

The basic wind speed for the model was considered as 130 mph with the exposure category B and the return period of 50 years. Depending on the geometric properties of the model, the calculated overall wind pressure coefficients were found to be 1.74 and 1.98 for short and long directions, respectively.

4.2.1.2 Building parameters According to BNBC-2020

The basic wind speed for the model was considered as 147 mph with the exposure category B and the return period of 50 years. Moreover, the wind gust coefficient and the directionality factor were 0.85. Depending on the geometric properties of the model, the calculated overall wind pressure coefficients were found to be 0.8 in the windward surface, and for the leeward surface, 0.45 and 0.50 were found in short and long directions, respectively.

4.2.1.3 Pressure Co-efficient from Numerical Wind Tunnel Test (NWTT)

A numerical wind tunnel test illustrated a graphical contours image of the wind pressure coefficient to visualize the various similar values on the surfaces of the simulated model. Figure 4.2 represents the pressure coefficient contours in the windward wall and sidewall of the six storied building in numerical wind tunnel test.

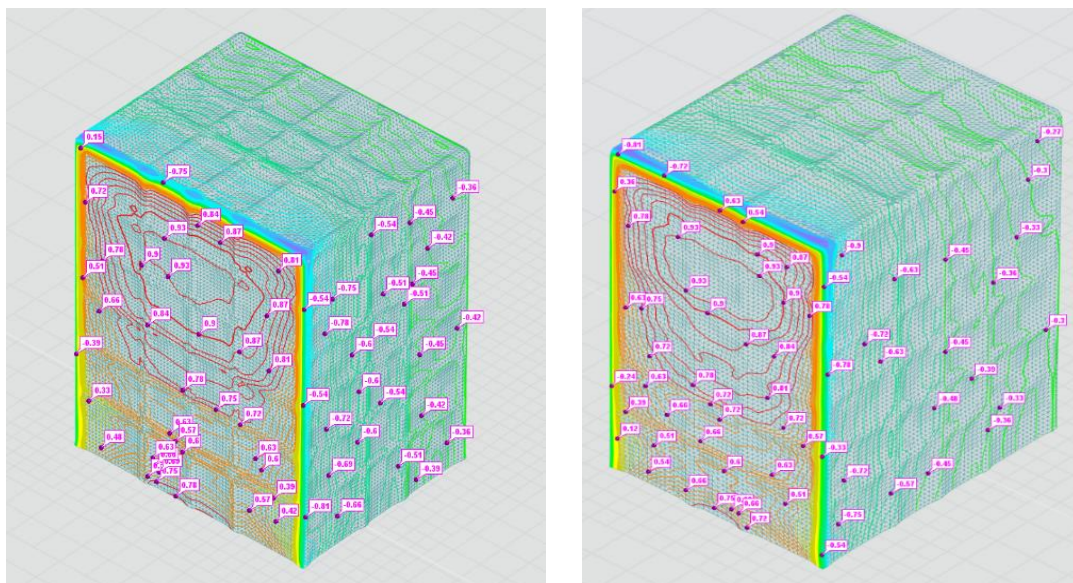


Figure 4.2: Contours of C_p in windward wall and side wall of the six storied building in the numerical wind tunnel test

The comparison of the story shear of the six storied-building in both directions can be seen in Figures 4.3 and 4.4. Up to the first story, the story shear was found to have an almost linearly proportional relationship with the height; story shear increased with an increase in height. Above that, the relationship is reversed; the story shear decreased with an increase in height.

BNBC-2020 and ASCE 7-05 showed similarity in determining the wind pressure coefficient; story-wise variation between the codes was found to be ranging from 0.55 to 1.36 percent with a mean variation of 1.08 percent in the long direction, while the variation range was 0.48 to 1.43 percent with a mean variation of 1.06 percent in the short direction, as shown in Figure 4.3 and Figure 4.4. On the other hand, BNBC-2006 and UBC- 94 had similar results with a story-wise variation ranging from 0.15 to 1.64 percent with a mean variation of 0.16 percent in the long direction, while the variation range was 0.21 to 2.14 percent with a mean variation of 0.67 percent in the short direction.

As observed from Figures 4.3 and 4.4, BNBC-2020 and BNBC-2006 showed a considerable variation in calculating the wind pressure coefficient. The story-wise variation ranged from 49.96 to 53.52 percent with a mean variation of 51.36 percent in the long direction, while the variation range was 45.67 to 49.44 percent with a mean variation of 47.14 percent in the short direction. The numerical wind tunnel for the BNBC 2020 showed relatively small variation with the BNBC-2020 manual with respect to what the numerical wind tunnel for the BNBC 2006 showed with the BNBC-2006 manual.

Story-wise variation of wind pressure coefficient between the numerical wind tunnel of BNBC 2020 with the BNBC-2020 manual calculation ranged from 15.30 to 25.59 percent in the long direction with a mean of 19.51 percent and 12.8 to 22.45 percent with a mean of 16.74 percent in the short direction. While the variation between the numerical wind tunnel of BNBC 2006 with the BNBC-2006 manual calculation ranged from 40.92 to 45.29 percent in the long direction with a mean of 43.15 percent and 33.77 to 38.36 percent with a mean of 36.17 percent in the short direction.

For detailed data, the Appendix-A of this paper was recommended.

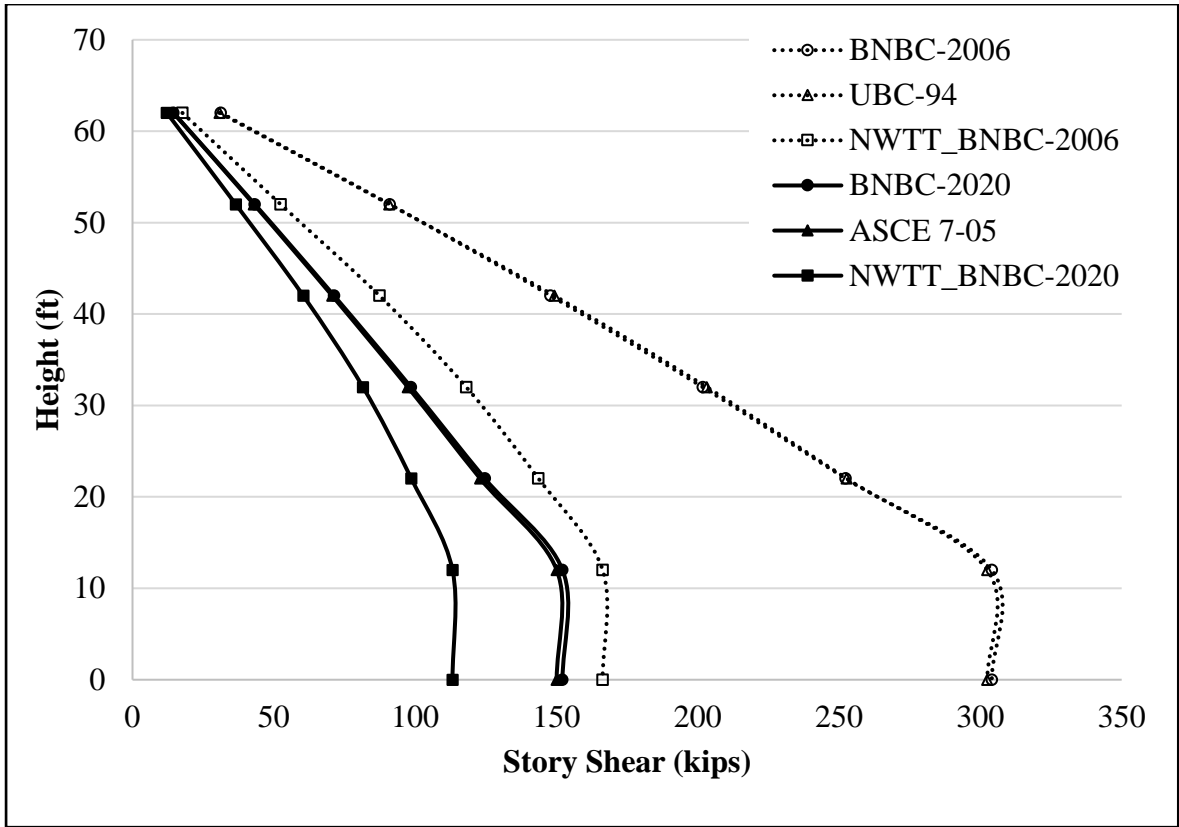


Figure 4.3: Comparison of story shear of the six storied building in the long direction

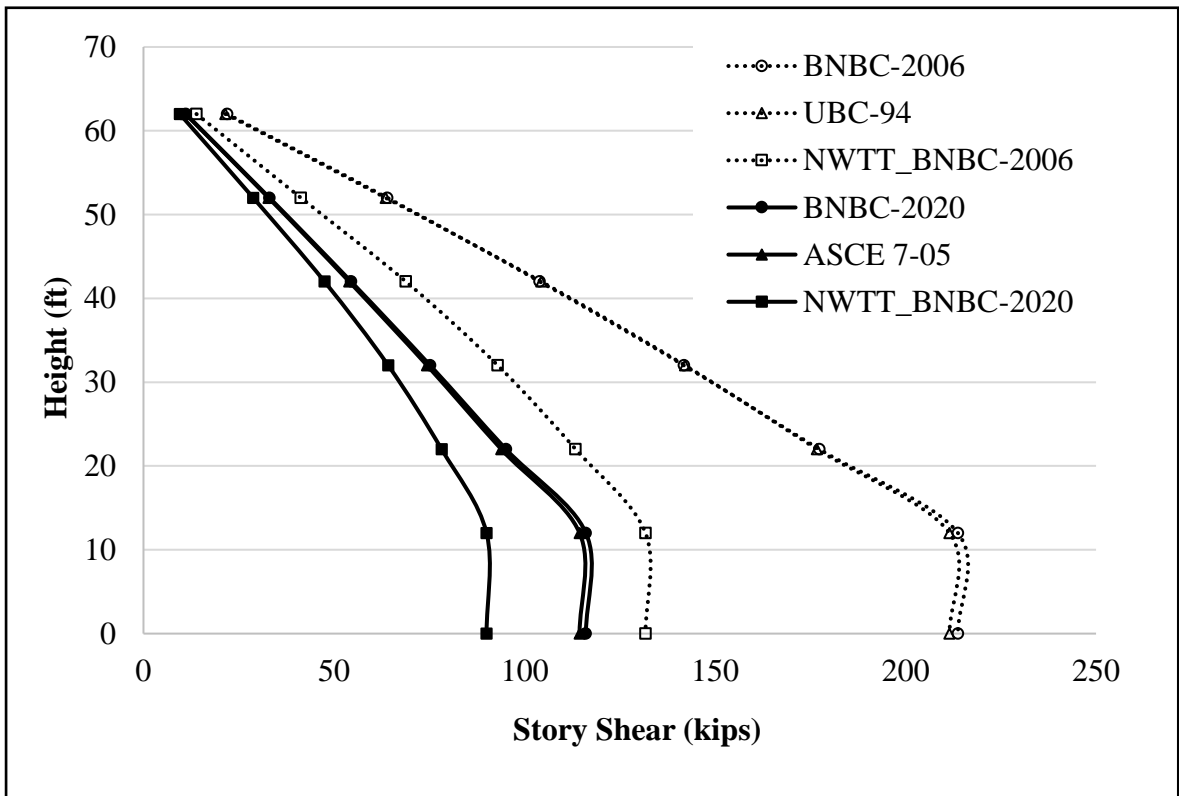


Figure 4.4: Comparison of story shear of the six storied building in the short direction

4.2.2 Ten Storied Regular Shape Building

Figure 4.5 represents a Main Wind Force Resisting System (MWFRS) with ten floors modelled in ETABS. The structure's total height is 100 feet, where the typical story height is 10 feet. The length and width of the structure are 75 feet and 50 feet, respectively.

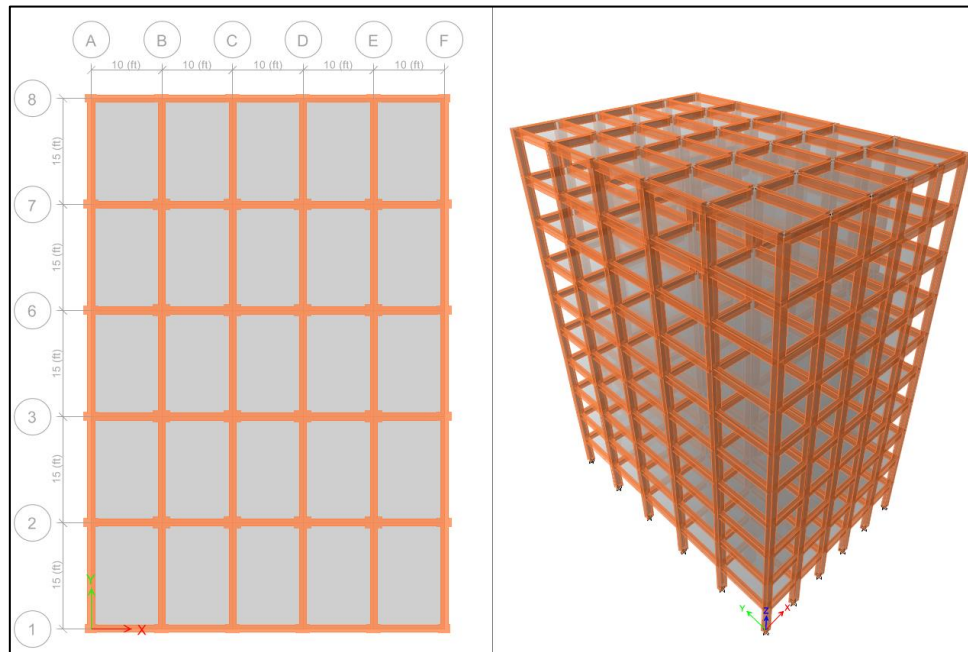


Figure 4.5: Ten Storied Building

4.2.2.1 Building Parameters According BNBC-2006

The basic wind speed for the model was considered as 130 mph with the exposure category A and the return period of 50 years. Depending on the geometric properties of the model, the calculated overall wind pressure coefficients were found to be 1.70 and 2.17 for short and long directions, respectively.

4.2.2.2 Building Parameters According to BNBC-2020

The basic wind speed for the model was considered as 147 mph with exposure category A and the return period of 50 years. The wind gust coefficients were 0.906 and 0.889 for short and long directions, respectively. Moreover, the directionality factor was 0.85. Depending on the geometric properties of the model, the calculated overall wind pressure coefficients were found to be 0.8 in the windward surface, and for the leeward surface, 0.40 and 0.50 were found in short and long directions, respectively.

4.2.2.3 Pressure Co-efficient from Numerical Wind Tunnel Test for Ten Storied Building

A numerical wind tunnel test illustrated a graphical contours image of the wind pressure coefficient to visualize the various similar values on the surfaces of the simulated model. Figure 4.6 represent the pressure coefficient contours in the windward wall and sidewall of the ten storied building in the numerical wind tunnel test.

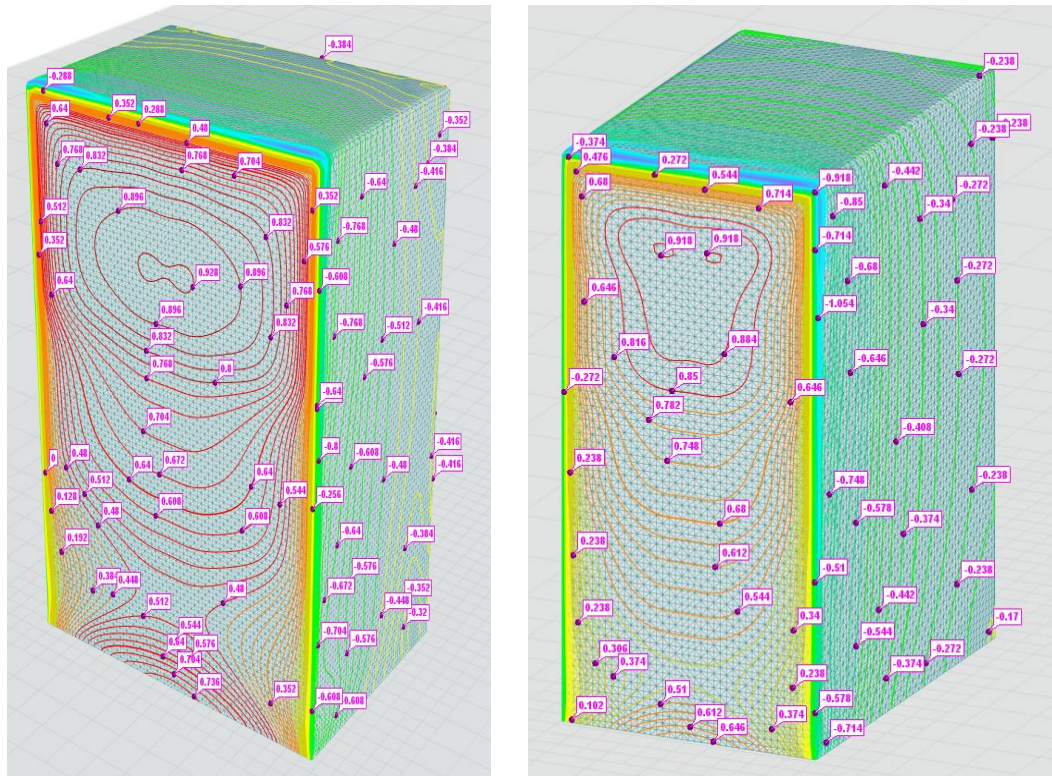


Figure 4.6: Contours of C_p in windward wall and sidewall of the ten storied building in the numerical wind tunnel test

The comparison of the story shear of the ten storied-building in both directions can be seen in Figures 4.7 and 4.8. Up to the first floor, it was found that the story shear is almost linearly proportional to the height. Story shear increased with an increase in height. On top of that, the relationship is reversed. Story shear decreased with an increase in height.

BNBC-2020 and ASCE 7-05 showed similarity in determining the wind pressure coefficient. The story-by-story variability between the codes ranged from 0.61 to 1.56 percent with an average variation of 1.16 percent in the long direction, while it was 0.65 to 1.71 percent and the average variation was 1.26 percent in the short direction as shown in Figure 4.7 and Figure 4.8. On the other hand, BNBC-2006 and UBC- 94 had similar results with a story-wise variation ranged from 0.18 to 4.32 percent with a mean variation of 0.48

percent in the long direction, while the variation range was 0.17 to 4.33 percent with a mean variation of 0.47 percent in the short direction.

As observed from Figures 4.7 and 4.8, BNBC-2020 and BNBC-2006 showed significant fluctuations in calculating the wind pressure coefficient. The story-wise variation ranged from 43.59 to 51.56 percent with a mean variation of 47.20 percent in the long direction, while the variation range was 32.92 to 41.85 percent with a mean variation of 36.91 percent in the short direction. The numerical wind tunnel for the BNBC 2020 showed relatively small fluctuations with the BNBC-2020 manual with respect to what the numerical wind tunnel for the BNBC 2006 showed with the BNBC-2006 manual.

Story-wise variation of wind pressure coefficient between the numerical wind tunnel of BNBC 2020 with the BNBC-2020 manual, ranged from 22.15 to 34.62 percent in the long direction with a mean of 28.33 percent and 26.93 to 37.75 percent with a mean of 31.65 percent in the short direction. While the variation between the numerical wind tunnel of BNBC 2006 with the BNBC-2006 manual, ranged from 49.38 to 58.05 percent in the long direction with a mean of 52.49 percent and 43.97 to 49.69 percent with a mean of 46.49 percent in the short direction.

For detailed data, the Appendix-B of this paper was recommended.

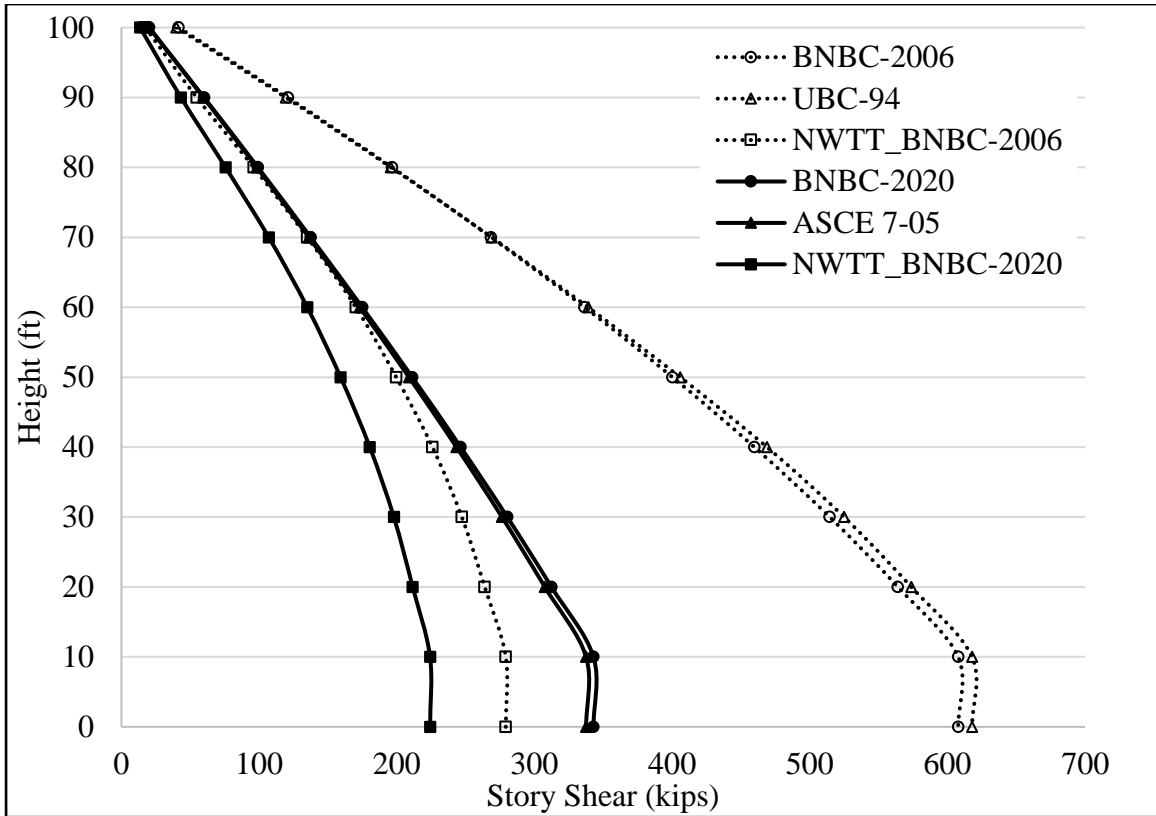


Figure 4.7: Comparison of story shear of the ten storied building in the long direction

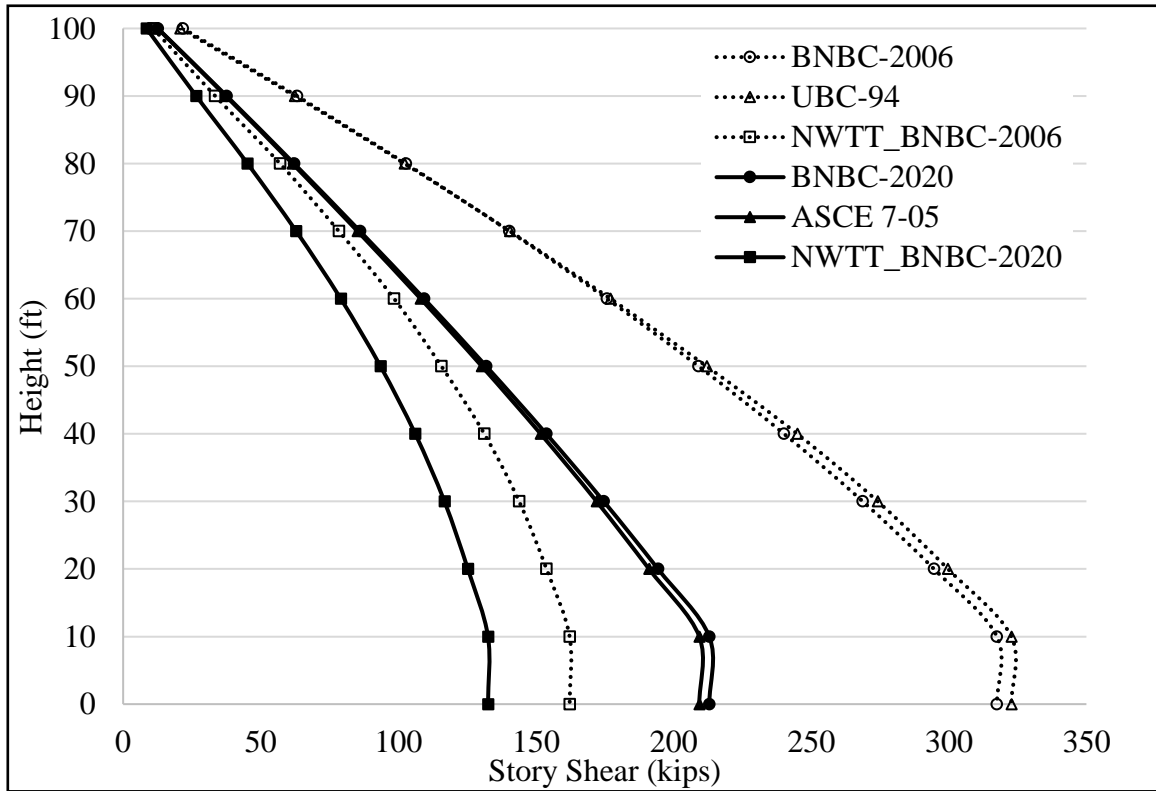


Figure 4.8: Comparison of story shear of the ten storied building in the short direction

4.2.3 Twenty Storied Regular Shape Building

Figure 4.9 represents a Main Wind Force Resisting System (MWFRS) with twenty floors modelled in ETABS. The structure's total height is 200 feet, where the typical story height is 10 feet. The length and width of the structure are 140 feet and 76 feet, respectively.

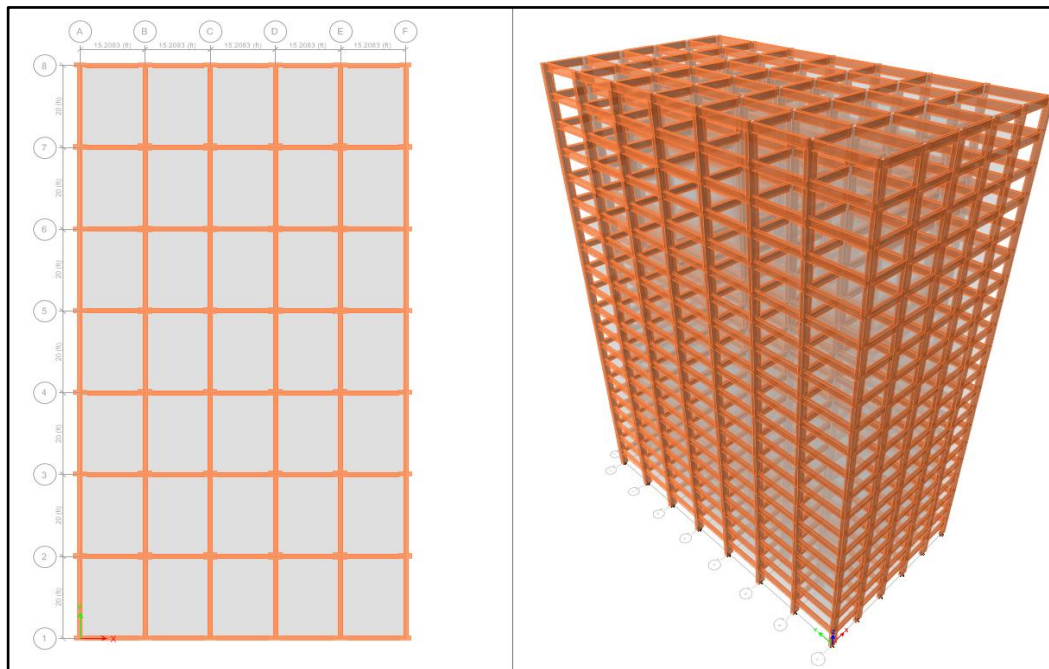


Figure 4.9: Twenty Storied Building

4.2.3.1 Building Parameters According BNBC-2006

The basic wind speed for the model was considered as 130 mph with the exposure category A and the return period of 50 years. Depending on the geometric properties of the model, the calculated overall wind pressure coefficients were found to be 2.08 and 1.56 for short and long directions, respectively.

4.2.3.2 Building Parameters According to BNBC-2020

The basic wind speed for the model was considered as 147 mph with exposure category A and the return period of 50 years. The wind gust coefficients were 0.903 and 0.932 for short and long directions, respectively. Moreover, the directionality factor was 0.85. Depending on the geometric properties of the model, the calculated overall wind pressure coefficients

were found to be 0.8 in the windward surface, and for the leeward surface, 0.33 and 0.50 were found in short and long directions, respectively.

4.2.3.3 Pressure Co-efficient from Numerical Wind Tunnel Test for Twenty Storied Building

A numerical wind tunnel test illustrated a graphical contours image of the wind pressure coefficient to visualize the various similar values on the surfaces of the simulated model. Figure 4.10 represent the pressure coefficient contours in the windward wall and sidewall of the twenty storied building in the numerical wind tunnel test.

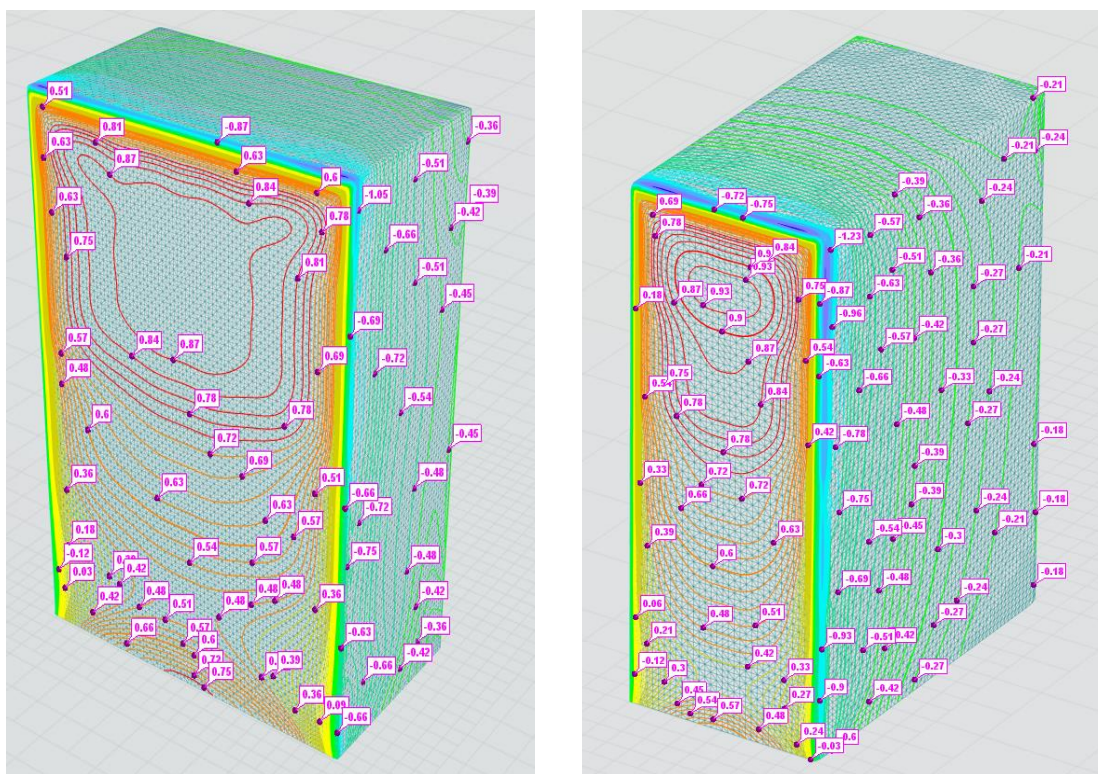


Figure 4.10: Contours of C_p in windward wall and sidewall of the twenty storied building in numerical wind tunnel test

The comparison of the story shear of the twenty storied-building in both directions can be seen in Figures 4.11 and 4.12. Up to the first story, the story shear was found to have an almost linearly proportional relationship with the height; story shear increased with an increase in height. Above that, the relationship is reversed; the story shear decreased with an increase in height.

BNBC-2020 and ASCE 7-05 showed similarity in determining the wind pressure coefficient; story-wise variation between the codes was found to be ranging from 0.30 to 0.95 percent with a mean variation of 0.62 percent in the long direction, while the variation range was 0.42 to 1.22 percent with a mean variation of 0.81 percent in the short direction as shown in Figure 4.11 and Figure 4.12. On the other hand, BNBC-2006 and UBC- 94 had relatively similar results with a story-wise variation ranged from 5.89 to 23.06 percent with a mean variation of 11.41 percent in the long direction, while the variation range was 5.84 to 23.02 percent with a mean variation of 11.36 percent in the short direction.

As observed from Figures 4.11 and 4.12, BNBC-2020 and BNBC-2006 showed a considerable variation in calculating the wind pressure coefficient. The story-wise variation ranged from 45.91 to 59.96 percent with a mean variation of 52.31 percent in the long direction, while the variation range was 36.51 to 52.05 percent with a mean variation of 43.40 percent in the short direction. The numerical wind tunnel for the BNBC 2020 showed relatively small variation with the BNBC-2020 manual with respect to what the numerical wind tunnel for the BNBC 2006 showed with the BNBC-2006 manual.

Story-wise variation of wind pressure coefficient between the numerical wind tunnel of BNBC 2020 with the BNBC-2020 manual, ranged from 23.59 to 40.11 percent in the long direction with a mean of 30.08 percent and 27.50 to 42.90 percent with a mean of 33.42 percent in the short direction. While the variation between the numerical wind tunnel of BNBC 2006 with the BNBC-2006 manual, ranged from 51.42 to 64.40 percent in the long direction with a mean of 54.00 percent and 48.40 to 60.35 percent with a mean of 50.68 percent in the short direction.

For detailed data, the Appendix-C of this paper was recommended.

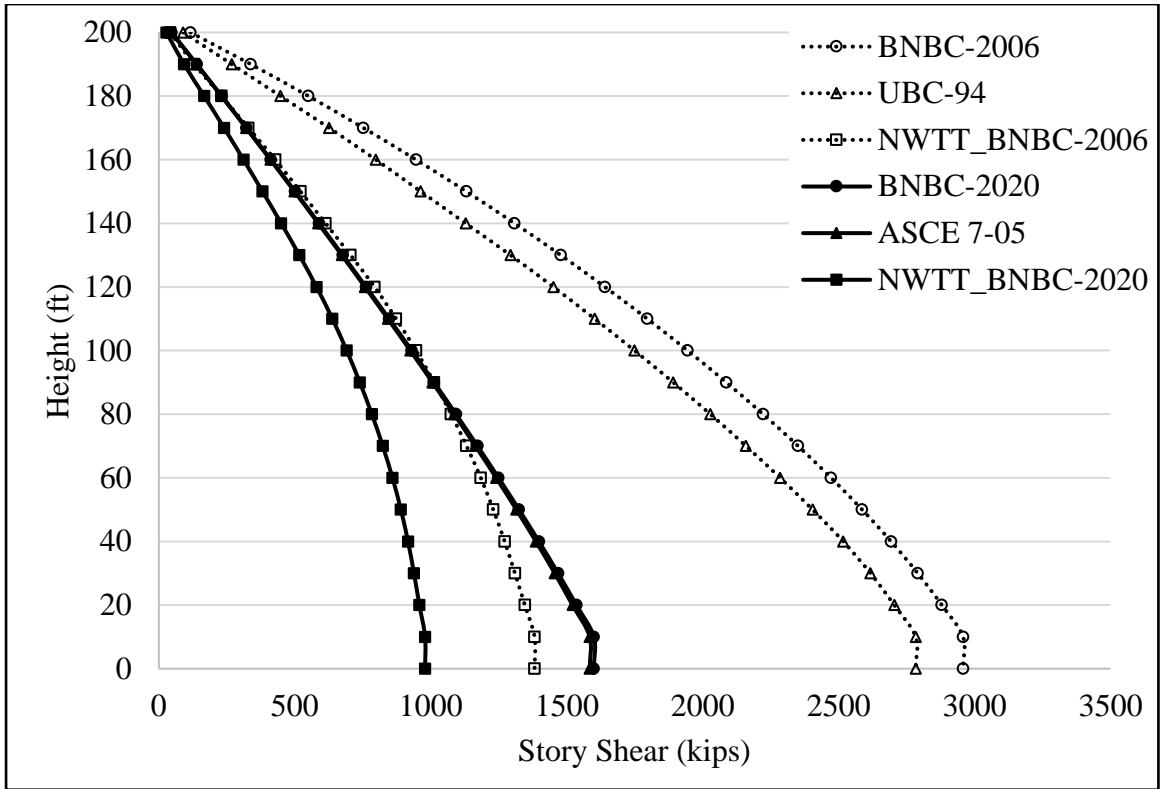


Figure 4.11: Comparison of story shear of the twenty storied building in the Long direction

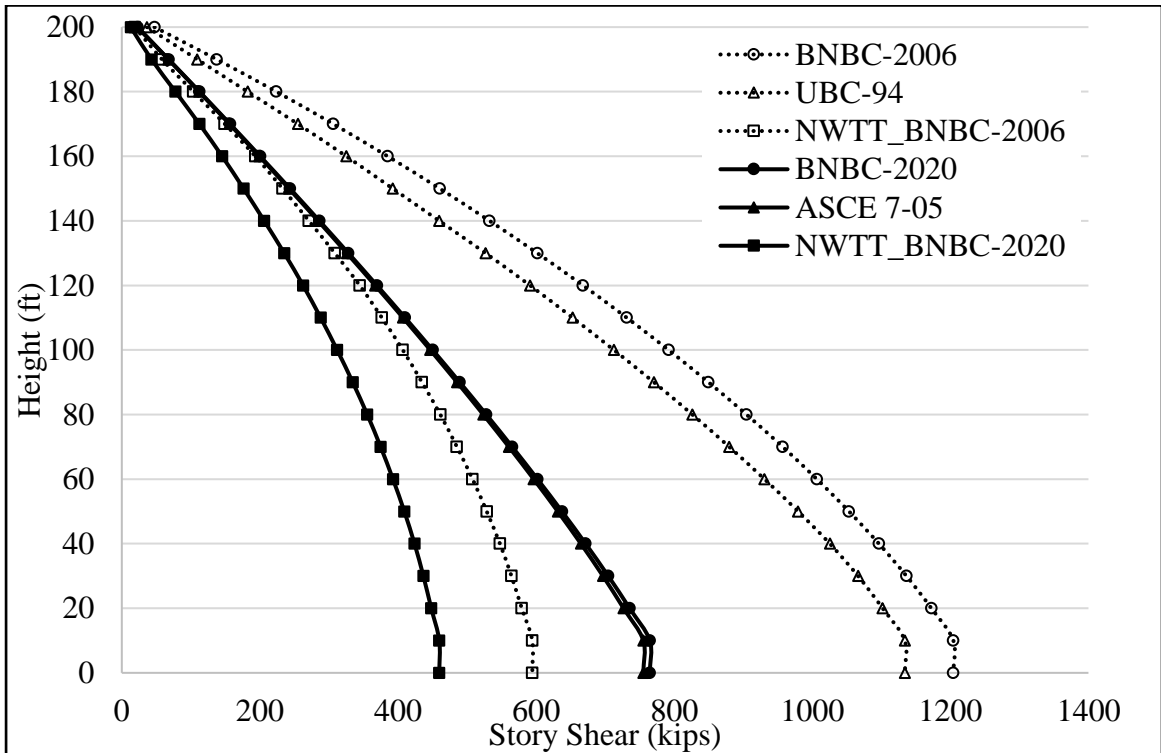


Figure 4.12: Comparison of story shear of the twenty storied building in the Short direction

4.2.4 Forty Storied Regular Shape Building

Figure 4.12 represents a Main Wind Force Resisting System (MWFRS) with forty floors modelled in ETABS. The structure's total height is 400 feet, where the typical story height is 10 feet. The length and width of the structure are 120 feet and 80 feet, respectively.

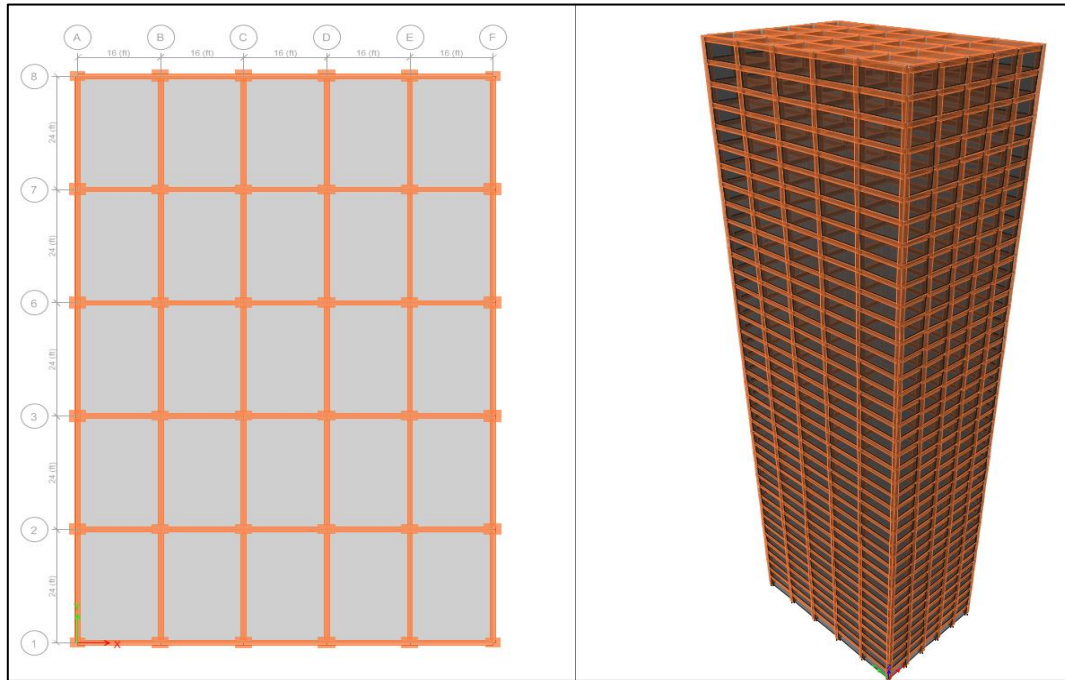


Figure 4.13: Forty Storied Building

4.2.4.1 Building Parameters According BNBC-2006

The basic wind speed for the model was considered as 130 mph with the exposure category A and the return period of 50 years. Depending on the geometric properties of the model, the calculated overall wind pressure coefficients were found to be 1.90 and 2.67 for short and long directions, respectively.

4.2.4.2 Building Parameters According to BNBC-2020

The basic wind speed for the model was considered as 147 mph with exposure category A and the return period of 50 years. The wind gust coefficients were 1.000 and 0.989 for short and long directions, respectively. Moreover, the directionality factor was 0.85. Depending on the geometric properties of the model, the calculated overall wind pressure coefficients

were found to be 0.8 in the windward surface, and for the leeward surface, 0.40 and 0.50 were found in short and long directions, respectively.

4.2.4.3 Pressure Co-efficient from Numerical Wind Tunnel Test for Forty Storied Building

A numerical wind tunnel test illustrated a graphical contours image of the wind pressure coefficient to visualize the various similar values on the surfaces of the simulated model. Figure 4.14 represent the pressure coefficient contours in the windward wall and sidewall of the forty storied building in the numerical wind tunnel test.

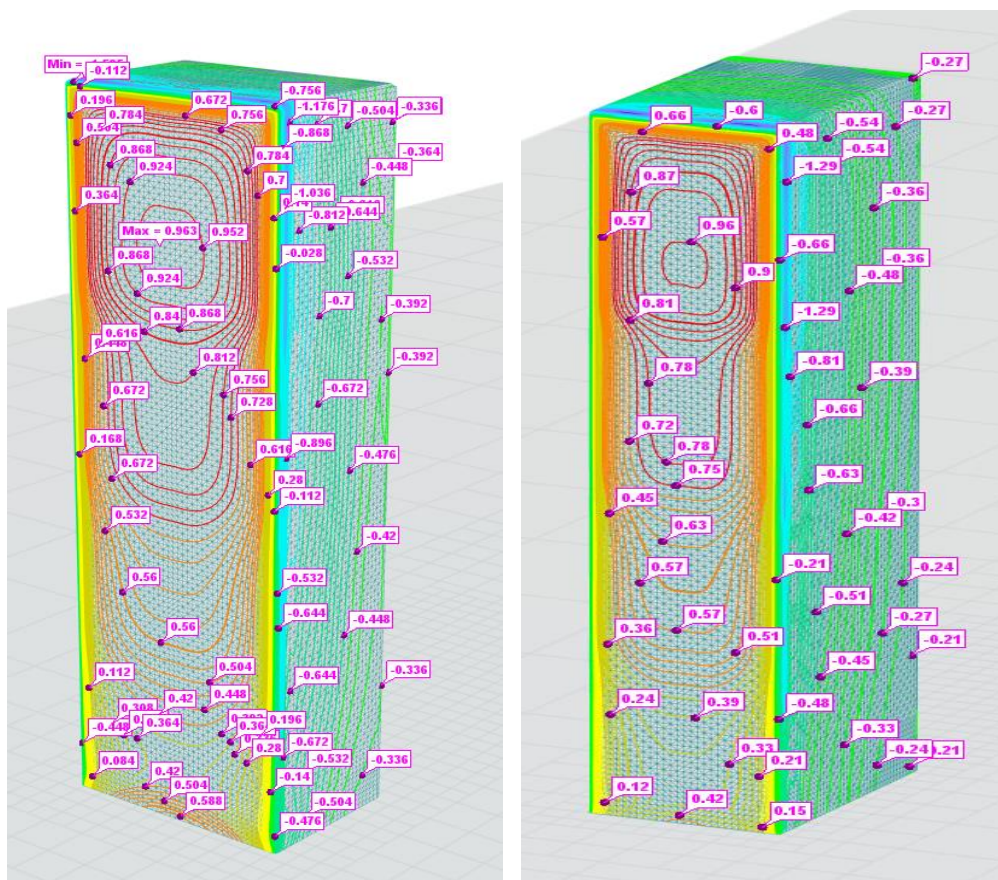


Figure 4.14: Contours of C_p in windward wall and sidewall of the forty storied building in numerical wind tunnel test

The comparison of the story shear of the forty storied-building in both directions can be seen in Figures 4.15 and 4.16. Up to the first story, the story shear was found to have an almost linearly proportional relationship with the height; story shear increased with an increase in height. Above that, the relationship is reversed; the story shear decreased with an increase in height.

BNBC-2020 and ASCE 7-05 showed similarity in determining the wind pressure coefficient; story-wise variation between the codes was found to be ranging from 0.15 to 0.55 percent with a mean variation of 0.32 percent in the long direction, while the variation range was 0.14 to 0.60 percent with a mean variation of 0.34 percent in the short direction as shown in Figure 4.15 and Figure 4.16. On the other hand, BNBC-2006 and UBC- 94 had similar results with a story-wise variation ranged from 0.98 to 6.79 percent with a mean variation of 5.52 percent in the long direction, while the variation range was 0.99 to 6.79 percent with a mean variation of 5.52 percent in the short direction.

As observed from Figures 4.15 and 4.16, BNBC-2020 and BNBC-2006 showed a considerable variation in calculating the wind pressure coefficient. The story-wise variation ranged from 50.01 to 56.88 percent with a mean variation of 53.99 percent in the long direction, while the variation range was 35.23 to 43.46 percent with a mean variation of 39.96 percent in the short direction. The numerical wind tunnel for the BNBC 2020 showed relatively small variation with the BNBC-2020 manual with respect to what the numerical wind tunnel for the BNBC 2006 showed with the BNBC-2006 manual.

Story-wise variation of wind pressure coefficient between the numerical wind tunnel of BNBC 2020 with the BNBC-2020 manual, ranged from 22.42 to 47.54 percent in the long direction with a mean of 28.86 percent and 21.96 to 43.46 percent with a mean of 39.96 percent in the short direction. While the variation between the numerical wind tunnel of BNBC 2006 with the BNBC-2006 manual, ranged from 60.87 to 74.21 percent in the long direction with a mean of 63.46 percent and 48.88 to 64.82 percent with a mean of 52.92 percent in the short direction.

For detailed data, the Appendix-D of this paper was recommended.

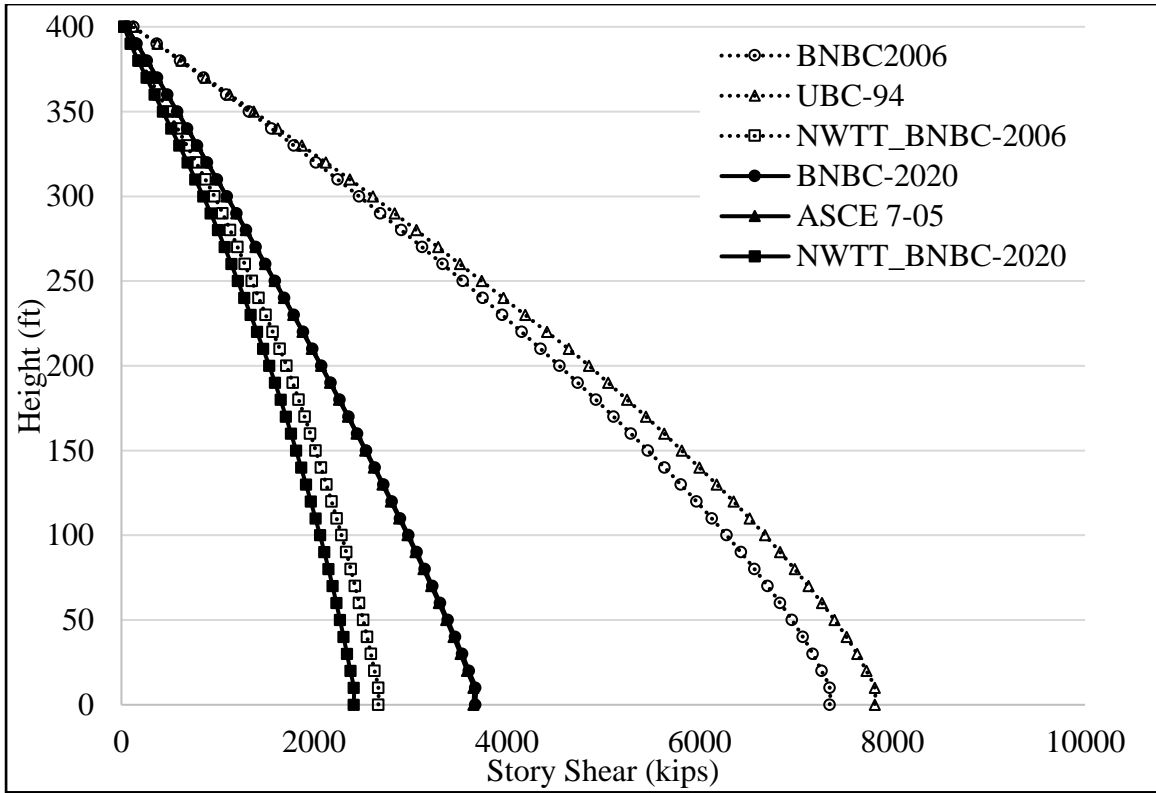


Figure 4.15: Comparison of story shear of the forty storied building in the long direction

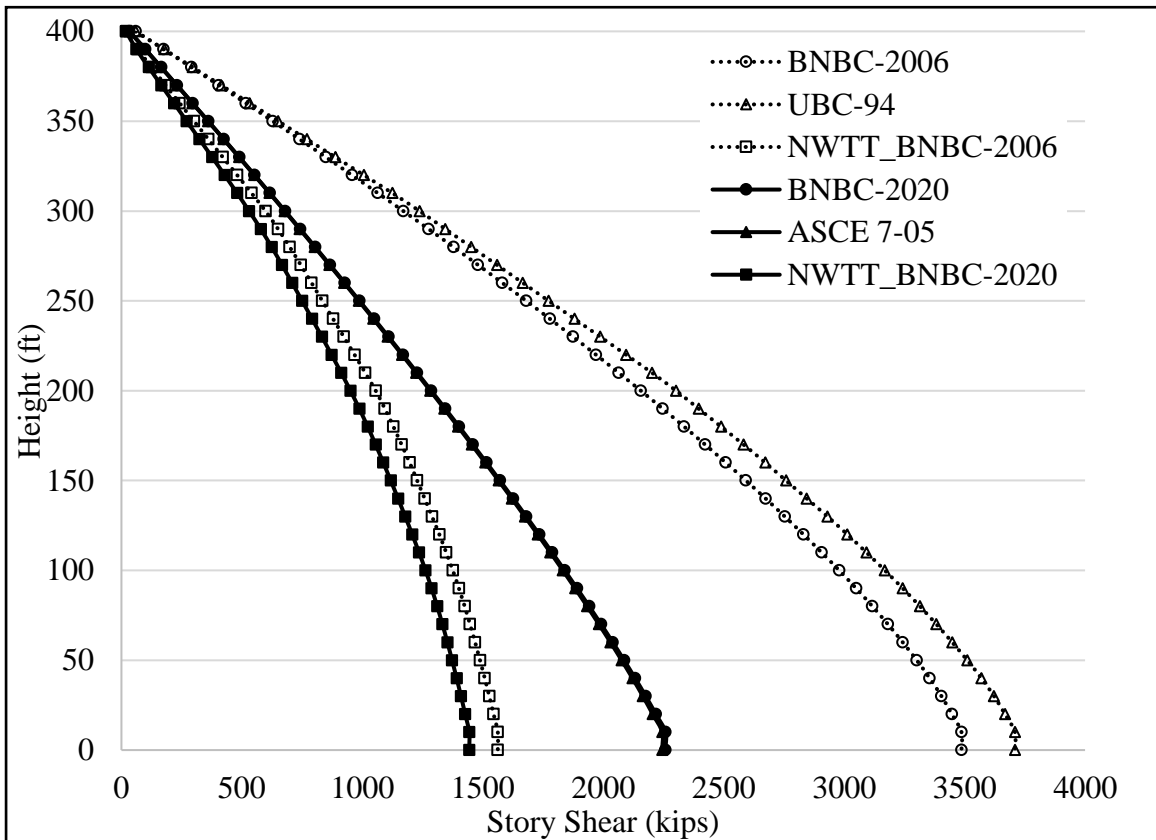


Figure 4.16: Comparison of story shear of the forty storied building in the short direction

4.3 Evaluation of Pressure Coefficient Due to Wind Force

The pressure coefficient depends on a wide range of parameters such as building geometry, facade detailing, position on the facade, the degree of exposure /sheltering, wind speed, and wind direction. Since this study was based on regular-shaped buildings only, the position and detailing of the façade were negligible. Thus, the building geometry became the most important parameter in addition to the attack angle and wind speed and boundary conditions.

A series of twenty flat-roofed rectangular buildings were used in the study, as shown in Table 4.24. The building geometry is described by two ratios (i) the length-width ratio and (ii) the aspect ratio. Length, L is the dimension of the building parallel to wind and the width, B indicates the dimension perpendicular to the wind, and height is denoted as h shown in Figure 4.17.

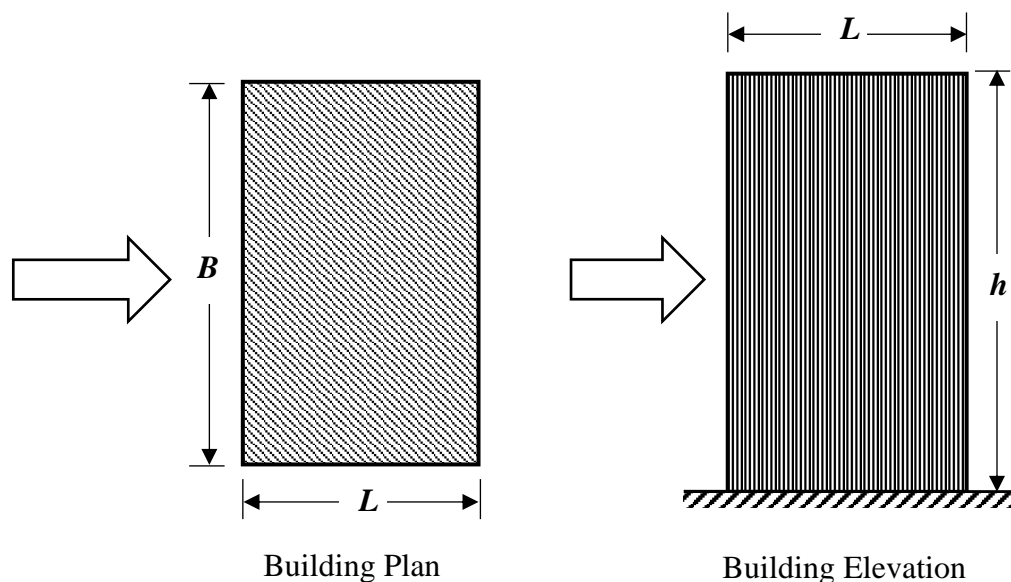


Figure 4.17: Geometry and wind direction of a typical building

The length-width ratio of a structure is one of the determiners of the wind pressure coefficient. In order to study the wind loads on rectangular high-rise buildings, the wind pressures on several rectangular high-rise buildings with various length-to-width ratios (0.5, 0.67, 1.0, 2.0, and 3.0) were tested in a wind tunnel where different categories were simulated. The sectional body shape coefficients with respect to wind azimuth and length-to-width ratio were calculated. The distribution of total body shape coefficients along with wind azimuth and the length-to-width ratio was studied.

Table 4.1: Length-width ratios of structures considered in modelling

Category	L/B is 0.5		L/B is 0.67		L/B is 1.0		L/B is 2.0		L/B is 3.0	
	B	L	B	L	B	L	B	L	B	L
Six Story (h = 60'-0")	60	30	60	40	60	60	60	120	60	180
Ten Story (h = 100'-0")	70	35	75	50	70	70	70	140	70	210
Twenty Story (h = 100'-0")	90	45	90	60	90	90	90	180	90	270
Forty Story (h = 400'-0")	120	60	120	80	120	120	120	240	120	360

The pressure coefficient values on any surface vary from center to edge. Central values are higher, whereas edges values are smaller but depend on length width and aspect ratio. The edge of the structure faces the most turbulence for those who are regular in shape. The surface was divided into five divisions are as follows A1, B1, C, B2, and A2; each division length was considered as 0.2B shown in Figure 4.17. The edge divisions A1 and A2, sub middle portions B1 and B2, were then merged into zone A and B, respectively, due to their characteristics to encounter with the wind flow.

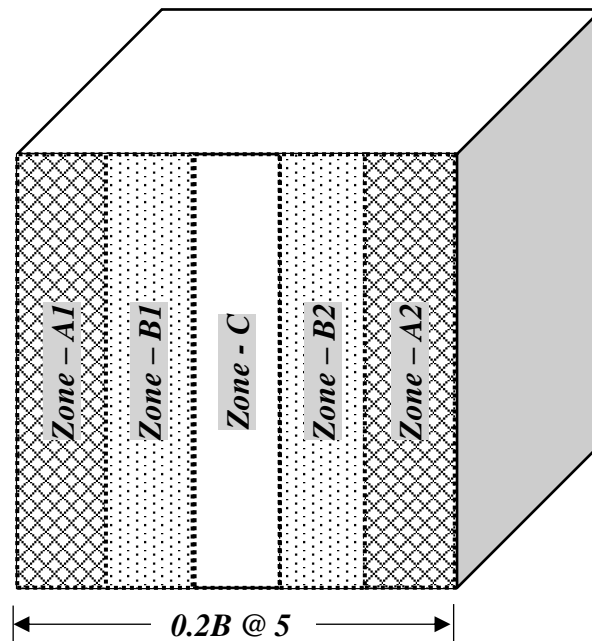


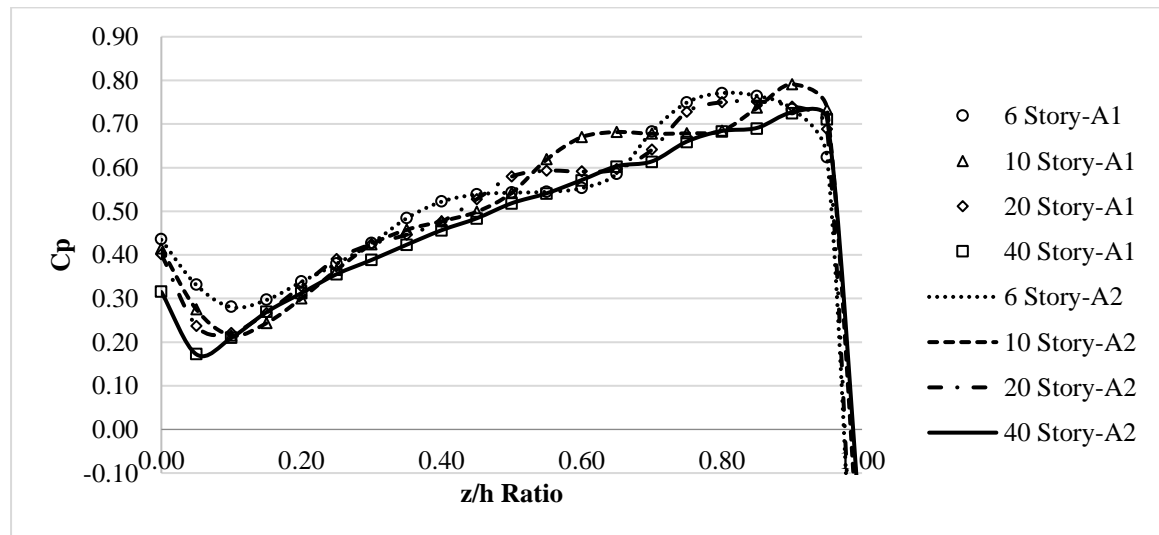
Figure 4.18: Considered zones of a structure

4.3.1 Pressure Coefficient for $L/B = 0.5$

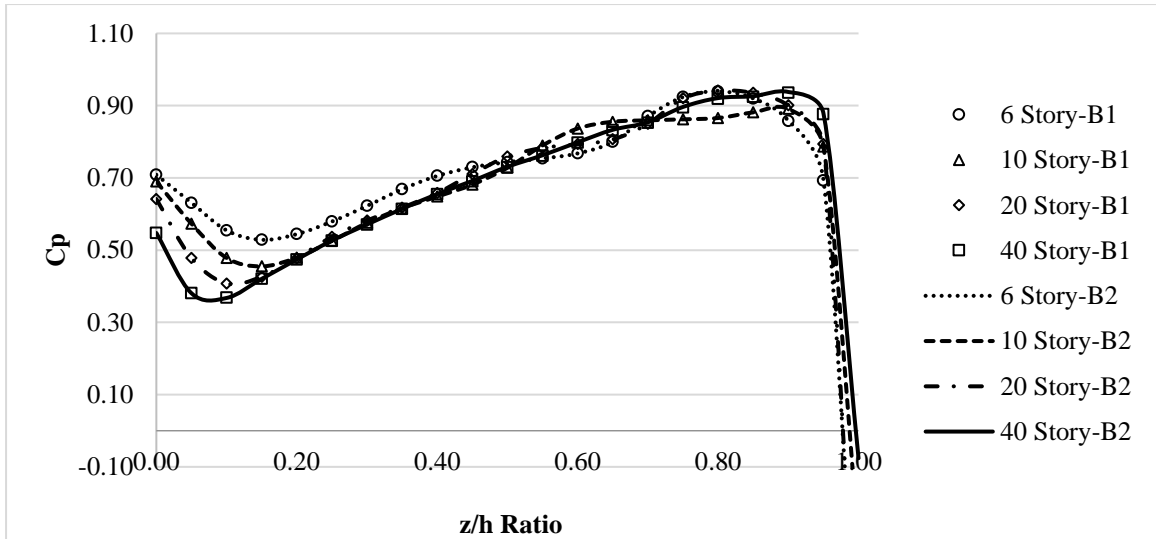
Initially, four buildings were considered with a length-width ratio of 0.5 for wind simulation in the numerical wind tunnel test. Simulated models are provided with the wind pressure coefficient over the zones of the surfaces (windward and leeward).

In the windward direction, the pressure coefficient up to 0.15 z/h ratio decreases from its origin and then increases almost linear proportionally. It becomes a coefficient of back pressure, suction at the top level, or the highest z/h ratio. Figure 4.19 represents the windward pressure coefficient for $L/B = 0.50$.

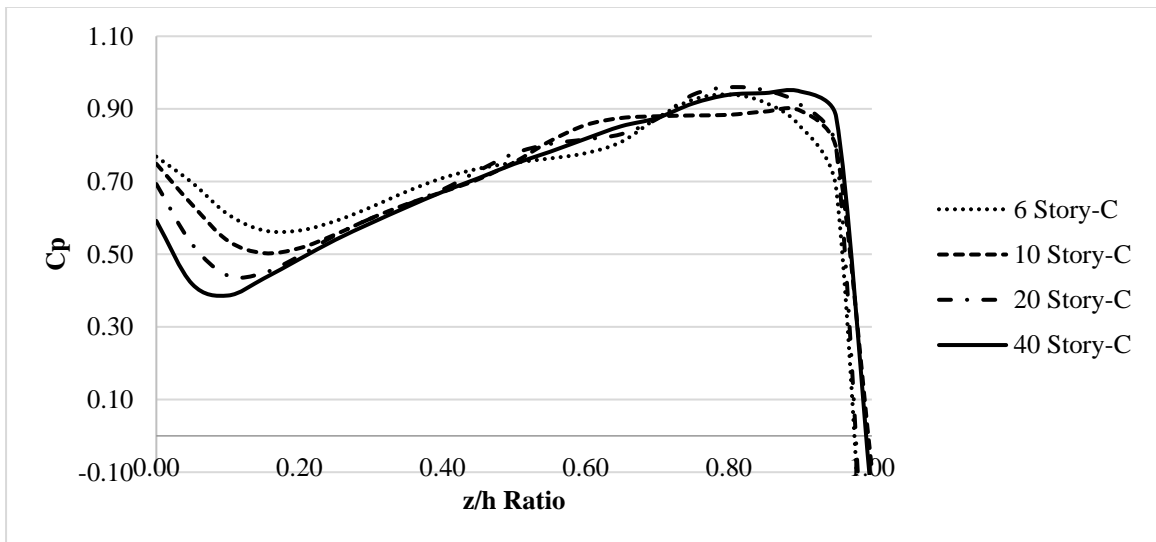
It was found that the C_p values in the windward direction were higher in the middle zone C and then the semi middle zone B edge zone A, respectively. Zone C started with an average value of 0.70, decreased to 0.49, and then before becoming negative, the average maximum was 0.93. While for zone B, the initial average value was 0.65, decreased to 0.45, and the average maximum was 0.92. On the other hand, for zone A, the initial average value was 0.39, decreased to 0.23, and the average maximum was 0.75. For detailed data, Appendix- E was recommended.



(a) Zone A



(b) Zone B



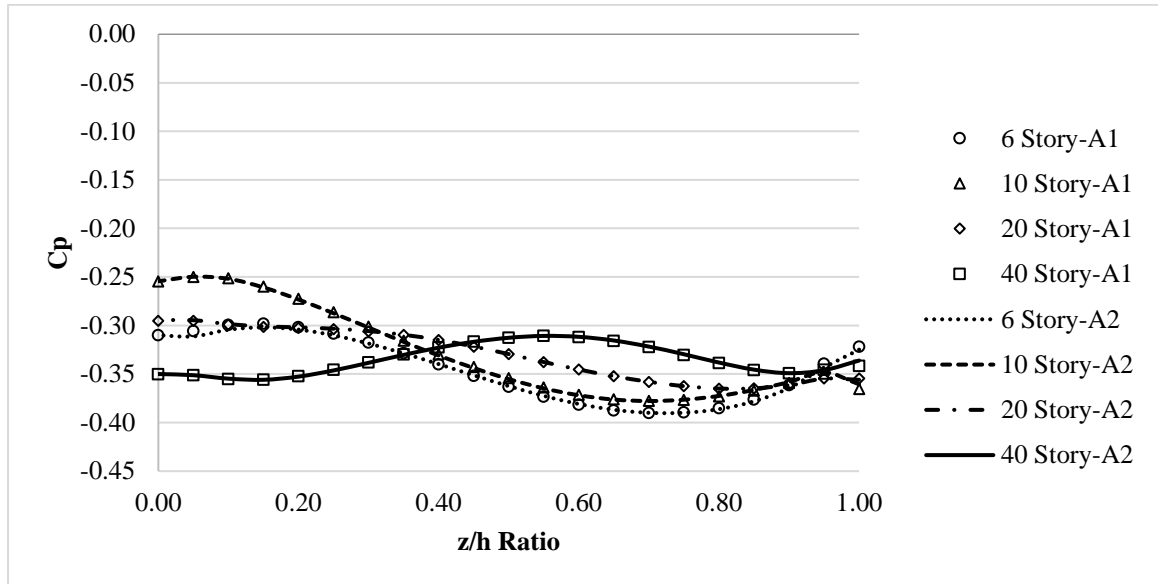
(c) Zone C

Figure 4.19: Windward pressure coefficient for $L/B = 0.50$

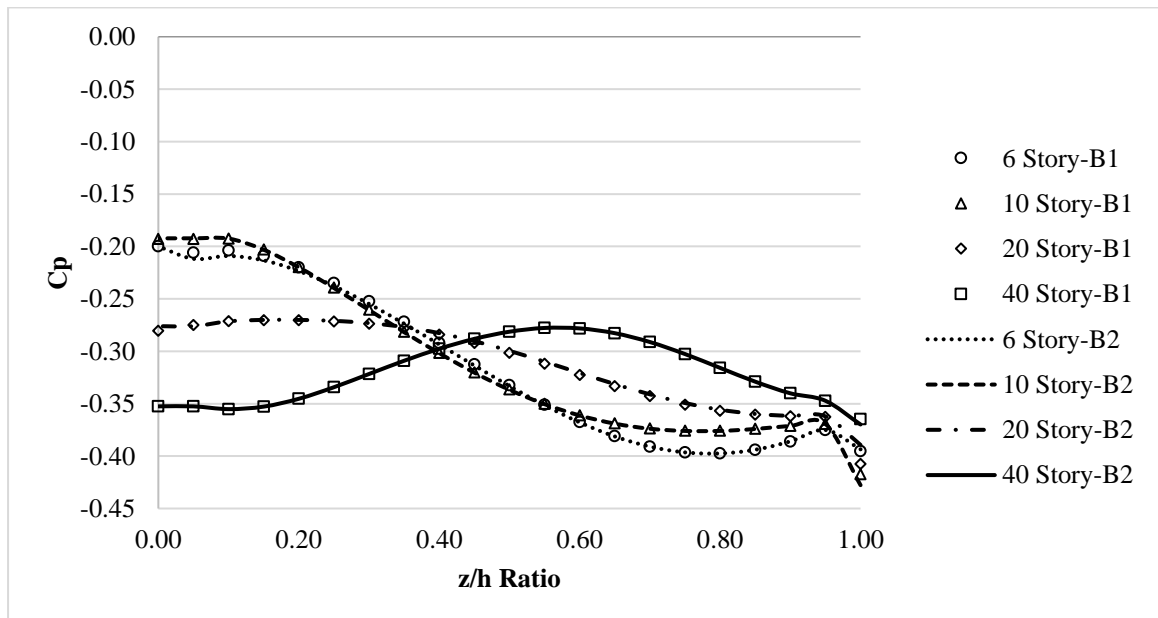
The pressure coefficients were negative as suction pressure acts on the surface in the leeward direction. The C_p values got a pick in the initial stage of the height ratio (z/h ratio), which soon decreased to the end portion of the z/h ratio except for the forty-storied building. Figure 4.20 represents the windward pressure coefficient for $L/B = 0.50$.

C_p values in the leeward direction were higher in the middle zone C and then the semi middle zone B edge zone A, respectively. Zone C had a maximum average C_p value of -0.11, and a minimum C_p value of -0.42. While for zone B, the maximum average C_p value was -0.14, and the minimum C_p value was -0.40. On the other hand, for zone A, the

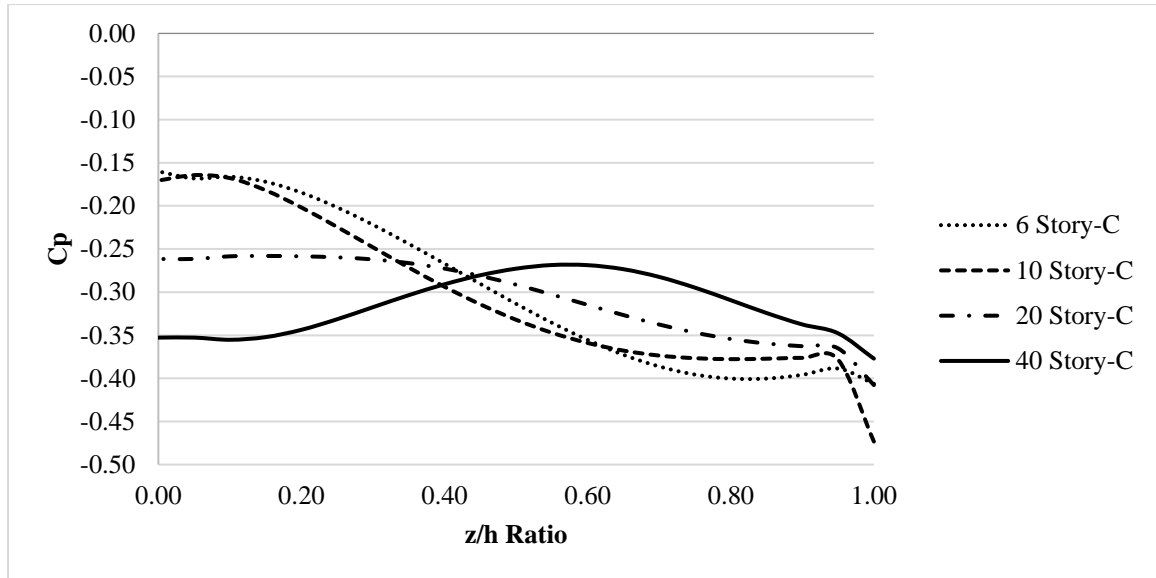
maximum average C_p value was -0.37, and the minimum C_p value was -0.24. For detailed data, Appendix- E was recommended.



(a) Zone A



(b) Zone B



(c) Zone C

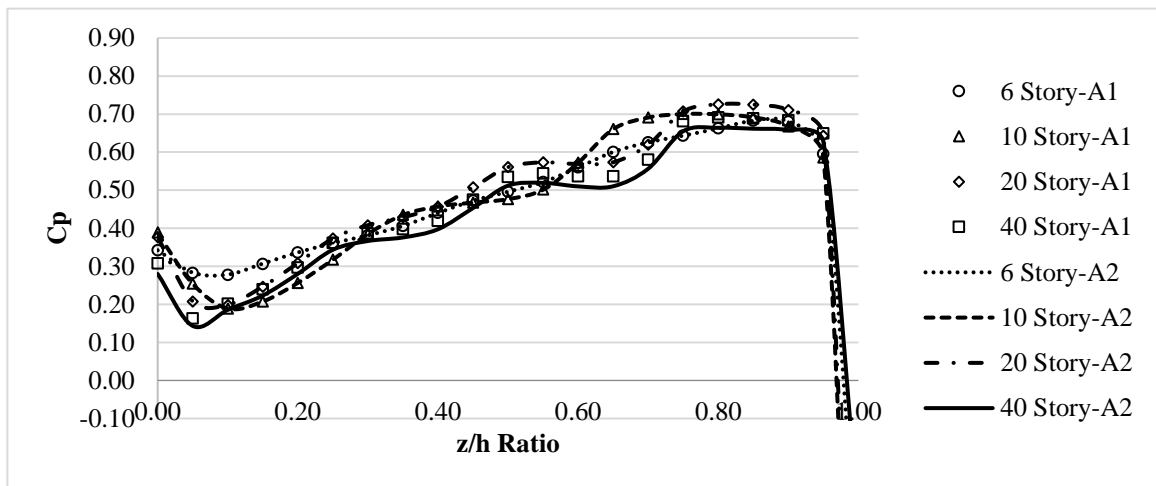
Figure 4.20: Leeward pressure coefficient for $L/B = 0.50$

4.3.2 Pressure Coefficient for Length to Width Ratio is 0.67

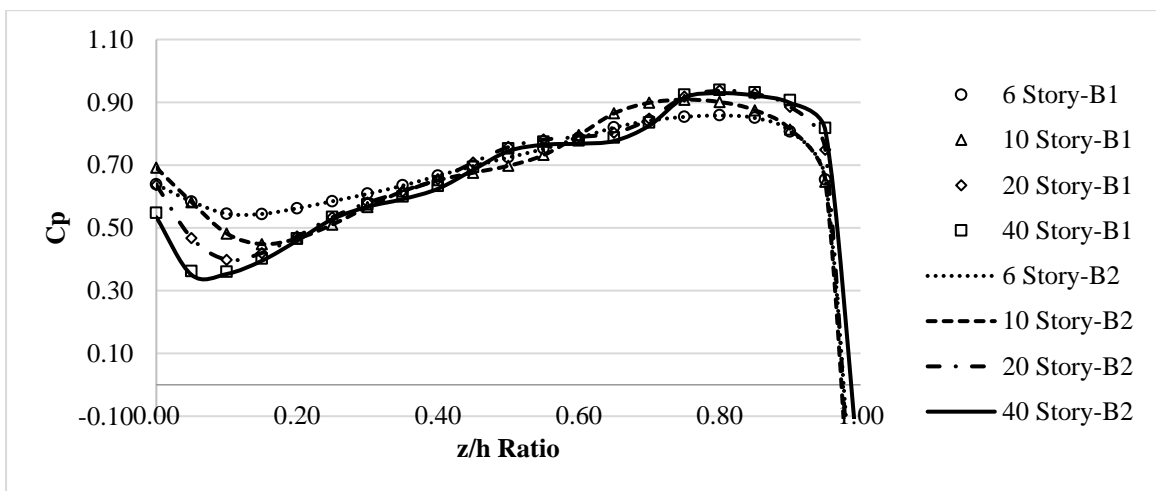
The buildings were then considered with a length-width ratio of 0.67 for wind simulation in the numerical wind tunnel test. Simulated models provided with the wind pressure coefficient over the zones of the surfaces (windward and leeward).

In the windward direction, the pressure coefficient up to a certain z/h ratio decrease from its origin and then increases almost linear proportionally and becomes a coefficient of back pressure, suction at the top level, or highest z/h ratio. Figure 4.21 represents the windward pressure coefficient for $L/B = 0.67$.

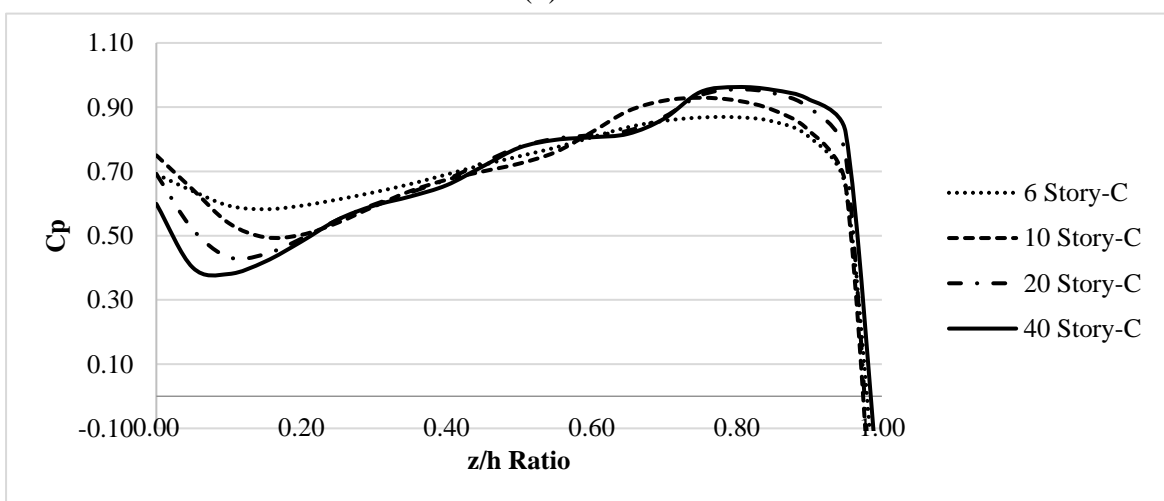
It was found that the C_p values in the windward direction were higher in the middle zone C and then the semi middle zone B edge zone A, respectively. Zone C started with an average value of 0.68, decreased to 0.48, and then before becoming negative, the average maximum was 0.93. While for zone B, the initial average value was 0.63, decreased to 0.45, and the average maximum was 0.91. On the other hand, for zone A, the initial average value was 0.35, decreased to 0.22, and the average maximum was 0.70. For detailed data, Appendix- F was recommended.



(a) Zone A



(b) Zone B

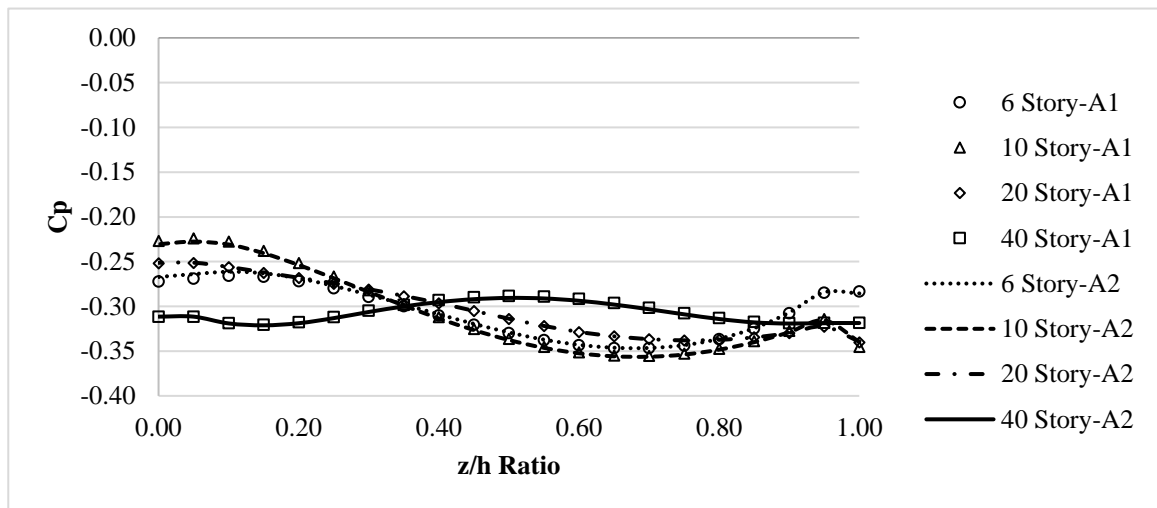


(c) Zone C

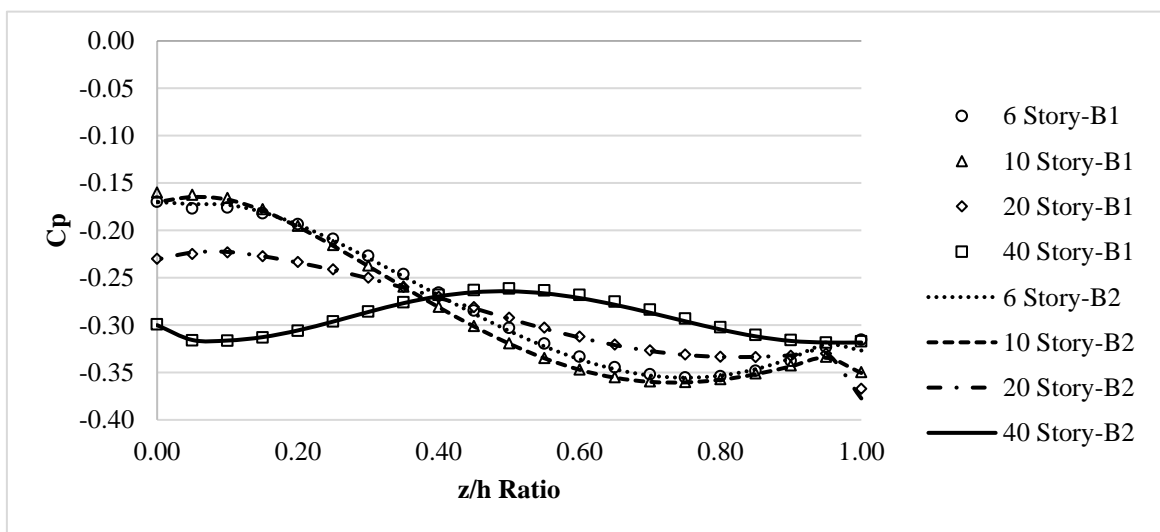
Figure 4.21: Windward pressure coefficient for $L/B = 0.67$

The pressure coefficients were negative as suction pressure acts on the surface in the leeward direction, The C_p values got a pick in the initial stage of the height ratio (z/h ratio), which soon decreased to the end portion of the z/h ratio except for the forty-storied building. Figure 4.22 represents the windward pressure coefficient for $L/B = 0.67$.

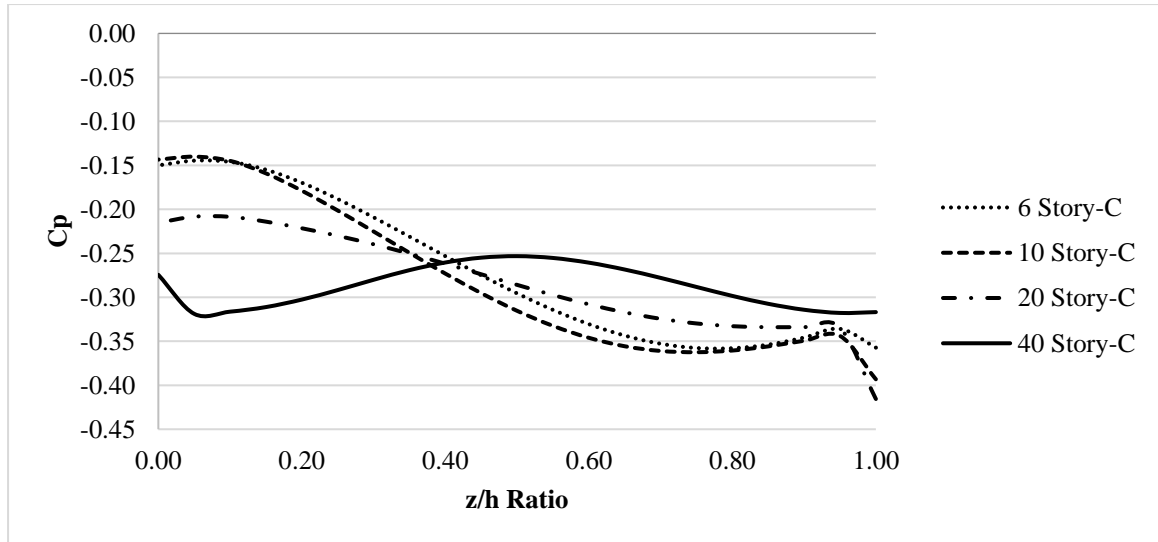
C_p values in the leeward direction were higher in the middle zone C and then the semi middle zone B edge zone A, respectively. Zone C had maximum average C_p value of -0.20, and the minimum C_p value of -0.37. While for zone B, the maximum average C_p value was -0.21, and the minimum C_p value was -0.34. On the other hand, for zone A, the maximum average C_p value was -0.24, and the minimum C_p value was -0.34. For detailed data, Appendix- F was recommended.



(a) Zone A



(b) Zone B



(c) Zone C

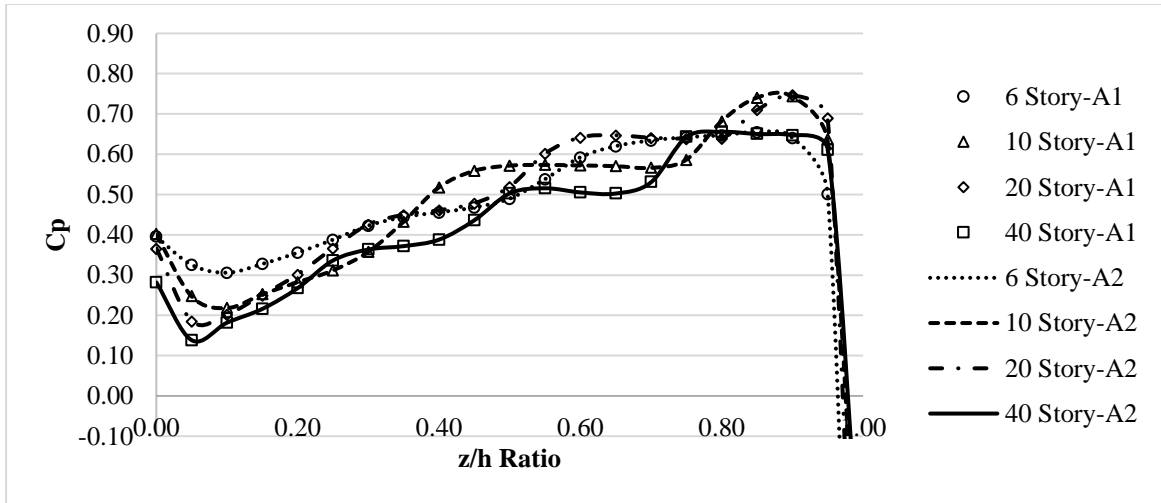
Figure 4.22: Leeward pressure coefficient for L/B = 0.67

4.3.3 Pressure Coefficient for Length to Width Ratio is 1.0

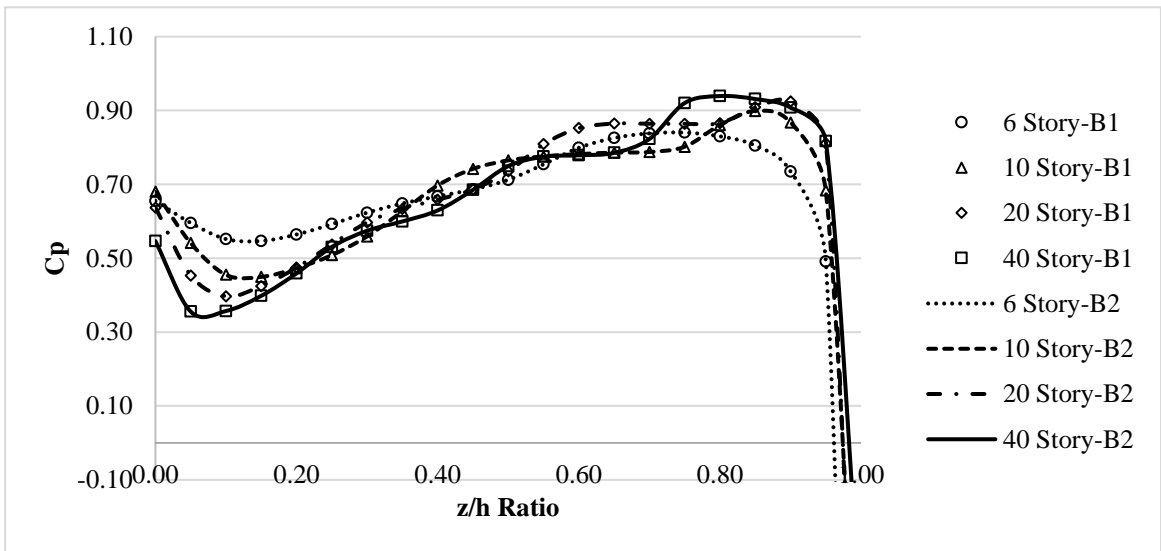
The buildings were then considered with a length-width ratio of 1.0 for wind simulation in the numerical wind tunnel test. Simulated models provided with the wind pressure coefficient over the zones of the surfaces (windward and leeward).

In the windward direction, the pressure coefficient up to a certain z/h ratio decrease from its origin and then increases almost linear proportionally and becomes a coefficient of back pressure, suction at the top level, or highest z/h ratio. Figure 4.23 represents the windward pressure coefficient for L/B = 1.0.

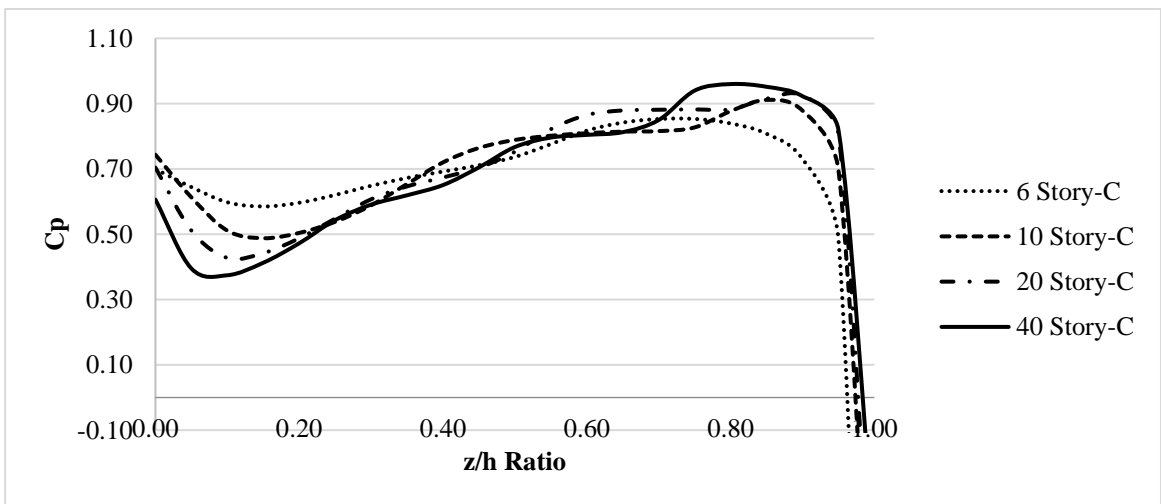
It was found that the C_p values in the windward direction were higher in the middle zone C and then the semi middle zone B edge zone A, respectively. Zone C started with an average value of 0.69, decreased to 0.48, and then before becoming negative, the average maximum was 0.90. While for zone B, the initial average value was 0.63, decreased to 0.44, and the average maximum was 0.89. On the other hand, for zone A, the initial average value was 0.36, decreased to 0.22, and the average maximum was 0.69. For detailed data, Appendix-G was recommended.



(a) Zone A



(b) Zone B

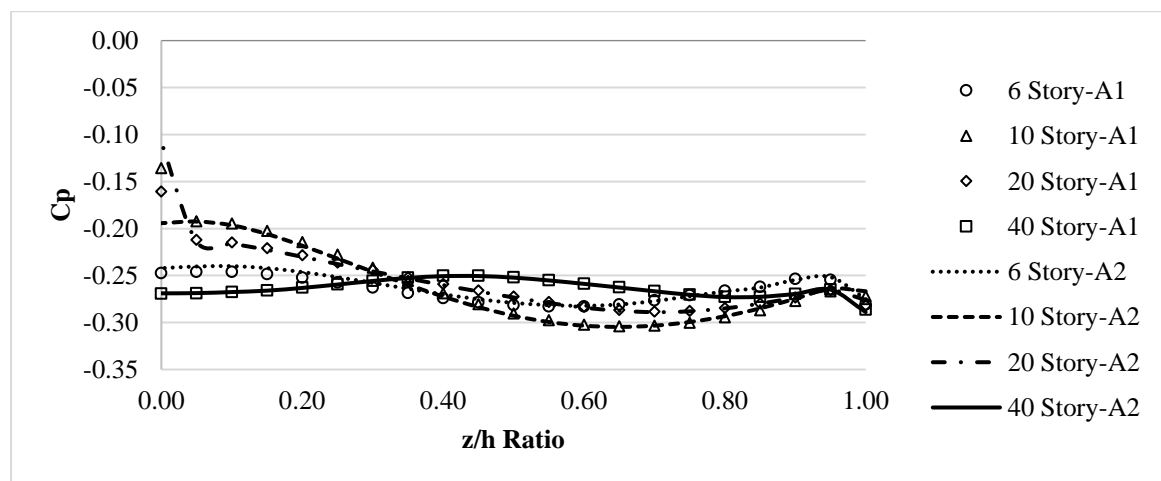


(c) Zone C

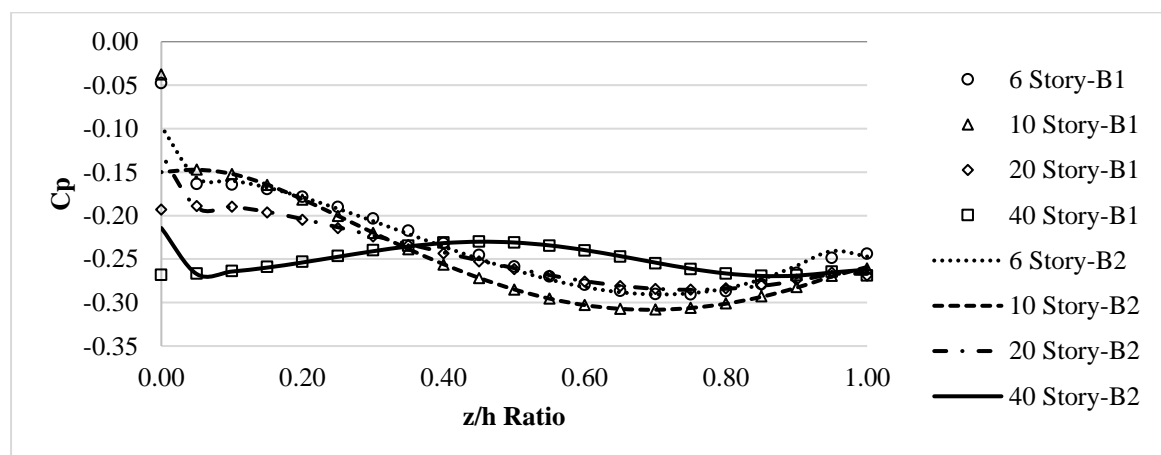
Figure 4.23: Windward pressure coefficient for $L/B = 1.0$

The pressure coefficients were negative as suction pressure acts on the surface in the leeward direction. The C_p values got a pick in the initial stage of the height ratio (z/h ratio), which soon decreased to the end portion of the z/h ratio except for the forty-storied building. Figure 4.24 represents the windward pressure coefficient for $L/B = 1.0$.

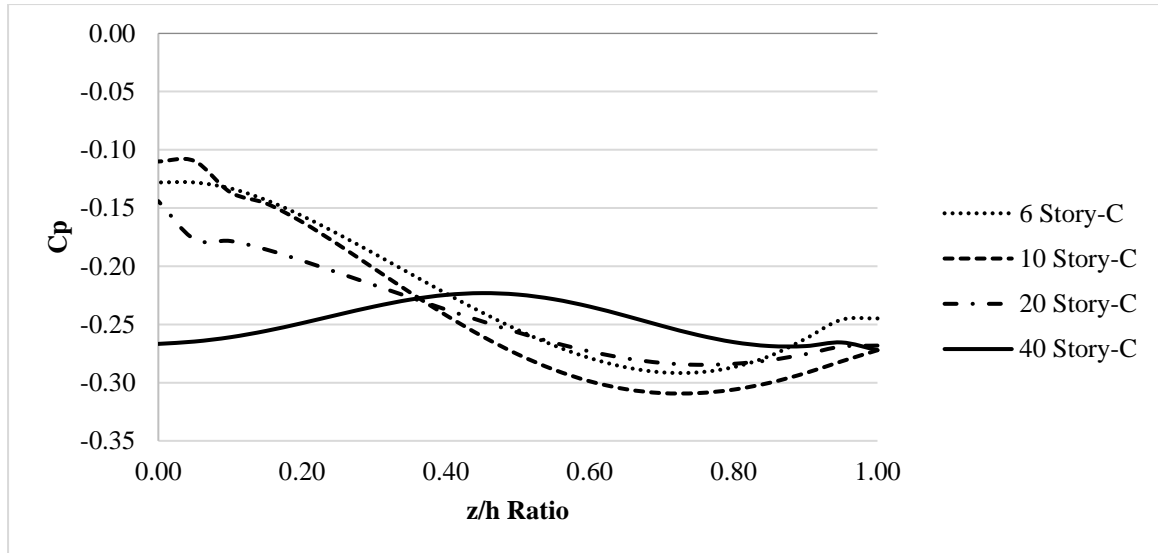
C_p values in the leeward direction were higher in the middle zone C and then the semi middle zone B edge zone A, respectively. Zone C had maximum average C_p value of -0.16, and the minimum C_p value of -0.29. While for zone B, the maximum average C_p value was -0.14, and the minimum C_p value was -0.29. On the other hand, for zone A, the maximum average C_p value was -0.20, and the minimum C_p value was -0.28. For detailed data, Appendix- G was recommended.



(a) Zone A



(b) Zone B



(c) Zone C

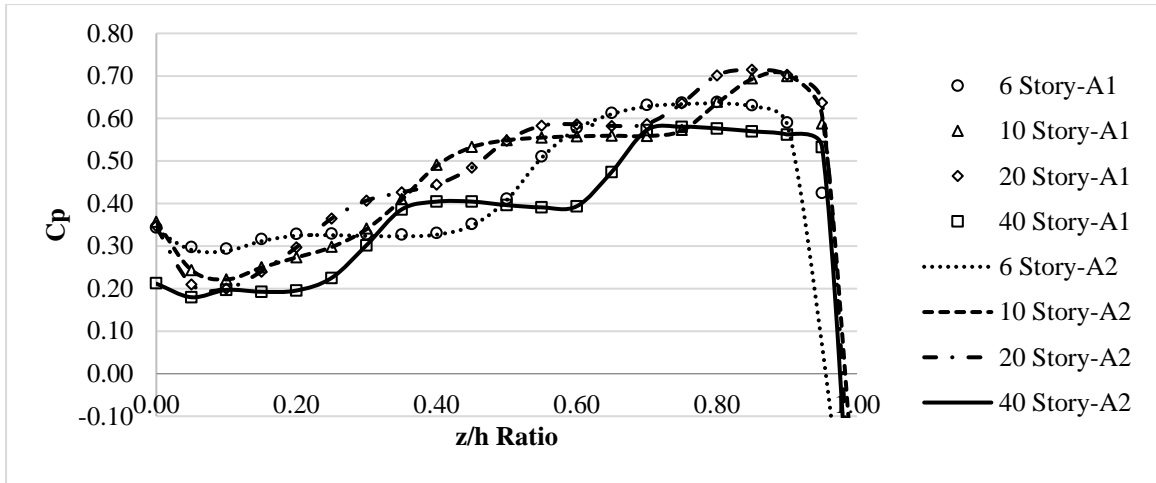
Figure 4.24: Leeward pressure coefficient for L/B = 1.0

4.3.4 Pressure Coefficient for Length to Width Ratio is 2.0

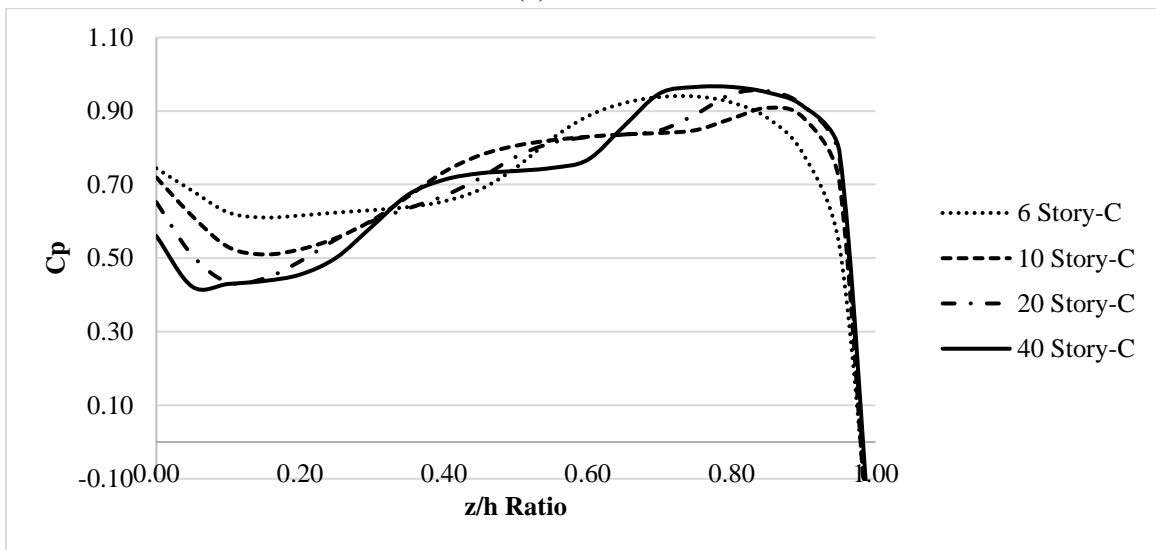
The buildings were then considered with a length-width ratio of 2.0 for wind simulation in the numerical wind tunnel test. Simulated models provided with the wind pressure coefficient over the zones of the surfaces (windward and leeward).

In the windward direction, the pressure coefficient up to a certain z/h ratio decrease from its origin and then increases almost linear proportionally and becomes a coefficient of back pressure, suction at the top level, or highest z/h ratio. Figure 4.25 represents the windward pressure coefficient for L/B = 2.0.

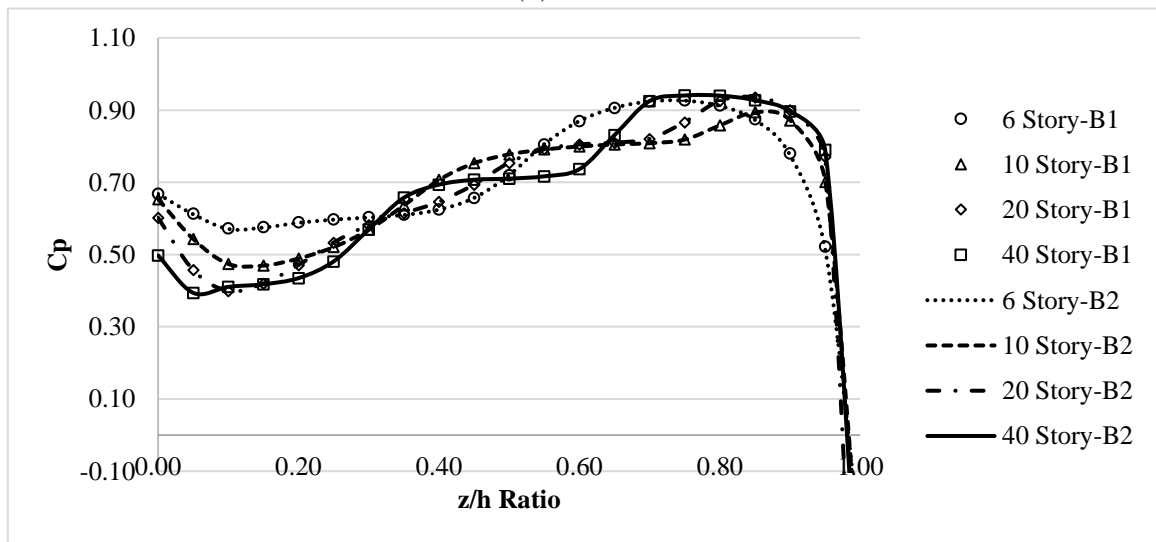
It was found that the C_p values in the windward direction were higher in the middle zone C and then the semi middle zone B edge zone A, respectively. Zone C started with an average value of 0.67, decreased to 0.50, and then before becoming negative, the average maximum was 0.93. While for zone B, the initial average value was 0.61, decreased to 0.46, and the average maximum was 0.91. On the other hand, for zone A, the initial average value was 0.32, decreased to 0.23, and the average maximum was 0.65. For detailed data, Appendix-H was recommended.



(a) Zone A



(b) Zone B

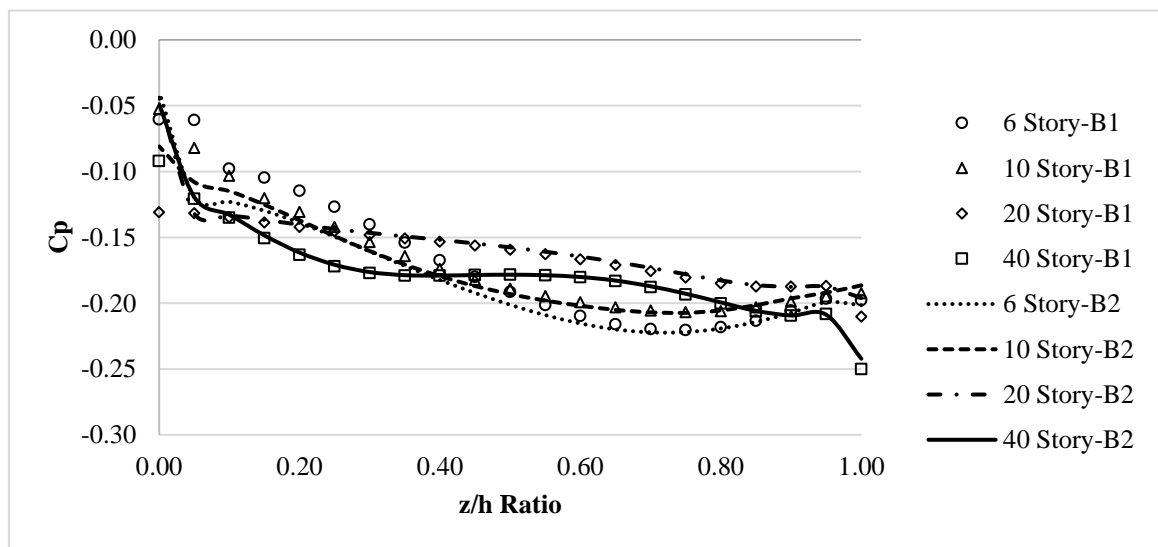


(c) Zone C

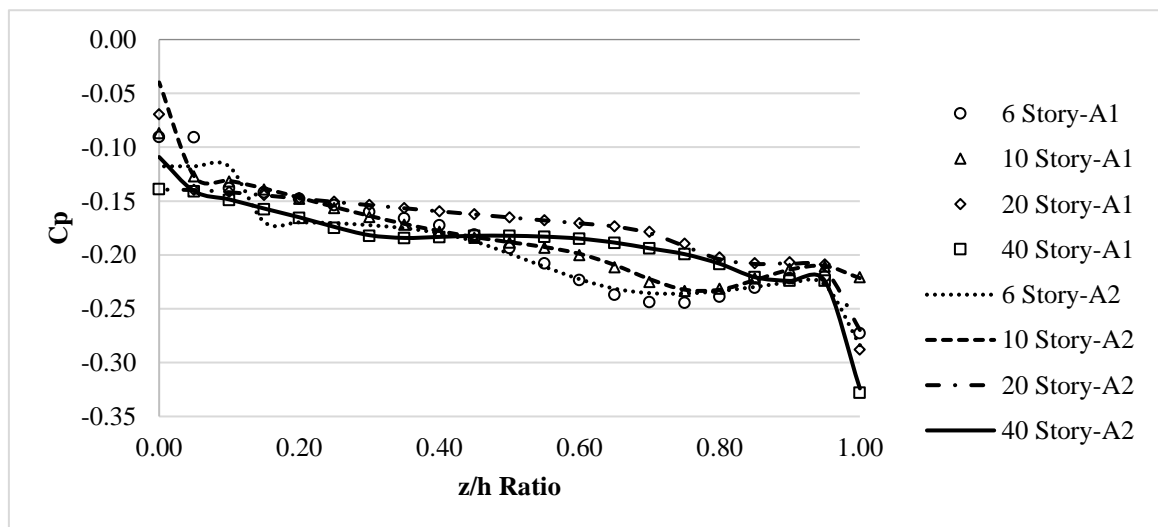
Figure 4.25: Windward pressure coefficient for $L/B = 2.0$

The pressure coefficients were negative as suction pressure acts on the surface in the leeward direction. The C_p values got a pick in the initial stage of the height ratio (z/h ratio), which soon decreased to the end portion of the z/h ratio except for the forty-storied building. Figure 4.26 represents the windward pressure coefficient for $L/B = 2.0$.

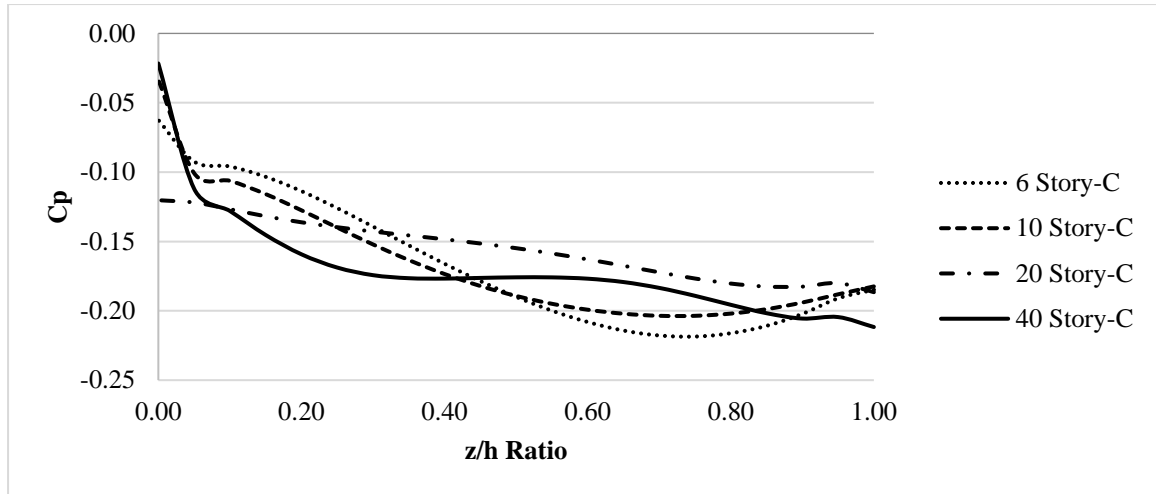
C_p values in the leeward direction were higher in the middle zone C and then the semi middle zone B edge zone A, respectively. Zone C had maximum average C_p value of -0.06, and the minimum C_p value of -0.20. While for zone B, the maximum average C_p value was -0.08, and the minimum C_p value was -0.21. On the other hand, for zone A, the maximum average C_p value was -0.10, and the minimum C_p value was -0.28. For detailed data, Appendix-H was recommended.



(a) Zone A



(b) Zone B



(c) Zone C

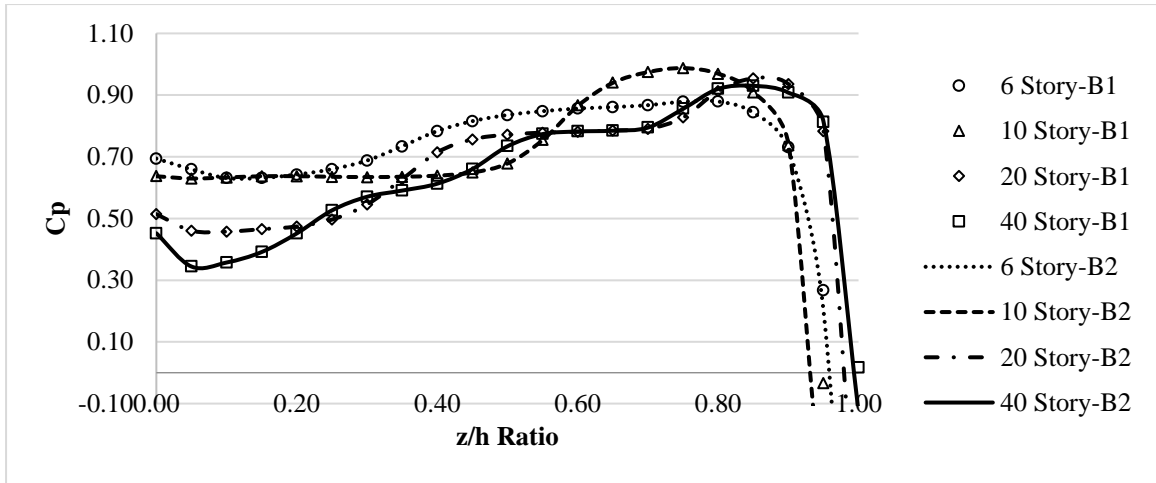
Figure 4.26: Leeward pressure coefficient for $L/B = 2.0$

4.3.5 Pressure Coefficient for Length to Width Ratio is 3.0

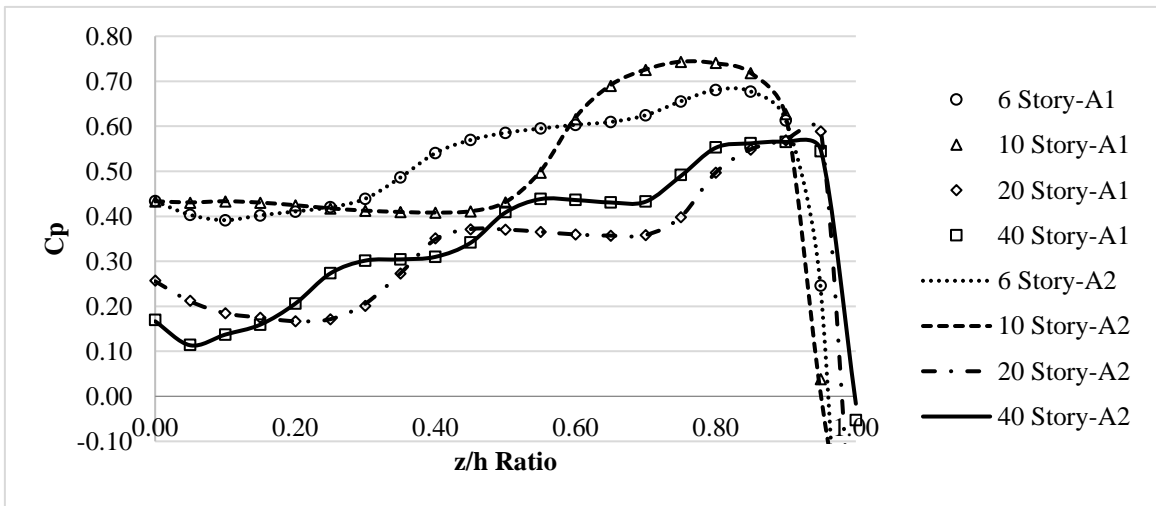
The buildings were then considered with a length-width ratio of 3.0 for wind simulation in the numerical wind tunnel test. Simulated models provided with the wind pressure coefficient over the zones of the surfaces (windward and leeward).

In the windward direction, the pressure coefficient up to a certain z/h ratio decrease from its origin and then increases almost linear proportionally and becomes a coefficient of back pressure, suction at the top level, or highest z/h ratio. Figure 4.27 represents the windward pressure coefficient for $L/B = 3.0$.

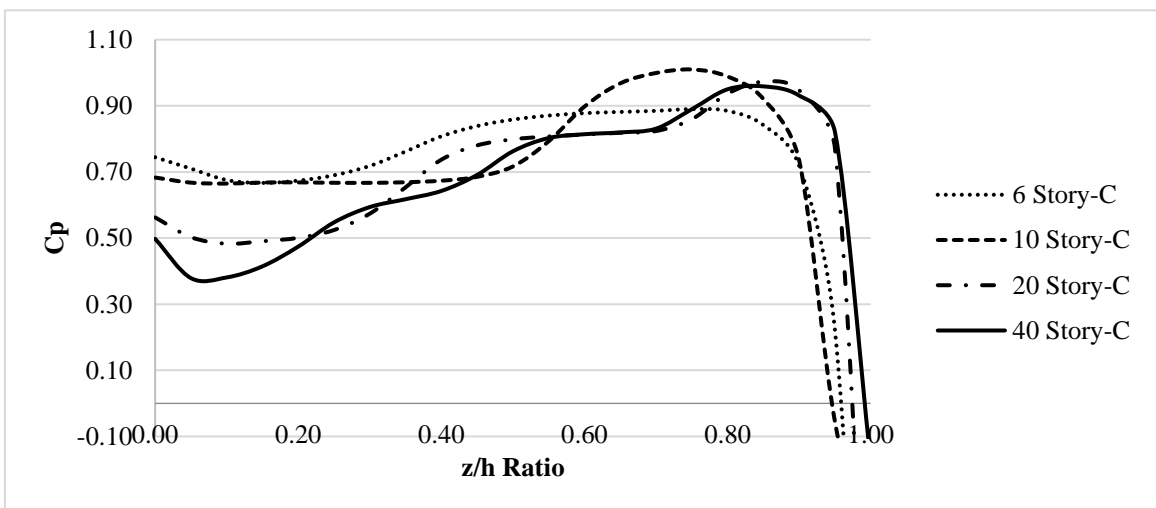
It was found that the C_p values in the windward direction were higher in the middle zone C and then the semi middle zone B edge zone A, respectively. Zone C started with an average value of 0.62, decreased to 0.44, and then before becoming negative, the average maximum was 0.94. While for zone B, the initial average value was 0.57, decreased to 0.46, and the average maximum was 0.92. On the other hand, for zone A, the initial average value was 0.32, decreased to 0.29, and the average maximum was 0.63. For detailed data, Appendix-I was recommended.



(a) Zone A



(b) Zone B

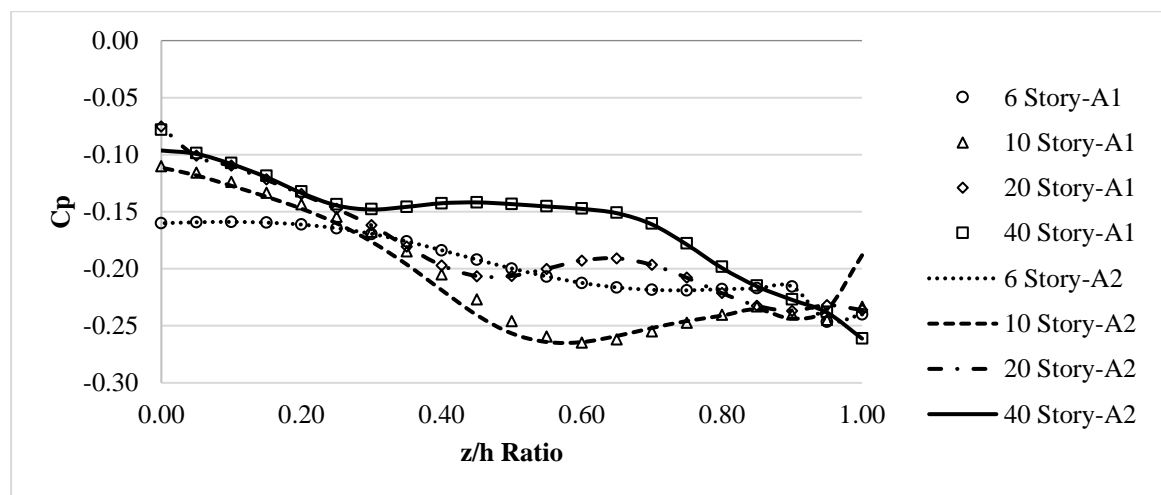


(c) Zone C

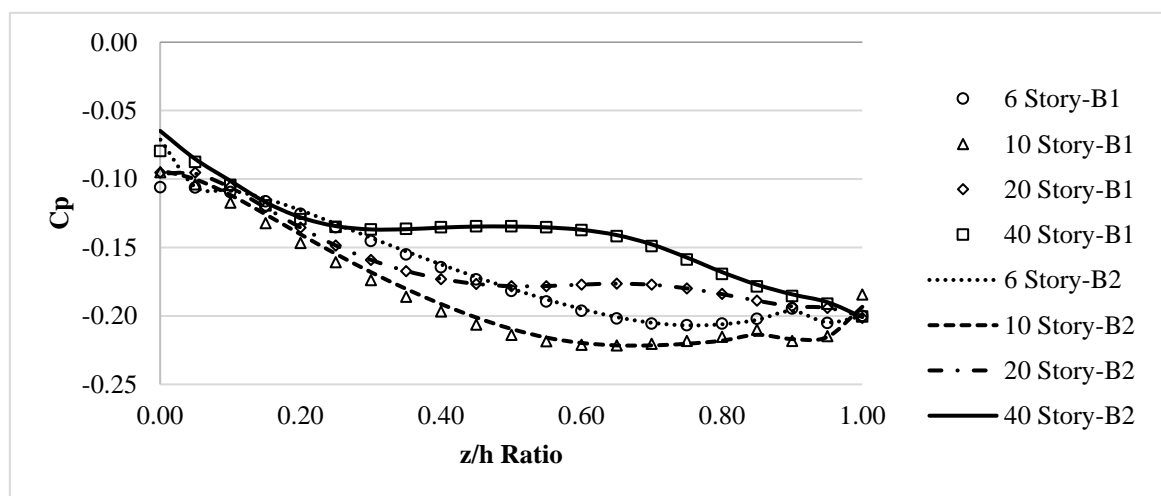
Figure 4.27: Windward pressure coefficient for $L/B = 3.0$

The pressure coefficients were negative as suction pressure acts on the surface in the leeward direction. The C_p values got a pick in the initial stage of the height ratio (z/h ratio), which soon decreased to the end portion of the z/h ratio except for the forty-storied building. Figure 4.28 represents the windward pressure coefficient for $L/B = 3.0$.

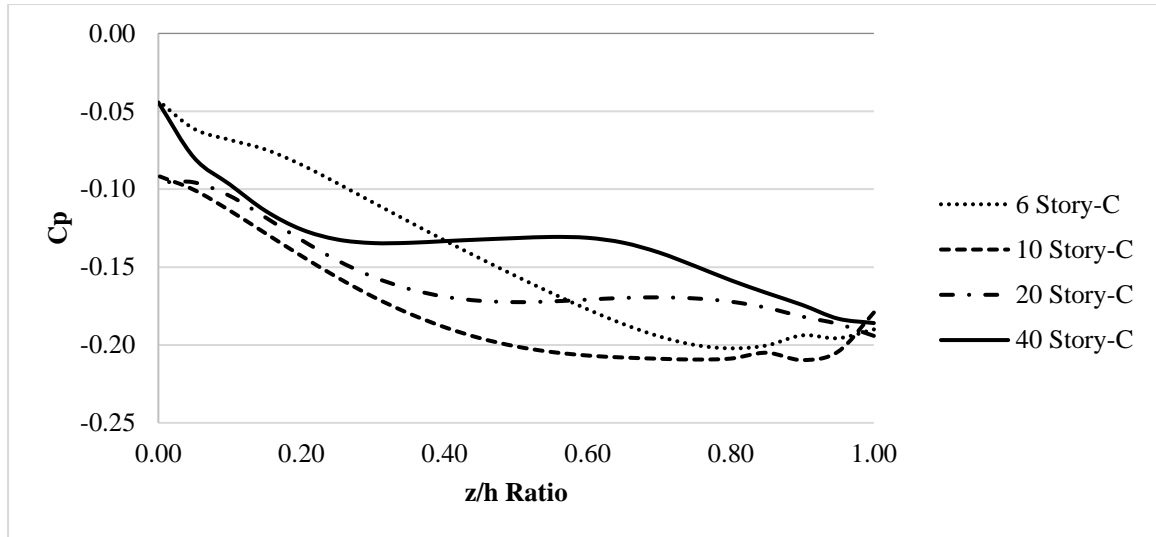
C_p values in the leeward direction were higher in the middle zone C and then the semi middle zone B edge zone A, respectively. Zone C had maximum average C_p value of -0.04, and the minimum C_p value of -0.21. While for zone B, the maximum average C_p value was -0.07, and the minimum C_p value was -0.24. On the other hand, for zone A, the maximum average C_p value was -0.11, and the minimum C_p value was -0.29. For detailed data, Appendix- I was recommended.



(a) Zone A



(b) Zone B



(c) Zone C

Figure 4.28: Leeward pressure coefficient for L/B = 3.0

4.4 Proposed Pressure Coefficient Equations

A wide variety of wind pressure coefficient values were observed during the result analysis. The use of variable wind pressure coefficient data provides a relatively good result. Therefore, a few linear equations are proposed for three different zones and directions, windward and leeward, as shown in Table 4.2. Table 4.2 also represents R-squared values. It shows good correlation.

Table 4.2: Proposed linear equations to calculate pressure coefficient

Zone	Windward		Leeward	
	Equation	R ²	Equation	R ²
A	$y = 0.5557x + 0.2359$	0.979	$y = -0.0813x - 0.2792$	0.639
B	$y = 0.509x + 0.4665$	0.948	$y = -0.1497x - 0.2266$	0.945
C	$y = 0.4715x + 0.5052$	0.927	$y = -0.1829x - 0.2029$	0.967

Those equations are found from the average pressure coefficient for different length to width and height ratios of the concerned buildings. Figure 4.29 to 4.34 represent the variation of average pressure coefficient to varying heights in windward and leeward sides.

In statistics, the standard deviation measures the amount of variation of a set of values. A low standard deviation indicates that the values tend to be close to the mean of the set, while a high standard deviation indicates that the values are spread out over a wider range. Mean plus double standard deviation was used to propose the empirical equations to ensure about 95.45% probability of the normal distribution of the data set.

Empirical equations for windward direction at zone A, B, and C were developed from five different data sets of L/B ratios (0.5, 0.67, 1.0, 2.0, 3.0). All the series of the L/B ratios showed similar sorts of graphs that were non-linear upward curves, as shown in the Figures from 4.29 to 4.31. However, for simplicity, a linear equation was proposed. Detailed data can be found in Appendix E to Appendix I.

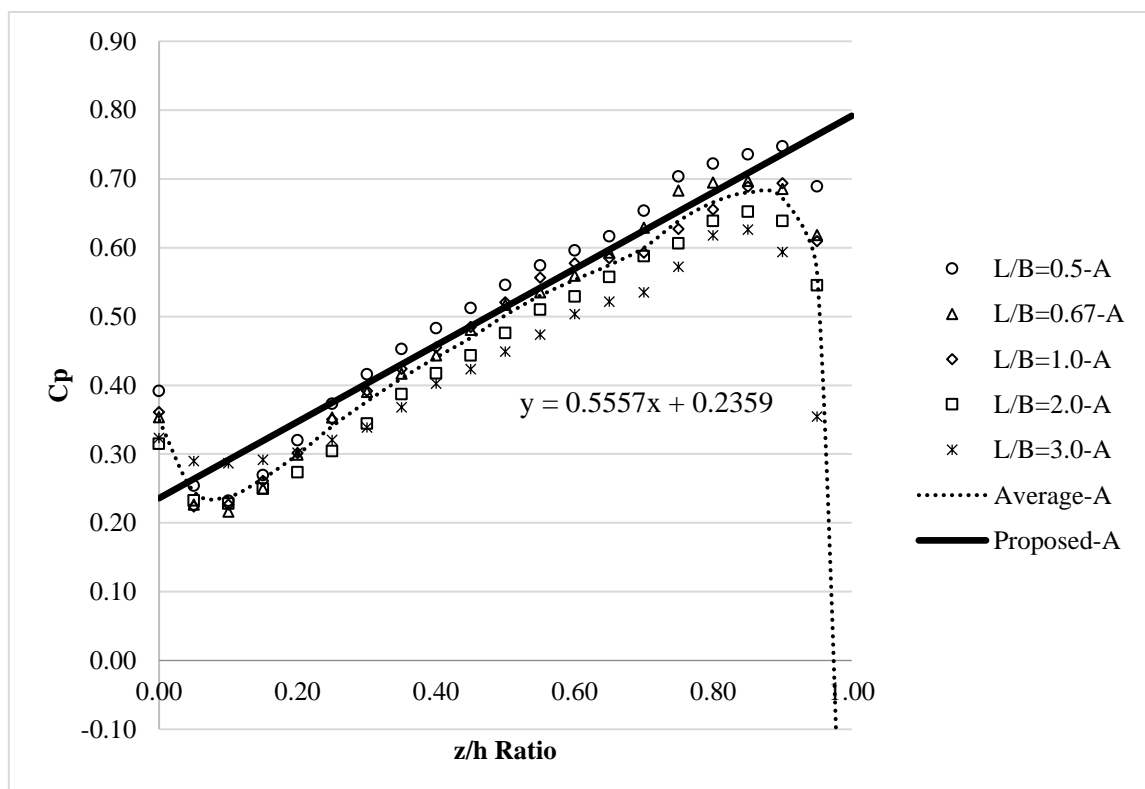


Figure 4.29: Proposed Windward pressure coefficient at zone A

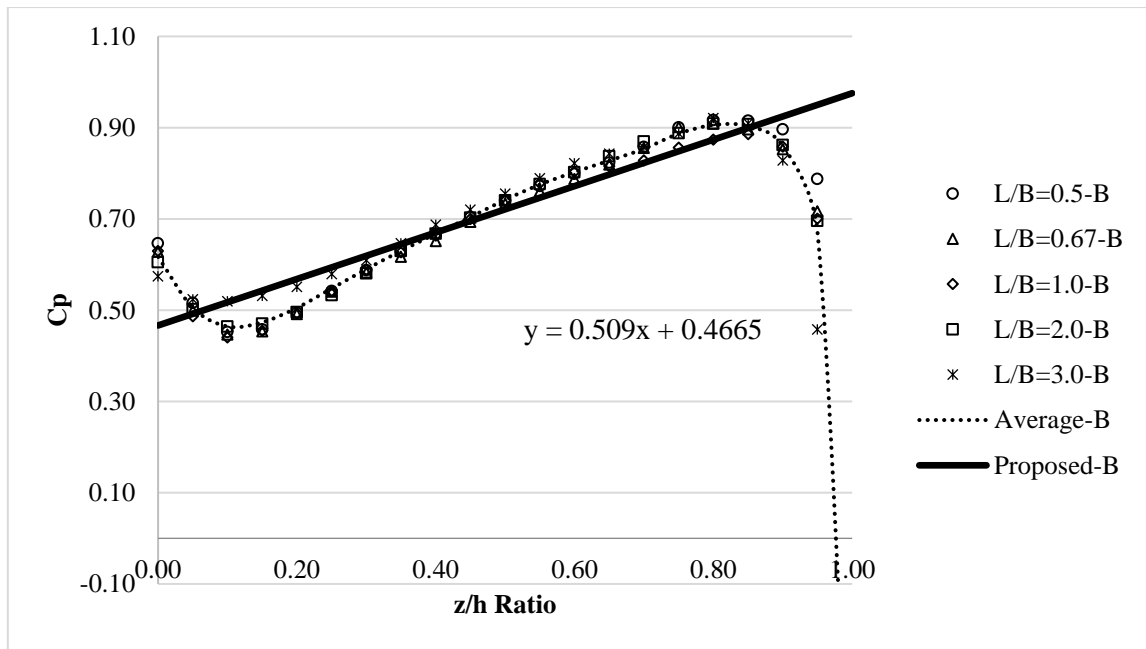


Figure 4.30: Proposed Windward pressure coefficient at zone B

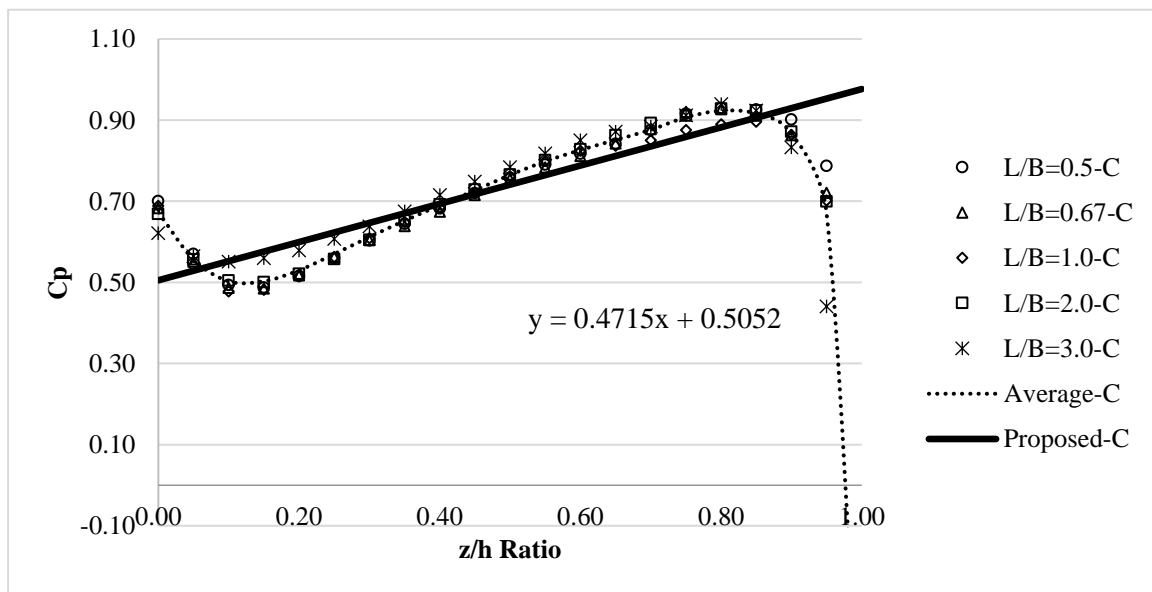


Figure 4.31: Proposed Windward pressure coefficient at zone C

Empirical equations for leeward direction at zone A, B, and C were also developed from five different data sets of L/B ratios (0.5, 0.67, 1.0, 2.0, 3.0). All the series of the L/B ratios showed similar sorts of graphs which were non-linear downward curves, which can be seen in the Figures from 4.32 to 4.34. However, for simplicity, a linear equation was proposed. Detailed data can be found in Appendix E to Appendix I.

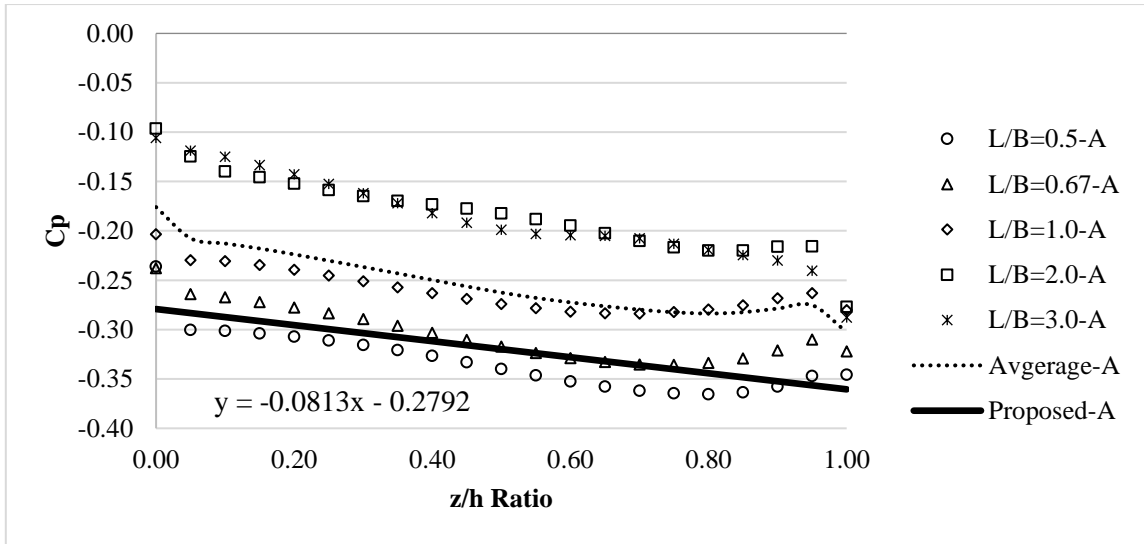


Figure 4.32: Proposed Leeward pressure coefficient at zone A

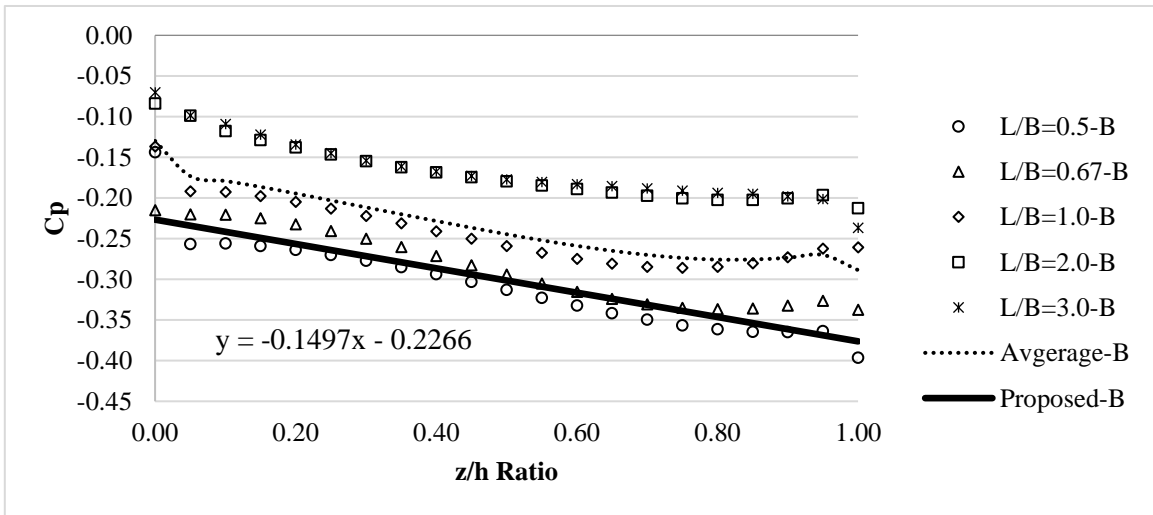


Figure 4.33: Proposed Leeward pressure coefficient at zone B

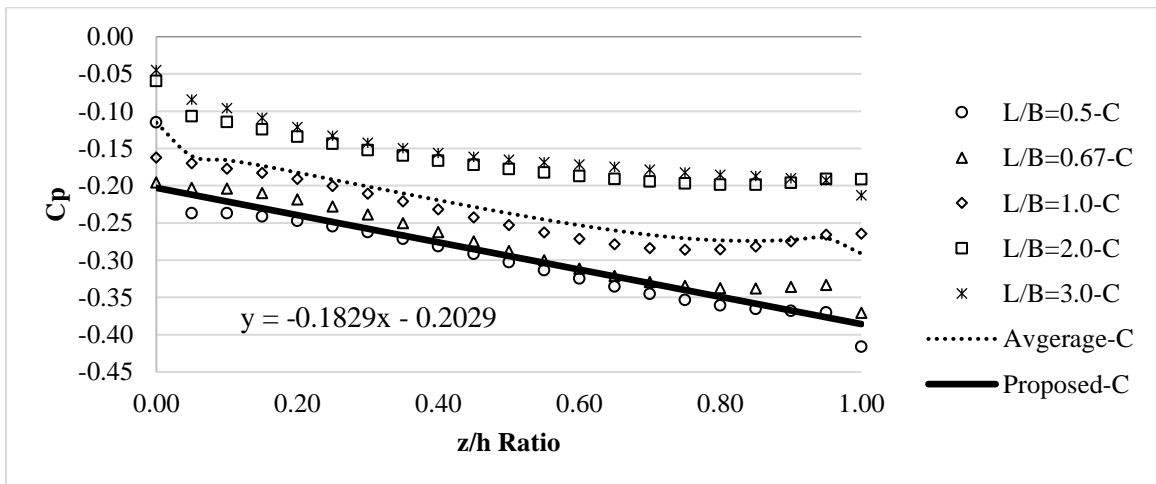


Figure 4.34: Proposed Leeward pressure coefficient at zone C

4.4.1 Comparison of Story Shear

A comparison was conducted as a part of this study between the story shear evaluating from proposed pressure coefficient equations and the equivalent numerical wind tunnel test according to the BNBC 2006 and the BNBC 2020. The wind speed profile was collected from these standards in the equivalent wind tunnel because of the goal to compare all of these standards and the equivalent numerical wind tunnel.

4.4.1.1 Six Storied Regular Shape Building

Figures 4.35 and Figure 4.36 represent the comparison of story shear of the six storied building in the long and the short direction, respectively. In determining the wind pressure coefficient, if calculated by the proposed empirical equations for BNBC 2020, the variation of story shear between the numerical wind tunnel to proposed empirical equations was found to be from 22.36 to 28.53 percent, and the average was 24.72 percent for the long direction of the six storied building as shown in Figure 4.35. Moreover, variation of story shear between the numerical wind tunnel and the proposed empirical equations for BNBC 2020 in the short direction was 22.96 to 35.73 percent, and the average was 26.29 percent as shown in Figure 4.36.

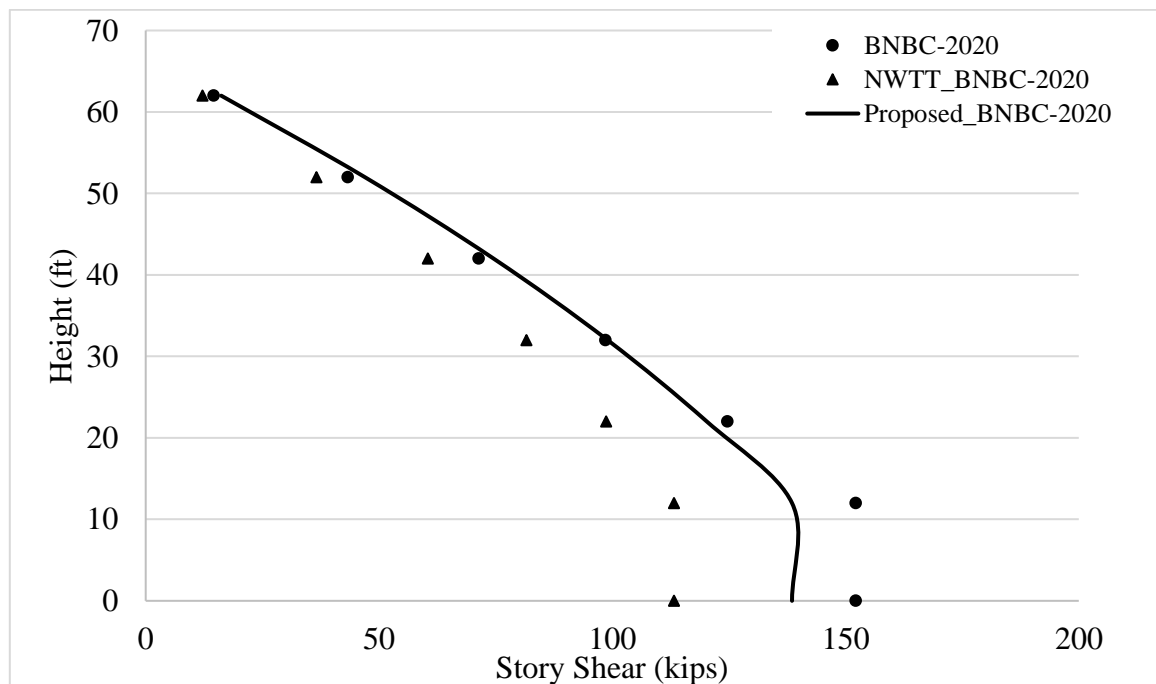


Figure 4.35: Comparison of story shear of the six storied building in the long direction

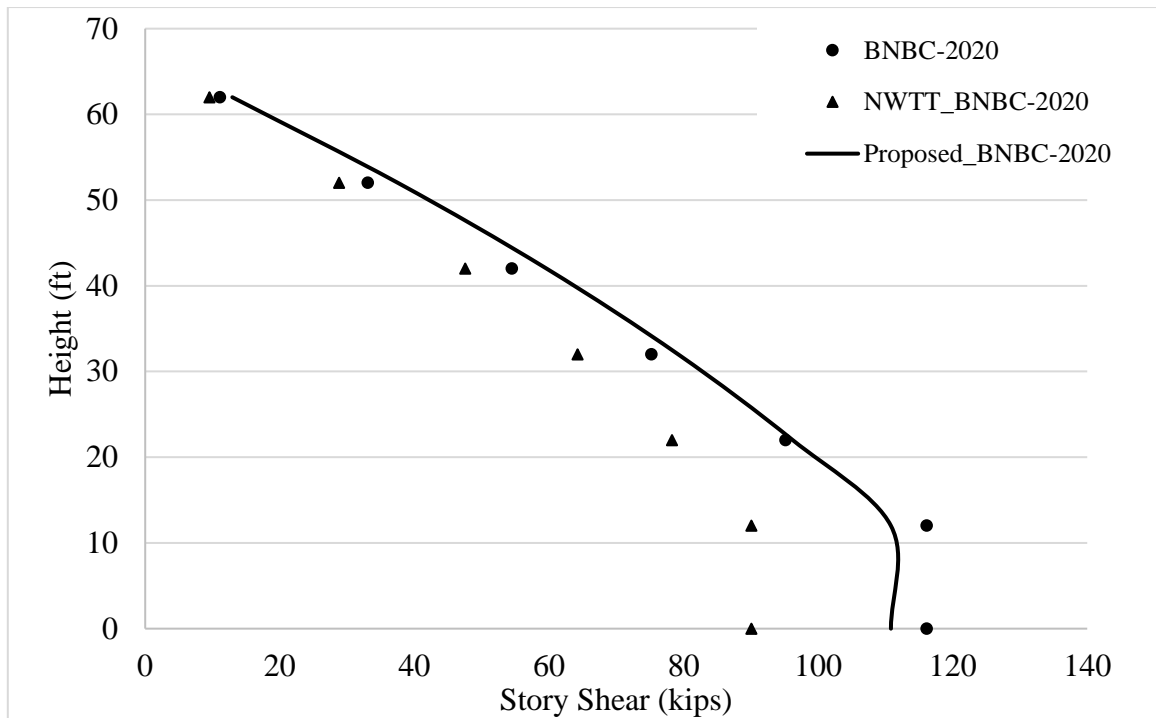


Figure 4.36: Comparison of story shear of the six storied building in the short direction

4.4.1.2 Ten Storied Regular Shape Building

Figures 4.37 and Figure 4.38 represent the comparison of story shear of the ten storied building in the long and the short direction, respectively. Wind pressure coefficient, if calculated by the proposed empirical equations for BNBC 2020, the variation of story shear between the numerical wind tunnel to proposed empirical equations was found to be from 7.45 to 23.99 percent, and the average was 13.54 percent for the long direction of the ten storied building as shown in Figure 4.37. Moreover, variation of Story shear between the numerical wind tunnel and the proposed empirical equations for BNBC 2020 in the short direction was 24.29 to 45.88 percent, and the average was 29.37 percent as shown in Figure 4.38.

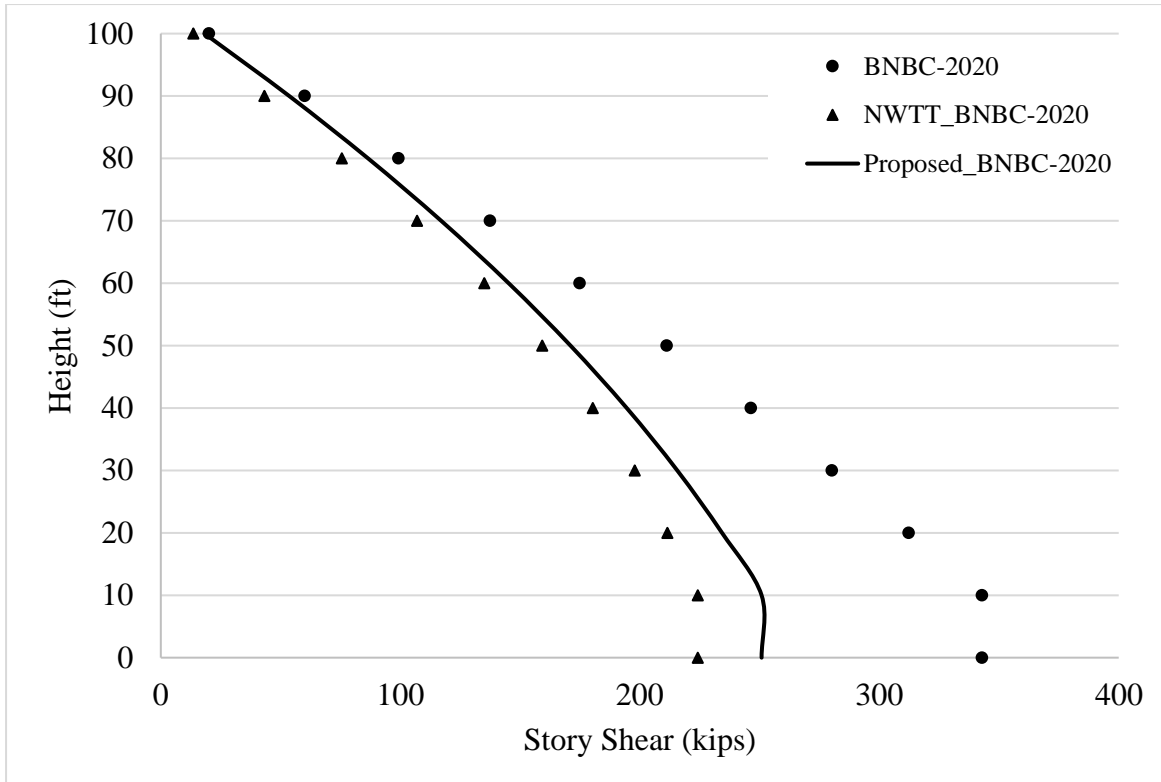


Figure 4.37: Comparison of story shear of the ten storied building in the long direction

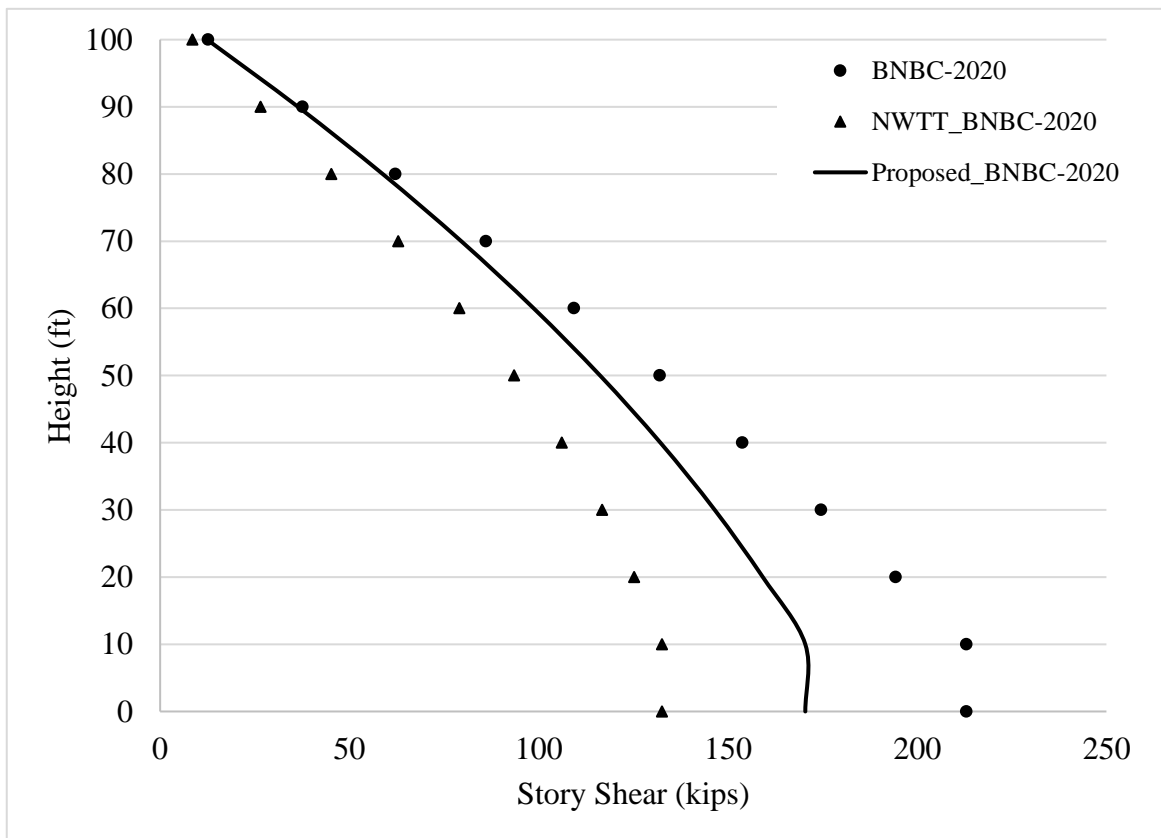


Figure 4.38: Comparison of story shear of the ten storied building in the short direction

4.4.1.3 Twenty Storied Regular Shape Building

Figures 4.39 and Figure 4.40 represent the comparison of story shear of the twenty storied building in the long and the short direction, respectively. Wind pressure coefficient, if calculated by the proposed empirical equations for BNBC 2020, the variation of story shear between the numerical wind tunnel to proposed empirical equations was found to be from 8.16 to 35.27 percent, and the average was 15.84 percent for the long direction of the twenty storied building as shown in Figure 4.39. Moreover, variation of story shear between the numerical wind tunnel and the proposed empirical equations for BNBC 2020 in the short direction was 34.27 to 63.21 percent, and the average was 40.81 percent as shown in Figure 4.40.

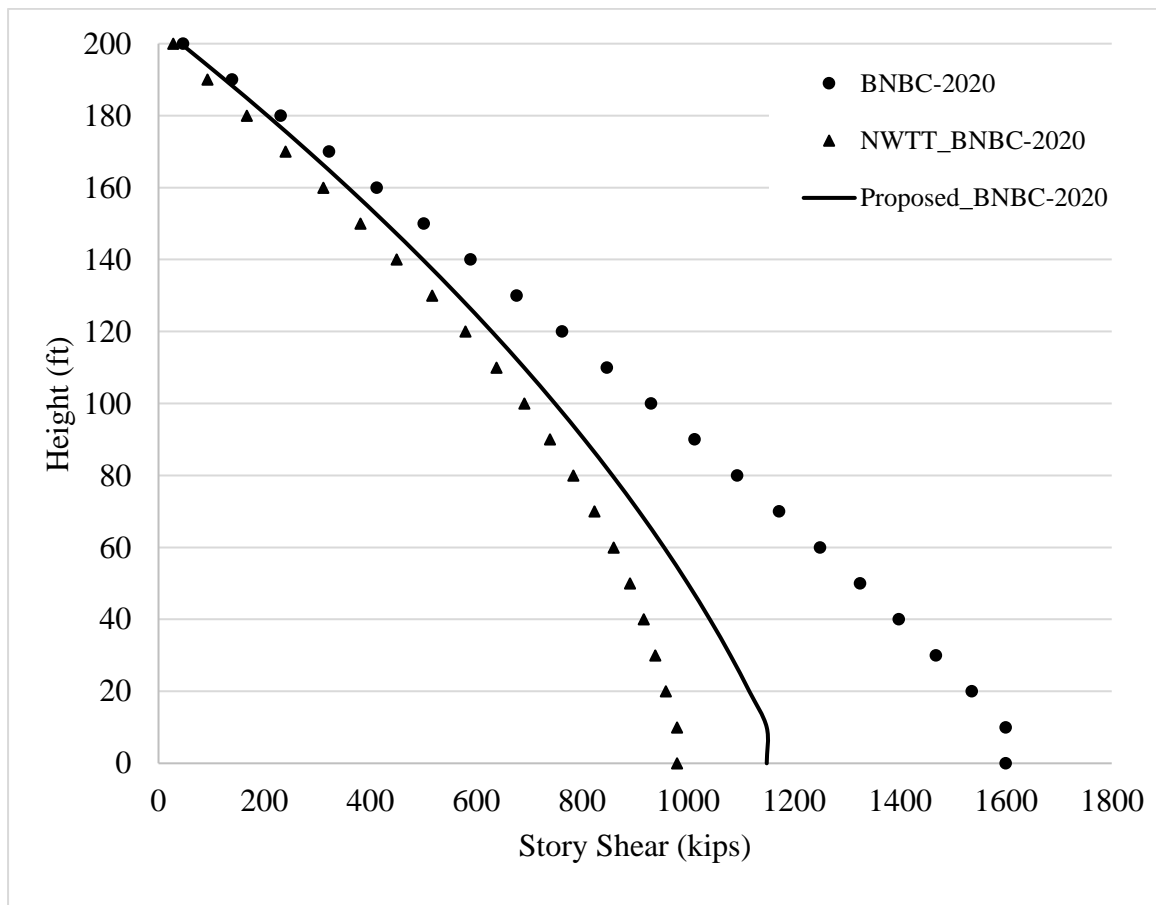


Figure 4.39: Comparison of story shear of the twenty storied building in the long direction

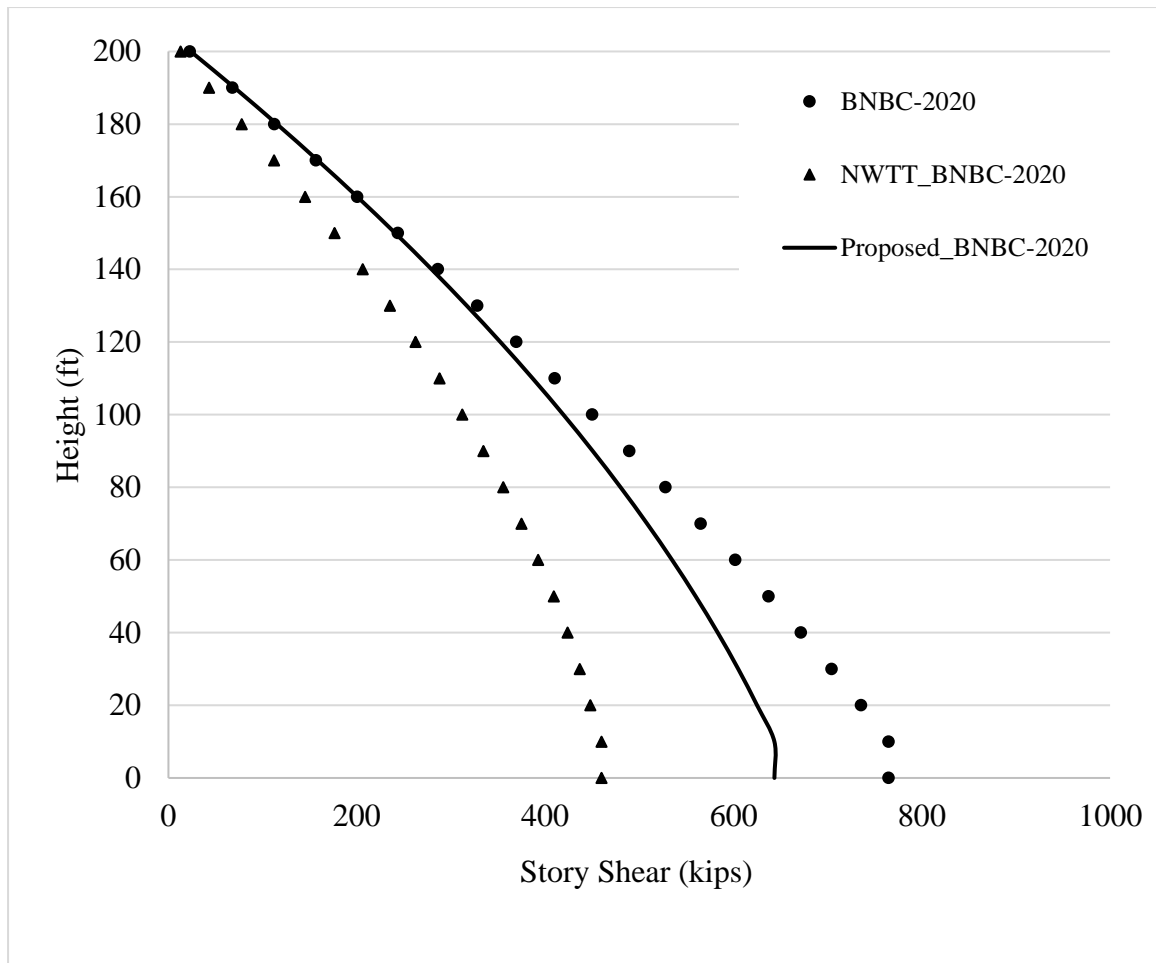


Figure 4.40: Comparison of story shear of the twenty storied building in the short direction

4.4.1.4 Forty Storied Regular Shape Building

Figures 4.41 and Figure 4.42 represent the comparison of story shear of the forty storied building in the long and the short direction, respectively.

Wind pressure coefficient, if calculated by the proposed empirical equations for BNBC 2020, the variation of story shear between the numerical wind tunnel to proposed empirical equations was found to be from 8.33 to 51.93 percent, and the average was 13.61 percent for the long direction of the forty storied building as shown in Figure 4.41. Moreover, variation of the story shear between the numerical wind tunnel and the proposed empirical equations for BNBC 2020 in the short direction was 18.06 to 56.29 percent, and the average was 23.35 percent as shown in Figure 4.42.

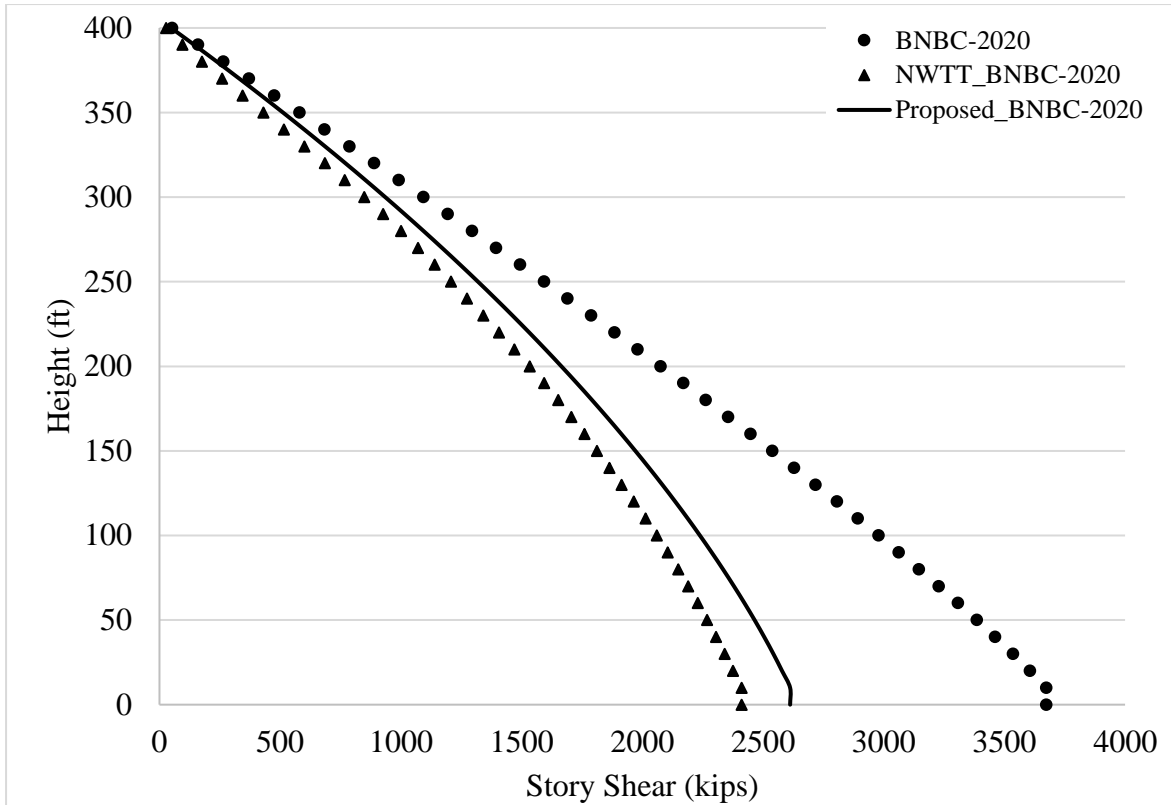


Figure 4.41: Comparison of story shear of the forty storied building in the long direction

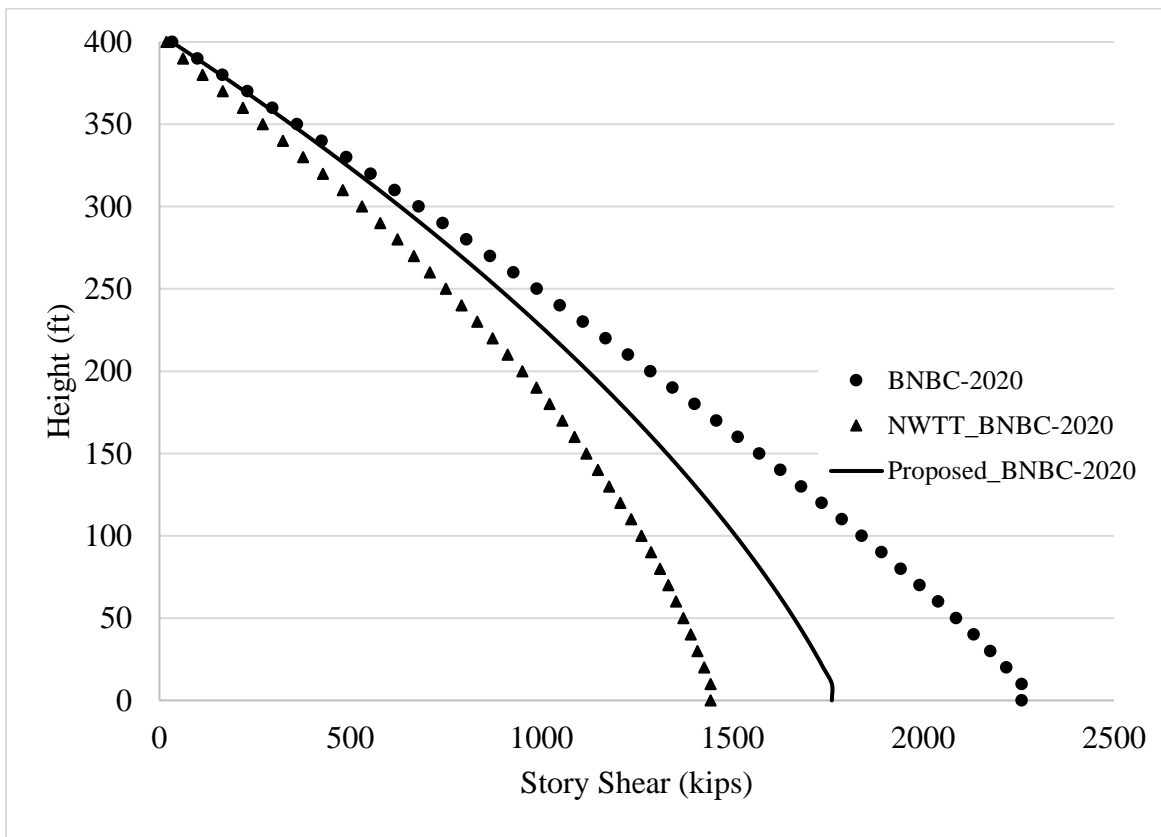


Figure 4.42: Comparison of story shear of the forty storied building in the short direction

4.4.2 Total Base Shear Comparison

Base shear due to wind force was calculated using BNBC-2020 manually, numerical wind tunnel of BNBC 2020, and the proposed empirical equations for four different buildings. Table 4.3 represents the comparison of base shear in the long direction. It was found that the manually calculated BNBC 2020 is relatively conservative with respect to the numerical wind tunnel test of BNBC 2020. It evaluated the base shear 35% to 64% higher than the numerical wind tunnel and the average for the calculated four building was 50.8% in the long direction. On the other hand, base shear calculated using the proposed empirical equations showed less variation with respect to the numerical wind tunnel test. It illustrated variations of 9% to 23% higher value than the numerical wind tunnel test data and the average for the calculated four building was 15% in the long direction.

In evaluation of the base shear by the guidelines are as follows- Manual calculation of BNBC 2020 > Proposed numerical Equation > Numerical wind tunnel test of BNBC 2020 as shown in Table 4.4. Figure 4.43 is an informative graph that represent the comparison of base shear in the long direction.

Table 4.3: Comparison of base shear in long direction

Story	NWTT BNBC 2020	Manual Calculation BNBC 2020	Variation (%) w.r.t NWTT BNBC 2020	Proposed Numerical Equation	Variation (%) w.r.t NWTT BNBC 2020
Six Story	113.22	152.15	34.4	138.53	22.4
Ten Story	224.19	342.90	53.0	250.87	11.9
Twenty Story	979.28	1600.06	63.4	1148.53	17.3
Forty Story	2411.63	3674.06	52.3	2612.50	8.3

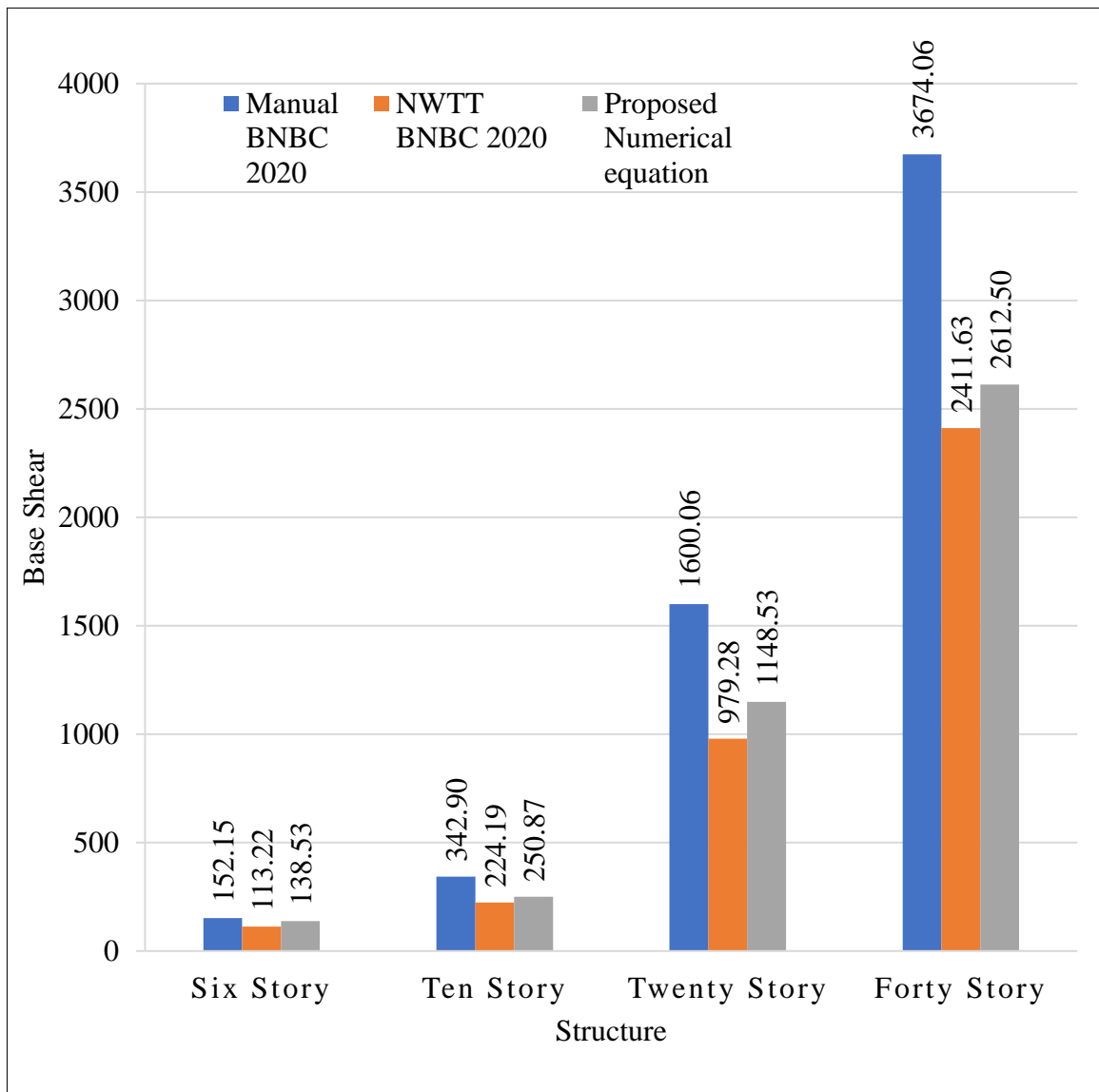


Figure 4.43: Comparison of base shear in the Long direction

Table 4.4 represents the comparison of base shear in the short direction. It was found that the manually calculated BNBC 2020 is relatively conservative with respect to the numerical wind tunnel test of BNBC 2020; it evaluated the base shear 29% to 66% higher than the numerical wind tunnel and the average for the calculated four building was 53.1% in the short direction. On the other hand, base shear calculated using the proposed empirical equations showed less variation with respect to the numerical wind tunnel test; it illustrated variations of 22% to 39% higher value than the numerical wind tunnel test data tunnel and the average for the calculated four building was 28.4% in the short direction.

Table 4.4: Comparison of base shear in short direction

Story	NWTT BNBC 2020	Manual Calculation BNBC- 2020	Variation (%) w.r.t NWTT BNBC 2020	Proposed Numerical Equation	Variation (%) w.r.t NWTT BNBC 2020
Six Story	90.05	116.12	29.0	110.83	23.1
Ten Story	132.57	212.97	60.6	170.45	28.6
Twenty Story	459.83	764.71	66.3	643.51	39.9
Forty Story	1443.74	2258.41	56.4	1761.04	22.0

Figure 4.44 is another informative graph that represent the comparison of base shear in the short direction. In evaluation of the base shear by the guidelines are as follows- Manual calculation of BNBC 2020 > Proposed numerical Equation > Numerical wind tunnel test of BNBC 2020.

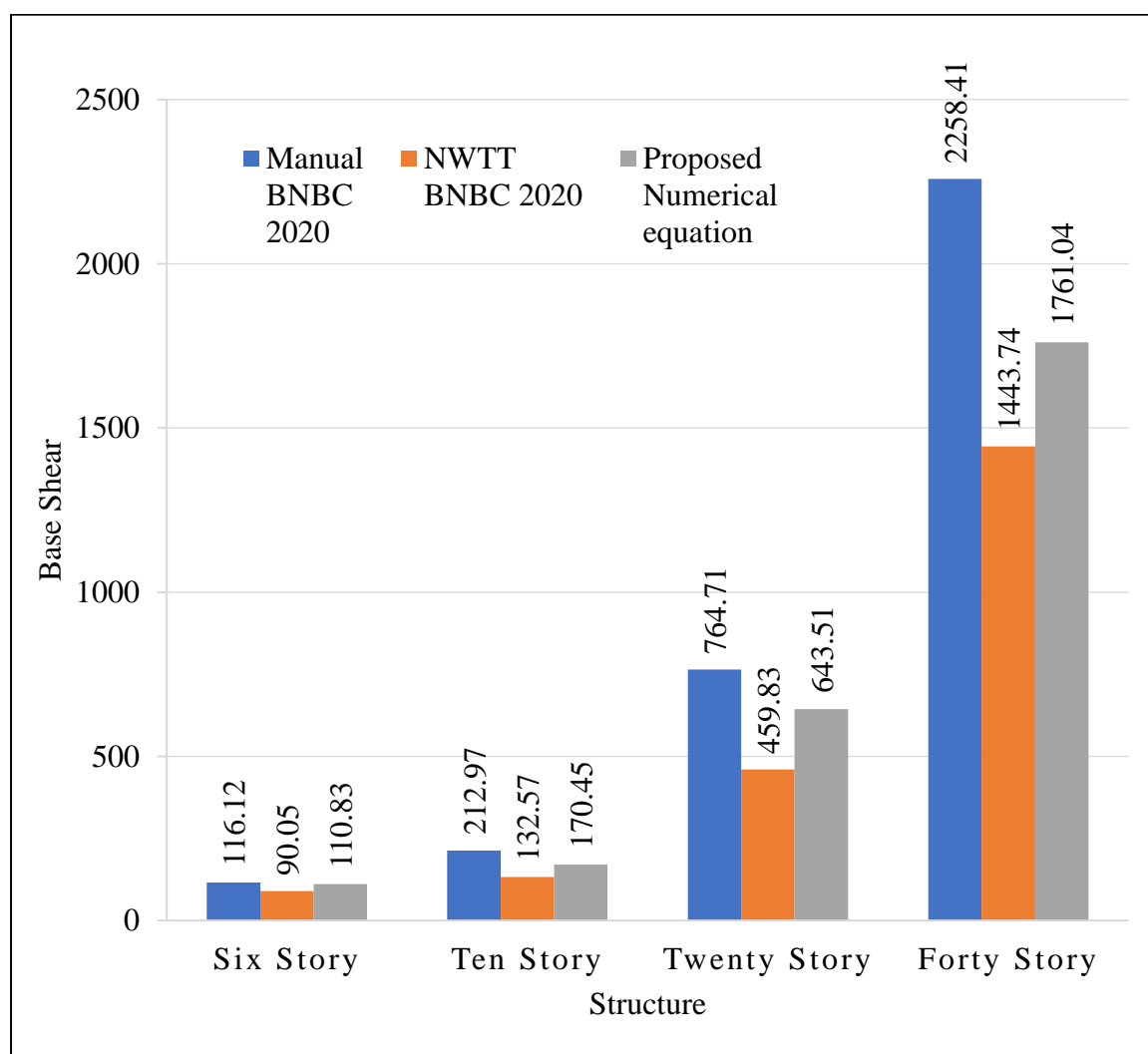


Figure 4.44: Comparison of base shear in the Short direction

4.5 Summary

A comparison of the story share of the BNBC 2006 manual, BNBC 2006 wind tunnel, BNBC 2020 manual, BNBC 2020 wind tunnel, ASCE 7-05, and UBC 94 was performed for different structures initially. Variable wind pressure coefficients were used, and structures were divided into three special zones for different structures with variable length-width ratios. After having the results, with the help of the standard deviation plus the average, a numerical equation for each zone was developed. The development of empirical equations was based on 20 different buildings of four different categories and five different length-width ratios. The results concluded that the proposed empirical equations evaluated the wind load effects on structures better than the BNBC 2020 concerning the numerical wind tunnel results. The study concluded with satisfactory results that the proposed empirical equations evaluate the wind loads better than the BNBC 2020.

CHAPTER 05

CONCLUSIONS AND RECOMMENDATIONS

5.1 Introduction

Wind tunnel tests have been industry-wide accepted tools for evaluating wind effects on tall buildings among wind-sensitive and complex-shaped structures. Aerodynamic wind tunnel tests are the most used tests for estimating design wind effects on a tall building. Since the building geometry is the only parameter modelled in aerodynamic wind tunnel tests, analytical procedures consider the effect of dynamic properties of the building. A numerical wind tunnel could be used as an alternative or equivalent to the physical wind tunnel.

The validation of the numerical wind tunnel performed satisfactorily, and the results are in good agreement with experimental data, and that's why the numerical wind tunnel ($k - \epsilon$) was chosen for this study. Four-building of the various geometric property was modeled and simulated to compare the evaluation characteristic of the codes in terms of the wind pressure coefficient. Another twenty models with different length-width ratios were simulated and analyzed to develop empirical equations for calculating the wind pressure coefficient.

This study attempted to assess the wind pressure coefficient on the surface of structures, an aerodynamic property, and evaluate the effects of different pressure coefficients on different surfaces of structures. Local and global standards were also studied, and comparison was performed in calculating the lateral base shear or story shear and numerical wind tunnel test results.

5.2 Conclusions

Investigation of this study could be divided into three sections, (i) calculation of the shear force due to the lateral wind load by the standards, (ii) effect of variable coefficients at different points of surfaces of structures using numerical wind tunnel test (CFD analysis), (iii) performance of proposed empirical equations for calculation of the variable coefficients at specified zones of structures. The conclusions of this study were as follows-

- i. BNBC-2020 and ASCE 7-05 showed similarity in determining the wind pressure coefficient; story-wise average variation was 0.32% to 1.08% in the long direction and 0.8% to 1.26% in the short direction.
- ii. BNBC-2006 and UBC- 94 had similar results with a story-wise average variation ranging from 0.16% to 11.41% in the long direction and 0.47% to 11.36% in the short direction.
- iii. BNBC-2020 and BNBC-2006 showed a considerable variation in calculating the wind pressure coefficient. The story-wise average variation ranged from 47% to 53% in the long direction and 37% to 47% in the short direction.
- iv. The numerical wind tunnel for the BNBC 2020 showed relatively less variation in calculation of the shear force with the BNBC-2020 manual, and the average variation was 20% to 30% in the long direction and 16% to 33% in the short direction. Variations were significant for the BNBC-2006 to the numerical wind tunnel, where average variation was 54% to 63% in the long direction and 50% to 53% in the short direction.
- v. In determining base shear, the proposed equations demonstrated better performance as they showed a mean variation of 15% to the numerical wind tunnel in the long direction. In contrast, the BNBC 2020 showed about 50%. Moreover, in the short direction, the proposed equations showed a mean variation of 28% compared to 53% of the BNBC 2020.
- vi. The empirical equation performs better than methods 1 and 2 according to BNBC in calculating wind pressure on structures and has good agreement with numerical wind tunnel results. As a result, the wind pressure on the structure can be calculated using those empirical equations.

5.3 Recommendations for Future Work

- i. This research concluded with empirical equations in evaluating the effect of wind load based on only 20 models with regular-shaped buildings. However, the same study can be done with irregular structures.
- ii. The K-epsilon model was used throughout this research; the latest model, such as the LES (Large Eddy Simulation) and others, could have been considered for higher accuracy.

- iii. Wind tunnel tests were highly recommended for complex-shaped and super-tall structures for accuracy.

REFERENCES

- Abuku, M., Blocken, B., & Roels, S. (2009). Moisture response of building facades to wind-driven rain: field measurements compared with numerical simulations. *Journal of Wind Engineering and Industrial Aerodynamics*, 97(5-6), 197-207.
- Adam, B., 1896. Chain Pier destroyed by storm. [Online] Available: https://workwithgoat.com/cool_timeline/chain-pier-destroyed-storm. [5 February 2022].
- Anderson, J. D., & Wendt, J. (1995). *Computational Fluid Dynamics*. New York: McGraw-Hill.
- ASCE/SEI 7-10. (2010). *Minimum design loads for buildings and other structures*. In American Society of Civil Engineers.
- Assaad, B. (2015). *Wind Effect on Super-tall Buildings Using Computational Fluid Dynamics and Structural Dynamics* (Doctoral dissertation, Florida Atlantic University).
- Bangladesh National Building Code, BNBC, 2006, Housing and Building Research Institute and Bangladesh Standard and Testing Institute, Bangladesh.
- Bangladesh National Building Code, BNBC, 2020, Housing and Building Research Institute and Bangladesh Standard and Testing Institute, Bangladesh
- Baskaran, A., & Stathopoulos, T. (1994). Prediction of wind effects on buildings using computational methods—review of the state of the art. *Canadian Journal of Civil Engineering*, 21(5), 805-822.
- Bitsuamlak, G. T., Dagnew, A., & Gan Chowdhury, A. (2010). Computational assessment of blockage and wind simulator proximity effects for a new full-scale testing facility. *Wind and Structures*, 13(1), 21.
- Bitsuamlak, G., & Simiu, E. (2010, May). CFD's potential applications: a wind engineering perspective. In *The fifth International Symposium on Computational Wind Engineering*. Chapel Hill, North Carolina, USA.

- Blocken, B. (2014). 50 years of computational wind engineering: past, present and future. *Journal of Wind Engineering and Industrial Aerodynamics*, 129, 69-102.
- Braun, A. L., & Awruch, A. M. (2009). Aerodynamic and aeroelastic analyses on the CAARC standard tall building model using numerical simulation. *Computers & Structures*, 87(9-10), 564-581.
- Charisi, S., Thiis, T. K., & Aurlien, T. (2019). Full-scale measurements of wind-pressure coefficients in twin medium-rise buildings. *Buildings*, 9(3), 63.
- Computers and Structures Inc., (2022). ETABS Integrated Software for Structural Analysis and Design. [Online] Available: <https://www.csiamerica.com/products/etabs>. [10 January 2022].
- Costola, D., Blocken, B., & Hensen, J. L. M. (2009). Overview of pressure coefficient data in building energy simulation and airflow network programs. *Building and environment*, 44(10), 2027-2036.
- Daemei, A. B., Aeinehvand, R., Kazemi, M., & Khotbehsara, E. M. (2019). Numerical Simulation of Wind Impacts on Building Blocks: Towards Sustainable Architecture Strategies. *European Journal of Sustainable Development Research*, 3(4).
- Dagneu, A. (2012). Computational evaluation of wind loads on low-and high-rise buildings (Doctoral dissertation, Florida International University).
- Dagneu, A. K., Bitsuamalk, G. T., & Merrick, R. (2009). Computational evaluation of wind pressures on tall buildings. In 11th american conference on wind engineering. San Juan, Puerto Rico.
- Dagneu, A., & Bitsuamlak, G. T. (2013). Computational evaluation of wind loads on buildings: a review. *Wind Struct*, 16(6), 629-660.
- Dlupal Software GmbH, (2022). RWIND Simulation, Wind Simulation (Wind Tunnel). [Online] Available: <https://www.dlupal.com/en/products/stand-alone-structural-analysis-software/rwind-simulation>. [6 March 2022].

- Dlubal Software GmbH, (2021). RWIND Simulation. [Online] Available: <https://www.dlubal.com/en/products/stand-alone-structural-analysis-software/rwind-simulation>. [24 February 2022].
- Girimaji, S., & Abdol-Hamid, K. (2005, January). Partially-averaged Navier Stokes model for turbulence: Implementation and validation. In 43rd AIAA Aerospace Sciences Meeting and Exhibit (p. 502). Reno, Nevada.
- Grosso, M. (1992). Wind pressure distribution around buildings: a parametrical model. *Energy and Buildings*, 18(2), 101-131.
- Holmes, J. D. (2007). *Wind loading of structures*. CRC press.
- Huang, S., Li, Q. S., & Xu, S. (2007). Numerical evaluation of wind effects on a tall steel building by CFD. *Journal of Constructional Steel Research*, 63(5), 612-627.
- Huang, S., Li, Q. S., & Xu, S. (2007). Numerical evaluation of wind effects on a tall steel building by CFD. *Journal of Constructional Steel Research*, 63(5), 612-627.
- Hui, Y., Tamura, Y., & Yoshida, A. (2012). Mutual interference effects between two high-rise building models with different shapes on local peak pressure coefficients. *Journal of Wind Engineering and Industrial Aerodynamics*, 104, 98-108.
- Kato, M. (1993). The modelling of turbulent flow around stationary and vibrating square cylinders. *Turbulent Shear Flow*, 1, 10-4.
- Kawamoto, S. (1998). Estimation of wind loading by computational fluid dynamics-Part2: High-rise building case. In *Proc. of AIJ Annual Meeting, 1998*.
- Kim, W., Tamura, Y., & Yoshida, A. (2011). Interference effects on local peak pressures between two buildings. *Journal of Wind Engineering and Industrial Aerodynamics*, 99(5), 584-600.
- Kim, Y. C., & Kanda, J. (2013). Wind pressures on tapered and set-back tall buildings. *Journal of Fluids and Structures*, 39, 306-321.

- Kondo, K., Murakami, S., & Mochida, A. (1997). Generation of velocity fluctuations for inflow boundary condition of LES. *Journal of Wind Engineering and Industrial Aerodynamics*, 67, 51-64.
- Köse, D. A., & Dick, E. (2010). Prediction of the pressure distribution on a cubical building with implicit LES. *Journal of wind engineering and industrial aerodynamics*, 98(10-11), 628-649.
- Kwon, D. K., & Kareem, A. (2013). Generalized gust-front factor: A computational framework for wind load effects. *Engineering structures*, 48, 635-644.
- Lam, K. M., Leung, M. Y. H., & Zhao, J. G. (2008). Interference effects on wind loading of a row of closely spaced tall buildings. *Journal of Wind Engineering and Industrial Aerodynamics*, 96(5), 562-583.
- Launder, B. E. (1993). Modeling flow-induced oscillations in turbulent flow around a square cylinder. In *ASME Fluid Engineering conference 1993*. Washington, DC.
- Liaw, K. F. (2005). Simulation of flow around bluff bodies and bridge deck sections using CFD (Doctoral dissertation, University of Nottingham).
- Lim, H. C., Thomas, T. G., & Castro, I. P. (2009). Flow around a cube in a turbulent boundary layer: LES and experiment. *Journal of Wind Engineering and Industrial Aerodynamics*, 97(2), 96-109.
- Lin, N., Letchford, C., Tamura, Y., Liang, B., & Nakamura, O. (2005). Characteristics of wind forces acting on tall buildings. *Journal of Wind Engineering and Industrial Aerodynamics*, 93(3), 217-242.
- Melbourne, W. H. (1980). Comparison of measurements on the CAARC standard tall building model in simulated model wind flows. *Journal of Wind Engineering and Industrial Aerodynamics*, 6(1-2), 73-88.
- Morgan, M., & Morgan, R. (1984). *South on the Sound: An Illustrated History of Tacoma and Pierce County*. Windsor Publications.

- Mou, B., He, B. J., Zhao, D. X., & Chau, K. W. (2017). Numerical simulation of the effects of building dimensional variation on wind pressure distribution. *Engineering Applications of Computational Fluid Mechanics*, 11(1), 293-309.
- Murakami, S., & Mochida, A. (1988). 3-D numerical simulation of airflow around a cubic model by means of the k- ϵ model. *Journal of Wind Engineering and Industrial Aerodynamics*, 31(2-3), 283-303.
- Murakami, S., Mochida, A., & Hibi, K. (1987). Three-dimensional numerical simulation of air flow around a cubic model by means of large eddy simulation. *Journal of Wind Engineering and Industrial Aerodynamics*, 25(3), 291-305.
- Nozawa, K., & Tamura, T. (2002). Large eddy simulation of the flow around a low-rise building immersed in a rough-wall turbulent boundary layer. *Journal of Wind Engineering and Industrial Aerodynamics*, 90(10), 1151-1162.
- Phillips, D. A., & Soligo, M. J. (2019). Will CFD ever replace wind tunnels for building wind simulations?. *International Journal of High-Rise Buildings*, 8(2), 107-116.
- Richards, P. J., & Hoxey, R. P. (2008). Wind loads on the roof of a 6 m cube. *Journal of Wind Engineering and Industrial Aerodynamics*, 96(6-7), 984-993.
- Selvam, R. P. (1996). Computation of flow around Texas Tech building using k- ϵ and Kato-Lauder k- ϵ turbulence model. *Engineering structures*, 18(11), 856-860.
- Selvama, P., & Landrus, K. (2010). GPU Computing for wind engineering. In *Proceedings: Fifth International International Symposium on Computational Wind Engineering (CWE2010)*, Chapel Hill, NC, May (pp. 23-27).
- Senthooran, S., Lee, D. D., & Parameswaran, S. (2004). A computational model to calculate the flow-induced pressure fluctuations on buildings. *Journal of Wind Engineering and Industrial Aerodynamics*, 92(13), 1131-1145.
- Smith, B. S., Coull, A., & Stafford-Smith, B. S. (1991). *Tall building structures: analysis and design (Vol. 5)*. New York: Wiley.

- Song, C. S., & Park, S. O. (2009). Numerical simulation of flow past a square cylinder using partially-averaged Navier–Stokes model. *Journal of Wind Engineering and Industrial Aerodynamics*, 97(1), 37-47.
- Stathopoulos, T. (2002). The numerical wind tunnel for industrial aerodynamics: Real or virtual in the new millennium?. *Wind and Structures*, 5(2-4), 193-208.
- Stathopoulos, T. (2003). Wind loads on low buildings: in the wake of Alan Davenport's contributions. *Journal of wind engineering and industrial aerodynamics*, 91(12-15), 1565-1585.
- Stathopoulos, T., & Baskaran, B. A. (1996). Computer simulation of wind environmental conditions around buildings. *Engineering structures*, 18(11), 876-885.
- Tanaka, H., Tamura, Y., Ohtake, K., Nakai, M., & Kim, Y. C. (2012). Experimental investigation of aerodynamic forces and wind pressures acting on tall buildings with various unconventional configurations. *Journal of Wind Engineering and Industrial Aerodynamics*, 107, 179-191.
- Taranath, B. S. (2004). *Wind and earthquake resistant buildings: Structural analysis and design*. CRC press.
- Tecele, A. S., Bitsuamlak, G. T., & Aly, A. M. (2013). Internal pressure in a low-rise building with existing envelope openings and sudden breaching. *Wind & structures*, 16(1), 25-46.
- The Business Standard , 2021. Story of the Iconic Legacy Tower in Bangladesh. [Online] Available: <https://www.tbsnews.net/feature/story-iconic-legacy-tower-bangladesh-219280>. [12 February 2022].
- Thornton Tomasetti, 2009. ONE INDIANA SQUARE. [Online] Available: <https://www.thorntontomasetti.com/project/one-indiana-square>. [12 February 2022].
- Tsuchiya, M., Murakami, S., Mochida, A., Kondo, K., & Ishida, Y. (1997). Development of a new $k-\epsilon$ model for flow and pressure fields around bluff body. *Journal of Wind Engineering and Industrial Aerodynamics*, 67, 169-182.

- Versteeg, H. K., & Malalasekera, W. (2007). An introduction to computational fluid dynamics: the finite volume method. Pearson education.
- Wright, N. G., & Easom, G. J. (2003). Non-linear k- ϵ turbulence model results for flow over a building at full-scale. *Applied Mathematical Modelling*, 27(12), 1013-1033.
- Yakhot, V. S. A. S. T. B. C. G., Orszag, S. A., Thangam, S., Gatski, T. B., & Speziale, C. (1992). Development of turbulence models for shear flows by a double expansion technique. *Physics of Fluids A: Fluid Dynamics*, 4(7), 1510-1520.
- Yilmaz, E., & Duffin, B. (2014). Computational fluid dynamics assessment of damaging wind loads on the One Indiana Square tower. *Environmental Fluid Mechanics*, 14(4), 795-819.
- Yu, X. F., Xie, Z. N., Zhu, J. B., & Gu, M. (2015). Interference effects on wind pressure distribution between two high-rise buildings. *Journal of Wind Engineering and Industrial Aerodynamics*, 142, 188-197.
- Zhang, A., & Gu, M. (2008). Wind tunnel tests and numerical simulations of wind pressures on buildings in staggered arrangement. *Journal of Wind Engineering and Industrial Aerodynamics*, 96(10-11), 2067-2079.

APPENDICES

Appendix A

Story share calculation of six storied regular shape building

Table A.1: Story shear in the long direction for the six storied building

Story	Height	BNBC-2006	UBC-94	Variation (%)	BNBC-2020	ASCE 7-05	Variation (%)
Roof	62	31.28	30.77	-1.64	14.54	14.46	-0.55
5th	52	91.06	90.88	-0.20	43.30	42.94	-0.83
4th	42	147.95	149.29	0.90	71.35	70.65	-0.98
3rd	32	201.78	203.23	0.72	98.55	97.44	-1.13
2nd	22	252.34	252.72	0.15	124.69	123.03	-1.33
1st	12	304.05	302.43	-0.53	152.15	150.08	-1.36
Base	0	304.05	302.43	-0.53	152.15	150.08	-1.36

Table A.2: Story shear in the long direction for the six storied building

Story	Height	BNBC-2006	NWTT_BNBC-2006	Variation (%)	BNBC-2020	NWTT_BNBC-2020	Variation (%)
Roof	62	31.28	17.66	-43.55	14.54	12.16	-16.35
5th	52	91.06	52.41	-42.45	43.30	36.55	-15.60
4th	42	147.95	87.40	-40.92	71.35	60.43	-15.30
3rd	32	201.78	118.11	-41.47	98.55	81.57	-17.23
2nd	22	252.34	143.66	-43.07	124.69	98.66	-20.88
1st	12	304.05	166.34	-45.29	152.15	113.22	-25.59
Base	0	304.05	166.34	-45.29	152.15	113.22	-25.59

Table A.3: Story shear in the long direction for the six storied building

Story	Height	BNBC-2006	BNBC-2020	Variation (%)	NWTT_BNBC-2006	NWTT_BNBC-2020	Variation (%)
Roof	62	31.28	14.54	-53.52	17.66	12.16	-31.13
5th	52	91.06	43.30	-52.45	52.41	36.55	-30.27
4th	42	147.95	71.35	-51.77	87.40	60.43	-30.86
3rd	32	201.78	98.55	-51.16	118.11	81.57	-30.94
2nd	22	252.34	124.69	-50.59	143.66	98.66	-31.32
1st	12	304.05	152.15	-49.96	166.34	113.22	-31.94
Base	0	304.05	152.15	-49.96	166.34	113.22	-31.94

Table A.4: Story shear in the short direction for the six storied building

Story	Height	BNBC-2006	UBC-94	Variation (%)	BNBC-2020	ASCE 7-05	Variation (%)
Roof	62	21.99	21.52	-2.14	11.12	11.07	-0.48
5th	52	64.02	63.56	-0.72	33.10	32.84	-0.78
4th	42	104.01	104.42	0.39	54.51	54.00	-0.92
3rd	32	141.85	142.14	0.21	75.25	74.43	-1.09
2nd	22	177.39	176.76	-0.36	95.14	93.91	-1.30
1st	12	213.75	211.53	-1.04	116.12	114.46	-1.43
Base	0	213.75	211.53	-1.04	116.12	114.46	-1.43

Table A.5: Story shear in the short direction for the six storied building

Story	Height	BNBC-2006	NWTT_BNBC-2006	Variation (%)	BNBC-2020	NWTT_BNBC-2020	Variation (%)
Roof	62	21.99	13.91	-36.74	11.12	9.54	-14.18
5th	52	64.02	41.32	-35.46	33.10	28.82	-12.92
4th	42	104.01	68.89	-33.77	54.51	47.53	-12.80
3rd	32	141.85	92.99	-34.45	75.25	64.25	-14.62
2nd	22	177.39	113.42	-36.06	95.14	78.26	-17.74
1st	12	213.75	131.76	-38.36	116.12	90.05	-22.45
Base	0	213.75	131.76	-38.36	116.12	90.05	-22.45

Table A.6: Story shear in the short direction for the six storied building

Story	Height	BNBC-2006	BNBC-2020	Variation (%)	NWTT_BNBC-2006	NWTT_BNBC-2020	Variation (%)
Roof	62	21.99	11.12	-49.44	13.91	9.54	-31.40
5th	52	64.02	33.10	-48.30	41.32	28.82	-30.26
4th	42	104.01	54.51	-47.59	68.89	47.53	-31.01
3rd	32	141.85	75.25	-46.95	92.99	64.25	-30.91
2nd	22	177.39	95.14	-46.37	113.42	78.26	-31.00
1st	12	213.75	116.12	-45.67	131.76	90.05	-31.66
Base	0	213.75	116.12	-45.67	131.76	90.05	-31.66

Appendix B

Story share calculation of ten storied regular shape building

Table B.1: Story shear in the long direction for the ten storied building

Story	Height	BNBC-2006	UBC-94	Variation (%)	BNBC-2020	ASCE 7-05	Variation (%)
Roof	100	41.58	39.79	-4.32	20.14	20.02	-0.61
9th	90	120.99	119.35	-1.35	60.05	59.56	-0.82
8th	80	196.65	195.76	-0.45	99.19	98.30	-0.90
7th	70	268.51	268.99	0.18	137.50	136.16	-0.97
6th	60	336.46	339.05	0.77	174.89	173.06	-1.04
5th	50	400.31	405.95	1.41	211.26	208.87	-1.13
4th	40	459.79	468.97	2.00	246.46	243.42	-1.23
3rd	30	514.54	524.95	2.02	280.28	276.45	-1.37
2nd	20	564.09	573.80	1.72	312.38	307.58	-1.54
1st	10	607.84	617.90	1.66	342.90	337.54	-1.56
Base	0	607.84	617.90	1.66	342.90	337.54	-1.56

Table B.2: Story shear in the long direction for the ten storied building

Story	Height	BNBC-2006	NWTT_BNBC-2006	Variation (%)	BNBC-2020	NWTT_BNBC-2020	Variation (%)
Roof	100	41.58	17.44	-58.05	20.14	13.57	-32.64
9th	90	120.99	54.71	-54.78	60.05	43.24	-27.99
8th	80	196.65	96.14	-51.11	99.19	75.65	-23.73
7th	70	268.51	134.98	-49.73	137.50	107.04	-22.15
6th	60	336.46	170.31	-49.38	174.89	135.01	-22.80
5th	50	400.31	199.60	-50.14	211.26	159.22	-24.63
4th	40	459.79	225.95	-50.86	246.46	180.42	-26.79
3rd	30	514.54	247.26	-51.95	280.28	197.90	-29.39
2nd	20	564.09	263.92	-53.21	312.38	211.58	-32.27
1st	10	607.84	279.18	-54.07	342.90	224.19	-34.62
Base	0	607.84	279.18	-54.07	342.90	224.19	-34.62

Table B.3: Story shear in the long direction for the ten storied building

Story	Height	BNBC-2006	BNBC-2020	Variation (%)	NWTT_BNBC-2006	NWTT_BNBC-2020	Variation (%)
Roof	100	41.58	20.14	-51.56	17.44	13.57	-22.23
9th	90	120.99	60.05	-50.37	54.71	43.24	-20.96
8th	80	196.65	99.19	-49.56	96.14	75.65	-21.31
7th	70	268.51	137.50	-48.79	134.98	107.04	-20.70
6th	60	336.46	174.89	-48.02	170.31	135.01	-20.73
5th	50	400.31	211.26	-47.23	199.60	159.22	-20.23
4th	40	459.79	246.46	-46.40	225.95	180.42	-20.15
3rd	30	514.54	280.28	-45.53	247.26	197.90	-19.96
2nd	20	564.09	312.38	-44.62	263.92	211.58	-19.83
1st	10	607.84	342.90	-43.59	279.18	224.19	-19.69
Base	0	607.84	342.90	-43.59	279.18	224.19	-19.69

Table B.4: Story shear in the short direction for the ten storied regular building

Story	Height	BNBC-2006	UBC-94	Variation (%)	BNBC-2020	ASCE 7-05	Variation (%)
Roof	100	21.72	20.78	-4.33	12.63	12.55	-0.65
9th	90	63.20	62.34	-1.37	37.64	37.31	-0.89
8th	80	102.72	102.24	-0.47	62.13	61.52	-0.98
7th	70	140.25	140.49	0.17	86.05	85.14	-1.05
6th	60	175.74	177.08	0.76	109.35	108.11	-1.13
5th	50	209.08	212.02	1.41	131.95	130.34	-1.22
4th	40	240.14	244.93	2.00	153.76	151.70	-1.34
3rd	30	268.74	274.17	2.02	174.63	172.04	-1.48
2nd	20	294.62	299.69	1.72	194.34	191.08	-1.68
1st	10	317.47	322.72	1.65	212.97	209.34	-1.71
Base	0	317.47	322.72	1.65	212.97	209.34	-1.71

Table B.5: Story Shear in the Short direction of the ten storied regular building

Story	Height	BNBC-2006	NWTT_BNBC-2006	Variation (%)	BNBC-2020	NWTT_BNBC-2020	Variation (%)
Roof	100	21.72	10.93	-49.69	12.63	8.51	-32.60
9th	90	63.20	33.47	-47.04	37.64	26.56	-29.44
8th	80	102.72	57.01	-44.50	62.13	45.21	-27.24
7th	70	140.25	78.37	-44.12	86.05	62.88	-26.93
6th	60	175.74	98.46	-43.97	109.35	79.08	-27.68
5th	50	209.08	115.66	-44.68	131.95	93.52	-29.12
4th	40	240.14	131.23	-45.35	153.76	106.14	-30.97
3rd	30	268.74	143.88	-46.46	174.63	116.75	-33.14
2nd	20	294.62	153.83	-47.79	194.34	125.24	-35.56
1st	10	317.47	162.22	-48.90	212.97	132.57	-37.75
Base	0	317.47	162.22	-48.90	212.97	132.57	-37.75

Table B.6: Story shear in the short direction for the ten storied regular building

Story	Height	BNBC-2006	BNBC-2020	Variation (%)	NWTT_BNBC-2006	NWTT_BNBC-2020	Variation (%)
Roof	100	21.72	12.63	-41.85	10.93	8.51	-22.11
9th	90	63.20	37.64	-40.44	33.47	26.56	-20.65
8th	80	102.72	62.13	-39.52	57.01	45.21	-20.70
7th	70	140.25	86.05	-38.65	78.37	62.88	-19.77
6th	60	175.74	109.35	-37.78	98.46	79.08	-19.68
5th	50	209.08	131.95	-36.89	115.66	93.52	-19.14
4th	40	240.14	153.76	-35.97	131.23	106.14	-19.12
3rd	30	268.74	174.63	-35.02	143.88	116.75	-18.86
2nd	20	294.62	194.34	-34.04	153.83	125.24	-18.58
1st	10	317.47	212.97	-32.92	162.22	132.57	-18.28
Base	0	317.47	212.97	-32.92	162.22	132.57	-18.28

Appendix C

Story share calculation of twenty storied regular shape building

Table C.1: Story shear in the long direction for the twenty storied building

Story	Height	BNBC-2006	UBC-94	Variation (%)	BNBC-2020	ASCE 7-05	Variation (%)
Roof	200	116.27	89.45	-23.06	46.55	46.41	-0.30
19th	190	338.06	268.36	-20.62	139.23	138.67	-0.41
18th	180	549.81	447.27	-18.65	231.06	230.06	-0.43
17th	170	752.16	626.18	-16.75	322.00	320.55	-0.45
16th	160	945.68	798.16	-15.60	412.02	410.10	-0.47
15th	150	1130.87	963.21	-14.83	501.08	498.67	-0.48
14th	140	1308.17	1128.26	-13.75	589.14	586.21	-0.50
13th	130	1477.95	1293.31	-12.49	676.14	672.66	-0.51
12th	120	1640.53	1451.43	-11.53	762.03	757.97	-0.53
11th	110	1796.14	1602.62	-10.77	846.74	842.06	-0.55
10th	100	1944.95	1749.40	-10.05	930.19	924.86	-0.57
9th	90	2087.04	1891.78	-9.36	1012.29	1006.25	-0.60
8th	80	2222.42	2028.48	-8.73	1092.94	1086.14	-0.62
7th	70	2351.00	2159.51	-8.14	1172.01	1164.37	-0.65
6th	60	2472.57	2284.88	-7.59	1249.34	1240.77	-0.69
5th	50	2586.81	2404.57	-7.04	1324.73	1315.10	-0.73
4th	40	2693.23	2517.34	-6.53	1397.90	1387.04	-0.78
3rd	30	2791.20	2617.51	-6.22	1468.45	1456.10	-0.84
2nd	20	2879.87	2704.92	-6.07	1535.75	1521.56	-0.92
1st	10	2958.15	2783.83	-5.89	1600.06	1584.80	-0.95
Base	0	2958.15	2783.83	-5.89	1600.06	1584.80	-0.95

Table C.2: Story shear in the long direction for the twenty storied building

Story	Height	BNBC- 2006	NWTT_B NBC- 2006	Variation (%)	BNBC- 2020	NWTT_B NBC- 2020	Variation (%)
Roof	200	116.27	41.40	-64.40	46.55	27.88	-40.11
19th	190	338.06	129.93	-61.57	139.23	92.64	-33.46
18th	180	549.81	230.46	-58.08	231.06	166.70	-27.86
17th	170	752.16	329.65	-56.17	322.00	239.78	-25.53
16th	160	945.68	427.71	-54.77	412.02	311.20	-24.47
15th	150	1130.87	520.70	-53.96	501.08	381.23	-23.92
14th	140	1308.17	613.18	-53.13	589.14	449.89	-23.64
13th	130	1477.95	704.77	-52.31	676.14	516.64	-23.59
12th	120	1640.53	793.55	-51.63	762.03	579.97	-23.89
11th	110	1796.14	872.50	-51.42	846.74	638.17	-24.63
10th	100	1944.95	945.82	-51.37	930.19	690.86	-25.73
9th	90	2087.04	1012.29	-51.50	1012.29	739.08	-26.99
8th	80	2222.42	1075.05	-51.63	1092.94	783.36	-28.33
7th	70	2351.00	1131.63	-51.87	1172.01	823.56	-29.73
6th	60	2472.57	1184.17	-52.11	1249.34	859.23	-31.23
5th	50	2586.81	1229.97	-52.45	1324.73	890.24	-32.80
4th	40	2693.23	1271.88	-52.78	1397.90	916.38	-34.45
3rd	30	2791.20	1309.84	-53.07	1468.45	938.39	-36.10
2nd	20	2879.87	1346.17	-53.26	1535.75	958.24	-37.60
1st	10	2958.15	1382.02	-53.28	1600.06	979.28	-38.80
Base	0	2958.15	1382.02	-53.28	1600.06	979.28	-38.80

Table C.3: Story shear in the long direction for the twenty storied building

Story	Height	BNBC-2006	BNBC-2020	Variation (%)	NWTT_BNBC-2006	NWTT_BNBC-2020	Variation (%)
Roof	200	116.27	46.55	-59.96	41.40	27.88	-32.65
19th	190	338.06	139.23	-58.82	129.93	92.64	-28.70
18th	180	549.81	231.06	-57.97	230.46	166.70	-27.67
17th	170	752.16	322.00	-57.19	329.65	239.78	-27.26
16th	160	945.68	412.02	-56.43	427.71	311.20	-27.24
15th	150	1130.87	501.08	-55.69	520.70	381.23	-26.79
14th	140	1308.17	589.14	-54.96	613.18	449.89	-26.63
13th	130	1477.95	676.14	-54.25	704.77	516.64	-26.69
12th	120	1640.53	762.03	-53.55	793.55	579.97	-26.91
11th	110	1796.14	846.74	-52.86	872.50	638.17	-26.86
10th	100	1944.95	930.19	-52.17	945.82	690.86	-26.96
9th	90	2087.04	1012.29	-51.50	1012.29	739.08	-26.99
8th	80	2222.42	1092.94	-50.82	1075.05	783.36	-27.13
7th	70	2351.00	1172.01	-50.15	1131.63	823.56	-27.22
6th	60	2472.57	1249.34	-49.47	1184.17	859.23	-27.44
5th	50	2586.81	1324.73	-48.79	1229.97	890.24	-27.62
4th	40	2693.23	1397.90	-48.10	1271.88	916.38	-27.95
3rd	30	2791.20	1468.45	-47.39	1309.84	938.39	-28.36
2nd	20	2879.87	1535.75	-46.67	1346.17	958.24	-28.82
1st	10	2958.15	1600.06	-45.91	1382.02	979.28	-29.14
Base	0	2958.15	1600.06	-45.91	1382.02	979.28	-29.14

Table C.4: Story shear in the short direction for the twenty storied building

Story	Height	BNBC-2006	UBC-94	Variation (%)	BNBC-2020	ASCE 7-05	Variation (%)
Roof	200	47.34	36.44	-23.02	22.70	22.60	-0.42
19th	190	137.64	109.32	-20.57	67.87	67.50	-0.55
18th	180	223.85	182.21	-18.60	112.56	111.91	-0.58
17th	170	306.23	255.09	-16.70	156.76	155.81	-0.60
16th	160	385.02	325.15	-15.55	200.44	199.19	-0.62
15th	150	460.42	392.39	-14.78	243.58	242.02	-0.64
14th	140	532.61	459.62	-13.70	286.16	284.27	-0.66
13th	130	601.74	526.86	-12.44	328.15	325.91	-0.68
12th	120	667.93	591.27	-11.48	369.51	366.91	-0.70
11th	110	731.28	652.86	-10.72	410.21	407.22	-0.73
10th	100	791.87	712.66	-10.00	450.21	446.81	-0.75
9th	90	849.72	770.66	-9.30	489.45	485.62	-0.78
8th	80	904.84	826.35	-8.67	527.88	523.58	-0.81
7th	70	957.19	879.73	-8.09	565.43	560.61	-0.85
6th	60	1006.69	930.80	-7.54	602.00	596.62	-0.89
5th	50	1053.20	979.56	-6.99	637.48	631.46	-0.94
4th	40	1096.53	1025.50	-6.48	671.72	664.97	-1.01
3rd	30	1136.42	1066.30	-6.17	704.49	696.85	-1.08
2nd	20	1172.52	1101.91	-6.02	735.44	726.73	-1.18
1st	10	1204.39	1134.06	-5.84	764.71	755.36	-1.22
Base	0	1204.39	1134.06	-5.84	764.71	755.36	-1.22

Table C.5: Story shear in the short direction for the twenty storied building

Story	Height	BNBC- 2006	NWTT_ BNBC- 2006	Variation (%)	BNBC- 2020	NWTT_ BNBC- 2020	Variation (%)
Roof	200	47.34	18.77	-60.35	22.70	12.96	-42.90
19th	190	137.64	58.33	-57.62	67.87	43.02	-36.61
18th	180	223.85	103.58	-53.73	112.56	77.72	-30.95
17th	170	306.23	149.22	-51.27	156.76	112.32	-28.35
16th	160	385.02	193.44	-49.76	200.44	145.31	-27.50
15th	150	460.42	232.77	-49.44	243.58	176.36	-27.60
14th	140	532.61	271.00	-49.12	286.16	206.25	-27.93
13th	130	601.74	308.47	-48.74	328.15	235.24	-28.31
12th	120	667.93	344.63	-48.40	369.51	262.57	-28.94
11th	110	731.28	376.65	-48.49	410.21	287.98	-29.80
10th	100	791.87	407.00	-48.60	450.21	311.90	-30.72
9th	90	849.72	434.73	-48.84	489.45	334.46	-31.67
8th	80	904.84	461.31	-49.02	527.88	355.52	-32.65
7th	70	957.19	485.36	-49.29	565.43	374.89	-33.70
6th	60	1006.69	508.06	-49.53	602.00	392.73	-34.76
5th	50	1053.20	528.51	-49.82	637.48	409.18	-35.81
4th	40	1096.53	547.65	-50.06	671.72	423.93	-36.89
3rd	30	1136.42	564.31	-50.34	704.49	436.79	-38.00
2nd	20	1172.52	579.29	-50.59	735.44	448.19	-39.06
1st	10	1204.39	594.45	-50.64	764.71	459.83	-39.87
Base	0	1204.39	594.45	-50.64	764.71	459.83	-39.87

Table C.6: Story shear in the short direction for the twenty storied building

Story	Height	BNBC-2006	UBC-94	BNBC-2020	% of Variation	NWTT_BNBC-2006	NWTT_BNBC-2020	% of Variation
Roof	200	47.34	36.44	22.70	-52.05	18.77	12.96	-30.94
19th	190	137.64	109.32	67.87	-50.69	58.33	43.02	-26.24
18th	180	223.85	182.21	112.56	-49.72	103.58	77.72	-24.97
17th	170	306.23	255.09	156.76	-48.81	149.22	112.32	-24.73
16th	160	385.02	325.15	200.44	-47.94	193.44	145.31	-24.88
15th	150	460.42	392.39	243.58	-47.10	232.77	176.36	-24.24
14th	140	532.61	459.62	286.16	-46.27	271.00	206.25	-23.89
13th	130	601.74	526.86	328.15	-45.47	308.47	235.24	-23.74
12th	120	667.93	591.27	369.51	-44.68	344.63	262.57	-23.81
11th	110	731.28	652.86	410.21	-43.91	376.65	287.98	-23.54
10th	100	791.87	712.66	450.21	-43.15	407.00	311.90	-23.36
9th	90	849.72	770.66	489.45	-42.40	434.73	334.46	-23.06
8th	80	904.84	826.35	527.88	-41.66	461.31	355.52	-22.93
7th	70	957.19	879.73	565.43	-40.93	485.36	374.89	-22.76
6th	60	1006.69	930.80	602.00	-40.20	508.06	392.73	-22.70
5th	50	1053.20	979.56	637.48	-39.47	528.51	409.18	-22.58
4th	40	1096.53	1025.50	671.72	-38.74	547.65	423.93	-22.59
3rd	30	1136.42	1066.30	704.49	-38.01	564.31	436.79	-22.60
2nd	20	1172.52	1101.91	735.44	-37.28	579.29	448.19	-22.63
1st	10	1204.39	1134.06	764.71	-36.51	594.45	459.83	-22.65
Base	0	1204.39	1134.06	764.71	-36.51	594.45	459.83	-22.65

Appendix D

Story share calculation of forty storied regular shape building

Table D.1: Story shear in the long direction for the forty storied building

Story	Height	BNBC-2006	UBC-94	Variation (%)	BNBC-2020	ASCE 7-05	Variation (%)
Roof	400	123.55	124.76	0.98	53.27	53.19	-0.15
39th	390	368.37	374.28	1.60	159.57	159.25	-0.20
38th	380	610.90	623.80	2.11	265.39	264.83	-0.21
37th	370	851.11	873.33	2.61	370.73	369.92	-0.22
36th	360	1088.99	1122.85	3.11	475.57	474.51	-0.22
35th	350	1324.52	1372.37	3.61	579.91	578.59	-0.23
34th	340	1557.68	1621.89	4.12	683.73	682.15	-0.23
33rd	330	1788.46	1871.41	4.64	787.02	785.18	-0.23
32nd	320	2016.84	2120.93	5.16	889.78	887.66	-0.24
31st	310	2242.81	2370.45	5.69	991.99	989.59	-0.24
30th	300	2466.34	2608.19	5.75	1093.64	1090.95	-0.25
29th	290	2687.11	2834.15	5.47	1194.71	1191.73	-0.25
28th	280	2905.09	3060.11	5.34	1295.19	1291.91	-0.25
27th	270	3120.25	3286.06	5.31	1395.07	1391.48	-0.26
26th	260	3332.55	3512.02	5.39	1494.33	1490.42	-0.26
25th	250	3541.97	3737.98	5.53	1592.95	1588.71	-0.27
24th	240	3748.47	3963.93	5.75	1690.91	1686.34	-0.27
23rd	230	3952.02	4189.89	6.02	1788.20	1783.29	-0.27
22nd	220	4152.59	4415.85	6.34	1884.79	1879.53	-0.28
21st	210	4350.16	4641.80	6.70	1980.67	1975.03	-0.28
20th	200	4544.69	4853.20	6.79	2075.80	2069.79	-0.29
19th	190	4735.72	5050.05	6.64	2170.16	2163.76	-0.30
18th	180	4923.21	5246.90	6.57	2263.73	2256.92	-0.30
17th	170	5107.09	5443.74	6.59	2356.47	2349.23	-0.31
16th	160	5287.31	5632.97	6.54	2448.34	2440.66	-0.31
15th	150	5463.81	5814.56	6.42	2539.31	2531.17	-0.32
14th	140	5636.03	5996.16	6.39	2629.34	2620.71	-0.33

Story	Height	BNBC-2006	UBC-94	Variation (%)	BNBC-2020	ASCE 7-05	Variation (%)
13th	130	5803.87	6177.76	6.44	2718.38	2709.23	-0.34
12th	120	5967.22	6351.74	6.44	2806.37	2796.68	-0.35
11th	110	6125.97	6518.09	6.40	2893.25	2882.98	-0.35
10th	100	6280.02	6679.59	6.36	2978.95	2968.07	-0.37
9th	90	6428.34	6836.23	6.35	3063.39	3051.84	-0.38
8th	80	6570.65	6986.64	6.33	3146.47	3134.20	-0.39
7th	70	6706.68	7130.82	6.32	3228.06	3215.01	-0.40
6th	60	6836.16	7268.75	6.33	3308.02	3294.09	-0.42
5th	50	6958.81	7400.45	6.35	3386.15	3371.23	-0.44
4th	40	7072.24	7524.52	6.40	3462.20	3446.13	-0.46
3rd	30	7175.07	7634.73	6.41	3535.79	3518.32	-0.49
2nd	20	7265.94	7730.90	6.40	3606.33	3587.13	-0.53
1st	10	7350.31	7817.72	6.36	3674.06	3653.86	-0.55
Base	0	7350.31	7817.72	6.36	3674.06	3653.86	-0.55

Table D.2: Story shear in the long direction for the forty storied building

Story	Height	BNBC-2006	NWTT_BNBC-2006	Variation (%)	BNBC-2020	NWTT_BNBC-2020	Variation (%)
Roof	400	123.55	31.87	-74.21	53.27	27.95	-47.54
39th	390	368.37	107.56	-70.80	159.57	94.93	-40.51
38th	380	610.90	197.65	-67.65	265.39	175.50	-33.87
37th	370	851.11	291.28	-65.78	370.73	259.50	-30.00
36th	360	1088.99	387.26	-64.44	475.57	344.65	-27.53
35th	350	1324.52	484.45	-63.42	579.91	430.10	-25.83
34th	340	1557.68	581.45	-62.67	683.73	515.76	-24.57
33rd	330	1788.46	678.54	-62.06	787.02	600.83	-23.66
32nd	320	2016.84	775.26	-61.56	889.78	684.82	-23.03
31st	310	2242.81	870.77	-61.18	991.99	767.42	-22.64
30th	300	2466.34	964.97	-60.87	1093.64	848.40	-22.42
29th	290	2687.11	1049.67	-60.94	1194.71	926.56	-22.44
28th	280	2905.09	1129.51	-61.12	1295.19	1000.47	-22.76

Story	Height	BNBC- 2006	NWTT_ BNBC- 2006	Variation (%)	BNBC- 2020	NWTT_ BNBC- 2020	Variation (%)
27th	270	3120.25	1205.42	-61.37	1395.07	1071.25	-23.21
26th	260	3332.55	1279.54	-61.60	1494.33	1140.17	-23.70
25th	250	3541.97	1352.62	-61.81	1592.95	1207.69	-24.19
24th	240	3748.47	1425.17	-61.98	1690.91	1274.47	-24.63
23rd	230	3952.02	1497.63	-62.10	1788.20	1340.98	-25.01
22nd	220	4152.59	1570.30	-62.19	1884.79	1406.49	-25.38
21st	210	4350.16	1642.83	-62.24	1980.67	1470.52	-25.76
20th	200	4544.69	1714.18	-62.28	2075.80	1533.28	-26.14
19th	190	4735.72	1778.00	-62.46	2170.16	1593.78	-26.56
18th	180	4923.21	1840.05	-62.62	2263.73	1651.28	-27.05
17th	170	5107.09	1900.56	-62.79	2356.47	1706.44	-27.58
16th	160	5287.31	1959.94	-62.93	2448.34	1760.23	-28.11
15th	150	5463.81	2015.83	-63.11	2539.31	1812.79	-28.61
14th	140	5636.03	2071.20	-63.25	2629.34	1864.30	-29.10
13th	130	5803.87	2126.29	-63.36	2718.38	1914.86	-29.56
12th	120	5967.22	2181.02	-63.45	2806.37	1964.56	-30.00
11th	110	6125.97	2233.01	-63.55	2893.25	2013.42	-30.41
10th	100	6280.02	2284.19	-63.63	2978.95	2060.72	-30.82
9th	90	6428.34	2332.94	-63.71	3063.39	2105.94	-31.25
8th	80	6570.65	2380.06	-63.78	3146.47	2149.14	-31.70
7th	70	6706.68	2424.39	-63.85	3228.06	2190.52	-32.14
6th	60	6836.16	2467.80	-63.90	3308.02	2230.17	-32.58
5th	50	6958.81	2509.30	-63.94	3386.15	2268.37	-33.01
4th	40	7072.24	2549.86	-63.95	3462.20	2305.30	-33.42
3rd	30	7175.07	2588.96	-63.92	3535.79	2340.90	-33.79
2nd	20	7265.94	2627.31	-63.84	3606.33	2375.59	-34.13
1st	10	7350.31	2666.62	-63.72	3674.06	2411.63	-34.36
Base	0	7350.31	2666.62	-63.72	3674.06	2411.63	-34.36

Table D.3: Story shear in the long direction for the forty storied building

Story	Height	BNBC- 2006	BNBC- 2020	Variation (%)	NWTT_ BNBC- 2006	NWTT_ BNBC -2020	Variation (%)
Roof	400	123.55	53.27	-56.88	31.87	27.95	-12.31
39th	390	368.37	159.57	-56.68	107.56	94.93	-11.75
38th	380	610.90	265.39	-56.56	197.65	175.50	-11.21
37th	370	851.11	370.73	-56.44	291.28	259.50	-10.91
36th	360	1088.99	475.57	-56.33	387.26	344.65	-11.00
35th	350	1324.52	579.91	-56.22	484.45	430.10	-11.22
34th	340	1557.68	683.73	-56.11	581.45	515.76	-11.30
33rd	330	1788.46	787.02	-55.99	678.54	600.83	-11.45
32nd	320	2016.84	889.78	-55.88	775.26	684.82	-11.67
31st	310	2242.81	991.99	-55.77	870.77	767.42	-11.87
30th	300	2466.34	1093.64	-55.66	964.97	848.40	-12.08
29th	290	2687.11	1194.71	-55.54	1049.67	926.56	-11.73
28th	280	2905.09	1295.19	-55.42	1129.51	1000.47	-11.42
27th	270	3120.25	1395.07	-55.29	1205.42	1071.25	-11.13
26th	260	3332.55	1494.33	-55.16	1279.54	1140.17	-10.89
25th	250	3541.97	1592.95	-55.03	1352.62	1207.69	-10.71
24th	240	3748.47	1690.91	-54.89	1425.17	1274.47	-10.57
23rd	230	3952.02	1788.20	-54.75	1497.63	1340.98	-10.46
22nd	220	4152.59	1884.79	-54.61	1570.30	1406.49	-10.43
21st	210	4350.16	1980.67	-54.47	1642.83	1470.52	-10.49
20th	200	4544.69	2075.80	-54.32	1714.18	1533.28	-10.55
19th	190	4735.72	2170.16	-54.17	1778.00	1593.78	-10.36
18th	180	4923.21	2263.73	-54.02	1840.05	1651.28	-10.26
17th	170	5107.09	2356.47	-53.86	1900.56	1706.44	-10.21
16th	160	5287.31	2448.34	-53.69	1959.94	1760.23	-10.19
15th	150	5463.81	2539.31	-53.52	2015.83	1812.79	-10.07
14th	140	5636.03	2629.34	-53.35	2071.20	1864.30	-9.99
13th	130	5803.87	2718.38	-53.16	2126.29	1914.86	-9.94
12th	120	5967.22	2806.37	-52.97	2181.02	1964.56	-9.92
11th	110	6125.97	2893.25	-52.77	2233.01	2013.42	-9.83
10th	100	6280.02	2978.95	-52.56	2284.19	2060.72	-9.78

Story	Height	BNBC-2006	BNBC-2020	Variation (%)	NWTT_BNBC-2006	NWTT_BNBC-2020	Variation (%)
9th	90	6428.34	3063.39	-52.35	2332.94	2105.94	-9.73
8th	80	6570.65	3146.47	-52.11	2380.06	2149.14	-9.70
7th	70	6706.68	3228.06	-51.87	2424.39	2190.52	-9.65
6th	60	6836.16	3308.02	-51.61	2467.80	2230.17	-9.63
5th	50	6958.81	3386.15	-51.34	2509.30	2268.37	-9.60
4th	40	7072.24	3462.20	-51.05	2549.86	2305.30	-9.59
3rd	30	7175.07	3535.79	-50.72	2588.96	2340.90	-9.58
2nd	20	7265.94	3606.33	-50.37	2627.31	2375.59	-9.58
1st	10	7350.31	3674.06	-50.01	2666.62	2411.63	-9.56
Base	0	7350.31	3674.06	-50.01	2666.62	2411.63	-9.56

Table D.4: Story shear in the short direction for the forty storied building

Story	Height	BNBC-2006	UBC-94	Variation (%)	BNBC-2020	ASCE 7-05	Variation (%)
Roof	400	58.61	59.19	0.99	33.14	33.09	-0.14
39th	390	174.76	177.57	1.61	99.27	99.06	-0.21
38th	380	289.82	295.94	2.11	165.08	164.71	-0.23
37th	370	403.78	414.32	2.61	230.56	230.02	-0.23
36th	360	516.63	532.69	3.11	295.71	295.00	-0.24
35th	350	628.37	651.07	3.61	360.52	359.63	-0.25
34th	340	738.98	769.45	4.12	424.98	423.92	-0.25
33rd	330	848.46	887.82	4.64	489.08	487.84	-0.25
32nd	320	956.81	1006.20	5.16	552.82	551.40	-0.26
31st	310	1064.01	1124.58	5.69	616.19	614.58	-0.26
30th	300	1170.06	1237.36	5.75	679.18	677.39	-0.26
29th	290	1274.80	1344.56	5.47	741.79	739.79	-0.27
28th	280	1378.21	1451.76	5.34	804.00	801.80	-0.27
27th	270	1480.28	1558.96	5.31	865.80	863.39	-0.28
26th	260	1581.00	1666.15	5.39	927.18	924.56	-0.28

Story	Height	BNBC- 2006	UBC- 94	Variation (%)	BNBC- 2020	ASCE 7-05	Variation (%)
25th	250	1680.35	1773.35	5.53	988.13	985.30	-0.29
24th	240	1778.32	1880.55	5.75	1048.64	1045.58	-0.29
23rd	230	1874.89	1987.74	6.02	1108.70	1105.41	-0.30
22nd	220	1970.04	2094.94	6.34	1168.29	1164.76	-0.30
21st	210	2063.77	2202.14	6.70	1227.39	1223.61	-0.31
20th	200	2156.05	2302.43	6.79	1285.99	1281.96	-0.31
19th	190	2246.68	2395.82	6.64	1344.08	1339.78	-0.32
18th	180	2335.62	2489.21	6.58	1401.63	1397.05	-0.33
17th	170	2422.85	2582.59	6.59	1458.62	1453.76	-0.33
16th	160	2508.35	2672.36	6.54	1515.03	1509.86	-0.34
15th	150	2592.08	2758.52	6.42	1570.83	1565.35	-0.35
14th	140	2673.78	2844.67	6.39	1625.99	1620.18	-0.36
13th	130	2753.40	2930.82	6.44	1680.48	1674.33	-0.37
12th	120	2830.89	3013.36	6.45	1734.27	1727.75	-0.38
11th	110	2906.20	3092.28	6.40	1787.31	1780.41	-0.39
10th	100	2979.28	3168.90	6.36	1839.56	1832.24	-0.40
9th	90	3049.64	3243.21	6.35	1890.95	1883.18	-0.41
8th	80	3117.15	3314.57	6.33	1941.43	1933.18	-0.43
7th	70	3181.68	3382.97	6.33	1990.91	1982.12	-0.44
6th	60	3243.10	3448.41	6.33	2039.29	2029.90	-0.46
5th	50	3301.29	3510.89	6.35	2086.43	2076.38	-0.48
4th	40	3355.10	3569.75	6.40	2132.17	2121.34	-0.51
3rd	30	3403.88	3622.04	6.41	2176.25	2164.48	-0.54
2nd	20	3446.99	3667.66	6.40	2218.28	2205.34	-0.58
1st	10	3487.02	3708.85	6.36	2258.41	2244.80	-0.60
Base	0	3487.02	3708.85	6.36	2258.41	2244.80	-0.60

Table D.5: Story shear in the short direction for the forty storied building

Story	Height	BNBC-2006	NWTT_BNBC-2006	Variation (%)	BNBC-2020	NWTT_BNBC-2020	Variation (%)
Roof	400	58.61	20.62	-64.82	33.14	18.62	-43.83
39th	390	174.76	68.84	-60.61	99.27	62.20	-37.34
38th	380	289.82	125.10	-56.84	165.08	113.13	-31.47
37th	370	403.78	183.04	-54.67	230.56	165.44	-28.24
36th	360	516.63	241.91	-53.17	295.71	218.20	-26.21
35th	350	628.37	301.28	-52.05	360.52	270.99	-24.83
34th	340	738.98	360.91	-51.16	424.98	323.78	-23.81
33rd	330	848.46	420.65	-50.42	489.08	376.38	-23.04
32nd	320	956.81	480.33	-49.80	552.82	428.61	-22.47
31st	310	1064.01	539.64	-49.28	616.19	479.91	-22.12
30th	300	1170.06	598.14	-48.88	679.18	530.07	-21.96
29th	290	1274.80	650.08	-49.01	741.79	578.27	-22.04
28th	280	1378.21	698.43	-49.32	804.00	623.46	-22.45
27th	270	1480.28	744.25	-49.72	865.80	666.52	-23.02
26th	260	1581.00	789.20	-50.08	927.18	708.59	-23.58
25th	250	1680.35	833.87	-50.38	988.13	750.10	-24.09
24th	240	1778.32	878.42	-50.60	1048.64	791.22	-24.55
23rd	230	1874.89	923.03	-50.77	1108.70	831.96	-24.96
22nd	220	1970.04	967.59	-50.88	1168.29	872.34	-25.33
21st	210	2063.77	1011.88	-50.97	1227.39	912.05	-25.69
20th	200	2156.05	1055.43	-51.05	1285.99	950.64	-26.08
19th	190	2246.68	1093.51	-51.33	1344.08	987.41	-26.54
18th	180	2335.62	1129.00	-51.66	1401.63	1022.12	-27.08
17th	170	2422.85	1162.82	-52.01	1458.62	1055.15	-27.66
16th	160	2508.35	1196.24	-52.31	1515.03	1086.91	-28.26
15th	150	2592.08	1227.52	-52.64	1570.83	1117.84	-28.84
14th	140	2673.78	1258.52	-52.93	1625.99	1148.19	-29.39
13th	130	2753.40	1289.17	-53.18	1680.48	1177.92	-29.91
12th	120	2830.89	1319.53	-53.39	1734.27	1207.02	-30.40
11th	110	2906.20	1347.93	-53.62	1787.31	1235.32	-30.88
10th	100	2979.28	1375.43	-53.83	1839.56	1262.27	-31.38

Story	Height	BNBC-2006	NWTT- BNBC-2006	Variation (%)	BNBC-2020	NWTT- BNBC-2020	Variation (%)
9th	90	3049.64	1400.80	-54.07	1890.95	1287.42	-31.92
8th	80	3117.15	1424.78	-54.29	1941.43	1310.67	-32.49
7th	70	3181.68	1446.80	-54.53	1990.91	1332.41	-33.08
6th	60	3243.10	1468.15	-54.73	2039.29	1352.95	-33.66
5th	50	3301.29	1488.31	-54.92	2086.43	1372.52	-34.22
4th	40	3355.10	1508.11	-55.05	2132.17	1391.36	-34.74
3rd	30	3403.88	1526.91	-55.14	2176.25	1409.49	-35.23
2nd	20	3446.99	1544.71	-55.19	2218.28	1426.76	-35.68
1st	10	3487.02	1562.30	-55.20	2258.41	1443.74	-36.07
Base	0	3487.02	1562.30	-55.20	2258.41	1443.74	-36.07

Table D.6: Story shear in the short direction for the forty storied building

Story	Height	BNBC-2006	BNBC-2020	Variation (%)	NWTT- BNBC-2006	NWTT- BNBC-2020	Variation (%)
Roof	400	58.61	33.14	-43.46	20.62	18.62	-9.72
39th	390	174.76	99.27	-43.20	68.84	62.20	-9.65
38th	380	289.82	165.08	-43.04	125.10	113.13	-9.57
37th	370	403.78	230.56	-42.90	183.04	165.44	-9.61
36th	360	516.63	295.71	-42.76	241.91	218.20	-9.80
35th	350	628.37	360.52	-42.63	301.28	270.99	-10.05
34th	340	738.98	424.98	-42.49	360.91	323.78	-10.29
33rd	330	848.46	489.08	-42.36	420.65	376.38	-10.53
32nd	320	956.81	552.82	-42.22	480.33	428.61	-10.77
31st	310	1064.01	616.19	-42.09	539.64	479.91	-11.07
30th	300	1170.06	679.18	-41.95	598.14	530.07	-11.38
29th	290	1274.80	741.79	-41.81	650.08	578.27	-11.05
28th	280	1378.21	804.00	-41.66	698.43	623.46	-10.73
27th	270	1480.28	865.80	-41.51	744.25	666.52	-10.44
26th	260	1581.00	927.18	-41.35	789.20	708.59	-10.22
25th	250	1680.35	988.13	-41.19	833.87	750.10	-10.05

Story	Height	BNBC- 2006	BNBC- 2020	Variation (%)	NWTT _BNBC -2006	NWTT _BNBC -2020	Variation (%)
24th	240	1778.32	1048.64	-41.03	878.42	791.22	-9.93
23rd	230	1874.89	1108.70	-40.87	923.03	831.96	-9.87
22nd	220	1970.04	1168.29	-40.70	967.59	872.34	-9.84
21st	210	2063.77	1227.39	-40.53	1011.88	912.05	-9.87
20th	200	2156.05	1285.99	-40.35	1055.43	950.64	-9.93
19th	190	2246.68	1344.08	-40.17	1093.51	987.41	-9.70
18th	180	2335.62	1401.63	-39.99	1129.00	1022.12	-9.47
17th	170	2422.85	1458.62	-39.80	1162.82	1055.15	-9.26
16th	160	2508.35	1515.03	-39.60	1196.24	1086.91	-9.14
15th	150	2592.08	1570.83	-39.40	1227.52	1117.84	-8.94
14th	140	2673.78	1625.99	-39.19	1258.52	1148.19	-8.77
13th	130	2753.40	1680.48	-38.97	1289.17	1177.92	-8.63
12th	120	2830.89	1734.27	-38.74	1319.53	1207.02	-8.53
11th	110	2906.20	1787.31	-38.50	1347.93	1235.32	-8.35
10th	100	2979.28	1839.56	-38.25	1375.43	1262.27	-8.23
9th	90	3049.64	1890.95	-37.99	1400.80	1287.42	-8.09
8th	80	3117.15	1941.43	-37.72	1424.78	1310.67	-8.01
7th	70	3181.68	1990.91	-37.43	1446.80	1332.41	-7.91
6th	60	3243.10	2039.29	-37.12	1468.15	1352.95	-7.85
5th	50	3301.29	2086.43	-36.80	1488.31	1372.52	-7.78
4th	40	3355.10	2132.17	-36.45	1508.11	1391.36	-7.74
3rd	30	3403.88	2176.25	-36.07	1526.91	1409.49	-7.69
2nd	20	3446.99	2218.28	-35.65	1544.71	1426.76	-7.64
1st	10	3487.02	2258.41	-35.23	1562.30	1443.74	-7.59
Base	0	3487.02	2258.41	-35.23	1562.30	1443.74	-7.59

Appendix E

Pressure coefficient for $L/B = 0.5$

Table E.1: Average pressure coefficient in windward for length to width ratio is 0.5

Height Ratio	Zone-A1	Zone-B1	Zone-C	Zone-B2	Zone-A2
0.00	0.39	0.65	0.70	0.65	0.39
0.05	0.25	0.52	0.57	0.52	0.25
0.10	0.23	0.45	0.49	0.45	0.23
0.15	0.27	0.46	0.49	0.46	0.27
0.20	0.32	0.49	0.52	0.49	0.32
0.25	0.37	0.54	0.56	0.54	0.37
0.30	0.42	0.59	0.60	0.59	0.42
0.35	0.45	0.63	0.64	0.63	0.45
0.40	0.48	0.67	0.68	0.67	0.48
0.45	0.51	0.70	0.72	0.70	0.51
0.50	0.55	0.74	0.76	0.74	0.55
0.55	0.57	0.77	0.79	0.77	0.57
0.60	0.60	0.80	0.82	0.80	0.60
0.65	0.62	0.82	0.84	0.82	0.62
0.70	0.65	0.86	0.88	0.86	0.65
0.75	0.70	0.90	0.92	0.90	0.70
0.80	0.72	0.92	0.93	0.92	0.72
0.85	0.74	0.92	0.93	0.92	0.74
0.90	0.75	0.90	0.90	0.90	0.75
0.95	0.69	0.79	0.79	0.79	0.69
1.00	-0.66	-0.59	-0.47	-0.47	-0.60

Table E.2: Average pressure coefficient in leeward for length to width ratio is 0.5

Height Ratio	Zone-A1	Zone-B1	Zone-C	Zone-B2	Zone-A2
0.00	-0.24	-0.14	-0.11	-0.16	-0.15
0.05	-0.30	-0.26	-0.24	-0.26	-0.30
0.10	-0.30	-0.26	-0.24	-0.26	-0.30
0.15	-0.30	-0.26	-0.24	-0.26	-0.30
0.20	-0.31	-0.26	-0.25	-0.26	-0.31
0.25	-0.31	-0.27	-0.25	-0.27	-0.31
0.30	-0.32	-0.28	-0.26	-0.28	-0.32
0.35	-0.32	-0.29	-0.27	-0.29	-0.32
0.40	-0.33	-0.29	-0.28	-0.29	-0.33
0.45	-0.33	-0.30	-0.29	-0.30	-0.33
0.50	-0.34	-0.31	-0.30	-0.31	-0.34
0.55	-0.35	-0.32	-0.31	-0.32	-0.35
0.60	-0.35	-0.33	-0.32	-0.33	-0.35
0.65	-0.36	-0.34	-0.34	-0.34	-0.36
0.70	-0.36	-0.35	-0.34	-0.35	-0.36
0.75	-0.36	-0.36	-0.35	-0.36	-0.36
0.80	-0.37	-0.36	-0.36	-0.36	-0.37
0.85	-0.36	-0.36	-0.37	-0.36	-0.36
0.90	-0.36	-0.36	-0.37	-0.36	-0.36
0.95	-0.35	-0.36	-0.37	-0.36	-0.35
1.00	-0.35	-0.40	-0.42	-0.40	-0.34

Appendix F

Pressure coefficient for $L/B = 0.67$

Table F.1: Average pressure coefficient in windward for the length-width ratio is 0.67

Height Ratio	Zone-A1	Zone-B1	Zone-C	Zone-B2	Zone-A2
0.00	0.35	0.63	0.68	0.63	0.35
0.05	0.23	0.50	0.55	0.50	0.22
0.10	0.22	0.45	0.49	0.44	0.21
0.15	0.25	0.45	0.48	0.45	0.25
0.20	0.30	0.49	0.52	0.49	0.30
0.25	0.35	0.54	0.56	0.54	0.35
0.30	0.39	0.58	0.60	0.58	0.39
0.35	0.42	0.62	0.64	0.61	0.41
0.40	0.44	0.65	0.67	0.65	0.44
0.45	0.48	0.69	0.72	0.69	0.47
0.50	0.52	0.73	0.76	0.73	0.51
0.55	0.54	0.76	0.78	0.76	0.53
0.60	0.56	0.79	0.81	0.78	0.55
0.65	0.59	0.82	0.84	0.82	0.59
0.70	0.63	0.86	0.88	0.85	0.62
0.75	0.68	0.90	0.92	0.90	0.68
0.80	0.69	0.91	0.93	0.91	0.69
0.85	0.70	0.90	0.91	0.89	0.69
0.90	0.69	0.85	0.86	0.85	0.68
0.95	0.62	0.72	0.72	0.72	0.61
1.00	-0.91	-0.78	-0.68	-0.75	-0.86

Table F.2: Average pressure coefficient in leeward for the length-width ratio is 0.67

Height Ratio	Zone-A1	Zone-B1	Zone-C	Zone-B2	Zone-A2
0.00	-0.24	-0.21	-0.20	-0.23	-0.23
0.05	-0.26	-0.22	-0.20	-0.22	-0.26
0.10	-0.27	-0.22	-0.20	-0.22	-0.27
0.15	-0.27	-0.22	-0.21	-0.22	-0.27
0.20	-0.28	-0.23	-0.22	-0.23	-0.28
0.25	-0.28	-0.24	-0.23	-0.24	-0.28
0.30	-0.29	-0.25	-0.24	-0.25	-0.29
0.35	-0.30	-0.26	-0.25	-0.26	-0.30
0.40	-0.30	-0.27	-0.26	-0.27	-0.30
0.45	-0.31	-0.28	-0.27	-0.28	-0.31
0.50	-0.32	-0.29	-0.29	-0.30	-0.32
0.55	-0.32	-0.31	-0.30	-0.31	-0.32
0.60	-0.33	-0.32	-0.31	-0.32	-0.33
0.65	-0.33	-0.32	-0.32	-0.33	-0.33
0.70	-0.34	-0.33	-0.33	-0.33	-0.34
0.75	-0.34	-0.33	-0.33	-0.34	-0.34
0.80	-0.33	-0.34	-0.34	-0.34	-0.33
0.85	-0.33	-0.34	-0.34	-0.34	-0.33
0.90	-0.32	-0.33	-0.34	-0.33	-0.32
0.95	-0.31	-0.33	-0.33	-0.33	-0.31
1.00	-0.32	-0.34	-0.37	-0.34	-0.32

Appendix G

Pressure coefficient for $L/B = 1.0$

Table G.1: Average pressure coefficient in windward for the length-width ratio is 1.0

Height Ratio	Zone-A1	Zone-B1	Zone-C	Zone-B2	Zone-A2
0.00	0.36	0.63	0.69	0.63	0.36
0.05	0.22	0.49	0.54	0.49	0.22
0.10	0.23	0.44	0.48	0.44	0.23
0.15	0.26	0.45	0.48	0.45	0.26
0.20	0.30	0.49	0.52	0.49	0.30
0.25	0.35	0.54	0.56	0.54	0.35
0.30	0.39	0.59	0.61	0.59	0.39
0.35	0.42	0.63	0.65	0.63	0.42
0.40	0.46	0.66	0.68	0.66	0.46
0.45	0.48	0.70	0.72	0.70	0.49
0.50	0.52	0.74	0.76	0.74	0.52
0.55	0.56	0.78	0.80	0.78	0.56
0.60	0.58	0.80	0.82	0.80	0.58
0.65	0.58	0.82	0.84	0.82	0.59
0.70	0.59	0.83	0.85	0.83	0.59
0.75	0.63	0.86	0.88	0.86	0.63
0.80	0.66	0.87	0.89	0.87	0.66
0.85	0.69	0.89	0.90	0.89	0.69
0.90	0.69	0.86	0.86	0.86	0.69
0.95	0.61	0.70	0.70	0.70	0.61
1.00	-1.09	-1.09	-1.11	-1.24	-1.09

Table G.2: Average pressure coefficient in leeward for the length-width ratio is 1.0

Height Ratio	Zone-A1	Zone-B1	Zone-C	Zone-B2	Zone-A2
0.00	-0.20	-0.14	-0.16	-0.15	-0.20
0.05	-0.23	-0.19	-0.17	-0.19	-0.23
0.10	-0.23	-0.19	-0.18	-0.19	-0.23
0.15	-0.23	-0.20	-0.18	-0.20	-0.23
0.20	-0.24	-0.20	-0.19	-0.20	-0.24
0.25	-0.25	-0.21	-0.20	-0.21	-0.25
0.30	-0.25	-0.22	-0.21	-0.22	-0.25
0.35	-0.26	-0.23	-0.22	-0.23	-0.26
0.40	-0.26	-0.24	-0.23	-0.24	-0.26
0.45	-0.27	-0.25	-0.24	-0.25	-0.27
0.50	-0.27	-0.26	-0.25	-0.26	-0.27
0.55	-0.28	-0.27	-0.26	-0.27	-0.28
0.60	-0.28	-0.27	-0.27	-0.28	-0.28
0.65	-0.28	-0.28	-0.28	-0.28	-0.28
0.70	-0.28	-0.28	-0.28	-0.28	-0.28
0.75	-0.28	-0.29	-0.29	-0.29	-0.28
0.80	-0.28	-0.28	-0.29	-0.28	-0.28
0.85	-0.28	-0.28	-0.28	-0.28	-0.28
0.90	-0.27	-0.27	-0.27	-0.27	-0.27
0.95	-0.26	-0.26	-0.27	-0.26	-0.26
1.00	-0.28	-0.26	-0.26	-0.26	-0.28

Appendix H

Pressure coefficient for $L/B = 2.0$

Table H.1: Average pressure coefficient in windward for the length-width ratio is 2.0

Height Ratio	Zone-A1	Zone-B1	Zone-C	Zone-B2	Zone-A2
0.00	0.32	0.61	0.67	0.61	0.31
0.05	0.23	0.50	0.56	0.50	0.23
0.10	0.23	0.46	0.50	0.46	0.23
0.15	0.25	0.47	0.50	0.47	0.25
0.20	0.27	0.50	0.52	0.50	0.27
0.25	0.30	0.53	0.56	0.53	0.30
0.30	0.34	0.58	0.60	0.58	0.34
0.35	0.39	0.63	0.65	0.63	0.39
0.40	0.42	0.67	0.69	0.67	0.42
0.45	0.44	0.70	0.73	0.70	0.44
0.50	0.48	0.74	0.77	0.74	0.48
0.55	0.51	0.78	0.80	0.78	0.51
0.60	0.53	0.80	0.83	0.80	0.53
0.65	0.56	0.84	0.86	0.84	0.56
0.70	0.59	0.87	0.89	0.87	0.59
0.75	0.61	0.89	0.91	0.89	0.61
0.80	0.64	0.91	0.93	0.91	0.64
0.85	0.65	0.91	0.92	0.91	0.65
0.90	0.64	0.86	0.87	0.86	0.64
0.95	0.55	0.70	0.70	0.69	0.46
1.00	-0.67	-0.50	-0.52	-0.56	-0.55

Table H.2: Average pressure coefficient in leeward for the length-width ratio is 2.0

Height Ratio	Zone-A1	Zone-B1	Zone-C	Zone-B2	Zone-A2
0.00	-0.10	-0.08	-0.06	-0.05	-0.10
0.05	-0.12	-0.10	-0.11	-0.12	-0.13
0.10	-0.14	-0.12	-0.11	-0.13	-0.13
0.15	-0.15	-0.13	-0.12	-0.14	-0.15
0.20	-0.15	-0.14	-0.13	-0.14	-0.16
0.25	-0.16	-0.15	-0.14	-0.15	-0.16
0.30	-0.16	-0.15	-0.15	-0.16	-0.17
0.35	-0.17	-0.16	-0.16	-0.17	-0.17
0.40	-0.17	-0.17	-0.17	-0.17	-0.18
0.45	-0.18	-0.17	-0.17	-0.18	-0.18
0.50	-0.18	-0.18	-0.18	-0.18	-0.18
0.55	-0.19	-0.18	-0.18	-0.19	-0.19
0.60	-0.19	-0.19	-0.19	-0.19	-0.19
0.65	-0.20	-0.19	-0.19	-0.19	-0.20
0.70	-0.21	-0.20	-0.19	-0.20	-0.21
0.75	-0.22	-0.20	-0.20	-0.20	-0.21
0.80	-0.22	-0.20	-0.20	-0.20	-0.22
0.85	-0.22	-0.20	-0.20	-0.20	-0.22
0.90	-0.22	-0.20	-0.20	-0.20	-0.22
0.95	-0.22	-0.20	-0.19	-0.20	-0.22
1.00	-0.28	-0.21	-0.19	-0.21	-0.27

Appendix I

Pressure coefficient for $L/B = 3.0$

Table I.1: Average pressure coefficient in windward for the length-width ratio is 3.0

Height Ratio	Zone-A1	Zone-B1	Zone-C	Zone-B2	Zone-A2
0.00	0.32	0.57	0.62	0.57	0.32
0.05	0.29	0.52	0.56	0.52	0.29
0.10	0.29	0.52	0.55	0.52	0.29
0.15	0.29	0.53	0.56	0.53	0.29
0.20	0.30	0.55	0.58	0.55	0.30
0.25	0.32	0.58	0.61	0.58	0.32
0.30	0.34	0.61	0.64	0.61	0.34
0.35	0.37	0.65	0.68	0.65	0.37
0.40	0.40	0.69	0.72	0.69	0.40
0.45	0.42	0.72	0.75	0.72	0.42
0.50	0.45	0.76	0.78	0.75	0.45
0.55	0.47	0.79	0.82	0.79	0.47
0.60	0.50	0.82	0.85	0.82	0.50
0.65	0.52	0.84	0.87	0.84	0.52
0.70	0.54	0.86	0.88	0.86	0.54
0.75	0.57	0.89	0.91	0.89	0.57
0.80	0.62	0.92	0.94	0.92	0.62
0.85	0.63	0.91	0.92	0.91	0.63
0.90	0.59	0.83	0.83	0.83	0.59
0.95	0.35	0.46	0.44	0.34	0.34
1.00	-0.56	-0.64	-0.78	-0.75	-0.54

Table I.2: Average pressure coefficient in leeward for the length-width ratio is 3.0

Height Ratio	Zone-A1	Zone-B1	Zone-C	Zone-B2	Zone-A2
0.00	-0.11	-0.07	-0.04	-0.06	-0.11
0.05	-0.12	-0.10	-0.08	-0.10	-0.12
0.10	-0.12	-0.11	-0.10	-0.11	-0.13
0.15	-0.13	-0.12	-0.11	-0.12	-0.13
0.20	-0.14	-0.13	-0.12	-0.13	-0.14
0.25	-0.15	-0.14	-0.13	-0.14	-0.15
0.30	-0.16	-0.15	-0.14	-0.15	-0.16
0.35	-0.17	-0.16	-0.15	-0.16	-0.17
0.40	-0.18	-0.17	-0.16	-0.17	-0.19
0.45	-0.19	-0.17	-0.16	-0.17	-0.20
0.50	-0.20	-0.18	-0.17	-0.18	-0.20
0.55	-0.20	-0.18	-0.17	-0.18	-0.20
0.60	-0.20	-0.18	-0.17	-0.18	-0.20
0.65	-0.21	-0.19	-0.17	-0.18	-0.20
0.70	-0.21	-0.19	-0.18	-0.19	-0.21
0.75	-0.21	-0.19	-0.18	-0.19	-0.21
0.80	-0.22	-0.19	-0.19	-0.19	-0.22
0.85	-0.22	-0.19	-0.19	-0.20	-0.23
0.90	-0.23	-0.20	-0.19	-0.20	-0.23
0.95	-0.24	-0.20	-0.19	-0.20	-0.24
1.00	-0.29	-0.24	-0.21	-0.24	-0.28

Appendix J

Story shear comparison for six storied building using proposed equations

Table J.1: Story shear in the long direction for the six storied building

Story	Height	NWTT _BNBC -2006	Proposed Equation	Variation (%)	NWTT_ BNBC- 2020	Proposed Equation	Variation (%)
Roof	62	17.66	19.62	11.09	12.16	16.19	33.11
5th	52	52.41	54.43	3.86	36.55	46.97	28.53
4th	42	87.40	84.43	-3.40	60.43	74.57	23.40
3rd	32	118.11	109.69	-7.12	81.57	99.01	21.39
2nd	22	143.66	130.51	-9.15	98.66	120.29	21.92
1st	12	166.34	149.41	-10.18	113.22	138.53	22.36
Base	0	166.34	149.41	-10.18	113.22	138.53	22.36

Table J.2: Story shear in the short direction for the six storied building

Story	Height	NWTT _BNBC -2006	Proposed Equation	Variation (%)	NWTT_ BNBC- 2020	Proposed Equation	Variation (%)
Roof	62	13.91	15.69	-28.63	9.54	12.95	35.73
5th	52	41.32	43.55	-31.98	28.82	37.58	30.39
4th	42	68.89	67.54	-35.06	47.53	59.66	25.51
3rd	32	92.99	87.75	-38.14	64.25	79.21	23.29
2nd	22	113.42	104.41	-41.14	78.26	96.23	22.96
1st	12	131.76	119.53	-44.08	90.05	110.83	23.08
Base	0	131.76	119.53	-44.08	90.05	110.83	23.08

Appendix K

Story shear comparison for ten storied building using proposed equations

Table K.1: Story shear in the long direction for the ten storied building

Story	Height	NWTT _BNBC -2006	Proposed Equation	Variation (%)	NWTT _BNBC -2020	Proposed Equation	Variation (%)
Roof	100	17.44	22.97	31.69	13.57	18.28	34.71
9th	90	54.71	64.95	18.72	43.24	53.62	23.99
8th	80	96.14	103.07	7.21	75.65	86.55	14.40
7th	70	134.98	137.43	1.82	107.04	117.09	9.39
6th	60	170.31	168.18	-1.25	135.01	145.26	7.59
5th	50	199.60	195.44	-2.08	159.22	171.08	7.45
4th	40	225.95	218.93	-3.11	180.42	194.55	7.83
3rd	30	247.26	238.66	-3.48	197.90	215.66	8.97
2nd	20	263.92	254.71	-3.49	211.58	234.35	10.76
1st	10	279.18	268.33	-3.88	224.19	250.87	11.90
Base	0	279.18	268.33	-3.88	224.19	250.87	11.90

Table K.2: Story shear in the short direction for the ten storied building

Story	Height	NWTT _BNBC -2006	Proposed Equation	Variatio n (%)	NWTT _BNBC -2020	Proposed Equation	Variation (%)
Roof	100	10.93	15.31	40.14	8.51	12.42	45.88
9th	90	33.47	43.30	29.38	26.56	36.43	37.16
8th	80	57.01	68.71	20.52	45.21	58.80	30.07
7th	70	78.37	91.62	16.91	62.88	79.55	26.52
6th	60	98.46	112.12	13.87	79.08	98.69	24.80
5th	50	115.66	130.29	12.66	93.52	116.23	24.29
4th	40	131.23	145.95	11.21	106.14	132.18	24.53
3rd	30	143.88	159.10	10.58	116.75	146.52	25.50
2nd	20	153.83	169.81	10.39	125.24	159.22	27.13
1st	10	162.22	178.89	10.27	132.57	170.45	28.57
Base	0	162.22	178.89	10.27	132.57	170.45	28.57

Appendix L

Story shear comparison for twenty storied building using proposed equations

Table L.1: Story shear in the long direction for the twenty storied building

Story	Height	NWTT _BNBC -2006	Proposed Equation	Variation (%)	NWTT _BNBC -2020	Proposed Equation	Variation (%)
Roof	200	41.40	54.15	30.81	27.88	42.24	51.52
19th	190	129.93	157.79	21.44	92.64	125.32	35.27
18th	180	230.46	256.84	11.45	166.70	205.60	23.34
17th	170	329.65	351.39	6.59	239.78	283.10	18.07
16th	160	427.71	441.49	3.22	311.20	357.82	14.98
15th	150	520.70	527.23	1.26	381.23	429.78	12.74
14th	140	613.18	608.46	-0.77	449.89	499.00	10.92
13th	130	704.77	685.23	-2.77	516.64	565.48	9.45
12th	120	793.55	757.63	-4.53	579.97	629.23	8.49
11th	110	872.50	825.75	-5.36	638.17	690.26	8.16
10th	100	945.82	889.66	-5.94	690.86	748.58	8.35
9th	90	1012.29	949.09	-6.24	739.08	804.18	8.81
8th	80	1075.05	1004.09	-6.60	783.36	857.08	9.41
7th	70	1131.63	1054.74	-6.79	823.56	907.24	10.16
6th	60	1184.17	1101.11	-7.01	859.23	954.66	11.11
5th	50	1229.97	1143.30	-7.05	890.24	999.31	12.25
4th	40	1271.88	1180.71	-7.17	916.38	1041.11	13.61
3rd	30	1309.84	1213.16	-7.38	938.39	1079.97	15.09
2nd	20	1346.17	1240.55	-7.85	958.24	1115.68	16.43
1st	10	1382.02	1264.79	-8.48	979.28	1148.53	17.28
Base	0	1382.02	1264.79	-8.48	979.28	1148.53	17.28

Table L.2: Story shear in the short direction for the twenty storied building

Story	Height	NWTT _BNBC -2006	Proposed Equation	Variation (%)	NWTT _BNBC- 2020	Proposed Equation	Variation (%)
Roof	200	18.77	29.39	56.61	12.96	23.67	82.61
19th	190	58.33	85.66	46.86	43.02	70.22	63.21
18th	180	103.58	139.43	34.62	77.72	115.20	48.22
17th	170	149.22	190.75	27.83	112.32	158.62	41.22
16th	160	193.44	239.67	23.90	145.31	200.48	37.97
15th	150	232.77	286.21	22.96	176.36	240.80	36.54
14th	140	271.00	330.30	21.88	206.25	279.58	35.56
13th	130	308.47	371.98	20.59	235.24	316.83	34.68
12th	120	344.63	411.29	19.34	262.57	352.55	34.27
11th	110	376.65	448.26	19.01	287.98	386.75	34.30
10th	100	407.00	482.96	18.66	311.90	419.42	34.47
9th	90	434.73	515.22	18.52	334.46	450.58	34.72
8th	80	461.31	545.08	18.16	355.52	480.21	35.07
7th	70	485.36	572.57	17.97	374.89	508.32	35.59
6th	60	508.06	597.75	17.65	392.73	534.89	36.20
5th	50	528.51	620.65	17.43	409.18	559.90	36.84
4th	40	547.65	640.96	17.04	423.93	583.33	37.60
3rd	30	564.31	658.57	16.70	436.79	605.10	38.53
2nd	20	579.29	673.44	16.25	448.19	625.10	39.47
1st	10	594.45	686.60	15.50	459.83	643.51	39.95
Base	0	594.45	686.60	15.50	459.83	643.51	39.95

Appendix M

Story shear comparison for forty storied building using proposed equations

Table M.1: Story shear in the long direction for the forty storied building

Story	Height	NWTT_ BNBC- 2006	Proposed Equation	Variation (%)	NWTT_ BNBC -2020	Proposed Equation	Variation (%)
Roof	400	31.87	58.96	85.01	27.95	48.34	72.98
39th	390	107.56	174.29	62.04	94.93	144.22	51.93
38th	380	197.65	287.07	45.25	175.50	238.49	35.89
37th	370	291.28	397.31	36.40	259.50	331.16	27.61
36th	360	387.26	505.04	30.41	344.65	422.23	22.51
35th	350	484.45	610.27	25.97	430.10	511.71	18.97
34th	340	581.45	713.03	22.63	515.76	599.60	16.25
33rd	330	678.54	813.33	19.86	600.83	685.90	14.16
32nd	320	775.26	911.20	17.53	684.82	770.62	12.53
31st	310	870.77	1006.67	15.61	767.42	853.76	11.25
30th	300	964.97	1099.75	13.97	848.40	935.32	10.25
29th	290	1049.67	1190.33	13.40	926.56	1015.31	9.58
28th	280	1129.51	1278.45	13.19	1000.47	1093.74	9.32
27th	270	1205.42	1364.11	13.17	1071.25	1170.59	9.27
26th	260	1279.54	1447.35	13.11	1140.17	1245.89	9.27
25th	250	1352.62	1528.19	12.98	1207.69	1319.62	9.27
24th	240	1425.17	1606.64	12.73	1274.47	1391.80	9.21
23rd	230	1497.63	1682.74	12.36	1340.98	1462.42	9.06
22nd	220	1570.30	1756.50	11.86	1406.49	1531.49	8.89
21st	210	1642.83	1827.96	11.27	1470.52	1599.00	8.74
20th	200	1714.18	1897.14	10.67	1533.28	1664.96	8.59
19th	190	1778.00	1963.91	10.46	1593.78	1729.37	8.51
18th	180	1840.05	2028.30	10.23	1651.28	1792.23	8.54
17th	170	1900.56	2090.34	9.99	1706.44	1853.54	8.62
16th	160	1959.94	2150.04	9.70	1760.23	1913.29	8.70
15th	150	2015.83	2207.44	9.51	1812.79	1971.48	8.75
14th	140	2071.20	2262.41	9.23	1864.30	2028.11	8.79

Story	Height	NWTT _BNBC- 2006	Proposed Equation	Variation (%)	NWTT _BNBC -2020	Proposed Equation	Variation (%)
13th	130	2126.29	2314.95	8.87	1914.86	2083.17	8.79
12th	120	2181.02	2365.10	8.44	1964.56	2136.65	8.76
11th	110	2233.01	2412.87	8.05	2013.42	2188.55	8.70
10th	100	2284.19	2458.29	7.62	2060.72	2238.84	8.64
9th	90	2332.94	2501.11	7.21	2105.94	2287.51	8.62
8th	80	2380.06	2541.34	6.78	2149.14	2334.53	8.63
7th	70	2424.39	2578.96	6.38	2190.52	2379.87	8.64
6th	60	2467.80	2613.99	5.92	2230.17	2423.49	8.67
5th	50	2509.30	2646.42	5.46	2268.37	2465.32	8.68
4th	40	2549.86	2675.73	4.94	2305.30	2505.27	8.67
3rd	30	2588.96	2701.67	4.35	2340.90	2543.20	8.64
2nd	20	2627.31	2724.04	3.68	2375.59	2578.88	8.56
1st	10	2666.62	2744.30	2.91	2411.63	2612.50	8.33
Base	0	2666.62	2744.30	2.91	2411.63	2612.50	8.33

Table M.2: Story shear in the short direction for the forty storied building

Story	Height	NWTT _BNBC -2006	Proposed Equation	Variation (%)	NWTT _BNBC -2020	Proposed Equation	Variation (%)
Roof	400	20.62	39.30	90.60	18.62	32.59	75.04
39th	390	68.84	116.20	68.79	62.20	97.21	56.29
38th	380	125.10	191.38	52.98	113.13	160.76	42.10
37th	370	183.04	264.88	44.71	165.44	223.23	34.93
36th	360	241.91	336.69	39.18	218.20	284.62	30.44
35th	350	301.28	406.85	35.04	270.99	344.93	27.28
34th	340	360.91	475.35	31.71	323.78	404.18	24.83
33rd	330	420.65	542.22	28.90	376.38	462.35	22.84

Story	Height	NWTT _BNBC -2006	Proposed Equation	Variation (%)	NWTT _BNBC -2020	Proposed Equation	Variation (%)
32nd	320	480.33	607.47	26.47	428.61	519.46	21.20
31st	310	539.64	671.11	24.36	479.91	575.50	19.92
30th	300	598.14	733.16	22.57	530.07	630.48	18.94
29th	290	650.08	793.55	22.07	578.27	684.40	18.35
28th	280	698.43	852.30	22.03	623.46	737.27	18.25
27th	270	744.25	909.41	22.19	666.52	789.08	18.39
26th	260	789.20	964.90	22.26	708.59	839.83	18.52
25th	250	833.87	1018.79	22.18	750.10	889.53	18.59
24th	240	878.42	1071.09	21.93	791.22	938.19	18.58
23rd	230	923.03	1121.83	21.54	831.96	985.79	18.49
22nd	220	967.59	1171.00	21.02	872.34	1032.35	18.34
21st	210	1011.88	1218.64	20.43	912.05	1077.86	18.18
20th	200	1055.43	1264.76	19.83	950.64	1122.32	18.06
19th	190	1093.51	1309.27	19.73	987.41	1165.74	18.06
18th	180	1129.00	1352.20	19.77	1022.12	1208.11	18.20
17th	170	1162.82	1393.56	19.84	1055.15	1249.43	18.41
16th	160	1196.24	1433.36	19.82	1086.91	1289.71	18.66
15th	150	1227.52	1471.63	19.89	1117.84	1328.94	18.88
14th	140	1258.52	1508.27	19.84	1148.19	1367.11	19.07
13th	130	1289.17	1543.30	19.71	1177.92	1404.23	19.21
12th	120	1319.53	1576.73	19.49	1207.02	1440.28	19.33
11th	110	1347.93	1608.58	19.34	1235.32	1475.26	19.42

Story	Height	NWTT _BNBC -2006	Proposed Equation	Variation (%)	NWTT _BNBC -2020	Proposed Equation	Variation (%)
10th	100	1375.43	1638.86	19.15	1262.27	1509.16	19.56
9th	90	1400.80	1667.41	19.03	1287.42	1541.97	19.77
8th	80	1424.78	1694.23	18.91	1310.67	1573.66	20.07
7th	70	1446.80	1719.31	18.84	1332.41	1604.23	20.40
6th	60	1468.15	1742.66	18.70	1352.95	1633.63	20.75
5th	50	1488.31	1764.28	18.54	1372.52	1661.83	21.08
4th	40	1508.11	1783.82	18.28	1391.36	1688.76	21.37
3rd	30	1526.91	1801.11	17.96	1409.49	1714.33	21.63
2nd	20	1544.71	1816.03	17.56	1426.76	1738.38	21.84
1st	10	1562.30	1829.53	17.11	1443.74	1761.04	21.98
Base	0	1562.30	1829.53	17.11	1443.74	1761.04	21.98

Appendix N

Provisions for Wind Load – BNBC 2006

Table N.1: Structural Importance Factor, C_i (BNBC 2006)

Category	C_i
Essential facilities	1.25
Hazardous facilities	1.25
Special occupancy	1.00
Standard occupancy	1.00
Low-risk structure	0.80

Table N.2: Local topography coefficient, C_t (BNBC 2006)

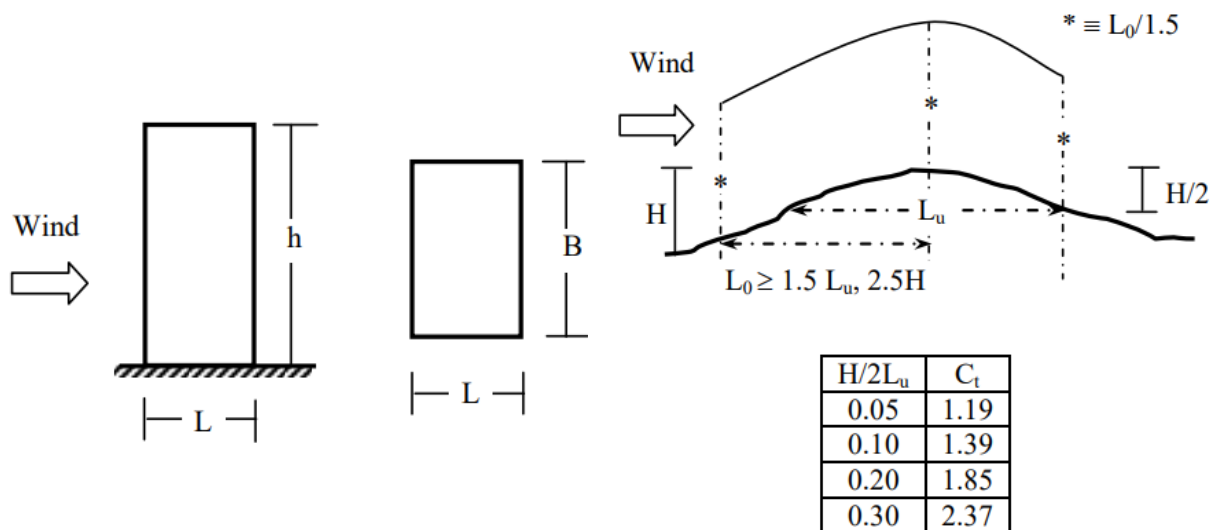


Table N.3: Overall Pressure Coefficient, C_p for Rectangular Building with Flat Roofs
(BNBC 2006)

h/B	L/B					
	0.1	0.5	0.65	1	2	≥ 3.0
≤ 0.5	1.4	1.45	1.55	1.4	1.15	1.1
1	1.55	1.85	2	1.7	1.3	1.15
2	1.8	2.25	2.55	2	1.4	1.2
≥ 4.0	1.95	2.5	2.8	2.2	1.6	1.25

Note:

- These coefficients to be used with Method-2, Use ± 0.7 for roof in all cases.
- Linear interpolation may be made for intermediate values of h/B and L/B

Table N.4: Wind Gust Co-efficient, C_G (BNBC 2006)

Height above ground level (meter)	Exposure A	Exposure B	Exposure C
0-4.5	1.654	1.321	1.154
6	1.592	1.294	1.140
9	1.511	1.258	1.121
12	1.457	1.233	1.107
15	1.418	1.215	1.097
18	1.388	1.201	1.089
21	1.363	1.189	1.082
24	1.342	1.178	1.077
27	1.324	1.170	1.072
30	1.309	1.162	1.067
35	1.287	1.151	1.061
40	1.268	1.141	1.055
45	1.252	1.133	1.051
50	1.238	1.126	1.046
60	1.215	1.114	1.039
70	1.196	1.103	1.033
80	1.180	1.095	1.028
90	1.166	1.087	1.024

Height above ground level (meter)	Exposure A	Exposure B	Exposure C
100	1.154	1.081	1.020
110	1.114	1.075	1.016
120	1.134	1.070	1.013
130	1.126	1.065	1.010
140	1.118	1.061	1.008
150	1.111	1.057	1.005
160	1.104	1.053	1.003
170	1.098	1.049	1.001
180	1.092	1.046	1.000
190	1.087	1.043	1.000
200	1.082	1.040	1.000

Table N.5: Combined Height and Exposure Coefficient, C_z (BNBC 2006)

Height above ground level (meter)	Exposure A	Exposure B	Exposure C
0-4.5	0.368	0.801	1.196
6	0.415	0.866	1.263
9	0.497	0.972	1.37
12	0.565	1.055	1.451
15	0.624	1.125	1.517
18	0.677	1.185	1.573
21	0.725	1.238	1.623
24	0.769	1.286	1.667
27	0.81	1.33	1.706
30	0.849	1.371	1.743
35	0.909	1.433	1.797
40	0.965	1.488	1.846
45	1.017	1.539	1.89
50	1.065	1.586	1.93
60	1.155	1.671	2.002
70	1.237	1.746	2.065

80	1.313	1.814	2.12
90	1.383	1.876	2.171
100	1.45	1.934	2.217
110	1.513	1.987	2.26
120	1.572	2.037	2.299
130	1.629	2.084	2.337
140	1.684	2.129	2.371
150	1.736	2.171	2.404
160	1.787	2.212	2.436
170	1.835	2.25	2.465
180	1.883	2.287	2.494
190	1.928	2.323	2.521
200	1.973	2.357	2.547

Appendix O

Provisions for Wind Load – BNBC 2020

Table O.1: Structural Importance Factor, I (BNBC 2020)

Occupancy Category	Structure Importance Category	V = 38~44 m/s	V > 44 m/s
(IV)	Essential Facilities, Hazardous Facilities*	1.15	1.15
(III)	Special Occupancy, Hazardous Facilities*	1.15	1.15
(II)	Standard Occupancy	1.00	1.00
(I)	Low Risk Structure	0.87	0.77

Table O.2: Pressure Co-efficient, C_p (BNBC 2020)

Surface	L/B	C_{pe}
Windward wall	All values	0.8
Leeward wall	≤ 0.10	-0.5
	0.65	-0.5
	1	-0.5
	2	-0.3
	≥ 4.00	-0.2
Sidewall	All values	-0.7

Table O.3: Velocity pressure exposure coefficient, K_z (BNBC 2020)

Height above Ground level, z	Exposure (Note 1)			
	A		B	C
(m)	Case 1	Case 2	Case 1 & 2	Case 1 & 2
0-4.6	0.70	0.57	0.85	1.03
6.1	0.70	0.62	0.90	1.08
7.6	0.70	0.66	0.94	1.12
9.1	0.70	0.70	0.98	1.16
12.2	0.76	0.76	1.04	1.22
15.2	0.81	0.81	1.09	1.27
18	0.85	0.85	1.13	1.31
21.3	0.89	0.89	1.17	1.34

K_z can be determined from the following formula:

$$\text{For } 4.57 \text{ m} \leq z \leq z_g \quad K_z = 2.01 (z/z_g)^{2/\alpha}$$

$$\text{For } z < 4.57 \text{ m} \quad K_z = 2.01 (4.57/z_g)^{2/\alpha}$$

Note: z shall not be taken less than 9.1 m, for Case 1 in exposure A.

α and z_g are tabulated in Table O.6.

Table O.4: Equations for Gust Effect Factor of Flexible structure, G (BNBC 2020)

Gust Effect Factor	G_f	$0.925[(1+1.7I_z\sqrt{[g_Q^2Q^2+g_R^2R^2]})/(1+1.7g_vI_z)]$
Items and Notation		Equations
Intensity of Turbulence	I_z	$c(33/z)^{1/6}$; where $Z=0.6h$ and Z_{min}
Resonant Response Factor	R	$\sqrt{[(1/b) R_n R_h R_B (0.53+0.47R_\ell)]}$
Background Response Factor	Q	$\sqrt{[1/(1+0.63((B+h)/L_z)^{0.63})]}$ Where $L_z = \ell(z/33)^\epsilon$
Peak factor for Background Response	g_Q	3.4
Peak factor for Resonant Response	g_R	$\sqrt{[2\ln(3600n_1)]} + 0.577/\sqrt{[2\ln(3600n_1)]}$
Peak factor for Wind Response	g_v	3.4

Table O.5: Parameters for Background Response Factor, R_n (BNBC 2020)

Equations	Sub Equations
$R_n = 7.47N_1/(1+10.3N_1)^{5/3}$	$N_1 = n_1 L_z/V_z$, $V_z = b(z/33)^{\bar{a}} \times (88/60) V$ $L_z = \ell(z/33)^\epsilon$
$R_h = R_\ell$ for $\eta = 4.6n_1 h/V_z$	$R_\ell = (1/\eta) - 1/(2\eta^2) (1 - e^{-2\eta})$ for $\eta > 0$
$R_B = R_\ell$ for $\eta = 4.6n_1 B/V_z$	$R_\ell = (1/\eta) - 1/(2\eta^2) (1 - e^{-2\eta})$ for $\eta > 0$
$R_L = R_\ell$ for $\eta = 15.4 n_1 L/V_z$	$R_\ell = (1/\eta) - 1/(2\eta^2) (1 - e^{-2\eta})$ for $\eta > 0$
$R_\ell = 1$ for $\eta = 0$	

<u>Parameters</u>	<u>Item Name</u>	<u>Explanation</u>
V	Basic Wind Speed	FPS Unit
n_1	Natural Frequency of the structure (Rigid <1 Hz ≤ Flexible)	Hz
h	Building Height	FPS Unit
B	The horizontal dimension of the building measured normal to wind direction	FPS Unit
b	Damping Ratio	Usually 5 percent

Table O.6: Constants Values FPS Unit for Gust (BNBC 2020)

Exposure	α	Z_g (ft)	\hat{a}	\hat{b}	\bar{a}	\bar{b}	c	l (ft)	$\bar{\epsilon}$	z_{min} (ft)*
A	7.0	1200	1/7	0.84	1/4.0	0.45	0.30	320	1/3.0	30
B	9.5	900	1/9.5	1.00	1/6.5	0.65	0.20	500	1/5.0	15
C	11.5	700	1/11.5	1.07	1/9.0	1/9.0	0.15	650	1/8.0	7

* z_{min} = Minimum height used to ensure that the equivalent height z is greater of $0.6h$ or z_{min}
For buildings with $h \leq z_{min}$, z shall be taken as z_{min} .

Table O.7: Parameters for Approximate Time Period (BNBC 2020)

Structure Type	C_t	m
Concrete moment-resisting frames	0.0466	0.9
Steel moment-resisting frames	0.0724	0.8
Eccentrically braced steel frames	0.0731	0.75
All other structural systems	0.0488	0.75

Note: Consider moment-resisting frames as frames that resist 100 percent of seismic force and are not enclosed or adjoined by components that are more rigid and will prevent the frames from deflecting under seismic forces.

Table O.8: Wind Directionality Factor K_d (BNBC 2020)

Structure Type	Directionality Factor K_d^*
Buildings	
Main Wind Force Resisting System	0.85
Components and Cladding	0.85
Arched Roofs, Chimneys, Tanks and Similar Structures	
Square	0.90
Hexagonal	0.95
Round	0.95
Solid Signs	0.85
Open Signs and Lattice Framework	0.85
Trussed Towers	
Triangular, Square, Rectangular	0.85
All other cross-section	0.95